A NEW MAGNETOMETER FOR THE NEUTRON EDM EXPERIMENT

by

Yacine Chibane

A thesis submitted in partial fulfilment
of the requirements for the
degree of Doctor of Philosophy

to

The University of Sussex

September 1990

Contents

ABSTRACT

A new magnetic field monitoring technique has been develloped to measure the average magnetic field seen by neutrons stored in a 40 litre cavity for times of the order 150 seconds. The precessing frequency of polarised Mercury atoms stored with the neutrons is measured by an optical technique and we expect to determine the magnetic field averaged over the storage time to 2 parts in 10^7.

CHAPTER I

INTRODUCTION

1.1.-Introduction

The motivation for the quest for a neutron EDM comes from the theoretical consequences resulting from the existence of such a quantity. Although a neutron is known to be electrically neutral, one can think of it as made up of two almost spherical charge distributions equal in size but opposite in sign separated by a small distance radially. As it will be shown below, any mechanism which gives rise to an EDM in a free particle must involve the violation of parity P and time reversal symmetry T. Consequently, a measurement of a finite neutron EDM implies the violation of T which has yet to be seen directly.

The work laid out in this thesis is associated with the neutron EDM experiment at the Institute Laue-Langevin (ILL) in Grenoble (France). This experiment is a result of a collaboration between the University of Sussex, the Rutherford Appleton Laboratory (RAL), the University of Washington, Harvard University and the ILL. The group uses for this experiment the high flux ultra cold neutron (UCN) source designed by the technical University of Munich and ILL. The actual EDM measurement uses polarised UCN that are stored in a neutron reflecting bottle. The neutrons are subjected to static aligned magnetic **B** and electric **E** fields. A change in the neutron resonance frequency correlated with the reversal of the **E** field is an

indication of the existence of a neutron EDM. This observation requires precise and continuous monitoring of the magnetic field B.

The aim of the work described in this thesis is to develop a new magnetometer system capable of monitoring the magnetic field to a precision of a few parts in 10^8 in the same volume as that occupied by the neutrons.

After presenting, in the present chapter, the ILL experiment in more detail, we discuss in chapter three the different possible magnetometer systems that could be implemented in this experiment and the likely performance of each of them. We establish that an optically pumped mercury system is probably the best system that could be accommodated in the ILL experiment. In chapter 2, a comprehensive review of optical pumping is presented. Chapter 4 deals with the work done on a Caesium magnetometer. We will show that Cs vapours can be optically pumped in large glass volumes (≈5 litres) but an attempt at polarising Cs in an aluminium container was unsuccessful and more research to find a suitable wall coating is required. General techniques of optical pumping in mercury vapours are dealt with in chapter 5 in which we describe experiments done with coated glass and quartz containers. This chapter serves as an introduction to the sixth chapter which is concerned with the outline of a prototype mercury magnetometer for the EDM experiment. In chapter 6, we will describe the successive stages in the realisation of such a system starting from the construction and concluding with the experimental results obtained. The thesis ends with a summary of the work and suggests improvements that could be implemented in the future.

1.2. - The Neutron EDM

Parity P, charge conjugation C and time reversal T play an important role in quantum theory. For a long time, it was believed that each of these symmetries was conserved until work done on weak decays of nuclei [Wu 57] and of pions and muons [Gar 57], [Fri 57] showed that P and C symmetries could be violated. In 1950, Landau proposed that these two symmetries should be replaced by a more general CP symmetry. In 1964, however, Christenson, Cronin, Fitch and Turlay [Chr 65] proved experimentally that CP was violated in decays of K° mesons. Fortunately, one could still construct an even stronger CPT symmetry suggested by Luders [Lud 57] and Pauli [Pau 55]. If this symmetry is indeed totally conserved then the observed CP violation implies an associated T violation. One can show that the existence of an intrinsic EDM in particles, such as the neutron, implies violation of T symmetry directly.

The neutron EDM can be written as

$$\mu_e = \langle \rho \, \mathbf{r}.\mathbf{S} \rangle \qquad (1.1)$$

where ρ is the charge density, $\mathbf{r}$ the position vector and $\mathbf{S}$ the neutron spin. Let us assume that the neutron is subjected to an electric field $\mathbf{E}$. The energy shift of the neutron due to the interaction of the electric dipole moment with the $\mathbf{E}$ field is

$$\Delta E = \langle \mu_e . \mathbf{E} \rangle \qquad (1.2)$$

Since the most important direction in a particle is the direction of its spin, a neutron EDM exists only if it has a component along the spin direction. The effective energy ΔE is then effectively

$$\Delta E = \langle(\mu_e \cdot \mathbf{S})(\mathbf{S}.\mathbf{E})\rangle \tag{1.3}$$

or

$$\Delta E = \langle(\rho\, \mathbf{r}.\mathbf{S})(\mathbf{S}.\mathbf{E})\rangle \tag{1.4}$$

Since the motion of $\mathbf{r}$ relative to $\mathbf{S}$ is much faster than the motion of $\mathbf{S}$ around $\mathbf{E}$, we can write that

$$\Delta E = \langle\rho\, \mathbf{r}.\mathbf{S}\rangle\langle\mathbf{S}.\mathbf{E}\rangle \tag{1.5}$$

The implication of a finite ΔE from the experiment shows that $\langle\rho\mathbf{r}.\mathbf{S}\rangle \neq 0$ for the neutron.

Applying T and P operators to this scalar yields

$$P(\mathbf{r}.\mathbf{S}) = (-\mathbf{r})(\mathbf{S})\, P \tag{1.6}$$

$$T(\mathbf{r}.\mathbf{S}) = (\mathbf{r})(-\mathbf{S})\, T \tag{1.7}$$

because $\mathbf{S}$ is an axial vector and $\mathbf{r}$ is a polar vector. We can immediately see that neither P nor T commute with $\mathbf{r}.\mathbf{S}$. If the Hamiltonian for the free neutron gives a neutron state which has a finite expectation value for an operator, eg. $(\mathbf{r}.\mathbf{S})$, which is odd under P and T, it can be shown that [Mes 65] the Hamiltonian does not commute with P and T. These arguments are only valid if the state concerned is not degenerate. We know that the neutron ground state is not degenerate from workings of the nuclear shell model.

According to quantum mechanics [Mes 65], the Hamiltonian

of a system is said to be invariant under the application of a symmetry operator A only if it commutes with A. Therefore both P and T symmetries are violated. Consequently, the existence of a neutron EDM is a definite manifestation of parity and time reversal violation.

The theoretical predictions for the neutron EDM are model dependent. They range from less than 10^{-30} e.cm in the Standard Model with three generations of quarks to 10^{-25} e.cm as predicted by the super-symmetric model.

Experimentally, the search for a neutron EDM started in the late 1940's on a neutron beam at Oak Ridge at the suggestion of N.F.Ramsey of Harvard University and the first result of $(-0.1 \pm 2.4)\times10^{-20}$ e.cm was obtained in 1951. Since then the measurement of the upper limit of the EDM has been improved at the rate of one order of magnitude every seven years. Most recent experiments (at ILL, Grenoble and Leningrad, USSR) use ultra cold bottled neutrons with speeds less than 6m/sec. The latest result published by the ILL collaboration is $< 12\times10^{-26}$ e.cm at the 95% confidence level, whereas the Leningrad group measures an upper limit of 26×10^{-26} e.cm [Alt 86].

1.3. - Measurement of the Neutron EDM at the ILL

The main features of the experiment are shown in Figure 1.1. The UCN from the source enter the apparatus through valve V_1. They are neutrons with velocities less than 6m/sec. Before reaching the storage bottle, only the UCN with the spin-up direction can pass through the 1µm magnetically saturated iron-cobalt polarising foil. Valve

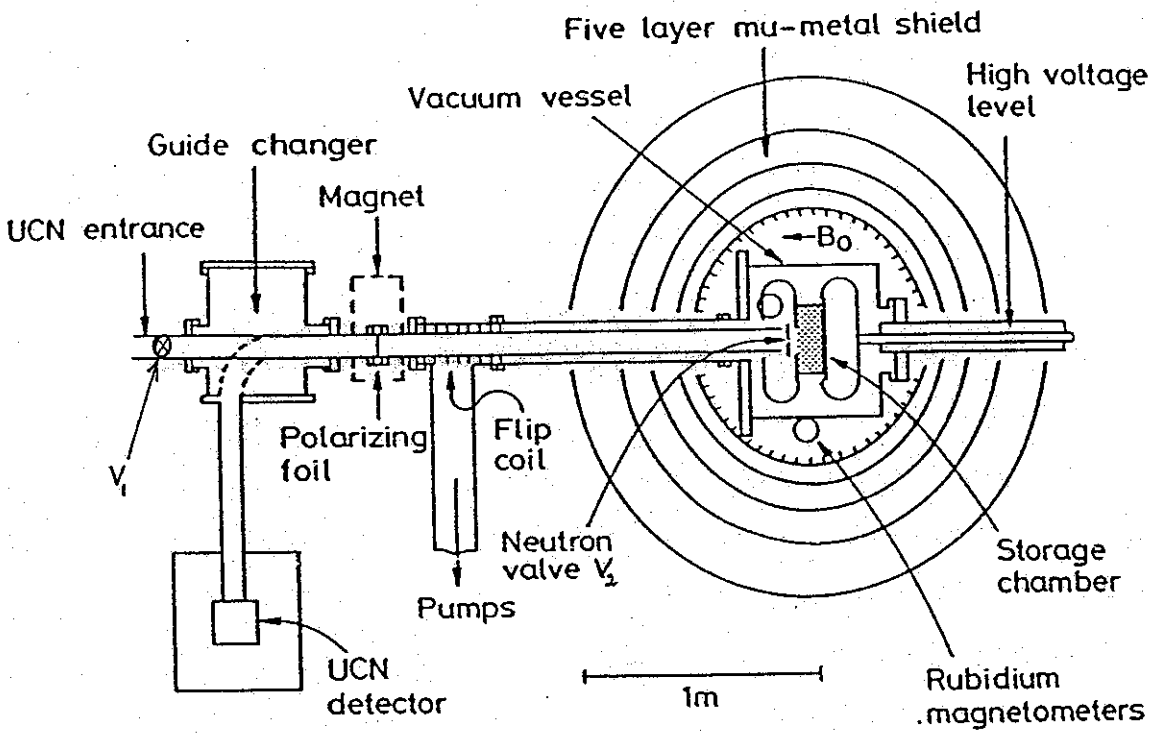

Figure 1.1 : Diagram showing the neutron EDM apparatus at ILL

V_2 is then closed to imprison the polarised neutrons for a period which is currently about 80 secs. The bottle consists of two beryllium electrodes, 25 centimetres in diameter, separated by a cylinder of beryllium oxide 10 centimetres high. The UCN then bounce around disappearing steadily till about 40% remain after time T.

A highly stabilised B_0 = 10 mGauss field is applied together with a 10 kvolt/cm electric field aligned with the magnetic field. A pressure of 10^{-4} torr of either dry nitrogen or Helium is maintained in the apparatus to help quench sparking. As they enter the bottle, the neutrons have their spins aligned parallel to $\mathbf{B}_0$. A few seconds after the V_2 valve is closed a 30 Hz resonant $\pi/2$ magnetic field oscillation perpendicular to $\mathbf{B}_0$ is applied for a time t of 4 seconds to turn the spins into the plane perpendicular to $\mathbf{B}_0$. The UCN continue precessing around $\mathbf{B}_0$ as they bounce around in the bottle until after a time T of 80 secs. a second burst of oscillating magnetic field phase coherent with the first one is applied for 4 seconds. At the end of this second $\pi/2$ pulse the UCN spins are either parallel or antiparallel to $\mathbf{B}_0$ with a probability which depends on the extent to which the precessing spins are in phase with the oscillating field during the second $\pi/2$ pulse. The change-over system has switched position allowing the neutrons in the guide tube outside the bottle to diffuse towards the detector. The neutrons pass back to the FeCo foil which now acts as an analyser by reflecting neutrons with reversed spin direction and transmitting neutrons with unchanged spin down a vertical guide to the detector. After a counting time of about 10 secs the neutrons that could not previously pass through are now

subjected to an adiabatic fast passage by energising the spin flipper coil in order to be counted. The first count is usually referred to as the " spin up" count and the second one as the " spin down " count. The whole cycle of operations takes about two minutes to complete. Valve V_1 is then opened again to start another machine cycle.

A typical curve of UCN counts as a function of the oscillating field frequency is shown in Figure 1.2. A working point is chosen half way up the central valley and the basic procedure is to look for a change in the UCN counts per machine cycle on reversing the electric field applied. Such a change would occur when the E-field acting on the EDM alters the UCN precession frequency, thereby slightly shifting the resonance. The precession frequency f_0 is given by

$$f_0 = \frac{1}{h} (2\mu_m B_0 \pm 2\mu_e E_0) \qquad (1.8)$$

where μ_m is the neutron magnetic dipole moment, and μ_e the neutron EDM. The ± refers to the $\mathbf{E}_0$ field being parallel to or anti-parallel to the $\mathbf{B}_0$ field. The change in precession frequency df when the $\mathbf{E}_0$ field is reversed is

$$df = \frac{4\mu_e E_0}{h} \qquad (1.9)$$

and a measurement of df yields an estimate of the neutron EDM as long as the B_0 field remains constant.

1.4- Need for a new magnetic field monitoring technique.

Unfortunately, some systematic phenomena correlated with

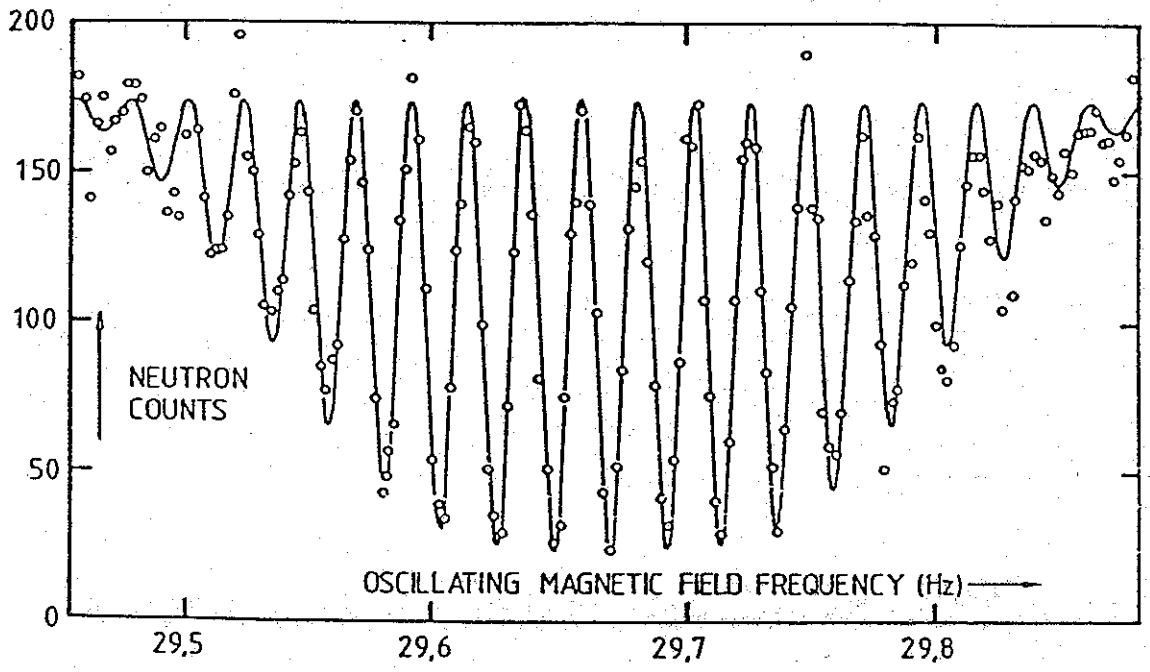

Figure 1.2 : A neutron magnetic resonance curve obtained with UCN stored for 40 secs in a 10 mGauss field when an oscillating magnetic field is applied for 4 secs at the beginning and the end of the storage period. The data points are fitted using the Ramsey theory which predicts a linewidth at the center of the pattern of 0.011 Hz.

the reversal of the electric field can cause a resonance frequency shift. This is the case of leakage currents flowing down the walls of the storage vessel created by the strong E_0 field. These currents generate their own magnetic field and are likely to change with the direction of the electric field and consequently exhibit a pseudo-EDM.

The magnetic field is monitored by three optically pumped Rubidium magnetometers positioned as close as possible to the neutron bottle and the neutron EDM is calculated as follows:

The neutron counts,over many cycles, with the E field in one direction are grouped in together and a neutron resonance frequency is calculated. The same operation is also done for the opposite direction of the E field. A neutron EDM (including any pseudo-EDM) is then calculated. The same treatment is repeated with the magnetometers and a magnetometer EDM μ_m is also computed. In order to calculate the real neutron EDM we take the difference between μ_N and μ_m in order to subtract any pseudo-EDM effects. The actual neutron EDM is then

$$\mu_e = (\mu_N - \mu_m) \pm \sqrt{(\delta\mu_N)^2 + (\delta\mu_m)^2} \qquad (1.10)$$

where $\delta\mu_N$ and $\delta\mu_m$ are the standard deviations in the neutron and the magnetometers EDM's respectively.

The fact that the magnetometers are placed outside the storage vessel does not make them ideal for field monitoring inside the bottle and an alternative technique should be implemented and that is the purpose of the work in this thesis.

The new technique which we have considered consists of storing spin polarised atoms with the neutrons, during the neutron storage period, and use them to monitor any magnetic field changes including those generated by leakage currents. Since, both neutrons and atoms are to be stored together they should average the same magnetic field. Among the types of atoms that could be utilised we have considered Helium atoms, Caesium atoms and Mercury atoms. We will show, in chapter 3, that the best system to be used is probably an optically pumped mercury gas.

1.5 - The UCN system as a magnetometer.

An effective magnetic field monitoring system should have a sensitivity greater than that which the neutrons provide (as a magnetometer). The neutrons themselves constitute a magnetometer which has its own performance in measuring the precession frequency. But, one needs an independent system with a better performance, running at the same time as the neutron system, and which is insensitive to the electric field (ie. that does not exhibit an EDM of its own). The different possible magnetometer systems under consideration are discussed in chapter 3, where we have also attempted to estimate the kind of precision each system should provide. Therefore, we will first estimate the precision achieved by the neutrons and take it as a reference for comparison with other magnetometer systems.

Figure 1.3 shows the central region of the Ramsey resonance curve where the frequency is determined. The spin-up neutrons counted as a function of the oscillating field frequency f can be described by

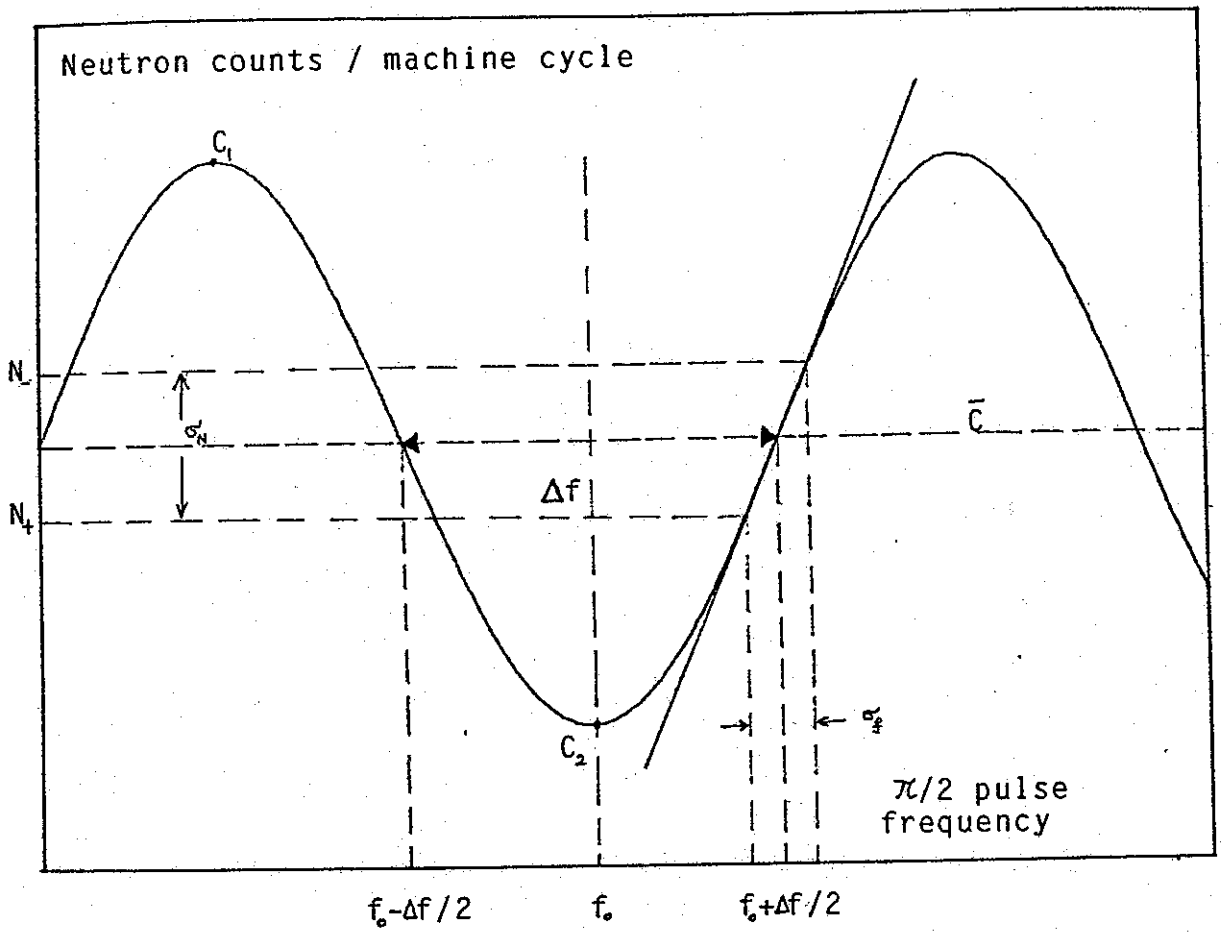

Figure 1.3 : Diagram showing the central region of the Ramsey resonance curve and the different parameters needed to determine σ_f the precision in the oscillating field frequency f . N_+ an N_- are the two points chosen to measure the uncertainty in the neutron count $\sigma_N = \sqrt{N}$

$$N(f) = \bar{C}\left[1 - a\,\mathrm{Cos}\left(\frac{\pi(f - f_0)}{\Delta f}\right)\right] \qquad (1.11)$$

where $\bar{C} = (C_1 + C_2)/2$, $a = (C_1 - C_2)/(C_1 + C_2)$, f_0 is the resonance frequency, Δf is the width of the central fringe, and C_1 and C_2 the maximum and minimum neutron counts. It is easy to see that at the working point ($f = f_0 + \Delta f/2$) we have

$$\frac{dN(f)}{df} = (\pi a \bar{C})/\Delta f \qquad (1.12)$$

We can write the relation between the standard deviation σ_N in the neutron count and the standard deviation σ_f in the frequency as

$$\sigma_N = \frac{dN}{df}\sigma_f \qquad (1.13)$$

Consequently,

$$\sigma_f = \frac{\Delta f\sqrt{N}}{\pi a \bar{C}} \qquad (1.14)$$

where we used the fact that the uncertainty in the neutron count is $\sqrt{N}$. In the central valley the linewidth at the working point is [Pen 90]

$$\Delta f = \frac{1}{2\,(T + 4t/\pi)} \qquad (1.15)$$

which reduces to $\Delta f = 1/2T$ for $t \ll T$. T is the time between the two $\pi/2$ pulses and t is the length of each pulse. The typical values involved are $T \approx 80$secs and $t = 4$ secs. Substituting for Δf and $\bar{C}$ in equation 1.14, we have

$$\sigma_f = \frac{1}{2\pi a T\sqrt{N}} \qquad (1.16)$$

a is usually of the order 0.6. Taking the number of neutrons to be 40,000 neutrons/cycle for the next experiment planned yields for one machine cycle

$$\sigma_f = 1.33\text{x}10^{-5}\ \text{Hz} \qquad (1.17)$$

which results in measuring the resonance frequency to a precision of

$$\left(\frac{\sigma_f}{f}\right) = 5.53\text{x}10^{-7} \qquad (1.18)$$

where we took f = 30 Hz. σ_f is the error made in measuring the frequency due to the error in the neutron counts. The magnetometer system to be implemented in the experiment should, at least, attain three times this precision in order to be fully effective.

CHAPTER II

Theory of Optical Pumping

2.1-INTRODUCTION

The term "OPTICAL PUMPING" was first suggested by Kastler in 1950 in Journal de Physique [Kas 50] and in a report presented the same year at the congress of radio-frequency spectroscopy in Amsterdam.

A system of atoms is said to be optically pumped when a light source is used to induce a population distribution very different from Boltzman.

Before we get to the subject of optical pumping in more detail it is worth asking the question :Why create population differences ?

The purpose behind this is to prepare atoms for a special kind of spectroscopic analysis. For instance, measurements of transfer collisional cross sections between the Zeeman sub-levels of an atomic system in the presence of foreign gases. The effect of the collisions is to "thermalise" the energy levels and to equalise their populations.

Therefore, the population distribution of the atoms amongst the different energy levels is used to measure the effect of atomic or molecular collisions of a given vapour in presence of a foreign gas. It is a means of probing matter.

2.2-Principles of Optical pumping

Let us consider a simplified atom with only three energy levels, which we shall call A, B and C [fig.2.1]. Levels A

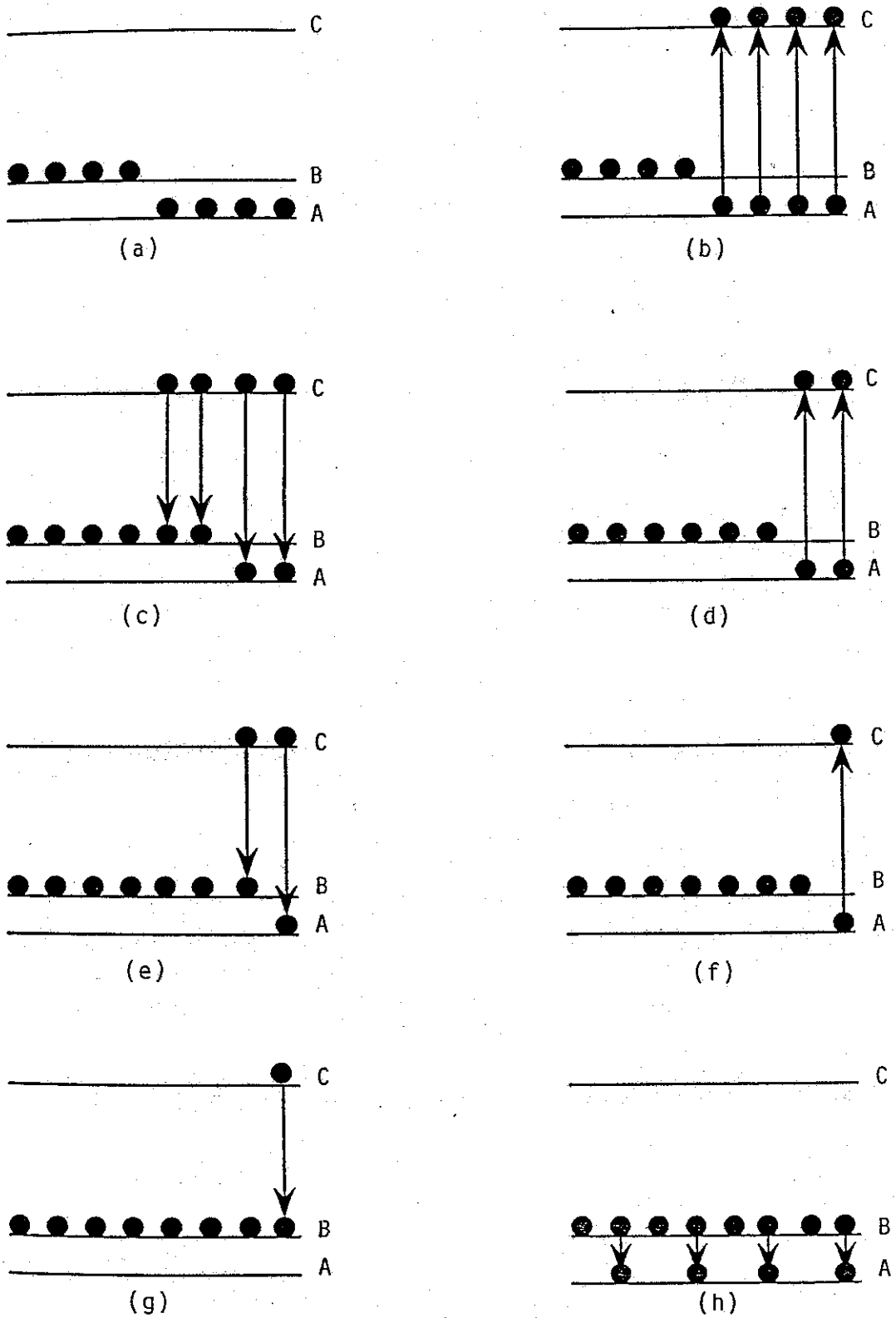

Figure2.1:The optical pumping process.

It start (a) with all the atoms equally distributed among A and B. Under the action of the pumping light (b)all the atoms in B are excited to C and subsequently decay (c) to both A and B states. This process continues untill all the atoms end up (g) in B and the pumping is complete. In (h), a RF field is applied to equalise the A and B populations.

and B are low-lying and the separation between them corresponds to a radio-frequency spectrum line,and in thermal equilibrium, levels A and B are equally populated when $hf_{AB} << kT$. However, the separations A-C and B-C correspond to lines lying in the optical spectrum. In other words, level C is much higher.

The system is now subjected to optical radiation, the nature of which is such as to stimulate only A⟶C transitions. The beam of photons brings the atoms from the A energy state to the upper state C where they stay for a very short time ($\sim 10^{-9}$ secs.).The depopulation of the excited level C is done in two ways : either by an emission of light which brings the atoms back to the original level A or by an emission of light which brings the atoms to level B. The proportion going to each state depends on the structure of the atoms. The important thing is that atoms that dropped into B can no longer be excited to level C because we arranged, somehow, to filter out the B⟶C transition. Nevertheless, the atoms that dropped back into A are raised again to the C state and again they will have some probability of dropping to B. After a long enough time, every atom must end up in the B state and no more light can be absorbed. The system is then said to be completely pumped.

The term *Optical Pumping* involves the two successive processes A⟶C and C⟶B. In practice, atoms do not stay indefinitely in state B and relaxation processes tend to re-establish thermal equilibrium between levels A and B. Furthermore, each of the levels A, B and C can consist of several sub-levels that are distinguished by their proper quantum numbers.

Detecting these non-thermal population distributions can be done in a number of ways, for example one can look at the characteristics of the absorbed light (absorption coefficient in the case of natural or polarised light) or those of the fluorescent light (intensity or state of polarisation). In one of the methods, one uses the fact that the intensity of the transmitted light through the vapour varies with the degree of pumping. As the atoms are removed from level A the transparency of the sample increases. When all the atoms are in the B state the pumping process is complete; the vapour is totally transparent and the intensity of the transmitted light is maximum.

We mentioned earlier that in order to have efficient pumping the transitions B⟶C have to be prevented. This can often be achieved by using circularly polarised pumping light. When light passes through a circular polariser and propagates along the z-direction, each photon carries a z-component of angular momentum of $+\hbar$ or $-\hbar$ according to the sense of the circular polarisation.If we assume the energy levels A, B and C to represent different m values of an atomic system, therefore, a σ^+ polarised light (photons carrying $+\hbar$ angular momenta) would take atoms from a $|m\rangle$ state to a $|m+1\rangle$ state. Consequently, one just makes sure that level B has at least the same m value as level C. No atom from B absorbing a σ^+ photon can be accepted in C.

2.3.- The Phenomenological Treatment of Optical Pumping

2.3.1.- Pumping and Relaxation in the Ground State.

In this section, we examine how the occupation of a given

magnetic sublevel of the ground state of an ensemble of atoms changes with time. A classical treatment of the dynamics of optical pumping can be achieved by using some phenomenological procedure based on population densities. In the general case, one considers a system of atoms with p sub-levels, then the rate of change of the population density N_k will be given by

$$-\frac{dN_k}{dt}=\sum_{i=1}^{p}(V_{ki}+W_{ki})N_k-\sum_{i=1}^{p}(V_{ik}+W_{ik})N_i \qquad (2.1)$$

with $k=1,2,\ldots,p$

where V_{ki} is the transition probability per unit time from the sublevel k of the ground state to the sub-level i of the same state via a certain intermediate optically excited level, and W_{ki} is the probability of the relaxation transitions between levels k and i directly. Usually the energy kT of the thermal motion is much larger than the distance E_i-E_k between the sublevels, therefore we can neglect the small difference between the equilibrium populations of the sublevels. In this case all the W_{ki} are the same,

$$\sum_{i=1}^{p}W_{ki}=pW=1/T_1 \qquad (2.2)$$

and

$$\sum_{i=1}^{p}W_{ki}N_i=\sum_{i=1}^{p}\frac{1}{pT_1}N_i=\frac{1}{pT_1}\sum_{i=1}^{p}N_i=\frac{1}{pT_1}N \qquad (2.3)$$

where N is the total number of atoms per unit volume and T_1 is the time characterising all the relaxation processes and is called the spin-lattice or the longitudinal relaxation

time for the system.

We also introduce the notation

$$\sum_{i=1}^{p} V_{ki} = 1/T_p \qquad (2.4)$$

where $1/T_p$ is the total rate of change of the difference in population densities under the action of the pumping light. Since V_{ki} is proportional to intensity, T_p is usually written as

$$T_p = \frac{1}{KI} \qquad (2.5)$$

where K is a constant and I the intensity of the incident light. The bigger the intensity I the smaller the time T_p. In other words, it takes a brighter light source a shorter time to pump an ensemble of atoms.

For the sake of simplicity, we will consider the case of a two-level system in the ground state like the one shown in figure 2.1. Equation (2.1) becomes

$$-\frac{dN_A}{dt} = (V_{AB} + W_{AB})N_A - (V_{BA} + W_{BA})N_B \qquad (2.6)$$

$$-\frac{dN_B}{dt} = (V_{BA} + W_{BA})N_B - (V_{AB} + W_{AB})N_A \qquad (2.7)$$

If we call polarisation the following quantity

$$P = \frac{N_A - N_B}{N_A + N_B} \qquad (2.8)$$

equations (2.6) and (2.7) reduce to

$$\frac{dP}{dt} = -\frac{1}{\tau_1}(P-P_0) \qquad (2.9)$$

where P_0 is the ultimate degree of polarisation attainable, expressed as

$$P_0 = \frac{T_1 X + T_p Y}{T_1 + T_p} \qquad (2.10)$$

and

$$1/\tau_1 = 1/T_1 + 1/T_p \qquad (2.11)$$

X and Y are defined as

$X = \frac{V_{BA} - V_{AB}}{V_{BA} + V_{AB}}$ the degree of polarisation of the atoms due to the light, and

$Y = \frac{W_{BA} - W_{AB}}{W_{BA} + W_{AB}}$ the small polarisation associated with the Boltzman distribution and no light. In the two level case T_p and T_1 take the form

$$1/T_p = V_{BA} + V_{AB} \qquad (2.12)$$

$$1/T_1 = W_{BA} + W_{AB} \qquad (2.13)$$

Since at t=0 the polarisation of the vapour is that associated with the Boltzman distribution, the solution to equation (2.9) is solved using the initial condition $P(0) = Y$ and reads

$$P(t) = P_0(1-e^{-t/\tau_1}) + Ye^{-t/\tau_1} \qquad (2.14)$$

We can see that the ultimate degree of polarisation reached

when $t>>\tau_1$ is equal to P_0.

Since $Y<<1$, P_0 takes the form

$$P_0 = -\left(1 + \frac{T_p}{T_1}\right)^{-1} \qquad (2.15)$$

The minus sign occurs because of our definition of P in equation (2.8). Note that when $T_p<<T_1$, P_0 can reach a value close to -1. This means that if the pumping action of the source is much quicker than the relaxation processes, the ultimate degree of polarisation can approach 100%. This would mean that the vapour could reach a state where the majority of the atoms are in level B. One can see that, in order to obtain an efficient pumping the condition $T_p<<T_1$ must be satisfied, ie. the contribution of the light to P_0 must exceed the contribution of the relaxation to P_0.

2.3.2.- The Bloch Equations for Optical Pumping

Let us assume now that our two-level system represents an atomic gas with a total spin quantum number F = 1/2. We can then characterise the system by a vector magnetisation **M** proportional to the degree of polarisation and defined by

$$\mathbf{M} = \boldsymbol{\mu} N P \qquad (2.16)$$

where $\boldsymbol{\mu}$ is the atomic magnetic moment.If the pumping light beam I_z is along the z direction, this equation becomes

$$M_z = \boldsymbol{\mu} N P_z \qquad (2.17)$$

Equation (2.9) can be written in terms of M_z:

$$\frac{dM_z}{dt} + \frac{1}{\tau_1}(M_z - M_{z0}) = 0 \qquad (2.18)$$

where

$$M_{z0} = \frac{T_1 M_z^P + T_{pz} M_z^T}{T_1 + T_{pz}} \qquad (2.19)$$

$$M_z^P = \mu N X_z \qquad (2.20)$$

and

$$M_z^T = \mu N Y_z \qquad (2.21)$$

Equation (2.19) is equivalent to equation (2.10) where polarisation was replaced by magnetisation induced by the I_z light beam. X_z is the contribution of the I_z light beam to the magnetisation and Y_z is the small magnetisation due to the Boltzman distribution. T_{pz} is exactly the same T_p defined earlier in equations (2.4) and (2.5), and the z index was only introduced to remind us that the pumping beam is along the z-axis.

If the direction of the applied magnetic field B does not coincide with the direction of the light beam I_z, we also have to take into account the moment of forces acting on the atom due to the external field in every direction. The expressions describing the time evolution of the magnetisation components M_x and M_y are obtained in a similar way. We have

$$\frac{dM_x}{dt} + \frac{1}{\tau_2}(M_x - M_{x0}) - \gamma[\mathbf{M} \times \mathbf{B}]_x = 0 \qquad (2.22.a)$$

$$\frac{dM_y}{dt} + \frac{1}{\tau_2}(M_y - M_{y0}) - \gamma[\mathbf{M} \times \mathbf{B}]_y = 0 \qquad (2.22.b)$$

$$\frac{dM_z}{dt} + \frac{1}{\tau_1}(M_z - M_{z0}) - \gamma[\mathbf{M} \times \mathbf{B}]_z = 0 \qquad (2.22.c)$$

$[\mathbf{M} \times \mathbf{B}]_x$ denotes the component of the cross product $\mathbf{M} \times \mathbf{B}$ in the x direction, and γ is the gyromagnetic ratio.
These expressions reduce to Bloch equations of nuclear magnetic resonance [Blo 46] when the light beam I_z is absent.

Let $M_\perp$ be the projection of the total magnetization M in the xy plane. $M_\perp$ is then the vector sum of M_x and M_y and is therefore called the " transverse magnetization". It is eligible to introduce a transverse relaxation time τ_2 defined as

$$1/\tau_2 = 1/T_2 + 1/T_p \qquad (2.23)$$

to describe the rate at which $M_\perp$ relaxes under both external relaxation phenomena and the pumping light. T_2 is the relaxation time of $M_\perp$ in the xy-plane without the effect of the I_z light beam.
The solutions to equations (2.22) depend on the boundary conditions,i.e on the experimental conditions

2.3.3.- Application to a Resonance Experiment

In the following, we will be restricting ourselves to a two-level atomic system like ^{199}Hg which will be used in the experimental part of this thesis.
We use a beam of light [fig. 2.2], circularly polarised, propagating along a static magnetic field B_z. The ensemble of atoms is at the same time subjected to rotating

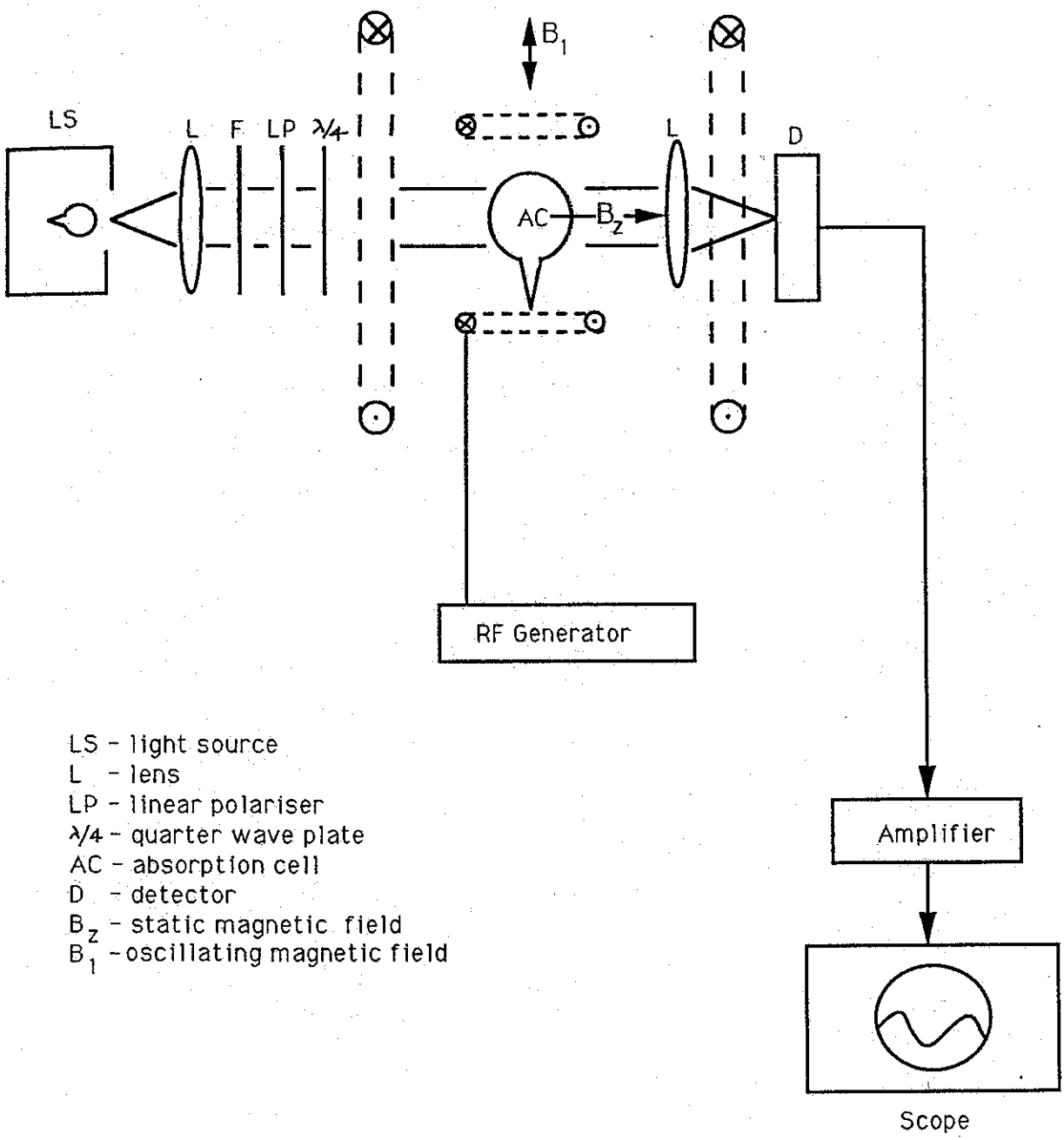

Figure 2.2 : An optical pumping apparatus

radio-frequency magnetic fields B_1 which rotate at the angular frequency ω in a plane perpendicular to the static field B_z. In practice an oscillating field, which can be decomposed into two counter-rotating components, is usually used. The field rotating in the same direction as the atomic precession has a large integrated effect on transition probabilities. The field rotating in the opposite direction averages almost to zero each precession cycle and can be ignored to first order. It only gives rise to a small shift, called the Bloch-Siegert shift [Blo 40].
The components of B_1 in the xy-plane are

$$B_x = B_1 \cos\omega t \qquad (2.24.a)$$

$$B_y = B_1 \sin\omega t \qquad (2.24.b)$$

in this case the rate equations take the form

$$\frac{dM_x}{dt} + \frac{1}{\tau_2}(M_x - M_{x0}) - \gamma(M_y B_z - M_z B_1 \sin\omega t) = 0 \qquad (2.25.a)$$

$$\frac{dM_y}{dt} + \frac{1}{\tau_2}(M_y - M_{y0}) - \gamma(M_z B_1 \cos\omega t - M_x B_z) = 0 \qquad (2.25.b)$$

$$\frac{dM_z}{dt} + \frac{1}{\tau_1}(M_z - M_{z0}) - \gamma(M_x B_1 \sin\omega t - M_y B_1 \cos\omega t) = 0 \qquad (2.25.c)$$

These equations are usually solved in a coordinate system rotating at the frequency ω around the z-axis [fig2.3], ie. a coordinate system rotating with B_1.
This amounts to replacing B_z by the effective field $B_1 + (B_z - \omega/\gamma)$. By doing so and assuming that the light beam is along the z-axis, we end up with the equivalent differential system

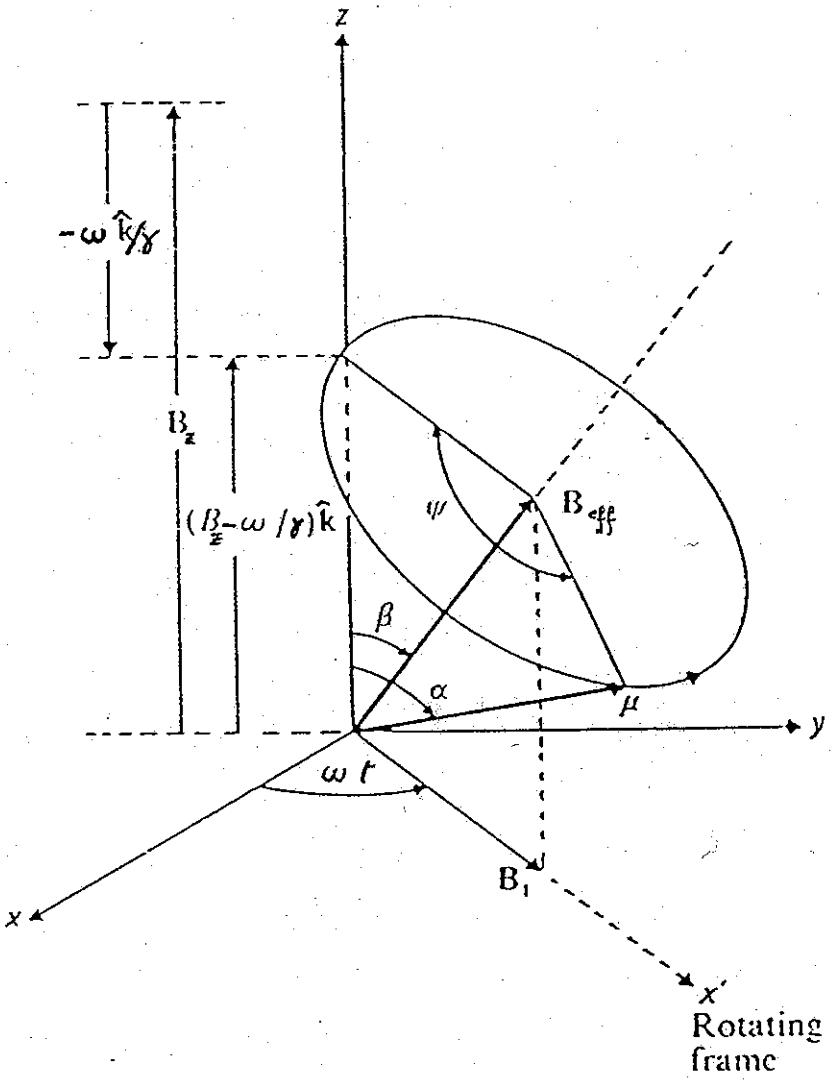

Figure 2.3 : The coordinate system x'y'z rotates around the z-axis at the angular frequency which is the frequency of the $\vec{B}_1$ field. In this frame, the magnetic moment $\vec{\mu}$ precesses around $\vec{B}_{eff}$ which is the sum of $\vec{B}_1$ and $(B_z-\omega/\gamma)\hat{k}$.

$$\frac{dM_x}{dt} = -\frac{M_x}{\tau_2} - (\omega_L - \omega)\, M_y \qquad (2.26.a)$$

$$\frac{dM_y}{dt} = (\omega_L - \omega)\, M_x - M_y/\tau_2 - \omega_1 M_z \qquad (2.26.b)$$

$$\frac{dM_z}{dt} = +\omega_1 M_y + (M_0 - M_z)/\tau_1 \qquad (2.26.c)$$

which has the following stationary solution in the rotating frame

$$M_z = M_0 \left(1 - \frac{\omega_1^{\,2}\tau_1/\tau_2}{1/\tau_2^{\,2} + \omega_1^{\,2}\tau_1/\tau_2 + (\omega_L - \omega)^2}\right) \qquad (2.27.a)$$

$$M_x = M_0 \left(\frac{\omega_1 (\omega_L - \omega)}{1/\tau_2^{\,2} + \omega_1^{\,2}\tau_1/\tau 2 + (\omega_L - \omega)^2}\right) \qquad (2.27.b)$$

$$M_y = -M_0 \left(\frac{\omega_1/\tau_2}{1/\tau_2^{\,2} + \omega_1^{\,2}\tau_1/\tau_2 + (\omega_L - \omega)^2}\right) \qquad (2.27.c)$$

Experimentally, one detects optical signals proportional to M_x, M_y and M_z. M_z is observed in the direction of the magnetic field B_z. When plotted as a function of $(\omega_L - \omega)$, M_z exhibits an absorption profile. M_x and M_y are detected by looking at the transverse magnetization $\mathbf{M}_\perp$ in a direction perpendicular to the static field. If the observation as a function of $(\omega_L - \omega)$ is done in the x direction (using a phase sensitive detector), M_x would be the in-phase component of $\mathbf{M}_\perp$ and behaves like a dispersion curve (fig.2.4.b), whereas M_y would be in quadrature and displays an absorption shape (fig.2.4.a).
When the observation is done without phase detection, the signal is proportional to $[M_x^{\,2} + M_y^{\,2}]$ [Coh 62].
By varying the angular frequency difference $(\omega_L - \omega)$, at

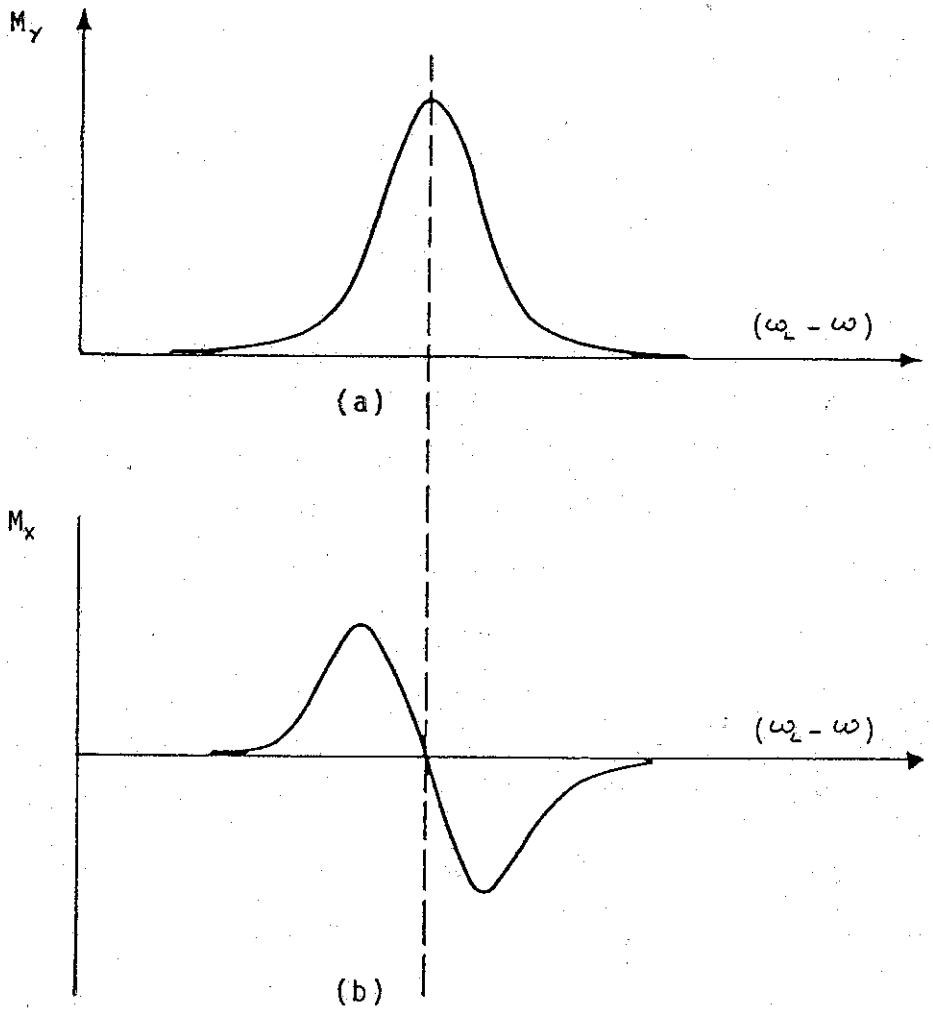

Figure 2.4 : These two profiles represent an NMR signal when it is phase detected (using a PSD).
(a) The signal is in quadrature
(b) The signal is in phase
In optical pumping, if the observation is done in the x-direction, figure (a) represents the component M_y of the transverse magnetisation and figure (b) the M_x component.

constant magnitude of B_1, the intensity of the transmitted light in the z-direction traces out a magnetic resonance absorption curve (fig.2.4.a). The transparency of the vapour is reduced by an amount that depends on $(\omega_L - \omega)$ and on the magnitude of B_1 (at resonance B_e is reduced to B_1).

The expression of the resonance signal linewidth, which is easily derived from equation (2.27.a) is

$$\Delta\omega_{\frac{1}{2}} = 2\left[\frac{1}{\tau_2{}^2} + \gamma^2 B_1{}^2 \frac{\tau_1}{\tau_2}\right]^{\frac{1}{2}} \qquad (2.28)$$

It should be noted that this expression is only valid for a two-level system in which only one transition is possible. The effect of the RF power on the linewidth is now apparent. By inducing transitions between two energy levels, the RF field shortens the lifetimes of these levels, and consequently broadens the resonance linewidth.

One should note that at zero RF power the linewidth is still finite. The remaining term $2/\tau_2$ represents the effect of the pumping light on the linewidth. The optical excitation destroys the phase memory of the precessing atoms. An optical pumping photon absorption pulls the atom out of the coherent superposition state in which it was set by the RF field. By measuring the linewidth for different RF powers and different light intensities and then extrapolating to zero both quantities, one can measure the intrinsic transverse relaxation time T_2. The linewidth reduces to

$$\Delta\omega_{\frac{1}{2}}^0 = 1/T_2 \qquad (2.29)$$

this relation can represent a definition of T_2 as being the relaxation time of the coherence between atoms that was introduced by the rotating B_1 field.

When the frequency of the applied B_1 field equals the Larmor angular frequency, ie. at resonance,

$$\omega = \omega_L = g_F \mu_B \frac{B_z}{\hbar} \qquad (2.30)$$

magnetic dipole transitions occur between the Zeeman levels. The RF field causes the atoms to shuttle back and forth between the two ground state Zeeman levels, thus effectively transferring some of them from level B to level A [fig 2.1]. The atom is said to be in a superposition of states. This happens at relatively low values of the amplitude of the RF field B_1. One needs only satisfy the relation

$$\gamma B_1 T_2 \approx 1 \qquad (2.31)$$

This condition is derived from the very well known Rabi formula, at resonance, that expresses the probability $P(t,t_0)$ of a transition from one spin state at t_0 to another spin state at a later time t,

$$P(t,t_0) = \frac{\omega_1^2}{\omega_1^2 + (\omega_L - \omega)^2} \sin^2\left[\frac{\omega_e (t - t_0)}{2}\right] \qquad (2.32)$$

where $\omega_1 = \gamma B_1$ and $\omega_e = \gamma B_e$. B_e is the effective field seen by the atoms in the rotating frame (fig. 2.3).
The time T_2, in these circumstances, is associated with the rate at which the precessing magnetic dipoles move out of phase with the RF field which forces their precessional

motion. For this reason, t in equation 2.32 is replaced by T_2 to obtain equation 2.31.

2.4- Relaxation processes

The ultimate degree of polarisation that can be attained in an optical pumping experiment depends critically on the relaxation rates in the ground state.
There are four main relaxation mechanisms:
(a)magnetic field inhomogeneities.
(b)wall collisions.
(c)atom-atom collisions.
(d)loss into the reservoir.
To each relaxation process is assigned a partial *relaxation time* T_{Ri}.
The overall relaxation time present in typical experimental conditions is a combination of the individual T_{Ri}'s in the form

$$\frac{1}{T_R} = \sum_i \frac{1}{T_{Ri}} \qquad (2.33)$$

2.4.1.- Magnetic field inhomogeneities

When an atom moves in an inhomogeneous magnetic field, its nuclear spin will not follow adiabatically the different directions of the applied field. The atom experiences randomly fluctuating magnetic fields. Because different atoms have different histories in the bulb,due to random nature of their paths, there is eventually a loss of coherence of the oscillating moments. However, these perturbations obey the motional narrowing condition

(the"flying atom" sees only the mean field value inside the cell) and their effects are small enough to be neglected. By careful design of the field coils this problem can be minimised.

2.4.2.- Wall collisions

When an atom strikes the walls of a container it usually sticks for a finite time before rebounding off. During this dwell, it is subjected to large local magnetic and electric field gradients that are produced by the molecules forming the container walls. The result is that the atomic spin interacts with these fields and "forgets" its initial direction. When it leaves the wall the spin magnetic moment finds itself randomly directed with respect to the applied magnetic field. Fortunately, this problem can be efficiently tackled by covering the cell walls with coatings of special organic compounds [Rob 58] and much longer relaxation times can be obtained.
The relaxation time associated with this mechanism can be identified with the mean time of flight T_W of the atoms between two collisions with the walls. This is given by

$$T_W = \frac{N}{n}\frac{V}{S} \qquad (2.34)$$

where V is the volume of the cell, S is the surface area, N is the atomic number density and n is the mean number of atoms of mass m hitting a unit area per second

$$n = \frac{1}{4} N \bar{v} \qquad (2.35)$$

where $\bar{v} = \left(\frac{8kT}{\pi m}\right)^{1/2}$ is the mean thermal velocity.
This relaxation time T_w applies in the case of vapours having electronic orientations, such as alkali atoms, in uncoated cells. In the case of pure nuclear orientations (odd mercury isotopes for example) the atoms can actually make many collisions with the walls before being depolarised.

2.4.3.- Atom-atom collisions

These can happen either with gaseous impurities present in the cell or between atoms of the vapour that is being pumped. Short lived molecules are likely to be formed in the process. The relaxation time associated with this phenomenon is given by

$$\frac{1}{T_c} = N_p \ \bar{v}_r \ \sigma(\bar{v}_r) \qquad (2.36)$$

where N_p is the atomic density of the foreign gas at the pressure p, $\bar{v}_r$ is the mean relative velocity, and $\sigma(\bar{v}_r)$ is the velocity averaged spin-disorientating collision cross-section.
On the other hand, some diamagnetic gases are intentionally put into the pumping cell to prevent the optically oriented atoms reaching the walls. These foreign gases are called "buffer gases" and the most widely used ones are H_2, N_2 and the noble gases. Bender [Ben 56] showed that S-state atoms (without orbital momentum) are insensitive to molecular collisions. However, one cannot increase the pressure of the buffer gas indefinitely because collisions between the excited atoms and those of the buffer gas do disorientate

the magnetic moments and therefore change the optical conditions. If the foreign gas pressure is considerably high the excited atoms will be uniformly distributed among the Zeeman states of the excited level and atoms will then return at the same rate to all states of the ground level.

2.4.4.- Loss into the reservoir

The vapour in an optical pumping cell is usually in equilibrium with a metallic drop of the same element. The life time of an atom in the cell is the time between leaving the drop and coming back to it. The collisions with the drop make the atoms lose their polarisation. In order to minimise this effect, the drop is placed in a stem separated from the main cell by a capillary. This effect can be sometimes completely avoided by sealing off the capillary and by working on a "dry vapour".

2.5- Modulation of a Light Beam by Precessing absorbing atoms.

In order to monitor the degree of polarisation of Hg vapours, we used (see chapters 5 and 6) a technique suggested by Dehmelt in 1957 [Deh 57],which consists of shining a polarised light beam onto an assembly of atoms precessing around a magnetic field perpendicular to the light beam direction. The output of such an experiment will be a modulation of the outgoing beam at the Larmor frequency of the precessing spins.
We aim, in this section, to show how such a modulation arises. We will not be giving the detailed calculations

until appendix 1, but only the main lines.

Let us assume a ground state total angular momentum F=1/2 and a complete polarisation of the atomic system. Let the system be an ensemble of ^{199}Hg atoms, of which the ground state is a $^1S_0$ state and the first excited state is a $^3P_1$. Note that the nuclear spin is equal to 1/2.
We assume the magnetisation **M** of the sample to be in a direction (θ,ϕ) taken as the quantization axis. In the ground state, such a system could be described by the state vector

$$|\psi\rangle=\text{Sin}\theta/2\ e^{i\phi/2}|-1/2\rangle + \text{Cos}\theta/2\ e^{-i\phi/2}|+1/2\rangle \qquad (2.37)$$

where $|-1/2\rangle$ and $|+1/2\rangle$ are the two eigenstates corresponding to $m_F=-1/2$ and $m_F=+1/2$.
We then apply a magnetic field **B** in the z-direction and shine a σ^+ polarised light beam along the x-axis.
The aim of this calculation amounts to evaluate the probability of finding the system in the excited $^3P_1$ state under the action of such a light beam. This probability P is written as

$$P=|\langle\tfrac{1}{2}\tfrac{1}{2}|\mathbf{E}.\mathbf{r}|\psi\rangle|^2+|\langle\tfrac{1}{2}-\tfrac{1}{2}|\mathbf{E}.\mathbf{r}|\psi\rangle|^2 \qquad (2.38)$$

which is the sum of the transition probabilities from the state $|\psi\rangle$ (equation 2.37) to either of the $|Fm_F\rangle$ of the $^3P_1$ excited state. **E** is the electric vector of the light beam defined by

$$\mathbf{E}=(E/\sqrt{2})(\mathbf{j}+i\mathbf{k}) \qquad (2.39)$$

and $\mathbf{r}=x\mathbf{i}+y\mathbf{j}+z\mathbf{k}$ is the position of the electron making the transition. The computation of equation (2.38) results in (see appendix 1)

$$P = k(1-\text{Sin}\theta\text{Cos}\phi) \qquad (2.40)$$

where k is a constant.
In the experiments to be described in chapters 5 and 6, the magnetisation of the sample lies in the xy-plane which makes $\theta=\pi/2$. The angle ϕ represents the extent to which the atoms have precessed in a time t, i.e $\phi=\omega t$ where ω is the Larmor precession frequency in the applied B field. Consequently,

$$P=k(1-\text{Cos}\omega t) \qquad (2.41)$$

The last expression, shows clearly the modulation in light absorption of the beam at the atomic precession frequency ω.

CHAPTER III

Possible Magnetometers for the EDM Experiment

3.1. - Introduction

As already mentioned in chapter I, the magnetic field in the neutron EDM experiment at ILL is monitored by three optical pumping magnetometers placed as near as possible to the neutron storage volume and arranged to average the field readings over the neutron storage cycle. The magnetometer output is analysed for correlation with electric field direction in the same way as the neutron counts in order to provide an indication of any pseudo-EDM associated with the magnetic fields produced by the leakage currents. Being outside the neutron storage vessel, the magnetometers do not average the same magnetic field seen by the neutrons during the storage period. In order to overcome this problem we decided to store optically pumped atoms with the neutrons and use them to extract any possible pseudo-EDM. We also think that the use of a SQUID, placed as near as possible to the neutron bottle, will help to stabilise the B_0 field considerably.

Three possible magnetometer systems are discussed in this chapter.

1.A Helium magnetometer. ^{3}He would be a very appropriate system for the experiment, but the difficulty involved in detecting its degree of polarisation makes its use less

likely.

2.A Caesium magnetometer. Caesium atoms provide a signal at 4KHz, higher than Helium by a factor 500, and the operating vapour pressure at room temperature, but we find that the difficulty in storing Cs atoms in metal containers and their tendency to form a metallic layer on the neutron bottle walls inducing a **E** field breakdown will surely prevent us from implementing such a system.

3.A Mercury magnetometer. This system seems to be the best. Hg atoms are easily polarised and kept for long periods of time. The Larmor frequency can be measured directly and the precision to which this system is likely to measure the average magnetic field seen by the neutrons is better than the UCN magnetometer discussed in chapter 1.

3.2. - A Helium Magnetometer

Although no work was done by the author of this thesis on Helium vapours, it is relevant to include such a magnetometer in the discussion. The idea of a Helium magnetometer was first suggested by Prof. N. F. Ramsey [Ram 79] and [Ram 84]. Polarised ^{3}He atoms injected into the storage volume just after the neutrons will, like the neutrons, be subjected to resonant $\pi/2$ oscillating field pulses at the beginning and end of the storage period. Measurement of the ^{3}He polarisation at the end of each cycle yields the ^{3}He resonance frequency during the cycle and the data handling program which correlates neutron frequencies with **E** field direction to give the neutron EDM

will, in the same way, correlate ^{3}He frequencies with **E** field direction to give what we call the magnetometer EDM, an estimate of the pseudo EDM.

^{3}He seems to be a good contender as a magnetometer for the EDM experiment for many reasons. Due to charge cloud compensation [Pur 50], [Sch 63], ^{3}He is expected to have negligible intrinsic EDM. It is also known to retain nuclear polarisation over long periods of time [Col 63]. Furthermore, polarisations as high as 70% have been reported in the literature [Pav 70].

On the other hand, the large neutron capture cross-section (5000b) [Mug 81] limits the density of ^{3}He that can be stored with the neutrons for 100secs to 3×10^{-4} torr, a density lower by a factor $\sim 10^4$ than other workers have used in practice. This makes accurate measurement of polarisation difficult.

Helium is optically polarised by first running a discharge to excite the atoms from the 1^1S_0 ground state to the 2^3S_1 metastable state (Figure 3.1). Infrared radiation of 10830 Å is then used to pump the atoms to the excited state 2^3P_0. Direct pumping to this level from the ground state requires light sources working in the vacuum UV. If the light beam is right-hand circularly polarised, the $m_F = +3/2$ and $m_F = +1/2$ sub-levels of the 2^3S_1 metastable state can be populated at the expense of the $m_F = -3/2, -1/2$ sub-levels via the 2^3P_0 level. This polarisation of the metastable state can then be transferred to the 1^1S_0 ground state through a metastability exchange collisions. During this exchange, angular momentum conservation laws imply a transfer of angular momentum from the metastable state to the ground state (which has no electronic angular

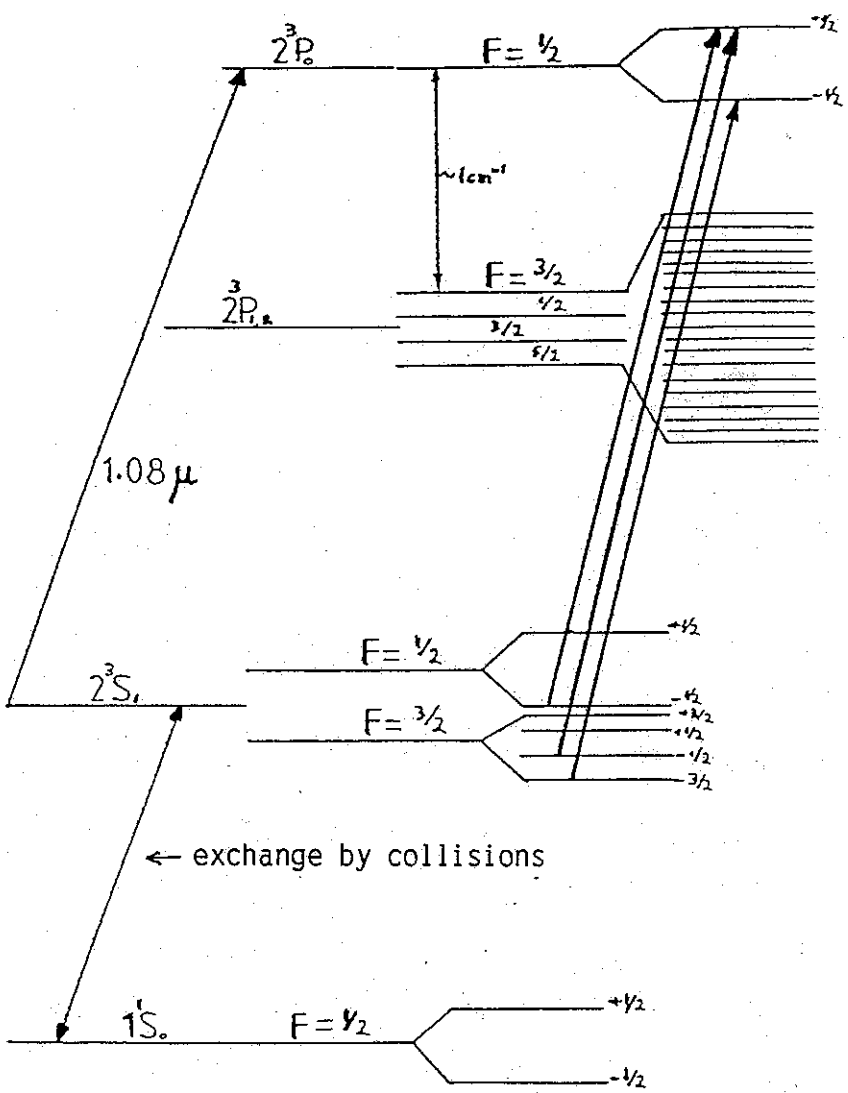

Figure 3.1 : Energy levels of ^{3}He in a weak magnetic field.

momentum). Orientation of the $^1S_0$ nuclear magnetic moment is extremely resistant to relaxation processes and lifetimes as long as a few hours can be achieved when the discharge is turned off.

3.2.1. - The Experimental Technique

As far as the neutron EDM experiment is concerned, ^{3}He could be polarised and then transferred to a storage volume already filled with neutrons. The transfer of polarised ^{3}He is done across magnetic field shaping solenoids to preserve maximum orientation. Once the neutron storage time has elapsed, ^{3}He atoms would be released before the neutrons into an analyser to measure the polarisation and give the ^{3}He precession frequency. Unfortunately, because the ^{3}He density in the storage bottle is limited to 10^{-4} torr, the measurement of polarisation after storage is difficult. In addition, the precession frequency estimated from polarisation measurements depends on the signal amplitude, requiring accurate stabilisation of initial density.

The three different methods which could be used to detect the degree of polarisation are described in the following section together with the performance expected from each of them.

1. Optical detection of polarisation :

The method developed by Pavlovic and Laloe in 1970 [Pav 70] could be used. This involves running a discharge in the vapour to excite some polarised atoms to energy levels above the 2^3P_0 level, thereby transferring their net

angular momenta to these higher states. When decaying back to some other lower excited states, these atoms emit circularly polarised light whose degree of polarisation is proportional to the polarisation achieved previously in the ground state. For example, if the discharge makes the polarised ground state atoms go to the 2^1P state, a subsequent decay to the 3^1D state is followed by the emission of a circularly polarised light at a wavelength of 6678 Å. The 3^1D state is very short lived with a low number density, so the probability of acquiring polarisation through collision with the metastable state is negligible. Nevertheless, the feasibility of this technique requires a ^3He pressure in the range 0.1 torr to a few torrs. Since the ^3He pressure used in the neutron bottle is only 10^{-4} torr, this means that the gas has to be compressed and, if necessary diluted with some additional unpolarised Helium. The whole operation has to be repeated for each neutron storage time.

In order to calculate the resonance frequency for ^3He the neutron result, equation (1.11), can be modified to yield polarisation oscillating with frequency between $-\beta$ and $+\beta$

$$P = \beta \, \mathrm{Cos}(\pi(f - f_0)/\Delta f) \qquad (3.1)$$

where β has a maximum of 1 and is likely to be near 1 in practice. Extending further the neutron analysis, replacing the standard deviation in neutron counts by the standard deviation in polarisation of 1% obtained by a French group [Smi 90] for $P = 0.7$, we obtain

$$\frac{\sigma_f}{f} = 9.5 \times 10^{-7} \qquad (3.2)$$

where we have taken T = 80 secs and f = 30Hz. This figure does not seem to be any better than the frequency precision measured by the neutrons themselves (see chapter 1). Furthermore, the French group worked at a ^{3}He pressure of 1 torr, very much bigger than we could use at ILL.

2. Detection by NMR :

Making reference to Dr. P. W. Franks' thesis [Fra 86] which was concerned with using ^{3}He as a magnetometer for the EDM experiment, we effectively quote his results and briefly describe the set-up he recommended.
Figure 3.2 shows the proposed NMR detection system. In a field of 1 Tesla generated by a super-conducting magnet over a region of a few centimetres, the ^{3}He magnetisation could be detected with a signal to noise ratio of the order of 100, with the NMR pick up coil emerged in liquid Helium. This figure is similar to the S/N achieved by the French group in the optical detection method. Therefore, the result obtained above (equation 3.2) is also applicable here and once again this detection method does not provide any better means of measuring the frequency than the neutrons. Furthermore, this method requires a good reproducibility in the number of the ^{3}He atoms arriving at the detector each cycle.

3. Detection using a SQUID :

This method is also dealt with in reference [Fra 86]. It is similar to the previous one except that the induced oscillating flux in the pick up coil is transferred to a rf SQUID via a flux transformer. The detection is done in a

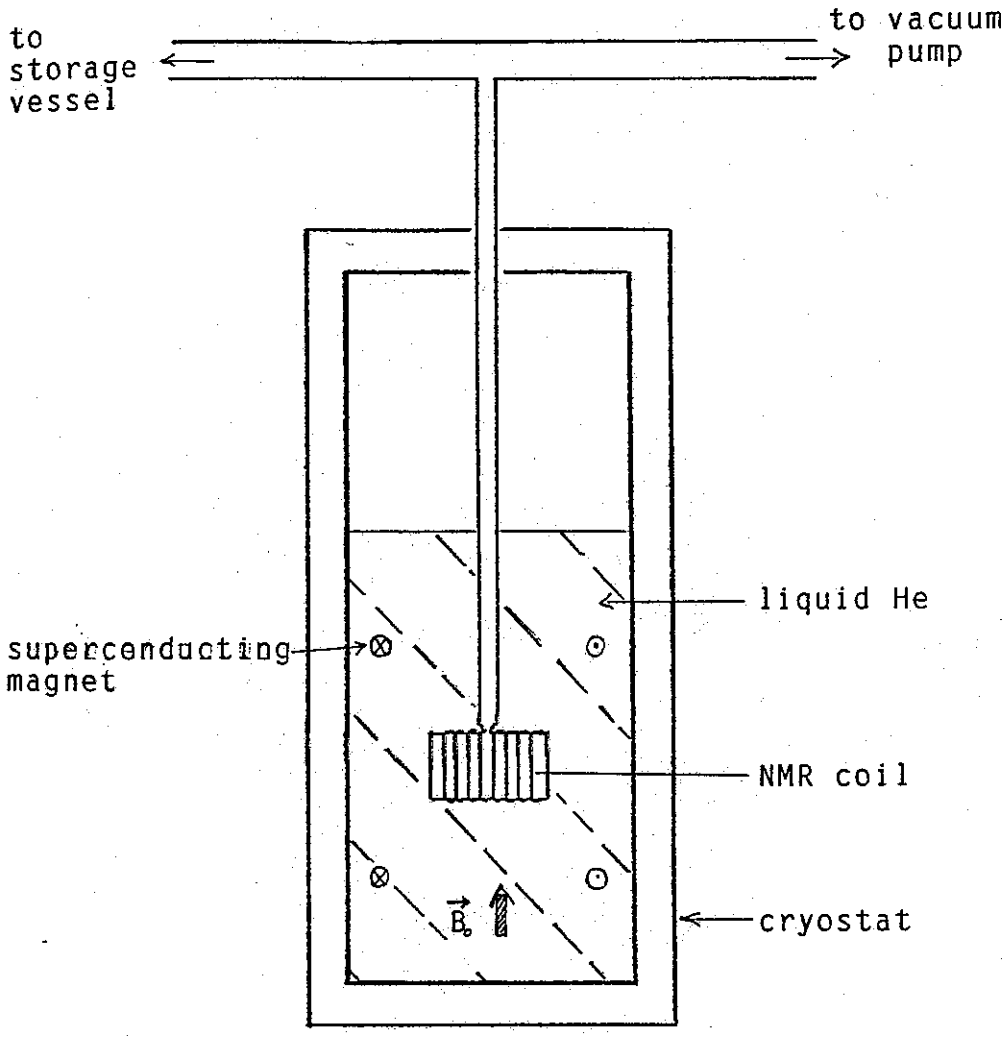

Figure 3.2 : A possible ^{3}He NMR detection system using a superconducting magnet. An oscillating current is induced in the NMR coil by the polarised Helium atoms.

low magnetic field and a super conducting magnet is not needed. The output of the SQUID is an AC voltage at the precession frequency and whose amplitude is proportional to the Helium polarisation. P. W. Franks estimated that with a degree of ^{3}He polarisation of 10% and a quantity of 10^{-4} torr cooled to 4.2K, the signal to noise ratio achievable is of the order of 100.
This is similar to the performance of the other detection methods described above which did not provide a better magnetometer than the neutrons.

3.3. - A Caesium Magnetometer

The main attractive features about Cs as a magnetometer for the EDM experiment is the high spin precession frequency involved and the low neutron capture cross-section (29b). Since Cs possesses an electronic spin as well as a nuclear spin, its total atomic nuclear moment is then about three orders of magnitude larger than the Hg or Helium magnetic moments, which scales up the precession frequency by the same factor. While the Hg precession frequency in a 10 mGauss field is about 8 Hz and that of ^{3}He about 30 Hz, Cs spins precess at about 3500Hz around the same field. This, of course, increases the accuracy to which the frequency is measured if the linewidth remains the same. However, the existence of an electronic spin makes the storage requirements more serious. A common wall coating for neutrons and Cs has to be found to store them together. The low Cs neutron capture cross-section allows the use of higher Cs densities but not too high to cause Cs deposition on the walls that could increase leakage

currents or initiate sparks. Since typical relaxation times obtained with Cs vapours are of the order of a few tenths of a second, and the mean transit time in the neutron bottle is of the order of 10^{-3} secs, it would be necessary to run it continuously during the neutrons storage period.
The vapour would be admitted to the vessel from a side tube through a small enough hole for the neutron loss to be negligible.
In chapter four, there is a description of the work we did in trying to set up a Caesium magnetometer.

3.4. - A Mercury magnetometer

Mercury has a number of particularly desirable features such as long relaxation times in some types of wall coatings and the fact that it has a rather small electric dipole moment $< 2 \times 10^{-26}$ e.cm [Lam 87].

Maybe the biggest advantage of using Hg is the possibility of a direct measurement of the precession frequency averaged over the storage time, a result which will, with careful analysis, be independent of signal amplitude variations from cycle to cycle.

Mercury atoms can be polarised inside a small chamber while the main storage volume is filling with neutrons. The polarised Hg is then transferred in ~ 1 sec. to mix with the neutrons just before the usual $\pi/2$ pulse is applied in the normal neutron cycle. A mercury $\pi/2$ pulse applied at the same time flips the spins into the xy plane and modulation of a second analysing beam at the Hg precession frequency will be recorded.

By registering the decaying Hg sinewave in the neutron storage vessel a computer program is used to do a fitting to the data and calculate the Hg resonance frequency in the applied magnetic field.

Estimate of σ_f/f after analysis of the ADC data:

We shall show in chapter 6 that the S/N for a free precession signal with 100% modulation, at the output of the detector, to be $\sim 5\times10^4$. Determination of σ_f/f depends on S/N from the light detector and the method of processing the data.

We are going to use a 16-bit ADC to store the data at 50 reads/sec. in order to reduce the effects of mains hum.

Let N be the number of readings collected in a time t, and let ϵ be the error associated with the measurement of each data point independently of the other points. Assuming a constant counting rate means that the number of points lying between A and B is N/2 (see figure 3.3). Since the slope of the curve does not change much in that region, all the N/2 points have the same error ϵ. It is then equivalent to taking one point at the zero crossing with an error of $\epsilon/\sqrt{N/2}$. If the sinewave is written as $y = \frac{S}{2}\,\mathrm{Sin}\phi$ where S is the peak to peak signal amplitude and ϕ the phase, then at maximum slope $\frac{dy}{d\phi} = \frac{S}{2}$.

The relation between the standard deviation in the amplitude and the phase is

$$\sigma_\phi = \frac{d\phi}{dy}\,\sigma_y \qquad (3.3)$$

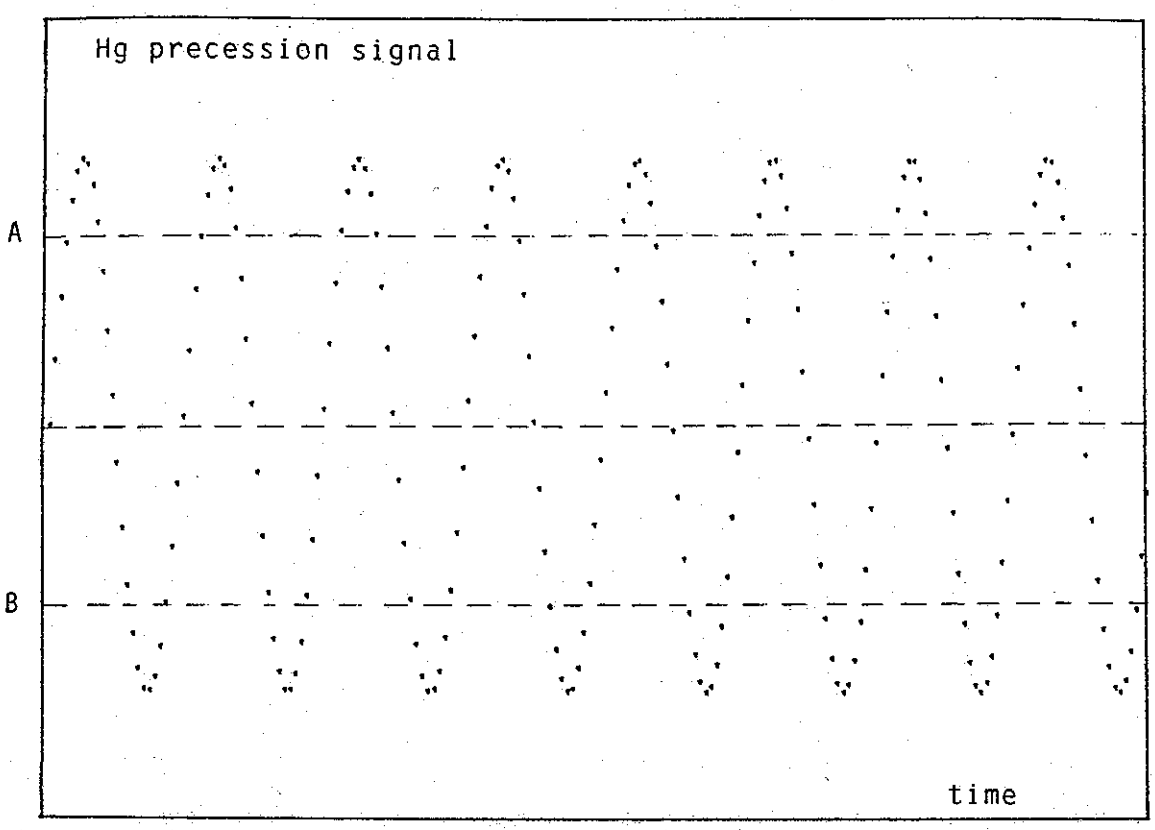

Figure 3.3 : Diagram showing the Hg precession signal as sampled by an ADC. The signal is written as $y=\$/2\sin(\varnothing)$. In the [A,B] interval, the slope of the signal is rather constant. If N is the total number of points collected in a time t then the number of points lying between A and B in time t is N/2 provided that the sampling rate is constant.

therefore,

$$\sigma_\phi = \frac{2}{S}.\frac{\epsilon}{\sqrt{N/2}} = \frac{2\sqrt{2}}{\sqrt{N}}\left(\frac{\epsilon}{S}\right) \qquad (3.4)$$

If the same measurement is done again T secs later for the same time t, at the point when the signal has decayed to 1/e of its size, the error in ϕ would then be

$$\sigma'_\phi = \frac{2\sqrt{2}}{\sqrt{N}} e \left(\frac{\epsilon}{S}\right) \qquad (3.5)$$

The combined error $\sigma_{\Delta\phi} = \sqrt{\sigma^2_\phi + \sigma'^2_\phi}$ is then

$$\sigma_{\Delta\phi} = \frac{2\sqrt{2}\sqrt{1+e^2}}{\sqrt{N}}\left(\frac{\phi}{S}\right) \qquad (3.6)$$

But, what we really want is the error in the measurement of the frequency. This can be expressed as

$$\frac{\sigma_f}{f} = \frac{\sigma_{\Delta\phi}}{\Delta\phi} = \frac{\sigma_{\Delta\phi}}{2\pi T f} \qquad (3.7)$$

where T is the time separating the two measurements. Substituting for $\sigma_{\Delta\phi}$ in the last equation gives

$$\left(\frac{\sigma_f}{f}\right) = \frac{2\sqrt{2}\sqrt{1+e^2}}{2\pi T f\sqrt{N}}\left(\frac{\epsilon}{S}\right) \qquad (3.8)$$

Taking T = 100 secs, f = 8Hz, $\epsilon/S = 1/(5\times10^4)$ and a counting rate of 50 reads/s for t = 4 secs (ie. N = 200) we obtain

$$\left(\frac{\sigma_f}{f}\right) = 2.3\times10^{-9} \qquad (3.9)$$

There will also be an additional ADC noise. Running the

fitting program [Smi 90] with a noise free signal of 20000 bits with no attenuation gives $\sigma_f/f = 6x10^{-8}$ which shows clearly the effect of ADC noise.

However,this is still much better than the figure of $2.54x10^{-7}$ obtained in chapter 7 for actual experimental conditions.

3.5. - Conclusion

A mercury magnetometer for the neutron EDM experiment seems to be the best possibility. The Larmor precession frequency is measured directly and not a big reproducibility in the signal amplitude is required. Mercury vapours are rather easy to polarise and it is equally easy to detect their polarisation. On the contrary, the rather elaborate techniques involved in detecting ^{3}He polarisation make it difficult to use in the EDM experiment. Moreover, a good signal reproducibility is required. As far as Caesium is concerned, the short relaxation times involved and the tendency to form a metallic layer on the neutron storage bottle walls causing a **E** field breakdown make it a more difficult magnetometer to use than mercury.

CHAPTER IV

Optical Pumping Experiments with Caesium Vapours

4.1. - Introduction

In this chapter we are presenting the actual practical side of optical pumping with Caesium vapours. The main apparatus which was shown in figure (2.2) chapter 2 is now described in more detail. We will also show how experiments were done in a 3-layer μmetal magnetic shield, as well as the changes operated on the apparatus in order to adapt it to the new environment. Different sizes of absorption cells were investigated. We started with cells of about 1/4 litre in volume, then 1 litre and finally 5 litres. In the first part of this chapter, we are concerned with the feasibility of optical pumping in these relatively big cells. We had to investigate whether some relaxation processes, like field inhomogeneities would not make the task impossible to achieve. We finish this first part by giving the results and discussing them.

We are concerned in the second part of this chapter with some attempts to optically polarise Cs atoms in a 7-litre aluminium vessel. Since the system has to be continuously pumped, a vacuum set-up was fixed to the vessel. Furthermore, we give the description of two different wall coatings that were used, namely Surfasil, and a solution of polystyrene we made in the laboratory. This second part is also closed with a discussion of the results obtained.

Before going to the experimental side in this chapter, it is rather necessary to give a description of optical pumping in Caesium vapours.

4.2.- Optical Pumping in Caesium

Like all alkali atoms, caesium is a very chemically reactive element. It is soft, silvery and rapidly tarnished in air. In nature, it always appears combined with other elements. Its orientation was first reported by Blandin and Barrat [Bla 56].

Caesium has a series of closed electron shells and one electron left over. The lowest state is a 6s. Because L=0 and S=1/2, the ground level is a $^2S_{1/2}$ state (fig 4.1). The first excited states $^2P_{3/2}$ and $^2P_{1/2}$ have the single electron in the 6p state.

The nuclear spin of the natural isotope ^{133}Cs is I=7/2. In the ground state there are two hyperfine levels F=3 and F=4. However, the excited states $^2P_{1/2}$ and $^2P_{3/2}$ are made up of the hyperfine levels F=3,4 and F=2,3,4,5 respectively. These hyperfine levels are separated by much smaller intervals than those of the ground state. The separation between the $^2S_{1/2}$ ground state and the $^2P_{1/2}$ and $^2P_{3/2}$ corresponds to wavelengths in the near infra red. The two transitions correspond to the D lines in sodium.

Usually, to obtain an efficient hyperfine pumping, the hyperfine components in the pumping light should be selected. Hyperfine component separation is done either with ordinary interference filters or by some other ingenious way like using the emission line of one isotope to pump the other. In the case of Cs, one uses interference

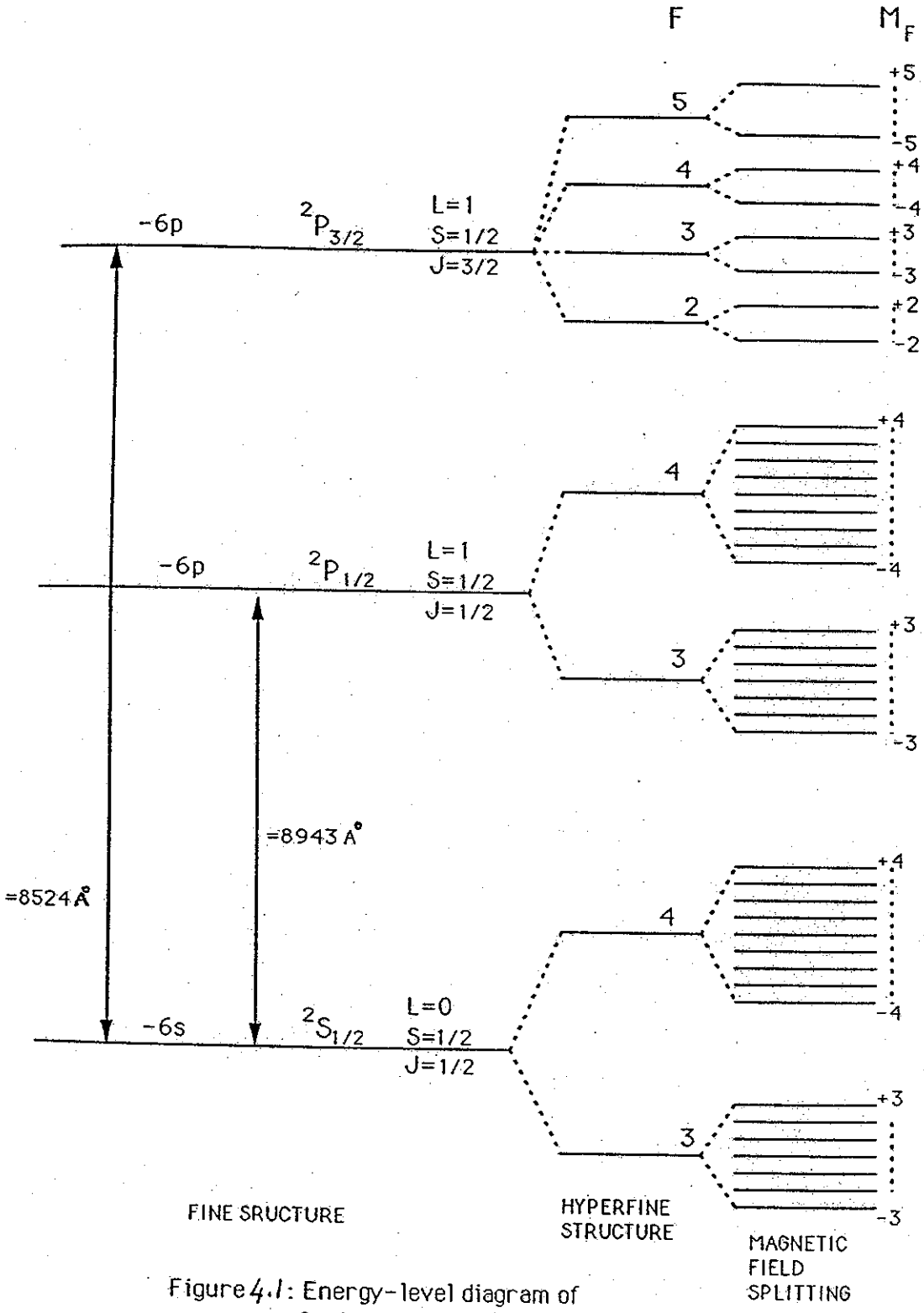

Figure 4.1: Energy-level diagram of Cesium.

filters. The $^2S_{1/2}$-$^2P_{1/2}$ transition corresponds to λ=8943 Å whereas the $^2S_{1/2}$-$^2P_{3/2}$ corresponds to λ=8524 Å. Optical pumping in Cs is commonly done using the 8943 Å line converted to circularly polarised light using a plane polariser and a quarter wave plate. This light must propagate along a steady magnetic field, through the resonance bulb onto a detector (photo diode or photo multiplier). Under these conditions, any transition induced by the light is subject to the selection rule ΔM_F=+1. Nevertheless, for the spontaneous decay, ΔM_F=0,±1 are possible with equal probability. Consequently, there is a tendency for atoms to be transferred from states of low values of M_F to states of higher values of M_F. When an atom falls into the highest M_F ground state, i.e. the level F=4, M_F=+4, it cannot be excited again because the $^2P_{1/2}$ multiplet of states does not contain a higher M_F value. In a time of the order of a few hundreds of milliseconds (in the case of alkali vapors) many of the atoms are transferred to the F=4, M_F=+4 state and optical absorption reaches a minimum. This level corresponds to B of the three level system (see fig. 2.1). All the other ground state levels are playing the role of A and all the $^2P_{1/2}$ levels are playing the role of C.

If a radio-frequency field is applied resonant with the transition F=4, M_F=+4 to F=4, M_F=+3 in the ground state, pumping infra-red absorption increases and a measurement of g_F for the $^2S_{1/2}$ level can therefore be made. If both D lines are used, i.e. the interference filter is not used, the 8524 Å line will take the atoms to the $^2P_{3/2}$ multiplet which contains an F=5, M_F=+5 level. Some of the atoms which would have been trapped in F=4,

M_F=+4 of the ground state under the 8943Å line alone will be able to reach the excited M_F=+5 state. This reduction in the M_F=+4 population implies a less efficient pumping.

The degree of polarisation obtained in a Cs vapour is quite small, usually of the order of 1.5 % [Bla 56].

4.3. - Experiments with Glass Cells

4.3.1. The Light Sources

Light sources used are electrodless spherical glass bulbs of about 2cm diameter on which a stem of 4 or 5cm is fixed (fig. 4.2.). A small drop of metallic Cs is located in this stem. The cell is excited by a high frequency power of the order 10 W at 60 MHz in order to generate the light necessary for pumping. The Caesium density remains low enough to minimise self-reversal of the resonance line. This happens when the excitation is not uniformly distributed in the cell. When the atoms are in the unexcited regions they tend to reabsorb the light emitted from the "good" regions before it leaves the cell. The absorption mainly happens at the centre of the line and leads to the apparition of a dip in the emission profile at the centre frequency.

Before being filled with Cs, the cells are thoroughly baked under vacuum. They are also cleaned with a high power discharge before admitting 2-5 mg of metallic Cs and 2 torr of Argon. When the discharge is running in the cell, a mixture of Cs, Argon, Cs ions, Argon ions and free electrons are present. Since Argon atoms have a metastable

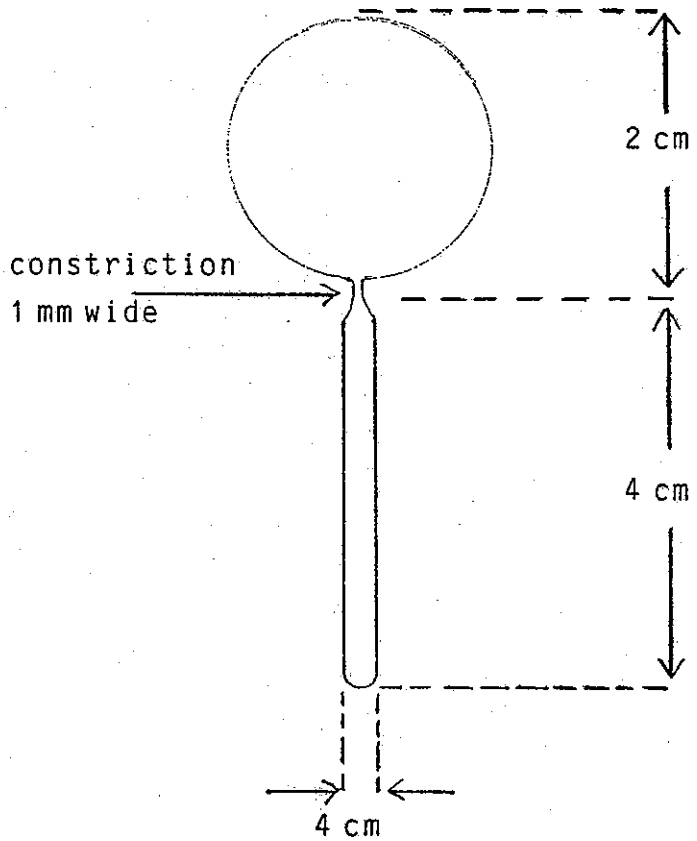

Figure 4.2: Light source bulb made in our laboratory. It is made out of pyrex and contains a drop of Caesium in the stem and two Torr of Argon.

excited state, Cs atoms are then more likely to be excited through a collision with a metastable Argon atom, and eventually radiate.

The pressure of Cs vapour present in the bulb is determined by the temperature of the stem which is controlled by a heater of Constantan wire wound on the stem. If the temperature is too high the line is self absorbed and pressure broadened. On the other hand, if the temperature is too low, there are not enough Cs atoms to emit light and the intensity of the lamp is rather low. Under favourable conditions, the vapour emits a rather bright and glowy bluish light.

4.3.2. The Absorption Cells

We used spherical absorption cells of 1/4 ℓ, 1 ℓ and 5ℓ made of Pyrex glass with a thin capillary side arms to introduce the Cs vapour. In some optical pumping experiments, cells are filled with a buffer gas to reduce the mean free path between collisions and minimise the number of collisions with the cell walls. The relaxation time T_1 does not increase indefinately with buffer gas pressure. It varies linearly at low pressures, reaches a maximum and then falls at high pressures (Fra 59). However, using this technique, does not allow the atoms to average the magnetic field by rapid motion from wall to wall.

To enable effective averaging the cell has to be coated with a material which does not flip the alkali spin. Dehmelt showed, in 1958 (Rob 58), that coatings of long chain parafines or silicones allow atoms to keep their polarisations for relatively long times. These long

molecules project into the cell protecting the atoms from the local electric fields present in the walls. Relaxation times of 0.1 sec were obtained in a Rb vapour by Franzen (Fra 59).

We used a siliconized agent called Surfasil. The cell is first cleaned with chromic acid and then thoroughly rinsed with deionised water and acetone. A solution made up of 2 cm^3 of Analar acetone and 1 cm^3 of Surfasil is then introduced. The bulb is then vigorously shaken to spread the solution all over the walls. After letting it dry up overnight, it was pumped down and then baked at 150°C for two days. A residual pressure of 2×10^{-6} torr was subsequently measured by an ionisation gauge fixed to the glassware. A small drop of Cs metal contained in an evacuated ampoule was then driven off to the side arm of the resonance cell by gentle heating. After sealing off and removing the cell from the vacuum system, it was gently heated in order to clear metal from the walls.

4.3.3. The Optical Components.

The optical accessories used to generate a parallel, mono-energetic and polarised light beam through the absorption cell consists of a lens, an interference filter, a plane polariser and a quarter wave plate. The glass lens used is positioned in such a way that the light source is at its focal centre. The light emerging from the other side is then reasonably parallel. It falls onto an interference infra-red filter that only transmits the light at the desired wavelength of 8943 Å. Most of our experiments were done with circularly polarised light σ^+. This is achieved

by making the light emerging from the filter propagate through a plane polariser and a $\lambda/4$ plate. These two components have to be orientated with respect to each other in order to achieve σ^+ light.

Setting up the circular polariser:

A light beam was propagated through the centre of a pair of linear polarisers LP_1 and LP_2 (fig 4.3) and LP_2 was made to rotate around the axis of the light beam at 50Hz using an AC powered motor driven directly from the mains. The light transmitted was detected by a semi-conductor photo-cell connected to a current to voltage converter (see section 4.3.5). The output voltage $V(\theta)$ obtained is a 50Hz sinewave whose peak value is V_p when the polarisers are parallel and a minimum when they are crossed. A $\lambda/4$ plate inserted between the two polarisers changes the amplitude of the sinewave and LP_1 and the $\lambda/4$ plate have the best relative orientation to give circularly polarised light when LP_2 has little effect on light emerging from the plate. In practise, this output is still a sinewave because LP_2 and $\lambda/4$ do not give a perfect σ polarised light.

As far as the detection of the transmitted light through the absorption cell is concerned, another lens could be placed after the absorption cell in order to focus as much light as possible onto the detector, but we did not judge that it was necessary.

4.3.4. The Magnetic Fields Coils

We used three sets of magnetic field coils shown in figure 4.5, a 50-turn, 64cm diameter Helmholtz coil to generate

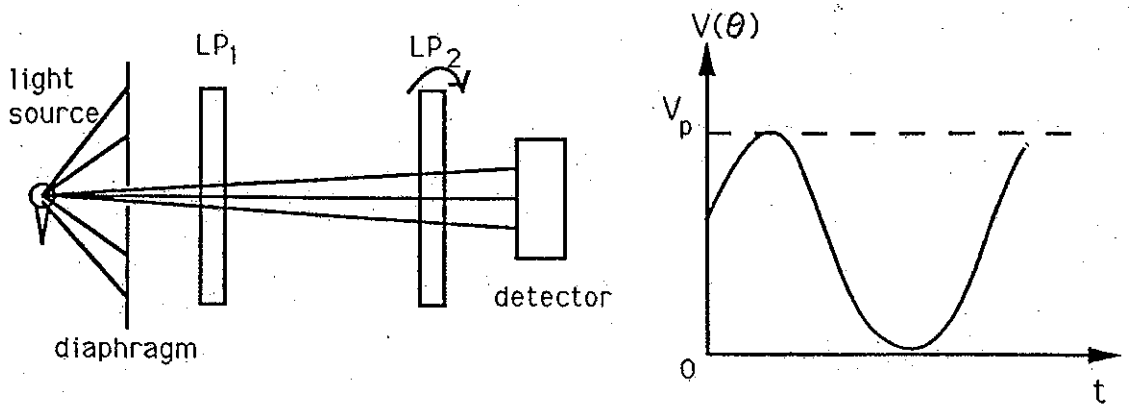

(a)

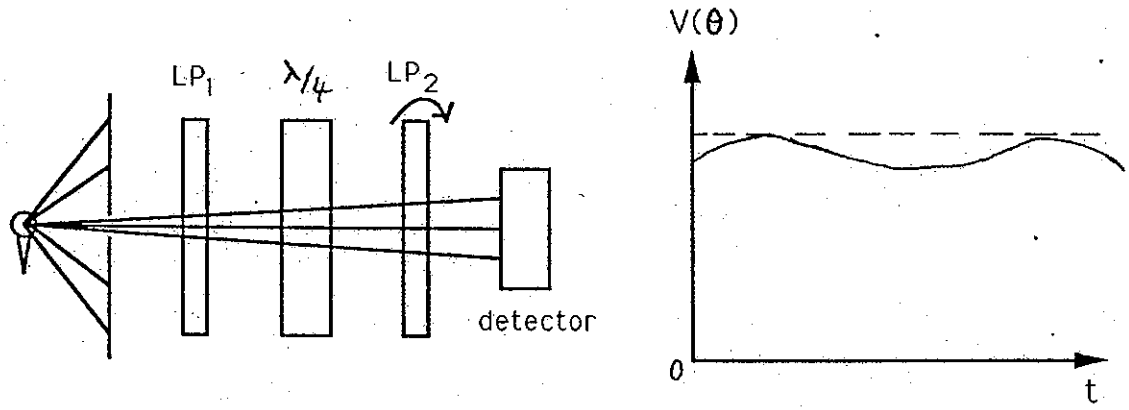

(b)

Figure 4.3: Setting LP_1 and the $\lambda/4$ plate to give σ polarised light. In (a) LP_1 is fixed and LP_2 rotating. In (b) the $\lambda/4$ plate is rotated by hand until the 50Hz output trace is minimum.

the static magnetic field B_z, a similar 5-turn Helmholtz coil fed with a low frequency ω_m sinewave signal in order to modulate the main B_z field and a small Helmholtz coil mounted around the resonance cell to give the radio-frequency field B_1 perpendicular to B_z. A frequency synthesizer (Wavetek 178) was usually used to feed the B_1 coil. the formula giving the magnitude of the magnetic field generated by a Helmholtz coil at its centre is

$$B=\frac{8\,\mu_0\,N\,I}{5^{3/2}\,a} \qquad (4.1)$$

where N is the number of turns, a the radius, μ_0 the permeability of free space and I the current.

4.3.5. The Detector and Associated Electronics

We used a Hamamatsu type of photodiode from the S1337 series with a typical radiant sensitivity of 0.5 A/W at the peak spectral response wavelength of 950±50 nm. It was connected to a current to voltage converter circuit, followed by a low frequency filter and an amplifying stage (fig 4.4). We chose C_1 and R_1 to filter out signals below 20 Hz and resistors to give an output of 1 V/µA. When running the experiment, one is primarily interested in the light DC level V_{DC}. The feedback capacitor (0.01 µF) is used to filter out the high frequency noise that could be picked up from the RF light source generator. The 355 op-amp used is a low noise field effect chip, whereas the 741 is just a general purpose op-amp. The whole circuit was battery operated to minimise 50 Hz pick-up.

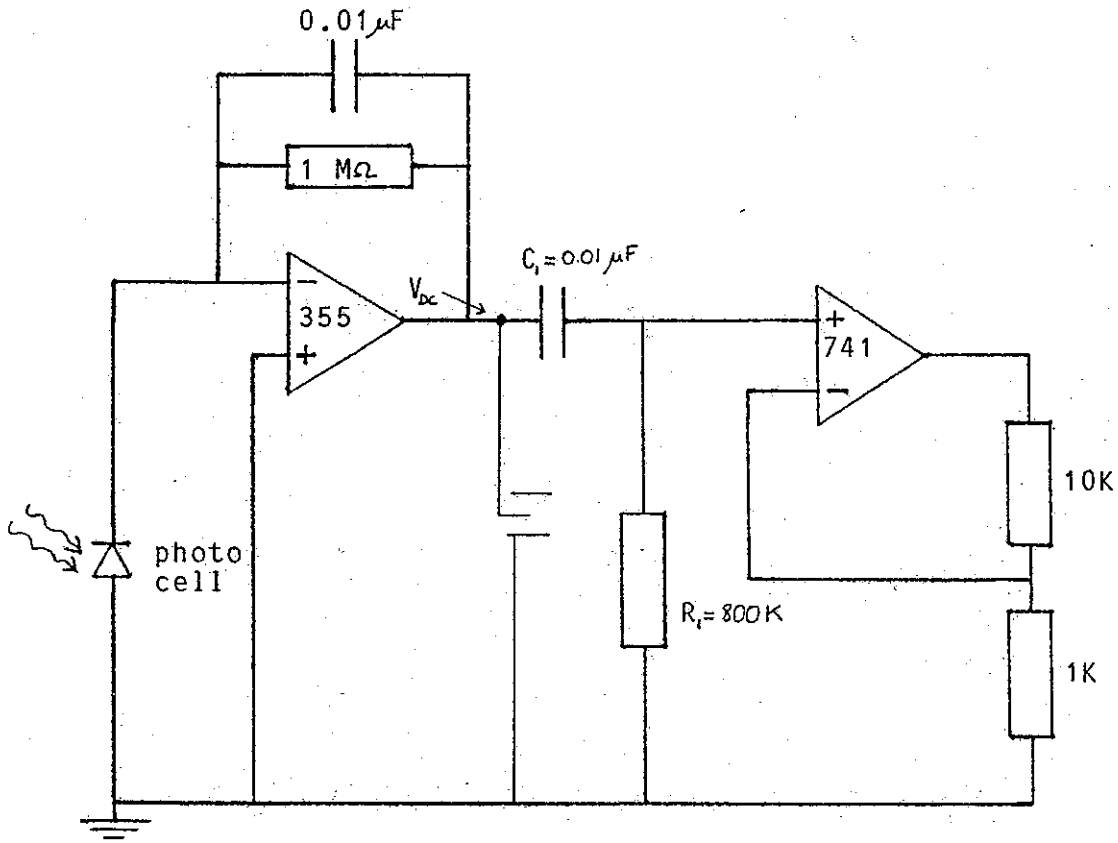

Figure 4.4: Diagram showing the current to voltage converter circuit. The components shown yield a conversion factor of 1 V/μAmp.

4.3.6. Results and Discussion

In figure 4.5 is shown the usual experimental set up we used for the detection of a resonance signal. Light scattered through the resonance cell was detected by the photocell connected to the current to the voltage converter. The signal was fed either to an oscilloscope or to a phase sensitive detector (PSD) for noise filtering. In the former case, we also displayed the signal used to modulate the B_z field, usually a sinewave of frequency ~35 Hz. When B_z sweeps through the resonant value, the intensity of the transmitted light is reduced, giving typically the pattern shown in figure 4.6. At resonance, the dips in light intensity are equidistant. The signal from the current to voltage converter was sometimes fed to a PSD using the modulating signal as reference. The PSD then amplifies signals at the reference frequency and behaves like a high Q frequency locked amplifier. Using a small sinewave modulation less than a linewidth and sweeping the rf frequency slowly we obtained a dispersion curve from which the signal linewidth Δf could be estimated. The frequency sweep was performed using the Wavetek synthesizer.

Measurement of an absorption curve linewidth requires considerable care. The rf power applied to the sample must be kept to a minimum and the field modulation should be considerably less than the linewidth. The strength of the rf field can be readily estimated from Rabi's formula on resonance, $\gamma B_1 T \approx 1$, where T is the total relaxation time.

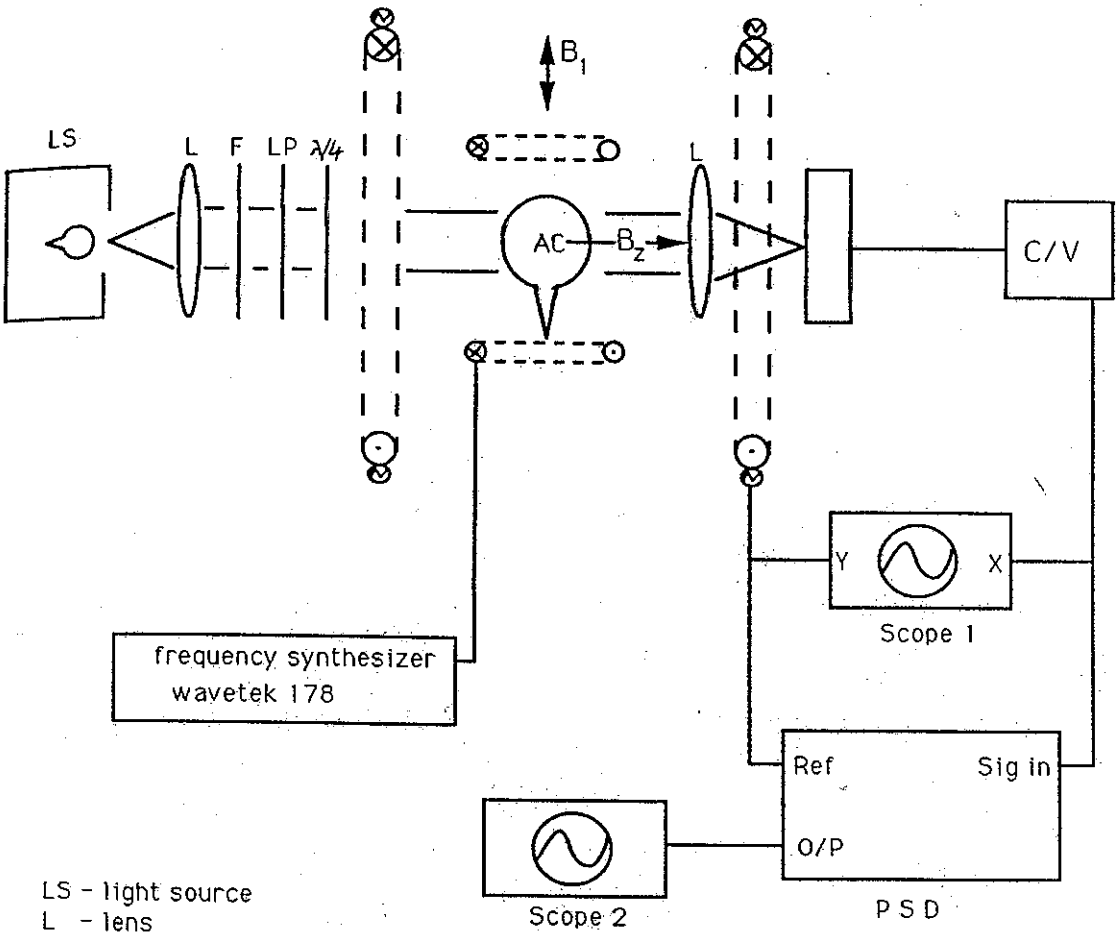

LS - light source
L - lens
LP - linear polariser
λ/4 - quarter wave plate
AC - absorption cell
D - detector
B_z - static magnetic field
B_1 - oscillating magnetic field

Figure 4.5: Observation of a resonance signal.

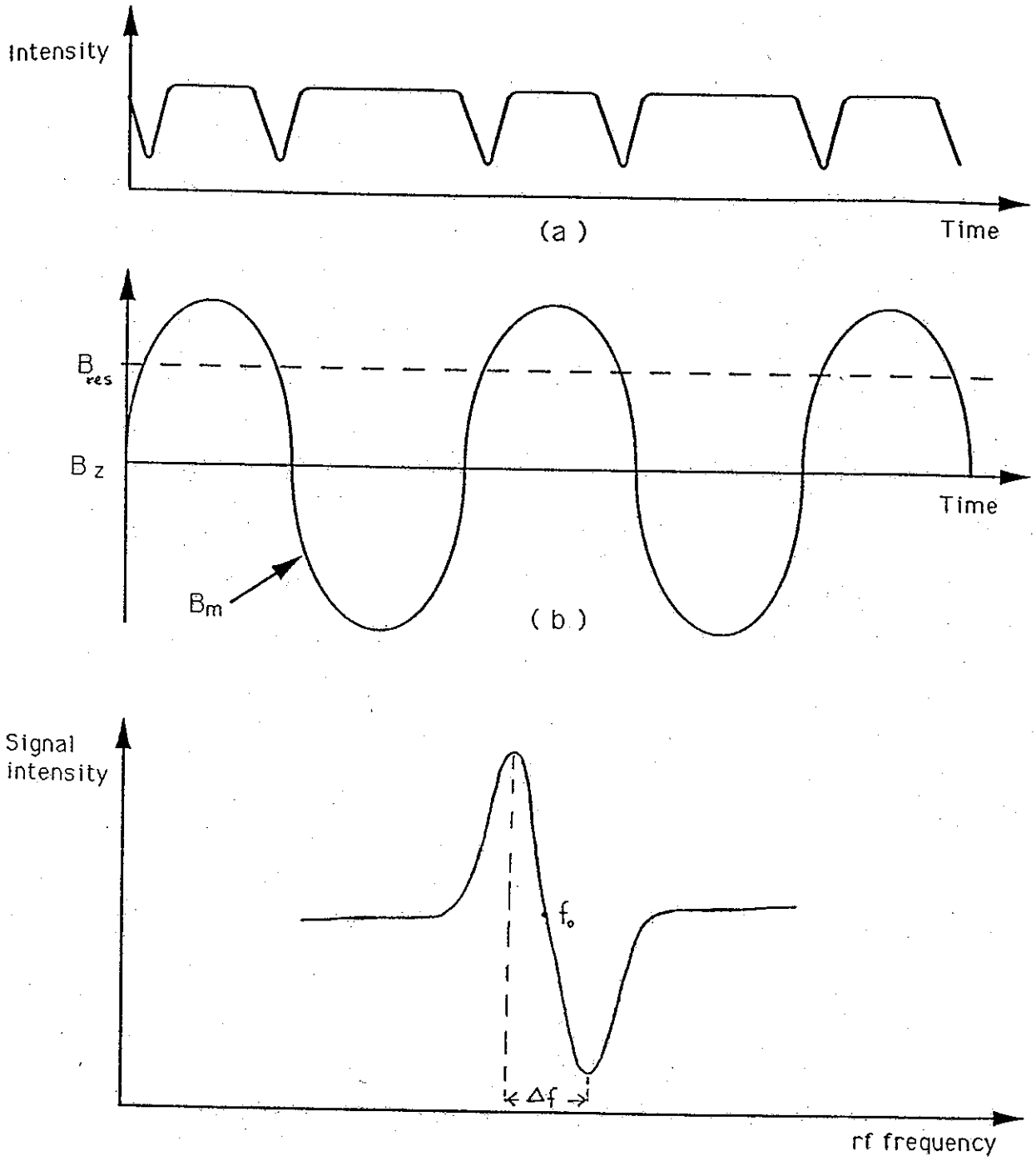

Figure 4.6 Resonance signals as a function of the magnetic field.
(a) light intensity as seen on a scope when resonance occurs;
(b) the sinewave represents the superimposed AC field;
(c) resonance signal out of a PSD when a small sinewave modulation is used. f_0 is the resonance frequency and Δf the linewidth.

Consequently, one starts off by estimating T, and the rf field B_1. The current needed to induce resonance with a single turn Helmholtz coil is

$$I_1 = \frac{5^{3/2}\, a\, \pi}{8\, \mu_0\, N\, T\, g_F\, (\mu_B/\hbar)} \qquad (4.2)$$

The wall relaxation time T_W for a spherical uncoated cell of diameter d is given by

$$T_W = \frac{2\, d}{3\, \bar{v}} \qquad (4.3)$$

this yields (d=22cm and $\bar{v}$=218 m/s at room temperature) the result $T_W = 6.7 \times 10^{-4}$ secs. Since the cell walls are coated, one hopes to improve this time by factor of at least 100. This gives T_W=67 msecs and the current I_1 is then estimated from equation (4.2) and found to be equal to about 0.3 mAmp (the coil radius a is equal to 12 cm). Note that we chose T_W rather than the relaxation time T_2 (due to field inhomogeneities), because in a coated cell the atoms tend to average the magnetic field by their rapid motion across the cell. We were able to estimate T_2 by measuring B_z as a function of position with a small absorption cell 6 cm in diameter. The results are summarised in table 4.1.

x(cm)	-9	-6	-3	0	3	6	9
f_0(KHz)	128.75	129.0	129.2	129.5	129.6	129.9	130.1
y(cm)	-9	-6	-3	0	3	6	9
f_0(KHz)	128.75	129.0	129.2	129.5	129.6	129.9	130.05

Table 4.1

The apparatus was moved from the working position ± 9 cm in one direction along the table (x direction), and the

procedure was then repeated in the perpendicular direction (y direction). We can now estimate the relaxation time T_2 describing the effect of field inhomegenieties. This is given, as it was pointed out in chapter 2, by the expression

$$T_2 = \frac{\pi^2}{\gamma^2 (\delta B)^2} (\bar{v}/Z) \qquad (4.4)$$

where δB is the DC field change over the distance Z and $\bar{v}$ is the atoms average velocity. Taking Z as the maximum distance over which f_0 was measured i.e. Z = 18cm we find that $\gamma\delta B$=(130.1-128.75)kHz=1.35 kHz. This gives T_2=6.6 msecs. The contribution of field homegenieties to the linewidth would be $\Delta f_2 = 1/\pi T_2$ =48 Hz.

Linewidth measurement in the 5 ℓ cell:

We carried out experiments in order to determine the linewidth of the absorption signal in the 5-litre bulb and get an idea about the size of signal to noise ratio. We modulated the DC field at 35.1 Hz in order to avoid mains pick up and measured the way the apparent linewidth varied with modulation. If the strength of the modulation B_m is bigger than the true linewidth, the absorption signal width is a measure of the field modulation. We found that a modulating current of 2.2 mAmps rms was suitable using the coil described in section 4.3.4 (diameter = 64 cm and number of turns N = 6). The light intensity was around 4 volts throughout the experiment with a conversion factor of 1V/μAmp in the current to voltage converter. The linewidth was subsequently measured as a function of the rf field amplitude generated by the 12 cm radius single turn rf

coil. The results are summarised in table 4.2.

rf current RMS (mA)	7.1	4.70	2.6	1.5	0.7
B_1 field RMS(mGauss)	0.53	0.35	0.21	0.1	0.03
Δf(Hz)	600	500	400	350	320

Table 4.2

By plotting the curve representing the linewidth as a function of the rf current and extrapolating to zero rf power, we find that the linewidth is of the order of 294 Hz (figure 4.7). The resonance frequency in the earth's field was estimated to be around 130 kHz and the rf frequency was swept through resonance in 500 seconds. The PSD time constant was set to one second.

For the sake of completeness we show in figure 4.8, an actual resonance signal in the earth's magnetic field obtained from the PSD output. This is a copy of a signal photograph taken from the scope. The rf frequency was swept from 149 kHz to 154 kHz in 200 seconds. The estimated resonance frequency and linewidth are 151.65 KHz and 600 Hz respectively. The PSD integrating time was set to 1 second. The peak to peak signal amplitude is 0.82 mvolts and the noise .005 mv. This yields a signal to noise ratio of 165. The total light DC amplitude used was 5.2 volts. Consequently, the change in transmitted light at resonance is about 0.016%. This is an indication of the amount of polarised atoms in the sample. This experiment was done at a modulating field frequency of 35.2 Hz and a rf current of about 7 mAmps rms corresponding to a rf B_1 field of 0.52 mGauss rms. Note that the earth's field as estimated from the resonance frequency is equal to 0.43

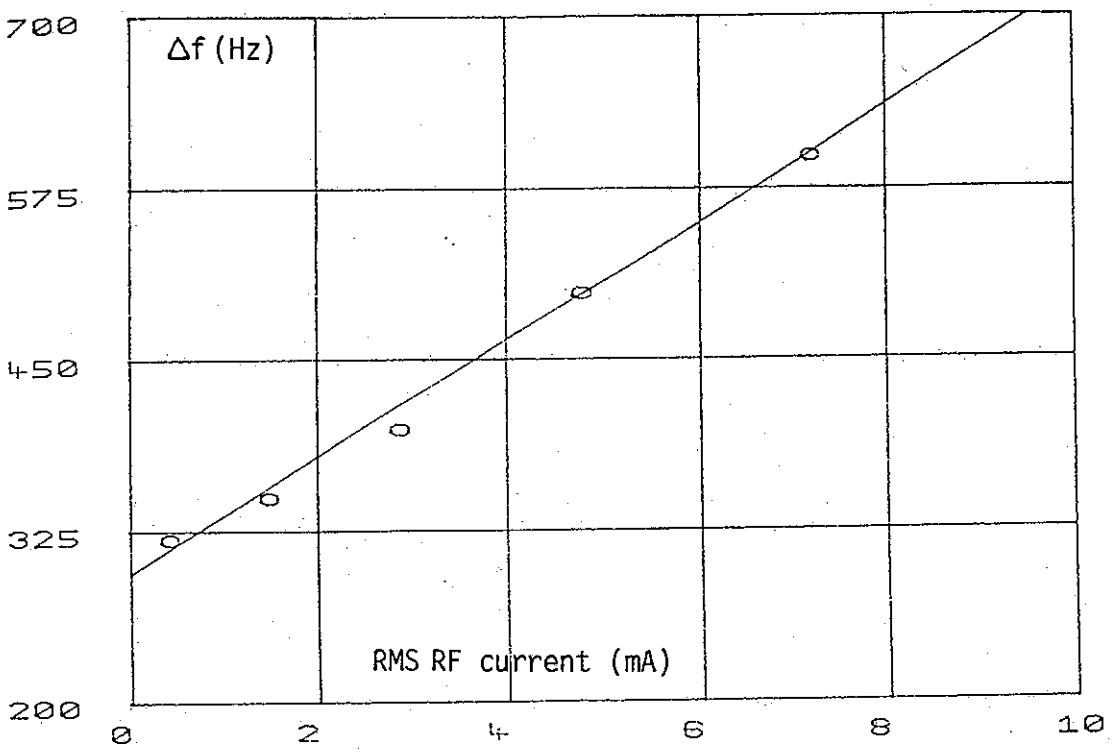

Figure 4.7: Variation of the signal linewidth with RF field amplitude.

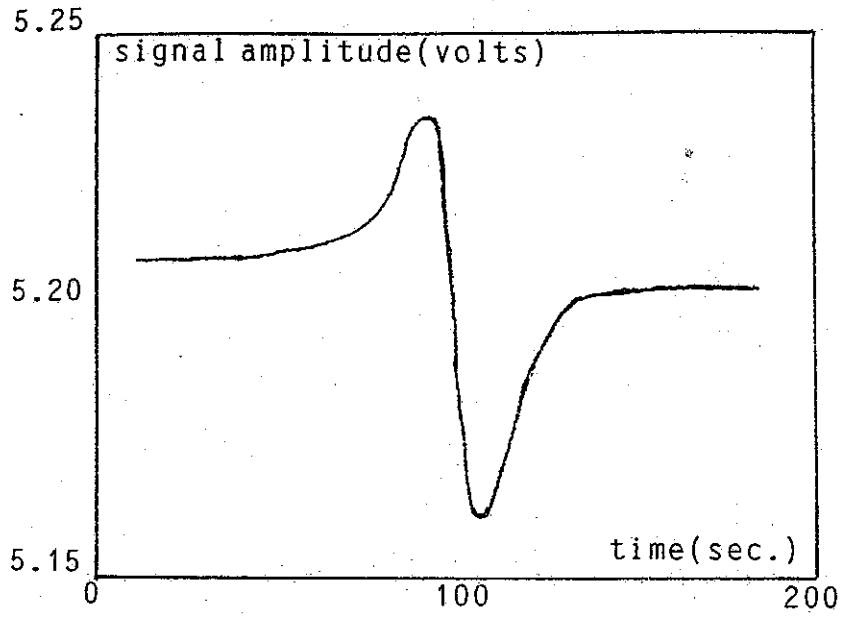

Figure 4.8: This is a copy of a photograph exhibiting a dispertion signal detected using a PSD. The RF frequency was swept from 149kHz to 154 kHz in 200 secs. The estimated resonance frequency and linewidth are 151.65 kHz and 600 Hz respectively. The PSD integrating time was set to 1 second.

Gauss.

To summarise the results obtained so far we have Δf_2=48 Hz due to field inhomogeneities and an apparent linewidth of 294 Hz. Therefore, we conclude that there must be either another source of relaxation, or one is not measuring the real linewidth but a modulation signal superimposed to the earth's magnetic field. This immediately suggests that one has to estimate the strength of the AC field present in the laboratory.

Measurement of the surrounding 50 Hz field:

We used a pick up coil located at the absorption cell position. But, the pick-up coil had to be calibrated against some well known field. An AC magnetic field generated by the 6-turn Helmholtz coil (section 4.3.4.) was used to calibrate the pick-up coil. This coil consisted of a shielded 1 cm radius solenoid containing about 5000 turns of thin enamelled copper wire. The AC voltage induced in the pick-up coil by the change of magnetic flux is amplified and measured by a PAR tuned amplifier set to a Q of 100 and a centre frequency corresponding to that of the applied AC field (77Hz). We give in figure 4.9 the calibration curve for the pick-up coil. The magnitudes of the applied fields are calculated using equation 4.1 in which a = 32cm, N = 6 and I the values of currents measured using a resistor in series with the coil.

In order to estimate the laboratory AC field, no current was fed to the 6 turn coil and the pick-up coil was left in the same position as previously. The picked up voltage at 50 Hz was 17 μV rms in the direction of the light beam. According to the calibration curve, this corresponds to a

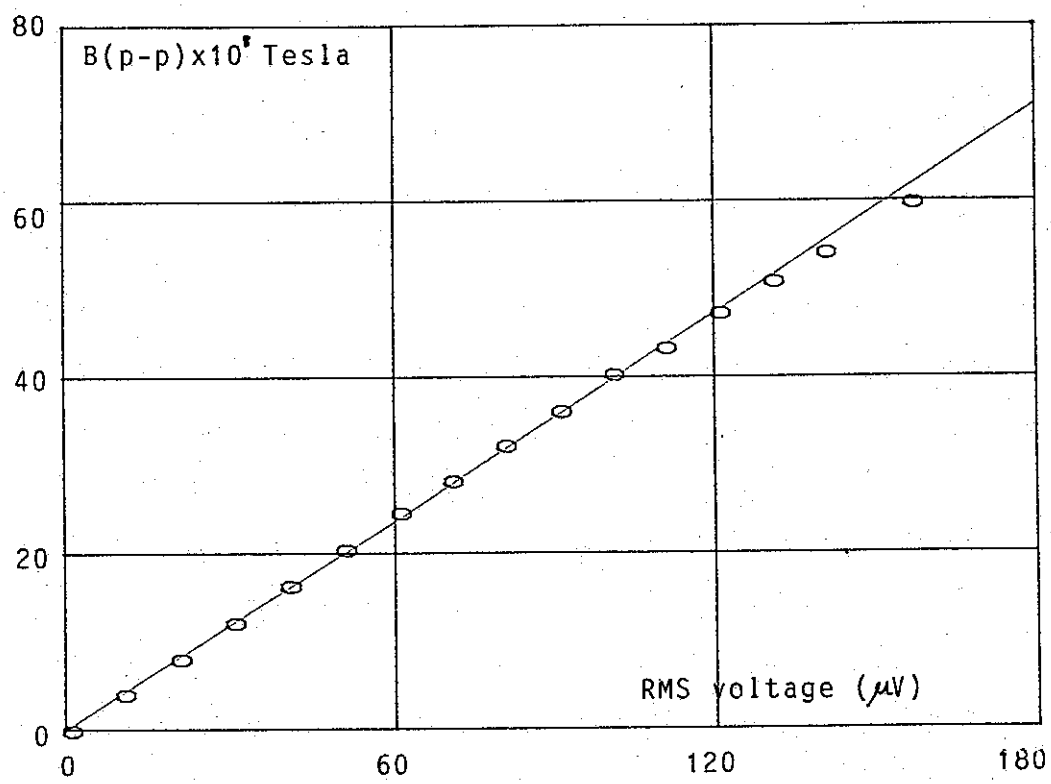

Figure 4.9: Calibration curve of the pick-up coil.

peak to peak value of 7.4×10^{-8} Tesla which in turn corresponds to a linewidth of 260 Hz in Caesium. This is in good agreement with the linewidth measured by optical pumping means (294 Hz) and therefore confirms the fact that it was not due to any relaxation phenomenon but merely was a measure of the AC surrounding field.

Consequently, we decided that the experiment ought to be carried out in a magnetic shield in order to avoid this effect, and be able to measure the actual linewidth.

Measurement of the pumping time T_p and the relaxation time T_2 :

In order to make these measurements, we chose to use the so called method of the magnetic resonance transients in the presence of the pumping light [Cag 61]. This method consists of the sudden application of a sufficiently large rf field, on resonance, to cause complete disorientation. First, the pumping exponential τ_1 is observed. When the pumping is complete, a resonant rf field is suddenly switched on and the atoms are placed in a superposition of $|+\frac{1}{2}\rangle$ and $|-\frac{1}{2}\rangle$ states. The signal is then modulated at the precession frequency γB_1. This behaviour would last indefinately if the action of B_1 was the only process present. However, both the action of the pumping light and the relaxation processes tend to dampen out this oscillation with a time constant θ. Cagnac [Cag 61] showed that this exponential time constant is given by

$$\frac{1}{\theta} = \frac{1}{2}\left(\frac{1}{\tau_1} + \frac{1}{\tau_2}\right) \qquad (4.5)$$

We carried out this experiment in such a way that the rf

field was switched on and off at a frequency of 10 Hz. This is achieved by modulating the rf waveform with a 10 Hz square wave signal. The total light level was 3.4 volts. We show in figure 4.10 the results of such a measurement to which an exponential was fitted in each region. The time constants found were

$$\tau_1 = 23 \text{ msecs.} \tag{4.6}$$

$$\theta = 8.2 \text{ msecs.} \tag{4.7}$$

These two equations are not sufficient to determine the three unknown quantities T_p, T_1 and T_2. However, one can make the assumption that T_1 is large compared to T_p (to have efficient pumping) and approximate $1/\tau_1$ to $1/T_p$. Therefore

$$T_p = 23 \text{ msecs.} \tag{4.8}$$

Using equation (4.7)

$$\frac{1}{\theta} \approx \frac{1}{2}\left(\frac{2}{T_p} + \frac{1}{T_2}\right) = \frac{1}{8.2\ 10^{-3}} \tag{4.9}$$

gives

$$T_2 = 6.4 \text{ msecs.}$$

This result is in good agreement with the value of T_2 calculated from field inhomogeneity measurements (Table 4.1) in which we found that $T_2 = 6.6$ msecs.
When doing the experiment in the magnetic shield, we expect

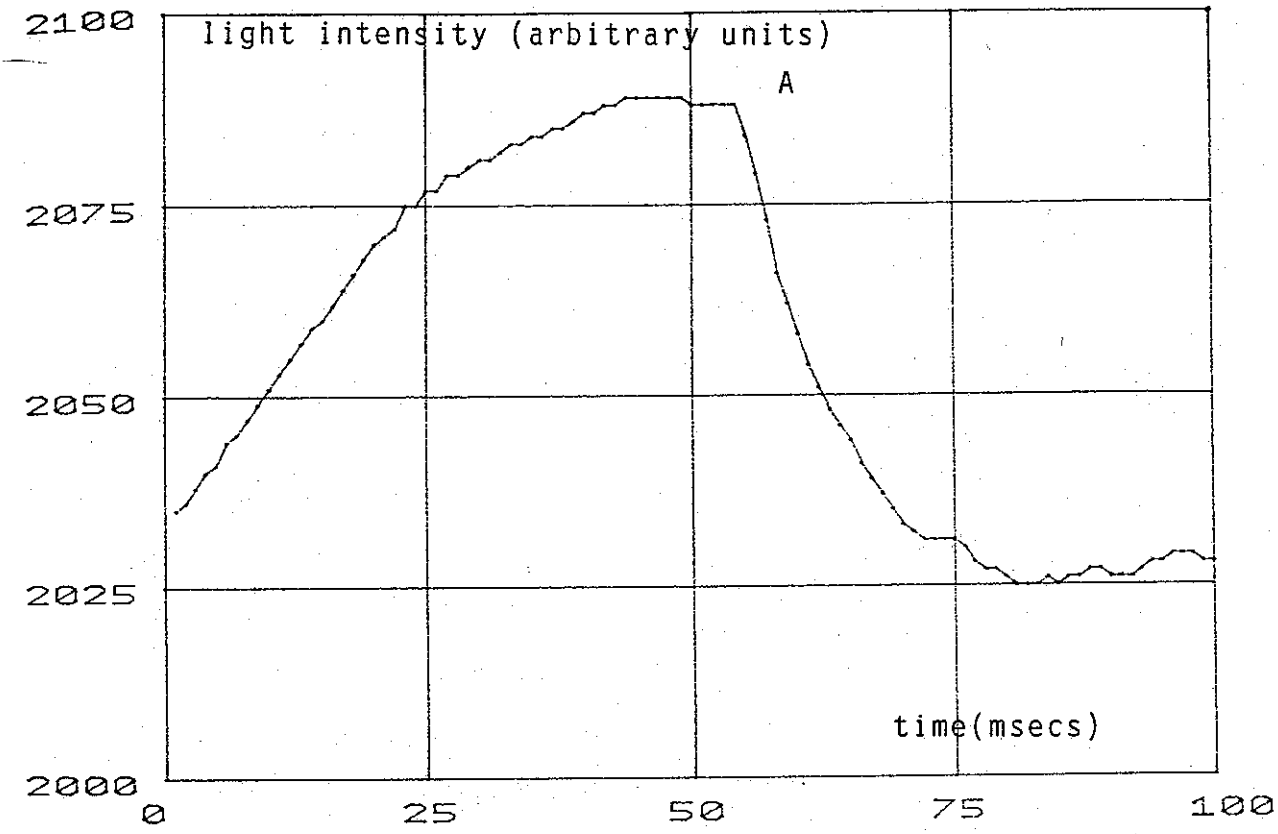

Figure 4.10: Magnetic resonance transients in the presence of the pumping light. At A the RF field is suddenly turned on.

T_2 to become longer (provided field drifts are less serious than they are outside the shield), but T_p and T_1 to remain relatively constant.

4.3.7. Experiments in the Shield

4.3.7.1. The 3-layer μ-Metal Shield

The magnetic shield in which the following experiments were performed consists of 3 layers of coaxial μ-metal cylinders 1.5 mm thick. On the base of each cylinder is welded a μ-metal circular plate with a 4cm radius hole through the centre. However, the other end of each cylinder is open ended and is provided with an endcap of the corresponding diameter with a 10cm radius hole in the centre. The dimensions of the 3 layers are as follows

- Outer most layer: 70cm in length and diameter.
- Central layer : 59.2cm in length and diameter.
- Inner most layer: 50cm in length and diameter.

This shield has a shielding factor of 3000.

4.3.7.2. The Demagnetiser

The shield is demagnetised using a thick multi-turn loop of copper wire passing through the centre. This cable is connected to a Solartron power supply delivering a current of 4 Amps at 13 volts. This current is sufficient to generate a magnetic field that saturates the μ-metal. A circuit is used to reverse the current every two seconds and to gradually reduce it to zero. The output of this circuit which is fed to the demagnetising coil is shown in

figure 4.11. The shield is usually demagnetised for about 10 minutes.

4.3.7.3. The B_z Solenoid

The static B_z field was produced by a solenoid wound on an aluminium former and positioned inside the innermost layer of the shield. It is made up of 460 turns of 48.2 cm diameter in a length of 46.3 cms. In fact, it consists of three solenoids connected in series (fig. 4.12.a). The two end solenoids have 28 turns and the middle one 404 turns. Resistors R_1 and R_2 are home-made bifilar wound copper wires. This insures the change in resistance due to temperature drifts to be the same for R_1, R_2 and the solenoid. R_1 and R_2 are used in order to have different currents flowing in the 3 solenoids. They were determined experimentally in the following manner:

A current was supplied to the solenoids so that the field at the centre of the shield was 10 mgauss. The field along the axis of the 3 solenoids is then measured using a fluxgate magnetometer with a resolution of 10^{-5} Gauss up to fields of one Gauss. The shape of the measured field, as a function of position, is bell shaped with hardly no flat regions. R_1 and R_2 are then adjusted, and the field remeasured until it becomes reasonably flat. The final values of $R_1 = 14.9\ \Omega$ and $R_2 = 57\ \Omega$ gave the magnetic field distribution shown in figure 4.13 for a current of 1.67 mAmps flowing in S_1. The circuit providing the current I_c is shown in figure 4.12.b. All the temperature sensitive components are thermally isolated in a box contained in a

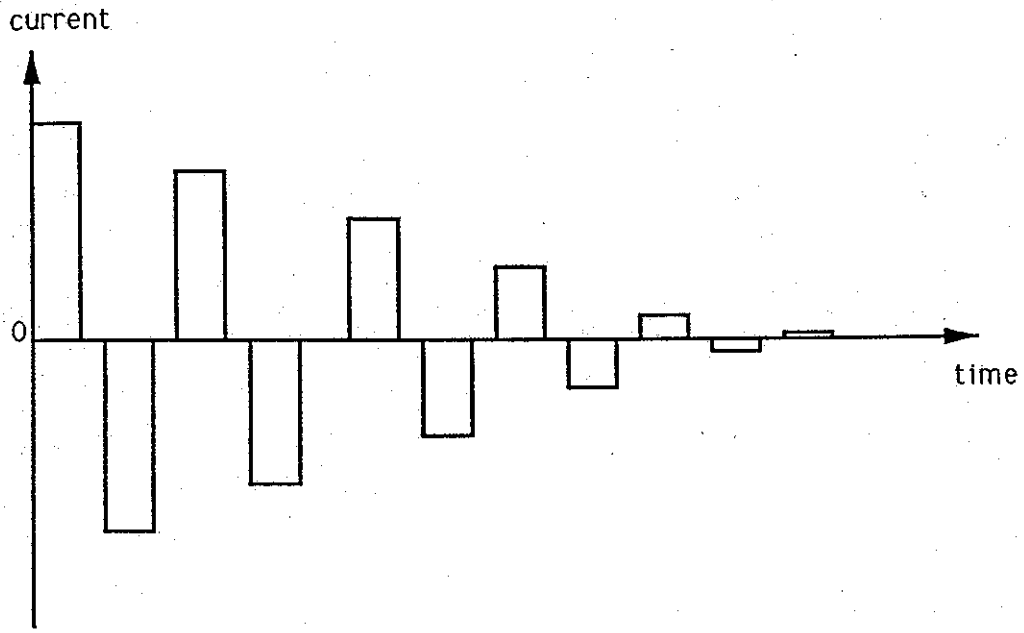

(a)

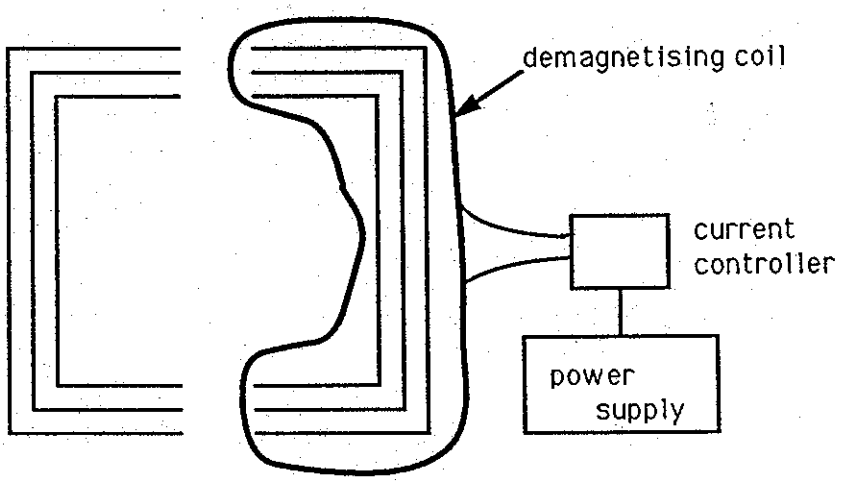

(b)

Figure 4.11: Shield demagnetisation. (a) Waveform of the demagnetising current. This is reversed every 2s. (b) The position of the demagnetising coil in the shield.

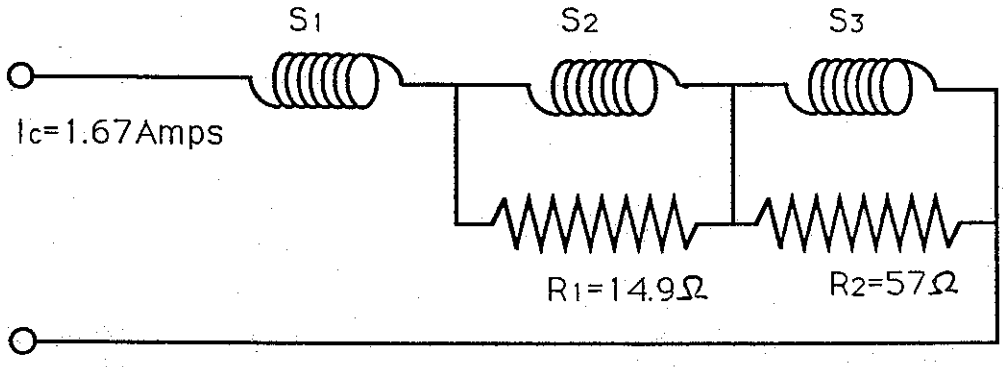

(a)

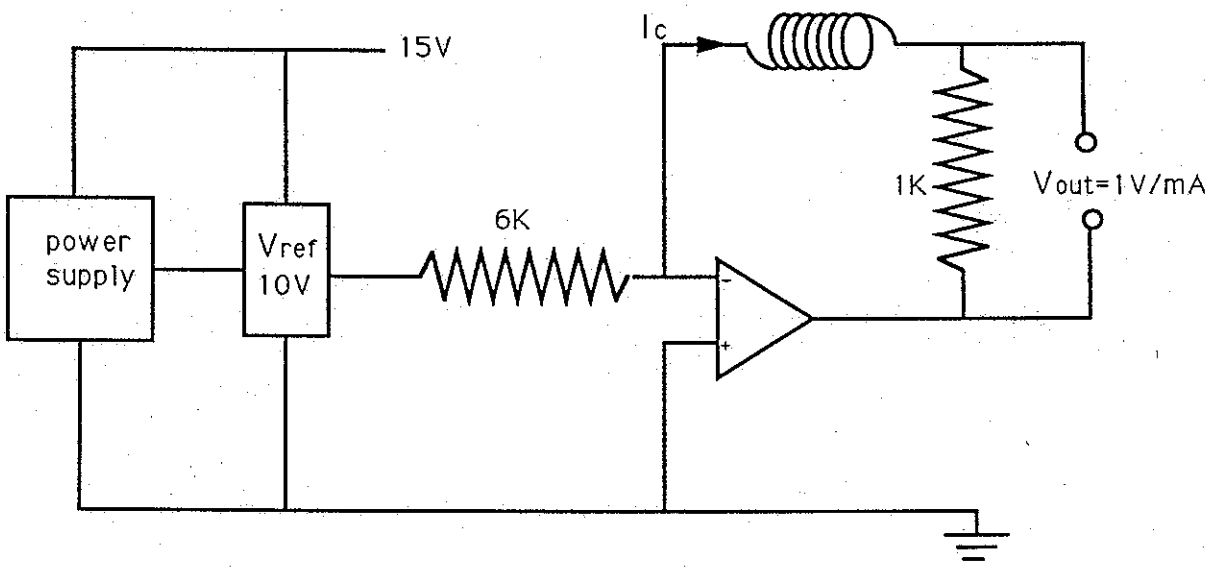

(b)

Figure 4.12: The B_z solenoid.
(a) The solenoid is made up of 3 solenoids in series.
(b) Circuit delivering a stable current to the coil.

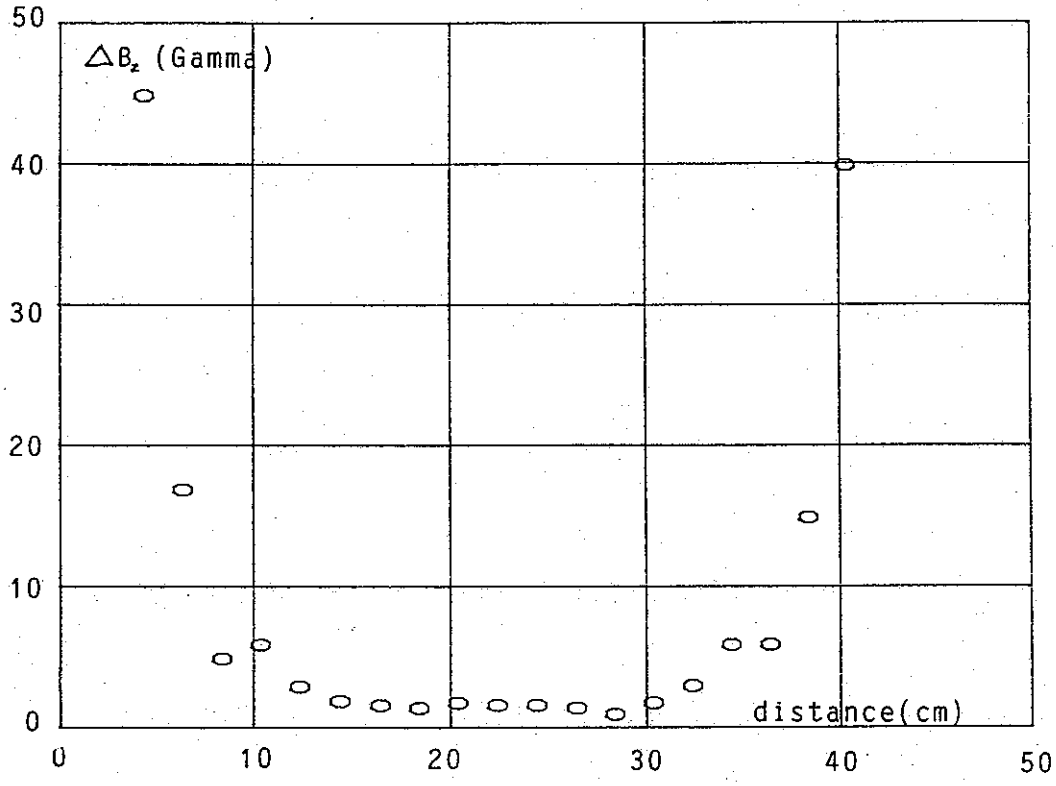

Figure 4.13: The B_z field profile along the axis of the shield.

water bath to ensure a high current stability. The chip used is a chopper chip chosen for its low offset voltage.

4.3.7.4. The Optical Components

We used the same optical components as in experiments done in section 4.3 (sub-section 4.3.3). However, one had to get the pumping light inside the shield from one of its sides. For this purpose, light was made to propagate from the source, through a set of optical fibres to the absorption cell positioned in the centre of the shield.

4.3.7.5. The Overall Set-Up

The absorption bulb is supported in the shield on a plastic tube as shown in figure 4.14. The diameter of this cylinder is such that it could hold all sizes of absorption cells used. Both the photocell, used to detect the resonance signal, and the RF field coil were fixed to this same cylinder. A Helmholtz coil used to modulate the Bz field was fixed to the inner surface of the aluminium former. This coil is 24cm in diameter with a separation of 25cm.

4.3.7.6. - Results and Discussion

Experiments to determine the linewidth and different relaxation times were performed in exactly the same way as in section 4.3.6.

Measurement of T_2 :

The results plotted in figure 4.13 yield a magnetic field

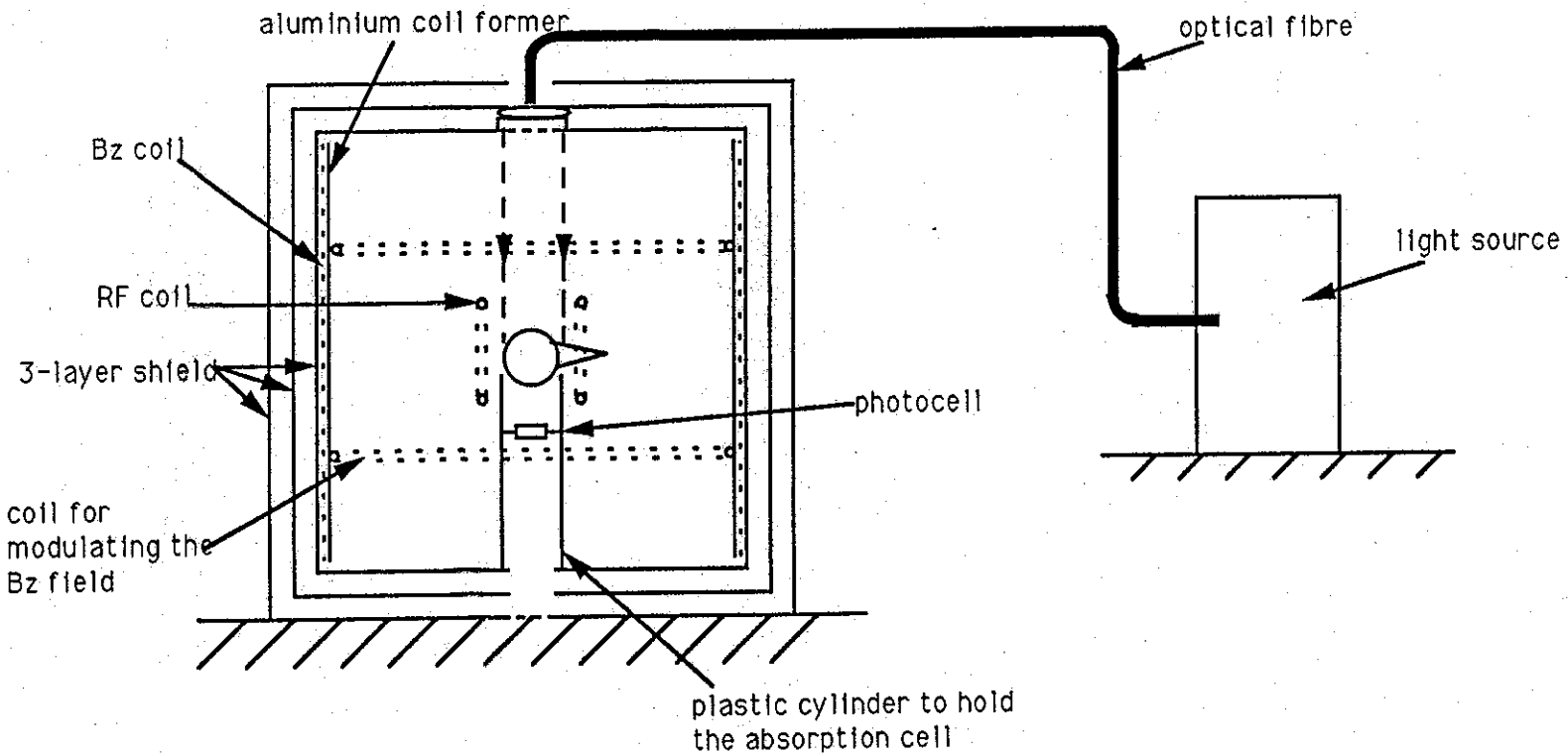

Figure 4.14: Experimental set-up in the magnetic shield.

inhomogeneity of about 3 Gamma across the radius of the 5 litre cell. Equation (4.4) then gives T_2 = 4.5 secs. This is an improvement factor of 682 from the value of T_2 measured in free space.

We expect T_1 to remain of the same order of magnitude as it would be measured outside the shield. Since it is primarily determined by the state of the cell walls. The pumping time T_p can be estimated from a measurement of the linewidth and the relation giving the expression for the linewidth of a resonance signal in terms of T_2 and T_p.

$$\Delta f = \frac{1}{\pi}\left(\frac{1}{T_2} + \frac{1}{T_p}\right) \qquad (4.10)$$

valid when the RF field magnitude is extrapolated to zero.

Measurement of the linewidth:

In the following, we give the details of the results obtained when an RF peak value of 4.5×10^{-3} mGauss was applied to the cell. This was generated by a peak current of 5×10^{-5} Amps running in a single turn Helmholtz coil 10 cm in radius. The frequency of the B_1 field was swept from the initial value of 3.6 kHz to 3.9 kHz in 100 seconds. The 10 mGauss Bz field was modulated at 4Hz and the resonance signal was measured using a PSD with an integration time constant of 4 secs. The total light output measured by the detector was 0.5 volts DC. Under these conditions (figure 4.15) a linewidth of 10 Hz and a resonance frequency of 3738 Hz were respectively measured.

The signal amplitude was 35 mvolts with a gain of 100 in

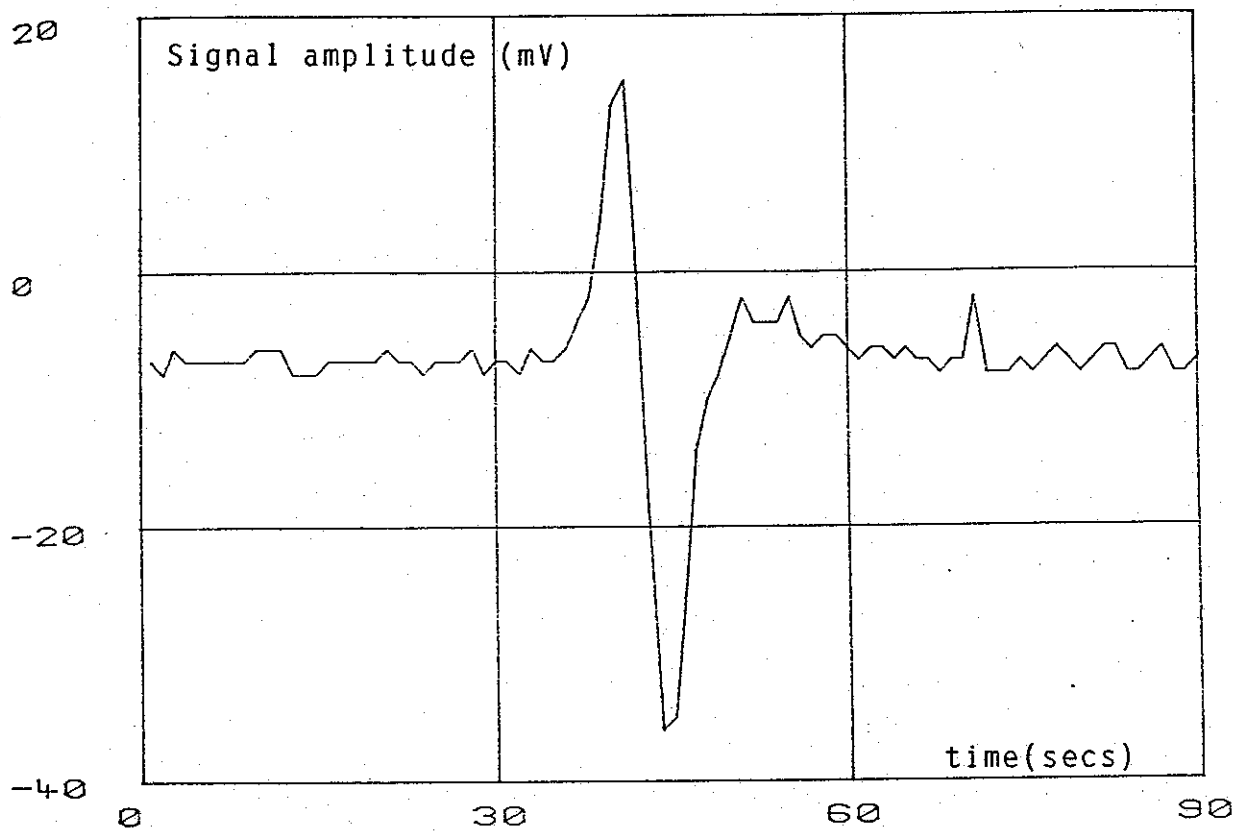

Figure 4.15: Magnetic resonance signal in the 3-layer μ-metal shield. This was detected using a PSD and sweeping the RF frequency from 3.6 kHz to 3.9 kHz in 100 seconds. We find f=3.738 kHz and Δf=10Hz.

the detector circuitry. The ratio of the signal to the total DC light is then 0.35/500≈0.07%. This represents the proportion of Cs atoms participating to the absorption. An estimate of the peak to peak signal to rms noise ratio from the data in figure 4.15 gives S/N = 42.

Measurement of T_p:

For this purpose, we used the method of magnetic resonance transients in the presence of light which was explained in section 4.3.6.

By switching the RF frequency on and off at 0.5 Hz, the pumping exponential with RF-off, and the decaying transients with RF-on were observed at a resonance frequency of 3696 Hz with a total light intensity of 373 mV. The B_1 field used to equalise the populations was 0.47 mGauss peak. The pumping curve obtained shown in figure 4.16 yields τ_1 = 63.5 msecs when an exponential is fitted to the data. Assuming $T_1 >> T_p$ we obtain 63.5 msecs for T_p, much less than the estimated T_2 of 4.5 secs. The linewidth estimated from equation 4.10 using T and T_p of 47 msecs at a light intensity of 0.5 volt, (assuming $1/T_p$ proportional to light intensity) is 6.8 Hz. This is in good agreement with the value measured experimentally for the same light intensity.

In conclusion, performing an experiment in a magnetic shield allowed us to reduce the signal linewidth from 300 Hz to 10 Hz. We established that it is mainly due to field inhomogeneities. We assumed that T_1 is essentially the same inside or outside the shield since it only depends on the state of the cell walls.

The aim of the work achieved in this section (4.3) is not

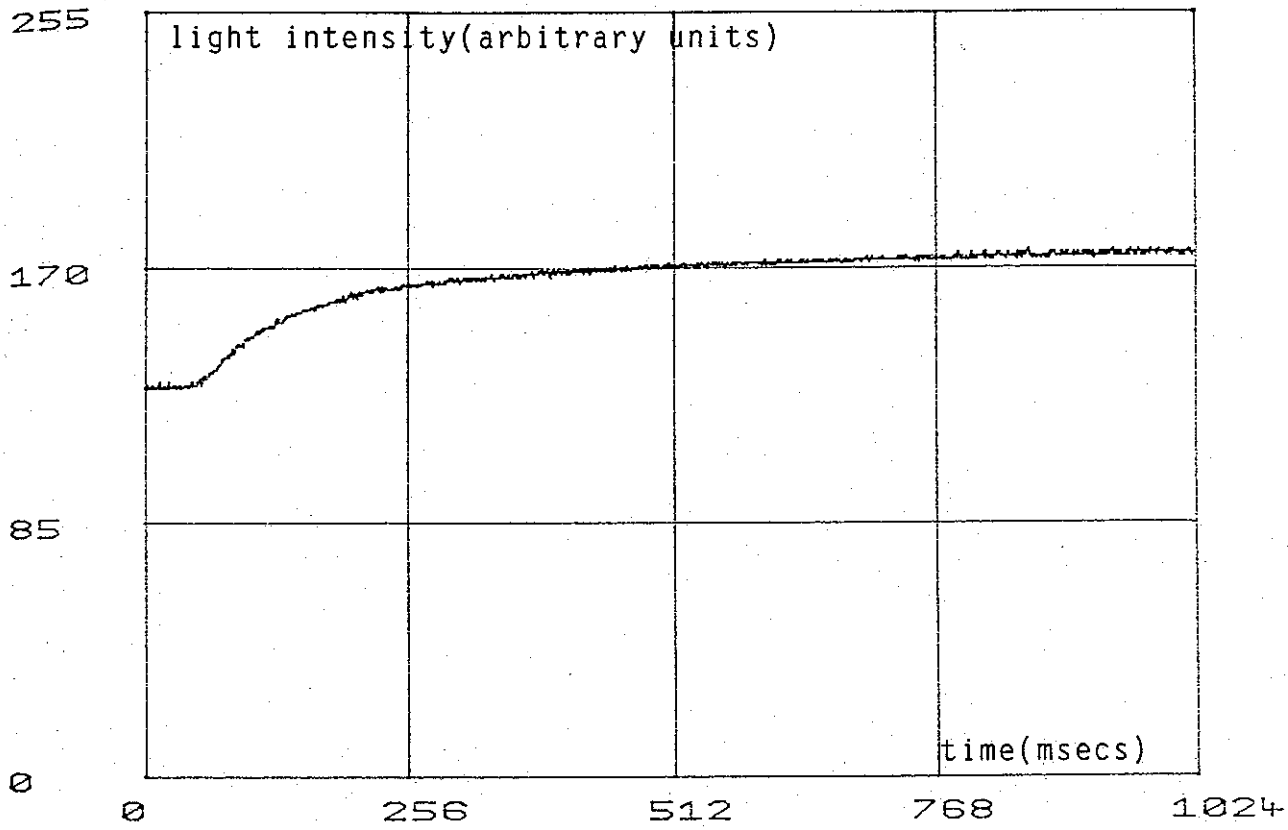

Figure 4.16: Pumping time curve.
The transparency of the vapour increases as more atoms are pumped.

to have an accurate measurement of the different relaxation times involved in the optical pumping process, but to show that such experiments can be done in such circumstances i.e in optical pumping absorption cells as big as 22 cm in diameter.

4.4. Optical Pumping Attempts in an Aluminium Vessel

4.4.1. Introduction

As it was mentioned in the previous stages of this work, the storage of ultra-cold neutrons in the EDM experiment is done in metallic containers coated with some non-depolarising substances. To be more precise, the container consists of a cylindrical insulator (for example BeO) with two conducting end-plates. These plates are usually made of aluminium or copper so that a high electric field can be applied across them. For this reason, one has to investigate the possibility of storing polarised atoms in metallic containers in order to be able to store them with polarised neutrons as it was pointed out in the introductory chapter.

We need a wall coating substance which allows polarised neutrons and polarised atoms to be stored at the same time. A prototype experiment was set up in Sussex to store and polarise Caesium atoms in a continously evacuated system. We shall be dealing, in this section with the structure of the vessel and the associated vacuum system. We shall also describe the coatings that were tested and the way that one of these, polystyrene, was made in the laboratory.

4.4.2. The Aluminium Vessel

It is similar to the EDM-type of bottle. It consists of a cylinder 13cm high with an inside diameter of 23cm, wall thickness of 1cm, and two end plates (figure 4.17). The end plates are sealed by Viton O-rings positioned in grooves which are cut in the cylinder. Each of the end plates contains a centre hole recessed to take a 4cm diameter glass window of 3mm thickness, sealed by Viton O-rings. This type of O-ring was used for their high temperature working range and low outgassing rate.

The vacuum is maintained through a 1cm hole in the bottom end plate. A home made air-actuated valve was used to maintain the pumping. This is shown in more detail in figure 4.18. Caesium vapour was admitted to the vessel through a 1cm hole in the upper plate. Figure 4.19 shows the Caesium glass container. It consisted of a glass tube with a teflon, vacuum tight, tap which controls the flow of Cs to the chamber. The small drop of Cs was admitted under vacuum after coating the inner walls of the glass tubing with surfasil in order to minimise the tendency of Cs to stick to the walls.

4.4.3 The Vacuum System and Overall Set Up

A diffstak 100 series from Edwards was connected to the chamber through a 1 inch copper tubing. This high vacuum pump is water cooled only and does not require any liquid nitrogen cooling. It is backed by a conventional rotary pump. The diffstak is supported on an aluminium frame underneath the 3-layer μ-metal shield. The rotary pump

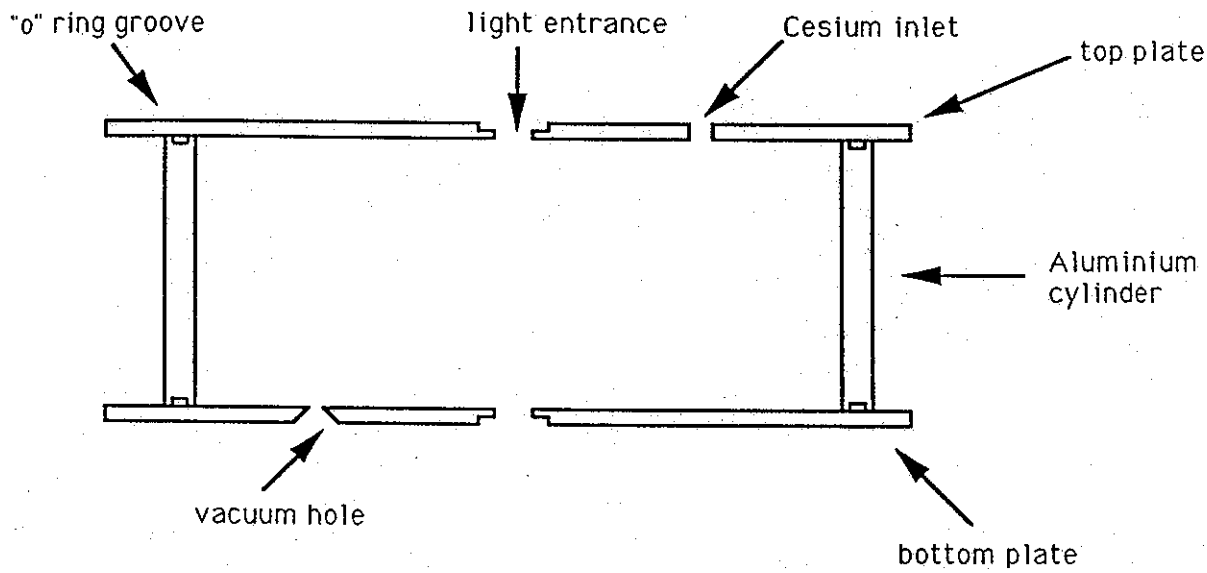

Figure 4.17: Diagram showing the Aluminium chamber used to store polarised Caesium atoms.

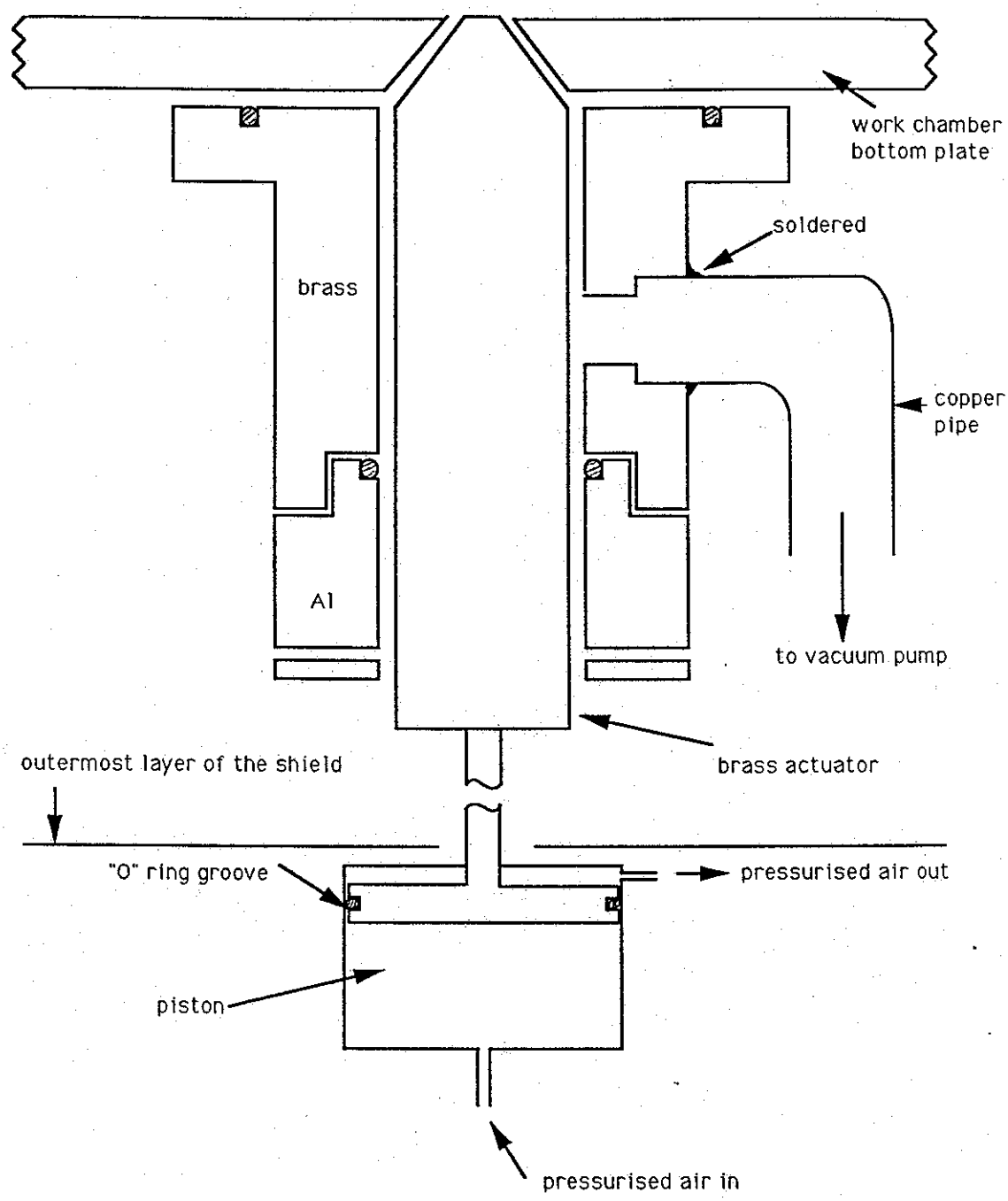

Figure 4.18 : The actuator valve in the closed position (not to scale).

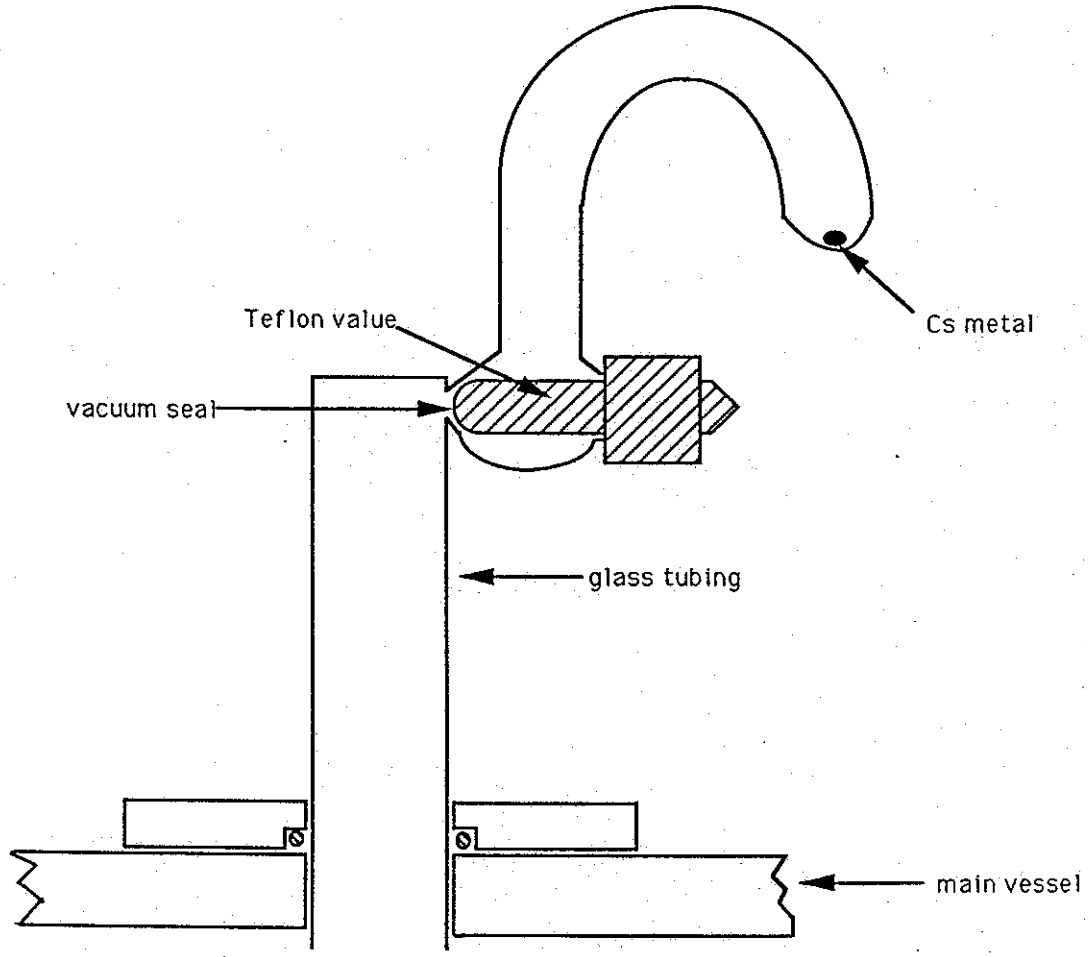

Fig 4.19: The Cesium container. The Teflon valve opens by screwing it out.

sits on a heavy block of concrete separated from the laboratory floor by some thick rubber tubing in order to minimise the low frequency vibrations transmitted to the work vessel. For the same reason, the connection between the rotary pump and the diffstak is done by means of a flexible vacuum pipe. The diffstak is equiped with a combined backing/roughing valve.

The overall set up is shown in figure 4.20. The aluminium vessel is supported inside the shield by 4 wooden stands. The optical components are fixed to the upper end plate whereas the light detecting photocell is fixed to the bottom end plate facing the central hole. Light crossed the vessel through the central holes after being admitted inside the shield through optical fibres.

4.4.4. The Surface Coatings

The surface coating is used to preserve spin polarisation and prevent the Cs atoms depositing on the walls. These substances are normally applied by brushing, spraying or dipping. There is a reasonable range of materials available and the choice is determined by the experimental conditions and the type of atoms to be stored. For example, it is well known that teflon (CF_{2n}) coated containers do not store alkali atoms because these attack the C-F bonds very strongly. However, teflon is a very convenient coating for Hg and Hydrogen.
We tried two coating agents, namely surfasil and polystyrene. The former was purchased from Pierce Chemical Company, whereas the latter was made in the laboratory from unpolymerised styrene.

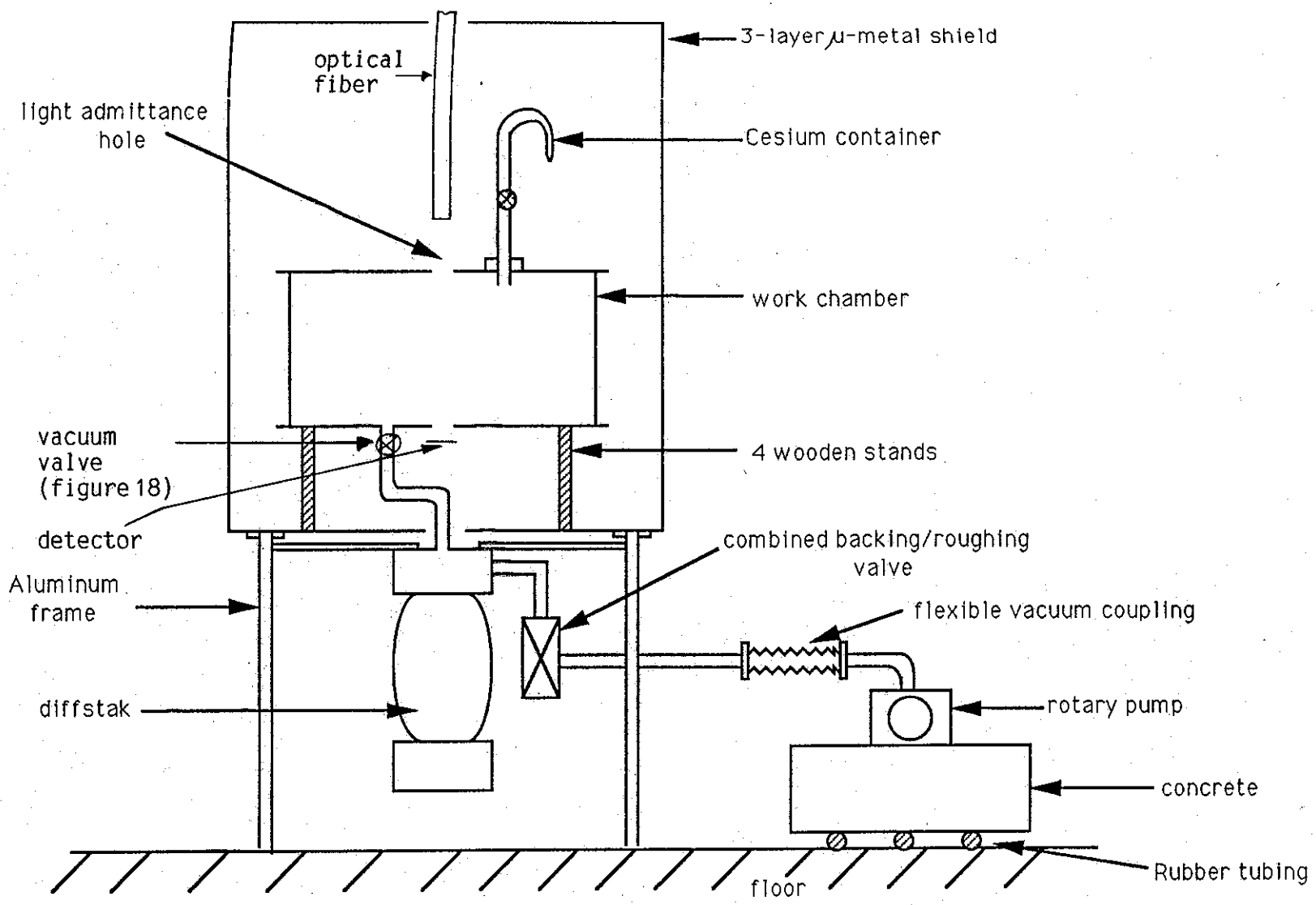

Figure 4.20: Vacuum system and overall set up

4.4.4.1. Surfasil

Surfasil is a siliconizing agent used for surface treatment of glass, quartz and other surfaces. It proved to be very effective when used in optical pumping glass containers. It is a very flammable material, corrosive and evolves small amounts of hydrochloride fumes during application. Consequently, special care is required with eyes, skin and clothing.

We found that the best results in glass cells were obtained when using a solution of $1cm^3$ Surfasil and 2 cm^3 analar acetone. A similar solution was applied to the aluminium vessel with a painting brush and left to dry up overnight. If the coating is thorough, pouring water on the surface would not wet it. It would just run freely without sticking to the container.

4.4.4.2. Polystyrene

One started off by purchasing a quantity of styrene (the monomer) from Sigma chemicals. This usually comes with a trace of an inhibitor (ex. hydroquinone) to prevent it from spontaneous polymerization. One straight forward way of polymerising it is through heat and pressure. Styrene is put in a sealed ampoule with thick walls capable to withstand up to 10 bar pressure (figure 4.21). The ampoule is then introduced in a stainless steel container heated from the outside with heater tape. The temperature is monitored by a Hg thermometer and the open end of the container is covered with glass wool to keep the heat in.

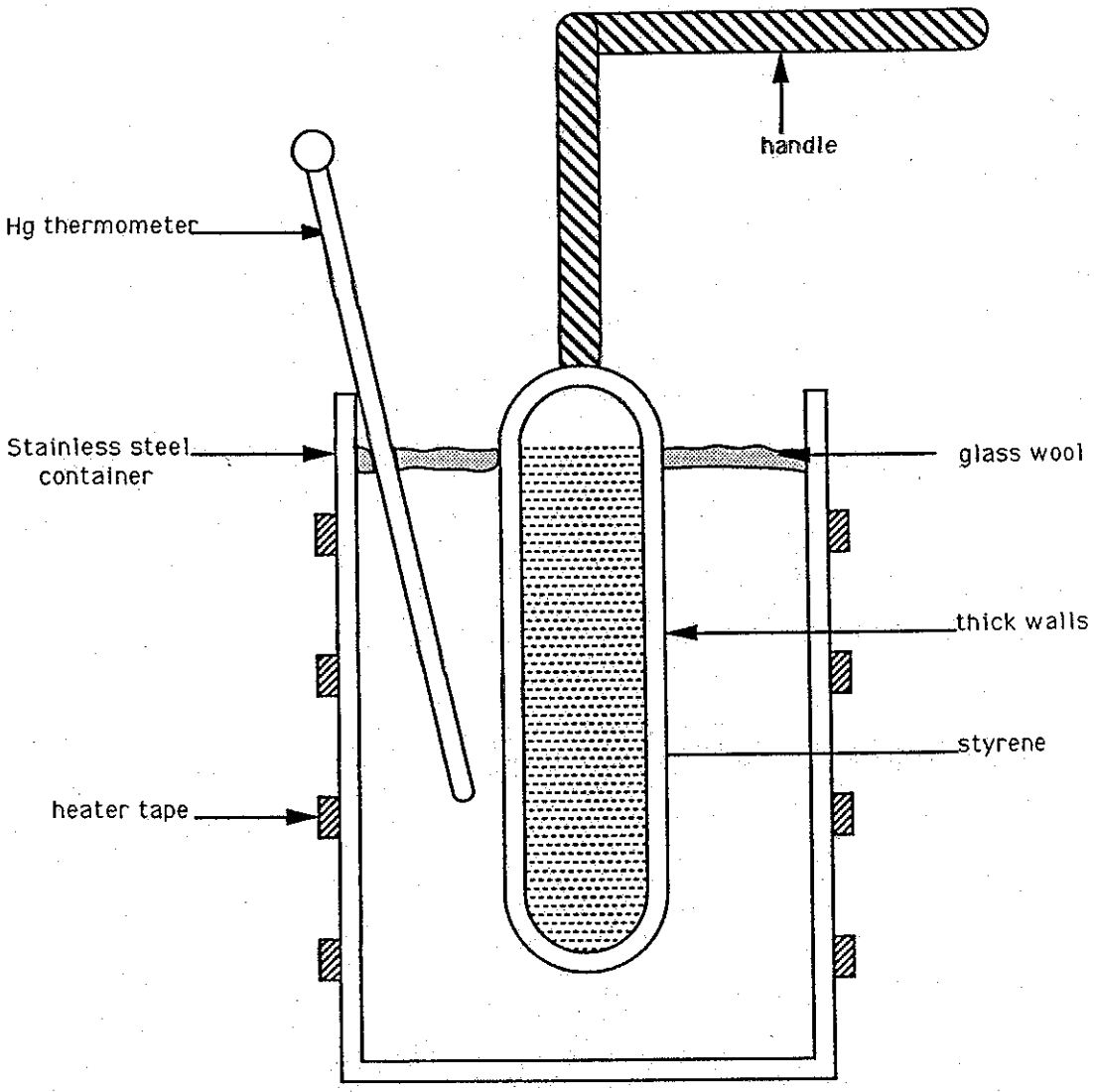

Figure 4.21: Polymerisation of styrene

The whole system is placed in a fume cupboard, and the temperature is then raised gradually until it reaches 180°C. This process takes about 4 or 5 hours and the entire operation is repeated 3 times. After the ampoule is allowed to cool down, it is taken out of the oven and wrapped in aluminium foil. It is then broken with a hammer and the pieces of glass separated from the polystyrene "rod" with a pair of clean tweezers. Polystyrene looks like glass, feels just as hard, but is a bit more opaque. It is then disolved in analar toluene over a period of about one day. The chemical formalae of styrene and polystyrene are shown in figure 4.22.

We found that application of polystyrene on surfaces requires a bit of care. It tends to dry rather quickly (a few seconds) and this makes brushing difficult. Dipping the container in polystyrene was also impossible because of the small quantities we had available and the high price of the substance. We also found that spraying is unsatisfactory; a sprayed surface shows very tiny uncovered holes. The best results were obtained by pouring a quantity of polystyrene on the surface and then wiping it with a piece of aluminium sheet held at an angle to the surface. This technique produced good uniform and shiny surfaces.

4.4.5.- Preliminary calculations

Before the experiment could be carried out, it was necessary to consider the conditions for an efficient optical pumping cycle.

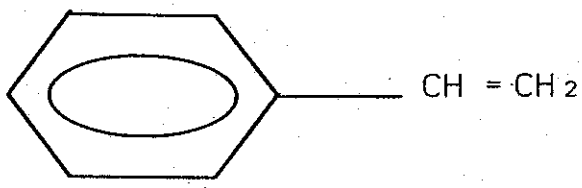

(a)

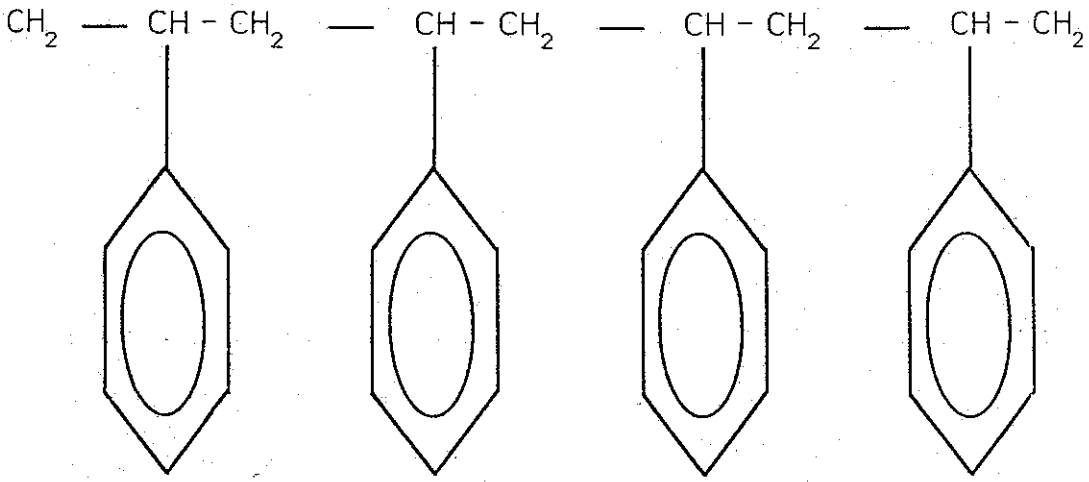

(b)

Figure 4.22: (a) Styrene, (b) Polystyrene.

1. Caesium pressure:

We start off by calculating the Cs vapor pressure needed for one absorption length across the chamber. This means that the light intensity drops by a factor of 1/e over a distance ℓ, which is in this case the height of the chamber.

The expression of light intensity, through a vapour, as a function of distance is given by

$$I(x) = I_0 \, e^{-\sigma x \rho} \tag{4.11}$$

where I_0 is the intensity at the source, x the distance travelled by the light, ρ the vapour density and σ is the light absorption cross-section for a given species of atoms at a given wavelength. In order to have one absorption length across the chamber one should have

$$I(\ell) = I_0 / e \tag{4.12}$$

thus

$$\sigma \rho \ell = 1 \tag{4.13}$$

from which the required vapour pressure could be calculated.The expression of σ, at resonance, is calculated from equation (9.11) given in reference [Cor 77] on page 273. Since the atoms absorbing the light are in constant motion, there has to be a correction that takes into account the Doppler width. We finally obtain,

$$\sigma = \frac{3}{2\pi}\lambda^2 \frac{\Delta\nu}{\Delta\nu_D} \qquad (4.14)$$

where $\Delta\nu$ is the natural width of the emitting excited state, and $\Delta\nu_D$ is the Doppler width at the working temperature. The lifetime of the excited state $6^2P_{\frac{1}{2}}$ in Cs is $\tau=3.8\times10^{-8}$ secs [Mit 71], which gives a natural width of 4.2 MHz. The Doppler width is given by the following expression

$$\Delta\nu_D = 7.2\times10^{-7}\sqrt{T/A}\,\nu_0 \qquad (4.15)$$

where ν_0 is the frequency of the transition, A is the atomic weight and T is the absolute temperature. For the 8943 Å Cs line at 300K we obtain $\Delta\nu_D$ = 363 MHz, giving 4.4×10^{-15} m^2 for σ.

Since the height of the chamber is ℓ=10 cm, the vapour pressure P needed to have one absorption length across the chamber is readily calculated from equation (4.13)

$$P = 6.7\times10^{-8} \text{ torr} \qquad (4.16)$$

In conclusion, maintaining this pressure in the chamber ensures that about a third of the total light reaches the detector.

2.Filling time:

The other parameter that ought to be known before the experiment is carried out is the filling time from the Cs container to the main vessel.

The pipe conductance C of the Caesium container (figure 4.19) is calculated to be equal to 0.9 ℓ/s. The vapour

pressure p_1 of Cs at room temperature is about 10^{-6} torr and the volume V of the chamber is 5 litres. The surface area of the Cs outlet is $A = 1\ cm^2$. This surface area acts as a depolarising agent since every atom hitting it would be absorbed by the Cs source. The differential equation describing the motion of the vapour from the Cs container to the vessel is written as

$$\frac{dn_2}{dt} = C\,(n_1 - n_2) - \frac{1}{4} n_2 \bar{v} A \qquad (4.17)$$

where n_1 and n_2 are the number of atoms in the Cs container and the main vessel respectively, and $\bar{v}$ the average speed of Cs atoms. The volume of the Cs container is assumed to be negligable compared to the main volume V.
In terms of pressure, this equation reduces to

$$\frac{dP_2}{dt} + p_2 \left(\frac{C + \beta}{V}\right) = \frac{C}{V} p_1 \qquad (4.18)$$

where $\beta = \frac{1}{4} \bar{v} A$, and has a solution of the form

$$p_2(t) = \frac{C}{C + \beta} p_1 \left(1 - \exp - \frac{C + \beta}{V} t\right) \qquad (4.19)$$

assuming p_1 remains constant compared with p_2.
If we want p_2 to be equal to 6.7×10^{-8} torr (equation 4.16), then t=0.5 sec. This time is rather short for the pneumatic valve controling the flow of Cs to the chamber. However, a time t of 2 secs. is rather suitable and the equilibrium pressure reached is 1.3×10^{-7} torr. This value would yield 2 absorption lengths across the chamber. It is resonable to use this amount of gas since it has already been shown that optical pumping signals were observed at pressures of 10^{-6}

torr which represent 10 absorption lengths across the small 6 cm diameter cells.

3. Emptying time:

After two seconds the Cs source valve is closed and the atoms inside the main vessel bounce around as long as the walls are coated with a non-sticking agent. The time taken to empty the chamber is given by the simple formula

$$t = \frac{V}{S} \ln \frac{p_0}{p} \qquad (4.20)$$

where S is the conductivity of the pipe connecting the chamber to the vacuum pump. This pipe, about 30 cm long and 2.5 cm in diameter, has a pumping speed of 6.4 ℓ/s. Therefore, the time taken to reduce the pressure by a factor of 100 is t=3.6 secs.

4.Depolarisation by atom-atom collisions:

Another possibility that has to be considered is the probability of spin depolarisation by atom-atom collisions. The main depolarising source would be oxygen molecules or Cs atoms themselves. As far as Cs-Cs collisions are concerned, there should not be any problems at a pressure of 1.3×10^{-7} torr. Optical pumping cells usually work with pressures of 10^{-6} torr. On the other hand, we were unseccessfull in finding, in the literature, a value for the spin flip collisional cross section between Cs atoms and oxygen molecules. If we assumed that $\sigma(Cs\text{-}O_2)$ is of the same order of magnetude as $\sigma(Cs\text{-}Cs)$ or $\sigma(Cs\text{-}Rb)$ i.e about 10^{-14} cm^2 [Cor 77], the collisional probability for spin flip is given by

$$P = N_0 \left(\frac{p}{p_0} \right) \sigma (\bar{v}_r) \bar{v}_r \qquad (4.21)$$

where N_0 is the atomic density of oxygen at the standard pressure p_0, p is the partial pressure of oxygen in the chamber and $\bar{v}_r$ is the mean relative velocity given by the relation

$$\bar{v}_r = \sqrt{\left(\frac{8kT}{\pi} \frac{M_{Cs} + M_{O2}}{M_{Cs} M_{O2}} \right)} \qquad (4.22)$$

from which we obtain $\bar{v}_r = 495$ m/s.

The residual pressure in the chamber was estimated from a measurement of the pressure near the vacuum pump and was found to be equal to 5×10^{-5} torr. The partial pressure p of O_2 in the chamber is then 1×10^{-5} torr. The density of Oxygen at N.T.P is 1.429 g/ℓ which allows us to calculate N_0. Substituting in 4.21 we obtain a spin flip probability of 176 collisions/sec. This yields a relaxation time T_c=6ms. We recall that the pumping time T_p measured in the 5-litre glass chamber was about 10 times this value, therefore, in order to achieve an efficient pumping cycle, we will have to use at least 10 times more light than usual. However this calculated value of T_c is rather guessed and could well be a factor of 10 larger. Furthermore, Cs metal acts as an oxygen absorber and therefore reduces the amount of O_2 in the chamber. This absorption process happens every time the Cs container is opened.

4.4.6.- Experiments and Discussion

One of the first problems we investigated was the effect

of an uncoated aluminium surface on the signal strength. We asked the glass blower to make a 1-litre glass cell coated with Surfasil containing a bare sheet of aluminium foil 25cm^2 in area. Since this sheet was loose and not fixed to the walls, it would look like a 50 cm^2 uncoated area. We then looked for an optical pumping signal and recorded both linewidth and signal strength. The experiment was then repeated under the same conditions (same light intensity, same rf power...etc...) with a similar cell without any aluminium sheet. The result was a reduction by a factor of 24 in the signal strength and almost no effect on the linewidth. This of no surprise because the linewidth is primarily concerned with field inhomogeneities. However, the serious effect on the signal amplitude suggests that special care should be taken when coating the aluminium chamber.

After coating the Aluminium vessel with Surfasil in the way described in section 4.4.4.1, we set out to look for an absorption signal, a reduction in light intensity when unpolarised Cs atoms were let into the cell. The light transmitted was monitored during a typical running sequence such as that set out below:

1.Close the high vacuum valve (pneumatically actuated).

2.Open the Cs tap for two seconds.

3.Wait for a few seconds and open the high vacuum valve to flush the chamber out.

In ideal circumstances, a gradual drop in light intensity would occur as soon as the Cs tap is opened, a drop with a time constant equal to the filling time constant. The light intensity should eventually stabilize around some level until the vacuum valve is opened. At this point, the light

DC level should return to its initial value with a time constant related to the conductance of the pumping pipe.

When we ran the experiment, however, a drop in light intensity was seen as soon as the vacuum valve (figure 4.23) was closed. No effect was recorded when the Cs tap was opened or closed but the light intensity recovered its initial level after the vacuum valve was closed. The experiment was repeated over and over again but each time the same behavior was recorded. Moreover, we ran with different parameters, changed the filling time and the temperature of the Cs source, but no sensible behavior was obtained. We had to assume that the change in light level when the pneumatic vacuum valve was actuated was due to a change in geometry caused by the forces exerted on the cell by the pneumatic valve.

In order to test this possibility, we closed the high vacuum valve of the diffstack pump itself instead of the pneumatic valve. This was done slowly by hand, making sure that nothing changed position in the system. The result was that there was no light variation.

More experiments were done to look for a resonance absorption signal. Two methods were utilized: the conventional method that we have been using so far, and a second method of zero-field crossings [Cor 77]. The latter one has the advantage that the experimenter does not need to know neither the frequency at which the resonance occurs nor the linewidth of the signal. Unfortunatelly, both methods led to negative results.

After so many attempts, it became apparent that the problem was related to the wall coating. Since one knows that Surfasil-coated glass containers stored Cs vapors, the

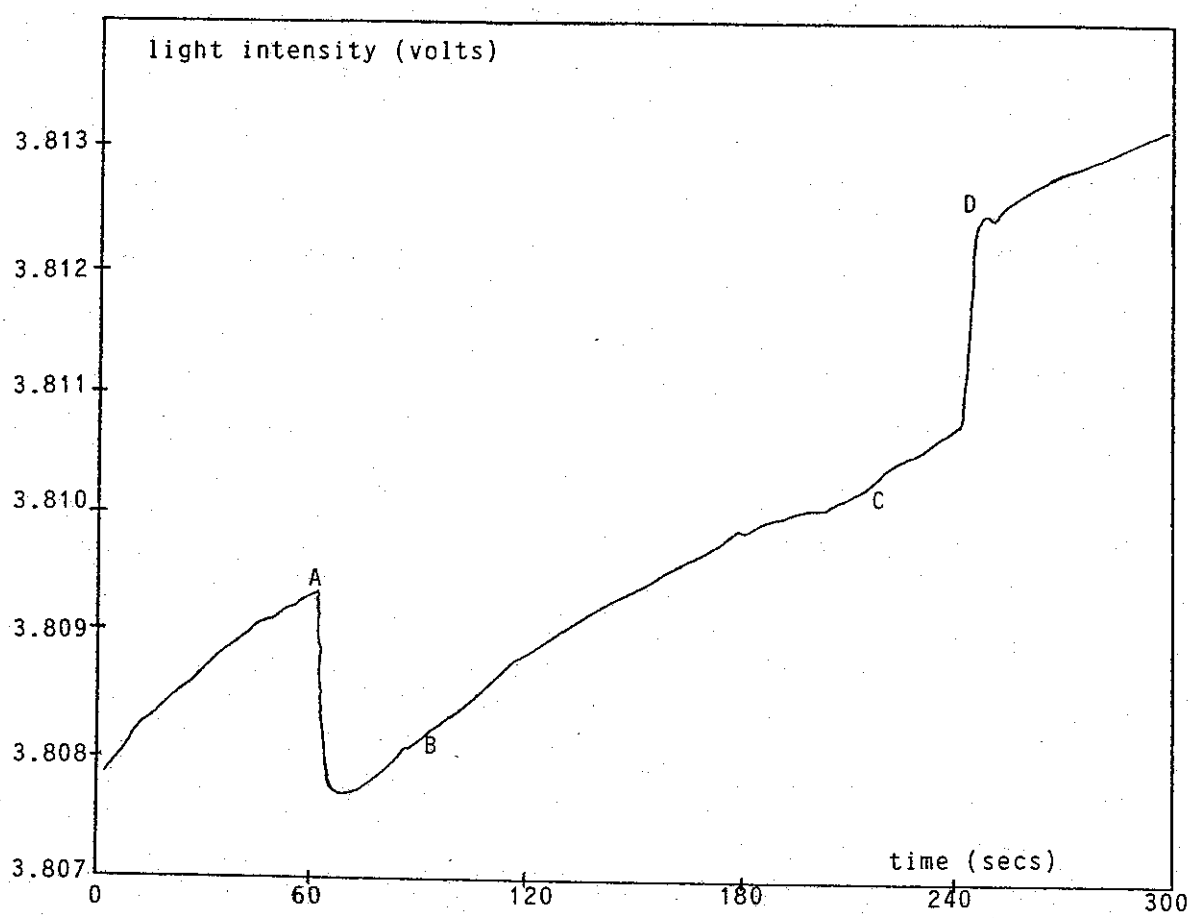

Figure 4.23: Monitoring of light absorption in the 5-litre vessel.
At B the Cs tap is opened and then close at C.
The vacuum valve is opened at A and closed at D.
There is no sign of absorption at B.

problem is then more likely to be that Surfasil does not cover aluminium surfaces adequately, and may well chemically react with them. We had another attempt to look for an absorption signal with a freshly coated chamber but, once again, we obtained no sensible results. The conclusion was that the use of Surfasil on aluminium surfaces was not advisable.

We decided to coat the work chamber with another agent, namely polystyrene. This was done in the manner described in section 4.4.4.2. The coated surfaces seemed to be in a satisfactory state both outside and under vacuum. However, any effort to store Cs atoms in the chamber ended up with a failure.

Having done that, it seemed rather interesting to look at the behavior of Cs with polystyrene in a "better" environment. We therefore asked the glass blower to make a 6 cm Cs absorption cell made out of pyrex treated with polystyrene. Immediately after it was made, we noticed that we could make Cs droplets run freely on the cell surface when this is tilted around. However, one day later, Cs seemed to be sticking more readily on the walls. In order to make it run towards the stem we heated the cell gently on a bunsen burner. A rather fast and vigourous reaction took place and the cell turned black making it impossible to use. Nonetheless, a second cell was made with all the Cs concentrated in the stem. Four days later an optical resonance experiment in the 3-layer shield was set up using this cell and subsequently a similar cell whose walls were coated with Surfasil. The two tests were done in the same conditions of light intensity, rf power...etc... We also made sure that the shield was demagnetised after it was

opened to put one or the other cell. Again the results showed no changes in the signal linewidth but a rather big change in the signal amplitude. The signal obtained with the polystyrene coated cell was about 6% of that registered with the cell coated with Surfasil. It is now clear that polystyrene is not as good a coating to be used with Cs vapours as Surfasil. Furthermore, as time passed by, the cell gradually discolored until it ended up being completely black within a few weeks.

At this point, we decided to stop any further attempts to store Cs atoms in a coated metallic container and start on the design and construction of a system using mercury vapour.

Clearly, the problem to solve is what sort of coating one should use that would, on one hand coat metallic surfaces (Al, Cu ...) thouroughly, and on the other hand not react with Cs (or alkalis in general).
Unfortunately, this most interesting problem was not tackled because of time constraints imposed on the neutron EDM experiment in Grenoble. Furthermore, some alternative ways to using Cs vapours in that experiment were coming from our collaborators in the University of Washington which seemed rather attractive. These suggestions were seriously considered in our research group to replace a possible caesium magnetometer for the neutron EDM experiment and the work laid down in the next pages of this thesis was soon undertaken.

CHAPTER V

Optical Pumping Experiments with Mercury Vapours in Sealed Quartz Cells

5.1. - Introduction

Optical pumping experiments with mercury atoms and alkalis are described by the same basic equations but the apparatus used tends to differ because the process works at a different wavelength. In this chapter we shall discuss the design and construction of the essential parts of system in which atomic mercury is pumped and free precession observed. We shall be describing the fabrication of light sources, absorption cells, the optical accessories used, the microwave generators and the electronic circuits used for the detection of resonance signals. We shall also show what could be done with such absorption cells and light sources. Some characteristics, such as light noise, are measured. Some of the used items were those used with Caesium experiments and they will not be described again but reference will be made to them.

Mercury is a very dense silvery-grey metal with a high surface tension which does not wet surfaces but forms small globules; hence its old name of *quicksilver*. Mercury is a poor conductor of heat and electricity compared to silver. The electronic configuration of the $^1S_0$ ground state of Hg is $2s^2\,2p^6\,3s^2\,3p^6\,3d^{10}\,4s^2\,4p^6\,4d^{10}\,4f^{14}\,5s^2\,5p^6\,5d^{10}\,6s^2$.

The natural isotopic abundances of mercury are summarised in table 5.1.

Isotope	204	202	201	200	199	198
Abundance (%)	6.85	29.8	13.22	23.13	16.84	10.02

Table 5.1

Mercury has a vapour pressure of 1.6×10^{-3} torr at room temperature and is consequently a very convenient element to pump optically.The vapour pressure as a function of temperature is given by the relation

$\log_{10} P(\text{torr}) = -3214/T(K) + 8.164$.

Optical pumping of Hg was first reported by Cagnac, Brossel, and Kastler [Cag 58a, b, c,]. Figure (5.1) shows the low-lying energy levels of mercury [Bro 52].

As far as optical pumping is concerned, one is only interested in the odd isotopes of Hg. Even isotopes have a completely diamagnetic ground state, i.e. they have no electronic spin angular momentum or nuclear spin (J=0, I=0) so their orientation is subsequently not feasible. The two odd isotopes ^{199}Hg and ^{201}Hg have nuclear paramagnetism with nuclear spins I=1/2 and I=3/2 (ground state 6^1S_0). By optically pumping these two isotopes, one obtains a purely nuclear orientation of the vapour.

The mercury spectrum contains two resonance lines in the ultraviolet region, the 6^1S_0-6^3P_1 transition at 2537 Å and the 6^1S_0-6^1P_1 transition at 1850 Å. The 1850 Å radiation cannot propagate in free space, because it is very strongly absorbed by oxygen. This photochemical reaction transforms oxygen into ozone and the less rapidly absorbed 2537 Å

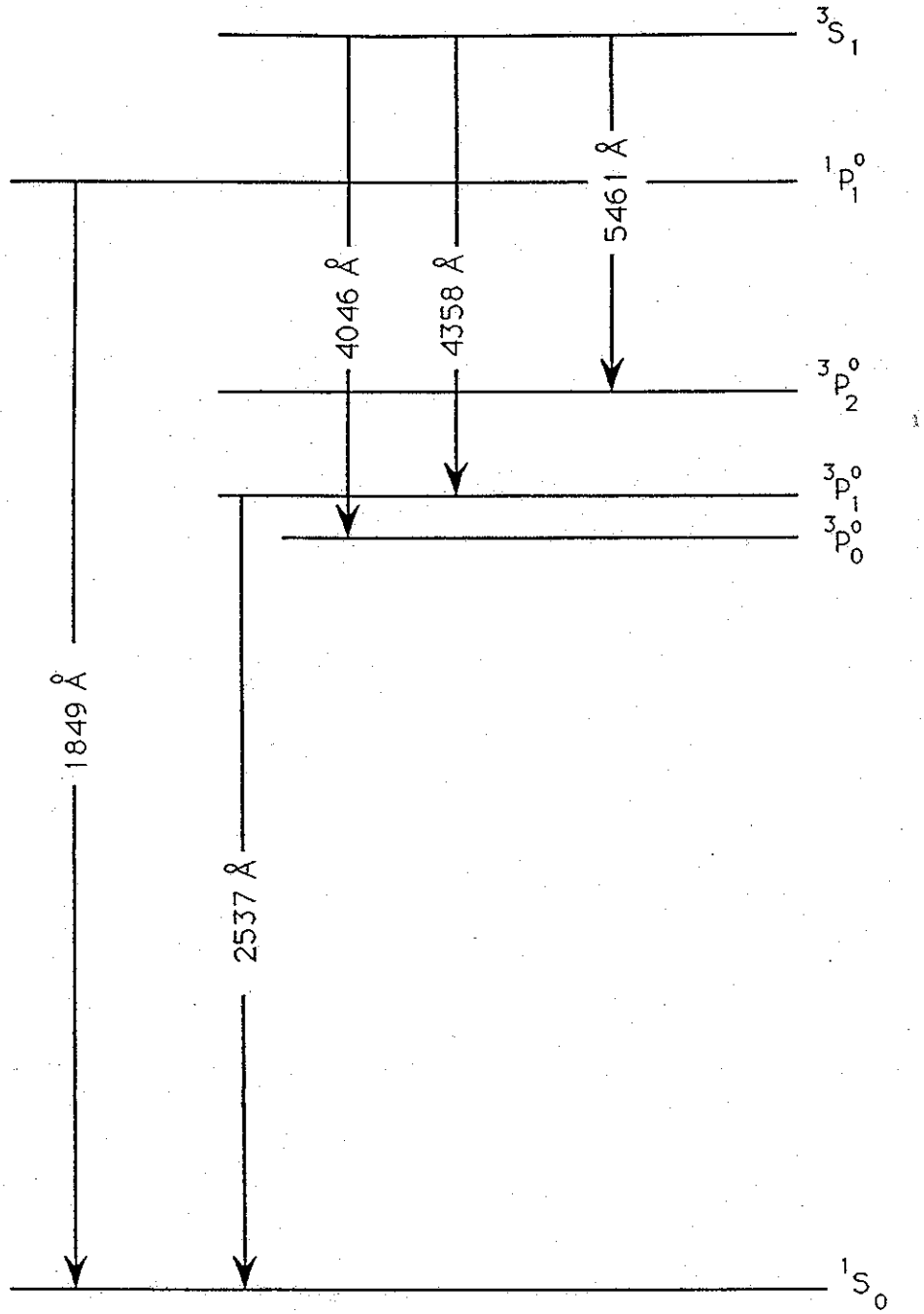

Figure 5.1: Low-lying energy levels of mercury.

radiation is preferred for optical pumping experiments. The excited state 6^3P_1 has a rather long lifetime of 1.2×10^{-7} sec., and the transition probability for the 6^1P_1-6^1S_0 line is a factor of 10 smaller than those of the resonance lines of the alkalis. As a result, the pumping time is rather long in this case and very intense light sources are necessary.

A transition from $^3P_1$ to $^1S_0$ is not allowed by the electric dipole transition selection rules for Russell-Saunders coupling because $\Delta S\neq0$. Mercury is a heavy atom, however, and some breakdown of LS coupling exists because of the spin-orbit interaction and the $^3P_1$ level is an admixture of pure $^3P_1$ and $^1P_1$. It must be noted that both these states have the same value of J since the spin-orbit interaction is diagonal in J. Transitions from $^1P_1$ to $^1S_0$ are allowed and are responsible for the intercombination line emitted.

Figure (5.2) shows the hyperfine structure of the 2537 Å natural Hg resonance line. It consists of the four single lines of the even isotopes 204, 202, 200, and 198 as well as the hyperfine components due to the odd isotopes 201 and 199.

The ^{201}Hg isotope has three components and ^{119}Hg has two of them (figure 5.3).

The lines emitted by the even isotopes are well resolved, but one notices the almost perfect coincidences between some of these lines and those of some of the components of the odd isotopes. The expression "almost perfect" means that the coincidence is well within a Doppler width. These coincidences are between ^{199}Hg(F=1/2) and ^{204}Hg, ^{201}Hg(F=5/2) and ^{204}Hg and also between ^{201}Hg(F=3/2)

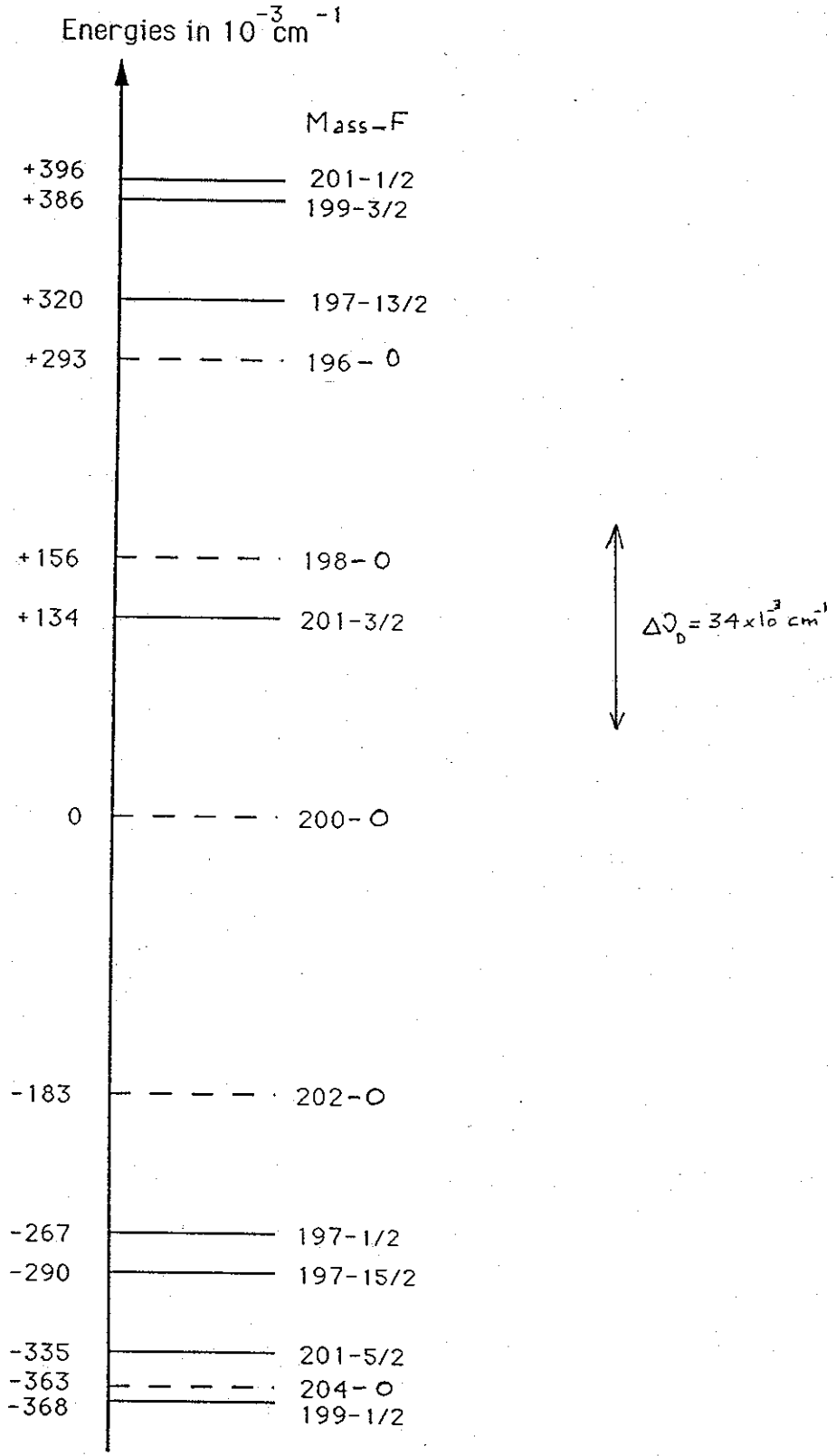

Figure 5.2 : Hyperfine structure of the 2537Å resonance line. $\Delta\nu_D$ is the Doppler width at room temperature.

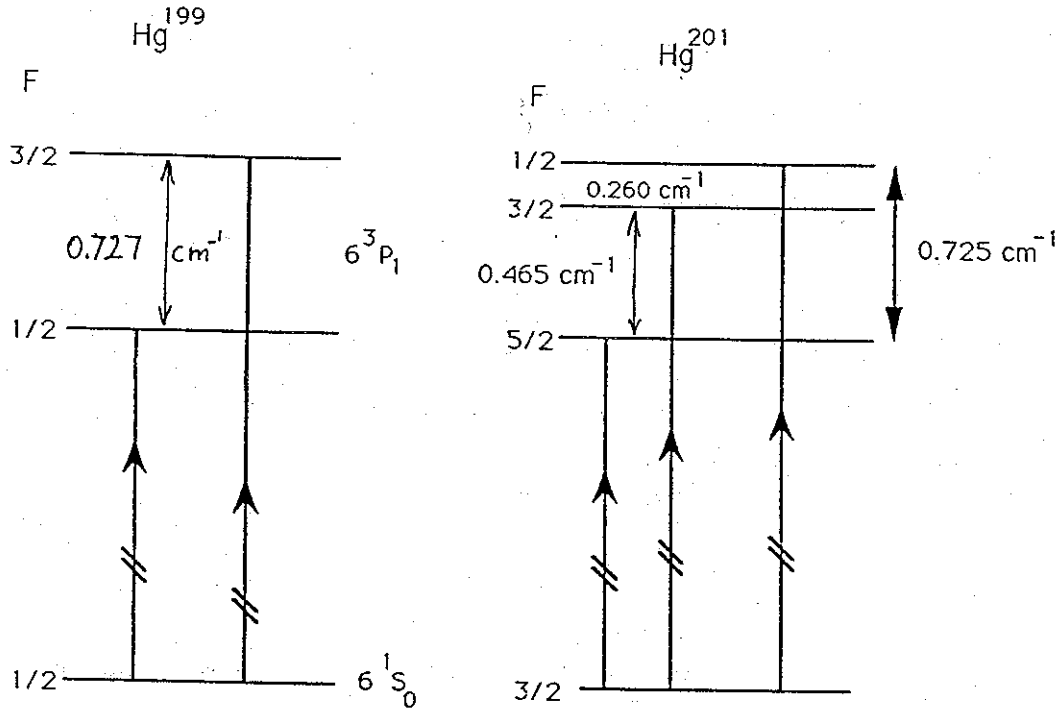

Figure 5.3: Energy scheme of the hyperfine structure of Hg 2537 Å for the odd isotopes ^{199}Hg (I=1/2) and ^{201}Hg (I=3/2).

and ^{198}Hg (table 5.2). The F value is that of the excited state 6^3P_1. These coincidences suggest the use of lamps with separated mercury isotopes to obtain a more efficient optical pumping on the ^{199}Hg and ^{201}Hg isotopes.

We shall, from now on, talk about pumping ^{199}Hg with a ^{204}Hg excitation light without making the explicit specification that we, in reality, mean the ^{199}Hg(F=1/2) component. The optical pumping mechanism in this case is quite straightforward and is exactly similar to the three level model of chapter 2 with the exception that the C level is now made up of two sub-levels. If the ^{204}Hg line is σ^+ polarised (by using a polariser and a $\lambda/4$ plate that transmits in the ultraviolet region of the spectrum) we can build up an excess of atomic population in the m_F=+1/2 of the 6^1S_0 ground state (figure 5.4).

^{199}Hg has served as an important test case for the basic theory of optical pumping. A well detailed comparison between theory and experiment can be found in the thesis of Cohen-Tannoudji [Coh 62a, b].

High degrees of polarisation reaching 80% could be obtained [Cag 61].

Finally, for the sake of comparison with orientations in the case of alkali atoms, two important differences occur: first the spin angular momemtum of the ground state is purely nuclear in the case of mercury. Therefore, one would expect to obtain long relaxation times. Secondly, however, the time constant to optically orientate Hg atoms with the 2537 Å resonance line is rather long due to the poor transition probability for this line as it was mentioned earlier. Very intense microwave light sources are therefore desirable for a successful orientation.

Isotope	Exited Level number F	Position of Component ($10^{-3}\ cm^{-1}$)
201	1/2	+ 229.4
199	3/2	+ 224.6
198	1	0.0
201	3/2	−22.6
200	1	− 160.4
202	1	− 337.2
201	5/2	− 489.3
204	1	− 511.1
199	1/2	− 514.3

Table 5.2: Hyperfine structure separations of the 2537 Å Hg resonance line. The Doppler width at room temperature is $34 \times 10^{-3} cm^{-1}$

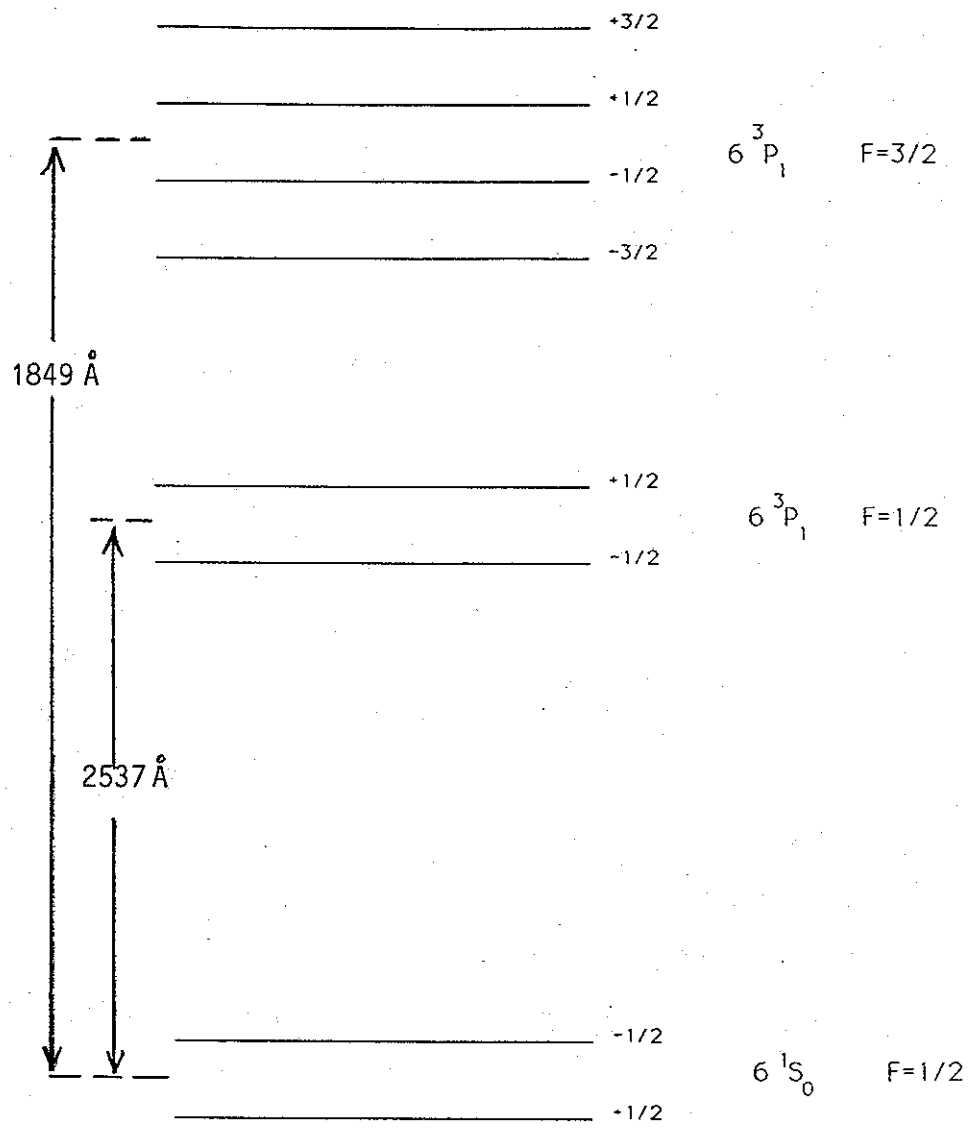

Figure5.4: Zeeman structure of 2537Å of ^{199}Hg.

5.2. - Experiments with Sealed Off Quartz Cells

5.2.1. - The Light Source

We used a conventional electrodeless quartz source bulb in a microwave cavity connected to a magnetron coupled to the cavity through an antenna $\lambda/4$ cm long. The stem of the light source sits inside an aluminium block which is fixed to a semiconductor cooler. Figure 5.5. shows the different components of the light source that we are going to describe individually and in more detail in the following sub-sections.

5.2.1.1. - Lamp Fabrication

We show, in figure 5.6., the glassware that was set up in the laboratory in order to make such lamps. These consist of a 1cm diameter, 2mm thick quartz discs fixed to a 4cm long quartz tubing and 2mm in diameter. In order to practise we first used natural Hg to fill a lamp. When we built up enough experience and confidence in the technique we then filled a few lamps with 58% enriched ^{204}Hg which is much more expensive than natural Hg. The filling technique adopted is as follows:

Valve A is always kept open unless the whole system is switched off, in which case it is closed so as to isolate the system from the rotary pump. The system is pumped down with a combination of a metal oil diffusion pump and a vac-ion pump when valves B and C are opened. The liquid nitrogen trap is used to prevent Hg coming off the

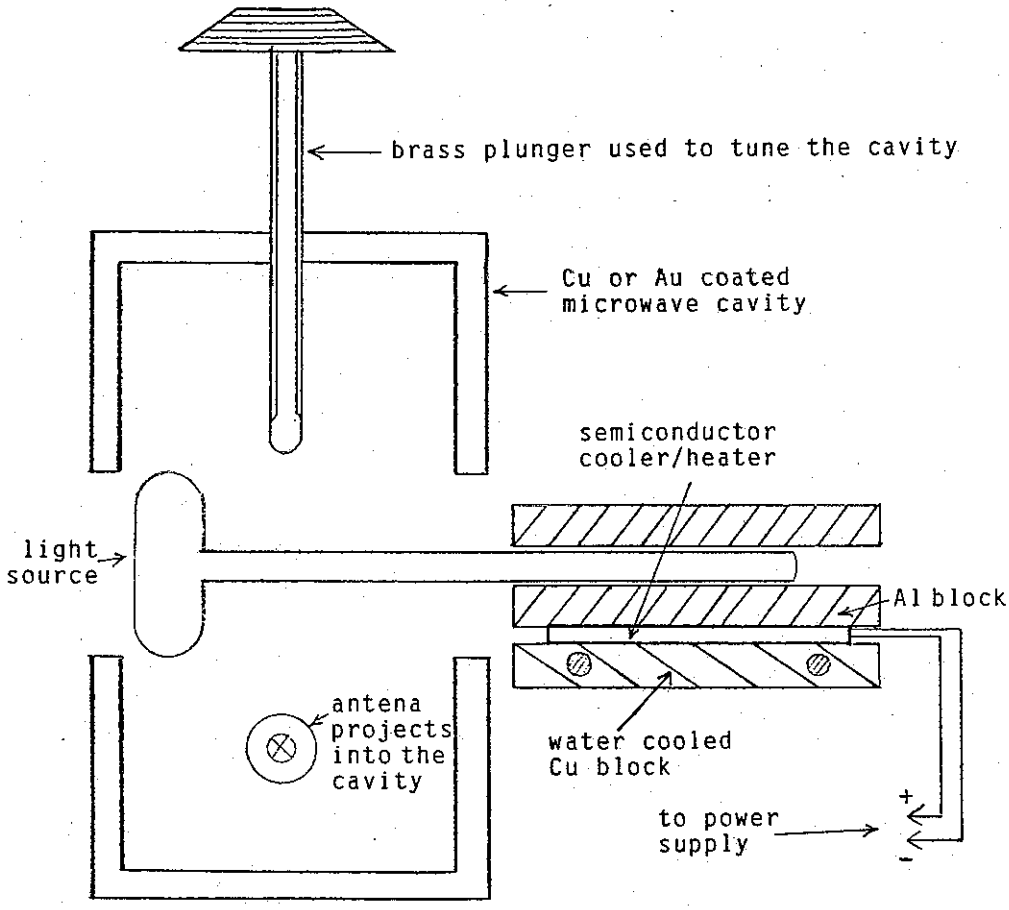

Figure 5.5: Diagram showing the light source in the microwave cavity. The stem of the source is fitted in a Aluminium block cooled with a semiconductor cooler.
(diagram not to scale).

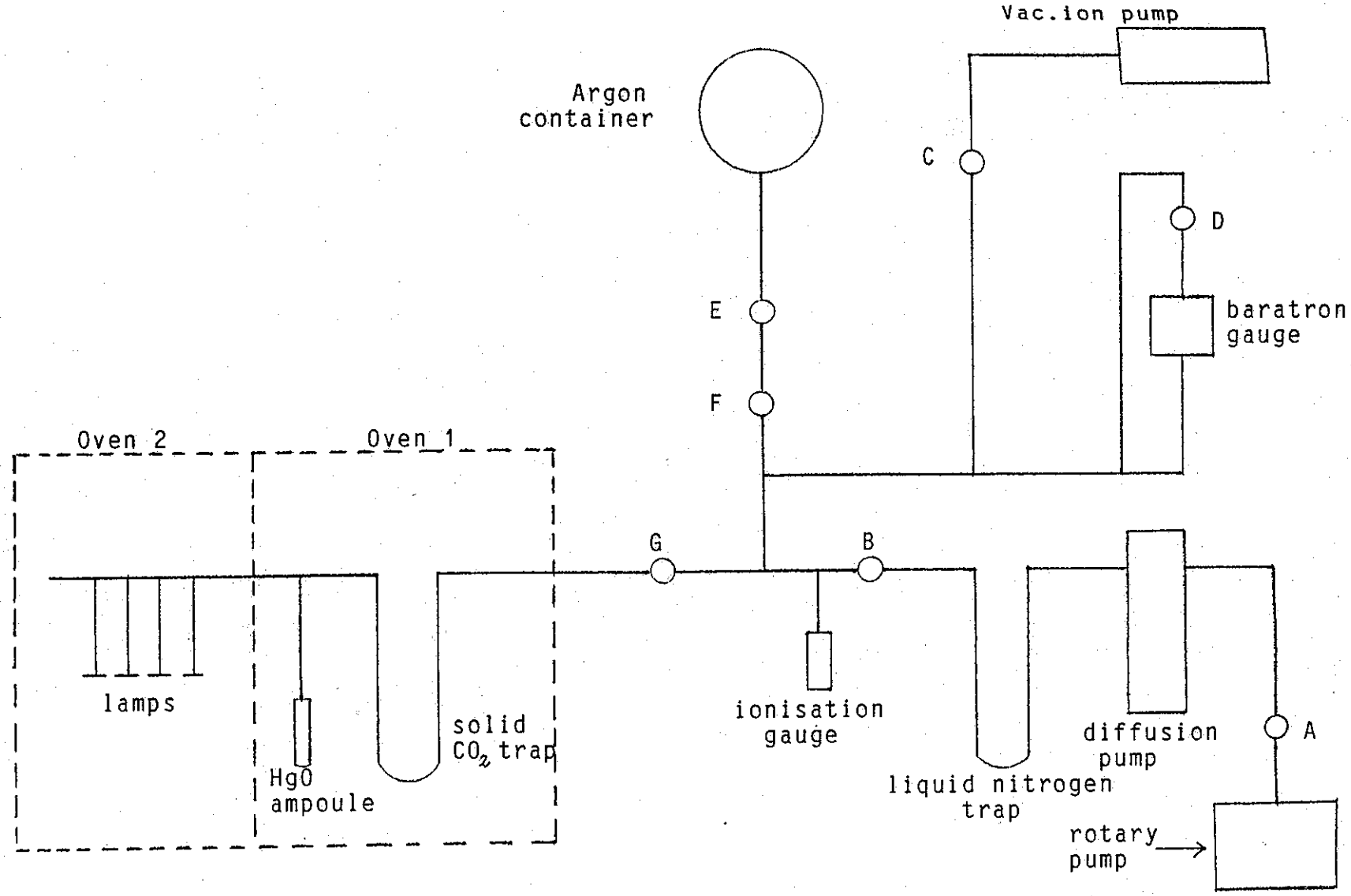

Figure 5.6: The Hg light source fabrication system.

diffusion pump from reaching the rest of the system. The system is gently heated with a torch in order to drive off any water vapour deposited on the glassware. The ion gauge fixed between valves B and G is used to measure the pressure in the system. The best pressure reached was 10^{-7} torr. The next step in the filling procedure is to outgas the quartz bulbs and glass. In order to do that, oven 2 is switched on for four hours with a running temperature of 1000°C. Oven 1 is also turned on but runs at a lower temperature of 400°C. Note that all the tubing in oven 2 is made out of quartz. Since valves G and B are open, any impurities released are pumped out of the system. After allowing the system to cool down to room temperature, valves B, C and D are closed. Valve E is then opened and a quantity of Argon is admitted in the piece of tubing between E and F. E is then closed and valve F opened. Two torrs of Argon are admitted to the whole system and F is closed. The Argon pressure is measured by the Baratron gauge. This actually measures the differential pressure between its sides. Since valve D was closed before any Argon was admitted the space between this gauge and D is at 10^{-7} torr, whereas the other side is at Argon pressure. The lamps are then further cleaned by driving a 5 GHz microwave discharge at 170 watts to bombard impurities off the walls. It is run for 1/2 hour after which the whole system is pumped out. This operation is repeated a few times until the light spectrum of the discharge (as observed with a hand held prism spectrometer) does not exhibit any spectral bands emitted by foreign molecules. Once the lamps are thoroughly cleaned the system is pumped out again and the internal break-seal of

the ampoule containing mercury oxide (HgO) powder is broken. This is done by dropping a piece of metal on the ampoule seal using a magnet from the outside. The HgO powder is then gently heated to 500°C using a torch. The trap near the ampoule is cooled down with dry ice alcohol mixture to trap Hg released from the HgO powder, letting oxygen gases escape to the pump. When all the powder has been decomposed valve G is closed and the dry ice trap is allowed to warm up. The lamps are then cooled down to liquid nitrogen temperature and the dry ice trap warmed gently in order to transfer Hg to the lamps. Hg is shared out among the lamps admitting about 1/2 mg in each lamp. Valve G is then opened and the lamps are sealed off after being filled with 2 torrs of Argon. Lamps made in this manner can run for hundreds of hours before they deteriorate [Lam 87].

5.2.1.2. -The Microwave Generator

Figure 5.7 shows the details of the microwave generator. It consists of a magnetron running at 3.5 Kvolts with a stabilised anode current of 20 mA. The input current to the magnetron is set by the voltage developed across R which is compared with a reference voltage and the magnetron high current-low voltage filament supply is produced by a switched mode power supply. The magnetron produces about 60 W of 2.45 GHz microwaves with an efficiency of 70-80 %, coupled into a 50 Ω coaxial cable using a cylindrical copper cavity on which the magnetron is mounted. The microwave power is fed to the smaller copper cavity which contains the source bulb.

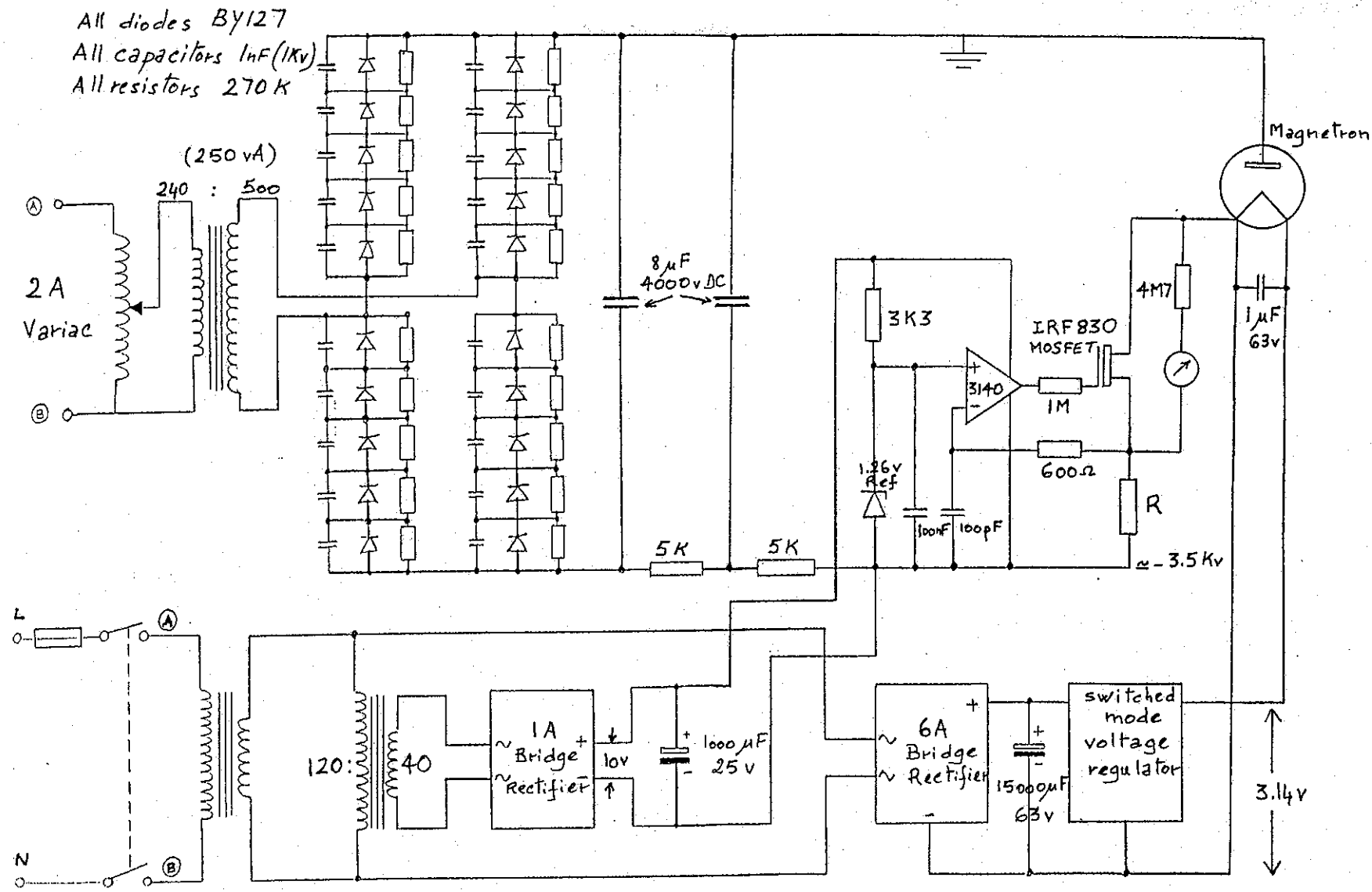

Figure 5.7: Stabilised magnetron power supply.

This small cavity consists of a 2 inch long square copper waveguide 1.25 inches wide. Two holes 1.5 cm in diameter are made on two opposite sides in order to place the lamp. The ends of the waveguide are closed with brass lids. From the end of the transmission cable, sticks out (into the cavity) a 1.5 cm long copper wire that serves as an antenna. The length of this antenna is approximately 1/4 of the microwave wavelength. In order to tune the cavity a 3/16 inch diameter brass rod is screwed in from one of its ends. When the lamp is placed in the cavity it is positioned in such a way that the discharge is concentrated in the main bulb and not in the stem. For best running conditions the inside of this cavity should be coated with silver or gold.

5.2.1.3. - The Semiconductor Stem Cooler

This is a 4cm x 4cm x 0.5cm solid state Peltier effect heat pump. when supplied with a suitable current it can either cool or heat. More precisely, it only transfers or pumps heat from one of its sides to the opposite side. We connected one of its sides to the aluminium block that holds the lamp and the other side to a water cooled copper block. Heat can then be removed from the lamp and transferred to water or vice versa. The main characteristics of this device is a 75 watts maximum heat pump capacity, a maximum temperature difference of 60°C, a maximum current of 9 Amps, a nominal voltage of 15.4 volts DC at maximum current and a maximum operating temperature of 150°C.

5.2.2.-The Absorption cell

We used two different absorption cells. The first one, given to us by Dr. S.Lamoreaux of the University of Washington is a quartz cylinder 7.5 cm in diameter and 7.5 cm high. It is closed on both sides with two circular glass windows fixed to it by means of a leak tight glue (Torr seal glue). The inner surface of this cell is coated with a transparent Teflon film. This cell contains 10^{-6} torr of gaseous 93% enriched ^{199}Hg. One expects over a long period, Hg to leak out of the cell seals and reduce the cell's lifetime. However, the advantage of putting a purely gaseous Hg in such cells, is to avoid cooling them down from room temperature in order to attain reasonable vapour pressures (at room temperature Hg absorbs practically 100% of an incident light beam).

One problem that one has to face up to when using UV light is the tendency of this kind of light to destroy the inner walls coating and the release of odd gases (such as O_2) into the cell.

The second cell we used (called the Sussex cell hereafter) was made in this laboratory in a manner very similar to the fabrication of the lamps as described in section 5.2.1.1. . The only difference is that the cell was first coated with Surfasil and subsequently baked for 4 hours at about 160°C and not at 1000°C as it was the case with the lamps. An amount of metallic 66% enriched ^{199}Hg (≈10 mg) was admitted into the stem of the cell before sealing it off and separating it from the fabrication system. We used a cylindrical quartz container 2.5 cm in diameter and 5 cm long. The main drawback of this kind of

cell is that the stem has to be cooled down in order to do any optical resonance experiments.

5.2.3.- **The Detector**

We used the Hamamatsu R166 solar blind photomultiplier. We found that shielding from ambient light is virtually unnecessary. It uses a Cs-Te photocathode which has a quantum efficiency of 17.6% at the Hg 2537 Å line. It has a cathode radiant sensitivity of 36.1 mA/W and a anode dark current of 0.02 nAmps. The window material is synthetic silica. The spectral response ranges between 160 nm and 320 nm peaking at 200 nm. The drive unit for this photomultiplier is shown in figure 5.8. We used a Hamamatsu high voltage power supply of the D.P. type. This features a built-in DC-DC regulated converter from a +15 v source supply voltage. The output voltage is controlled by a resistance programming technique (with a 5 KΩ potentiometer) and ranges between -300 to -900 volts enabling a control in the photomultiplier gain. The AC-AC transformer was intentionally built in a separate box from the rest of the circuit and kept a few feet away from it in order to minimize any 50 Hz magnetic pick-up.

The current out of the photomultiplier is fed to a conventional current to voltage converter with a feedback resistor of 1MΩ giving 1V/μAmp DC output. This amplifier has a low pass frequency response with a cut-off frequency of 16Hz. This frequency is determined by the 1 MΩ resistor and a feedback capacitor (10nF) in parallel with it. By changing C one can easily change the frequency response of this amplifier whenever required.

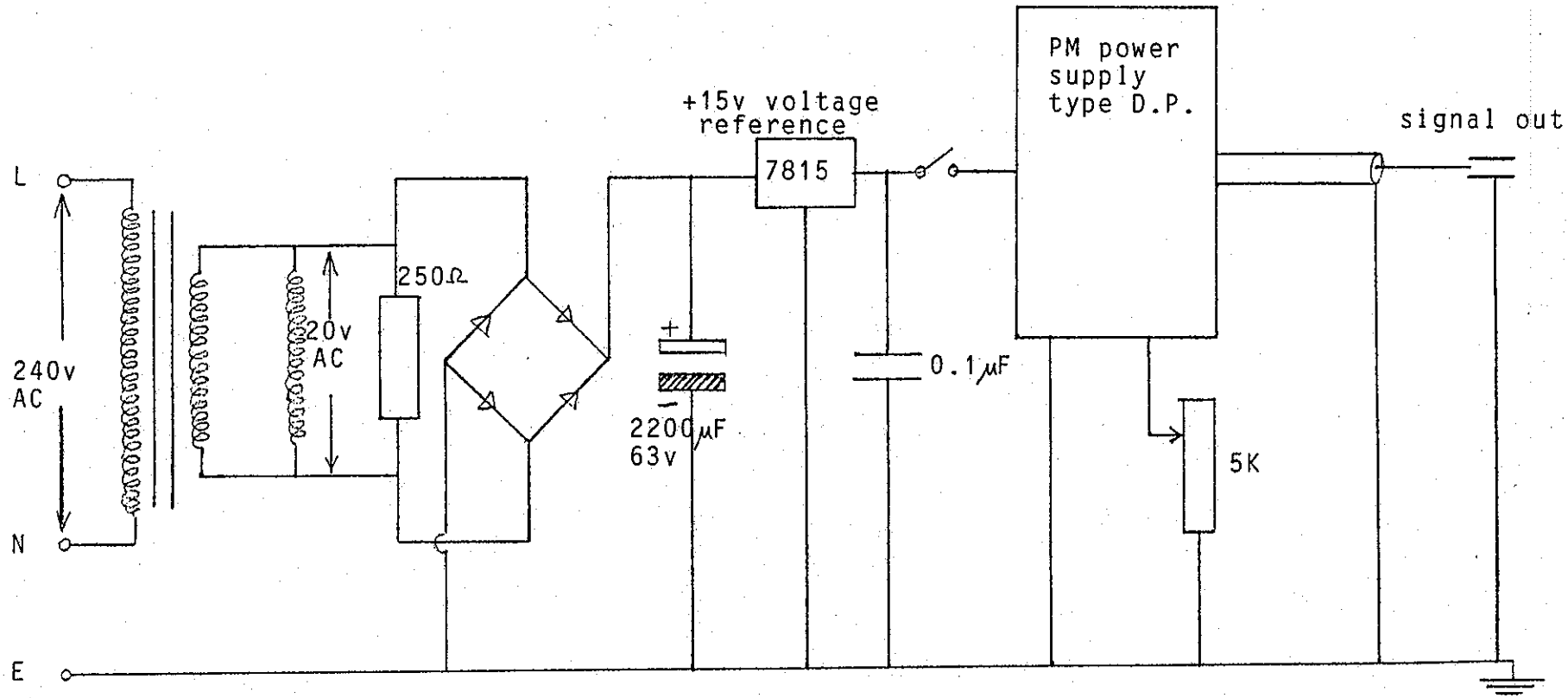

Figure 5.8: Circuit diagram of the photomultiplier drive unit. The PM power supply is of a Hamamatsu make.

5.2.4.-The Optical Components

As far as the optics is concerned, one is usually faced up to a compromise situation between the performance of a component and the light losses induced in it. Since we are interested in the UV part of the spectrum the choice offered by the manufacturers is rather limited.

1.The linear polariser (LP): We used the Oriel far UV-visible linear polariser. It employs polymer films which polarise light by dichroism. These films are deposited on a 1/16 inch thick quartz disc 2 inches in diameter. We measured the transmission of this polariser at the unpolarised Hg wavelength of 2537 Å and found it to be equal to 17.5%. Note that this figure is to be doubled if the incident light were fully polarised along the polariser axis. We used the above mentioned photomultiplier for the detection and a UV interference filter to single out the 2537 Å line.

2.The quarter wave plate: This was also purchased from Oriel. It is a 14.4 mm diameter zero order quartz plate. Unfortunately, this is a rather small diameter plate which restricts the amount of circularly polarised light to be used in the experiment. However, we found that the transmission of this plate at the wavelength of interest is rather good and amounts to 83.4%. The combined LP+$\lambda/4$ plate system transmits about 14% of an unpolarised incident beam. By applying the procedure outlined in section 4.3.3. and figure 4.3, we could find the optimum orientation of the $\lambda/4$ plate with respect to the LP for maximum circular polarisation. Assuming that this circular polariser produces mainly σ^+ light, we found that for an amount of

$7\sigma^+$ light there is $1\sigma^-$ polarised light. Defining the light polarisation as

$$P_L = \frac{\sigma^+ - \sigma^-}{\sigma^+ + \sigma^-} \qquad (5.1)$$

we calculate that the resulting light is 75% σ^+ polarised. In equation 5.1, σ^+ and σ^- represent the actual amount of one or the other light polarisation.

3.The light guide tube: We used highly polished aluminium coated mylar sheets rolled to form a cylindrical guide. We found that light polarisation deteriorates along the guide. So, we only used them when the light polarisation was unimportant, from the source to the polariser, for example, or from the cell to the detector. A tube 1 inch in diameter and 24 inches long transmits about 29% of the incident light with an exit angular divergence of about 10°.

4.Transmission through quartz windows: to be used in experiments done in an aluminium vessel. We used 3 mm thick and 40 mm in diameter polished spectrosil B discs purchased from Comar. Light transmission through these windows is measured to be about 92% in the UV. However, when they are coated with a film of polystyrene (as this will be required for the resonance experiment) the amount of transmitted light is found to be very dependent on the thickness of the film and its isotropy. For different coating thicknesses (typically a few microns) the transmission varied between 40% and 80%. This shows that these windows could be reasonably coated with polystyrene and still transmit 80% of the incident light. From this figure and the 92% transmission through uncoated windows we find that light

transmission through a layer of polystyrene a few microns thick (3 to 10μm) is around 87%.

5.Transmission through empty absorption cells: The purpose behind measuring light transmission through absorption cells walls is to take into account the amount of light absorbed by the walls off the total flux incident on the cell. This is rather important since it is the flux of photons interacting with the vapour that determines the time it takes to pump the atoms. The measurements were done by shining light onto the cell followed by a circular diaphragm that focuses the light onto the PM photocathode. The same experiment was done after removing the absorption cell. The two light intensities obtained were then compared. As far as the Sussex cell is concerned, this measurement was done using an empty identical cell. The transmission was 80% through the two walls which leads to 89% transmission through a single wall.

On the other hand, light transmission through the Washington cell was done by direct comparison of measured light intensity with the cell across and away from the beam. This experiment resulted in 55.3% transmission through the cell and thus a transmission of 74.4% through a single wall.

5.2.5.- Light source noise measurements.

Noise generated by the light source is of prime concern in optical pumping experiments. This plays an important role in the ultimate signal to noise ratio achievable in such experiments. If we wanted to determine the nutation frequency of a group of atoms in a given magnetic field,

the accuracy of the measurement would be at least limited by the source shot noise. For this reason, we set off to estimate the source noise under different conditions. Unfortunately, shot noise from the source is not the only noise involved in the experiment. There is an additional source noise due to the electron multiplication process in the photomultiplier. Since this noise is white noise, we will present our experimental results on noise measurements as if the light source noise were the only contributing noise and then take the photomultiplier noise into account.

In order to look at noise in a wide frequency bandwidth the low-pass cut-off frequency of the I/V converter was shifted to about 5 KHz by changing the feedback capacitor C from 10 nF to 33 pF. The source was set to shine light through the 3-layer μ-metal shield, onto the polarisers and the Washington absorption cell and finally collected by a light guide to the photomultiplier positioned on the opposite side of the shield (figure 5.10). The signal out of the I/V converter was then fed to a PAR wideband rms voltmeter (model 124 A) which has a tuned amplifier with Q variable from 1 to 100.

The equivalent noise bandwidth (ENBW) given by the PAR manufacturer is

$$\text{ENBW (Hz)} = \frac{f_0}{Q}\frac{\pi}{2} \qquad (5.2)$$

The rms noise was read from a display meter provided on the front panel of the PAR. The PM gain was set to its minimum with a supply voltage of -314 v. The light source stem was at a temperature of +26°C.

5.2.5.1.- Source noise as a function of frequency.

The PAR was set to work in a bandpass mode with Q=20. The center frequency was then varied and the corresponding noise was read from the meter. The results summarised in table 5.3 suggest that the nature of noise is rather white throughout the spectrum. The rms noise/$\sqrt{ENBW}$ values are practically constant except at 50 Hz and 100 Hz where one expects some mains pick-up. However, one cannot assume that it is of shot noise nature as yet.

5.2.5.2.-Determination of the photomultiplier gain from shot noise measurements.

The value of the PM gain to be determined in this section is not the definite one. The actual value will be calculated after considering the PM noise as well as the light source noise. Although gain figures are quoted by the manufacturer for each type of PM tube, we decided to measure our PM gain using shot noise measurements and the result

$$i_{RMS} = \sqrt{2GeI\Delta f} \qquad (5.3)$$

where G is the PM gain, e the electron charge, I the output current from the PM tube and Δf is the equivalent noise bandwidth over which the measurement was done.

In order to make sure that the noise measured is dominated by shot noise, we cut down the light intensity emerging from the source by a factor of 100 by placing a polythene sheet across the light. The measuring frequency

$f_0(Hz)$	total photo-current (μA)	RMS noise (pA)	ENBW (Hz)	$\frac{RMSnoise}{\sqrt{ENBW}}$ (pA/$\sqrt{Hz}$)
3000	5.34	1200	235.6	78.2
2000	5.33	1100	157.1	87.8
1000	5.32	800	78.5	90.3
500	5.30	580	39.3	92.5
400	5.28	520	31.4	92.8
300	5.28	450	23.6	92.6
200	5.22	370	15.7	93.4
100	5.11	380	7.85	135.6
90	5.09	260	7.07	97.8
80	5.09	230	6.30	91.6
70	5.10	220	5.5	93.8
60	5.10	230	4.7	106.1
50	5.10	770	3.9	390
40	5.11	170	3.14	95.9
30	5.11	150	2.36	97.6
20	5.12	120	1.57	95.8
8.33	5.12	65	0.65	80.6
3	5.12	40	0.24	81.6

Table 5.3: light source noise in different frequency domains. ENBW is the equivalent noise bandwidth.

f_0 was set to 1000 Hz, well above the onset of flicker noise, and the rms noise was measured as a function of bandwidth. The same measurement was then repeated at $f_0 = 8.33$ Hz, the Hg resonance frequency in the 10mGauss magnetic field used in our experiments. These measurements are presented in tables 5.4 and 5.5 respectively. They show that the rms noise is proportional to the square root of the ENBW which confirms that the noise is of shot noise nature. By applying equation 5.3 to the whole set of data in table 5.4 we calculate an average value for the PM gain of 4550 (as it was mentioned before this is not the final value of G). From table 5.5 it seems that some 50 Hz pick up is present at $f_0 = 8.33$ Hz which can be seen at low values of Q.

In section 5.2.5.1. it was said that noise from 3 kHz down to 3 Hz was rather white (table 5.3). Since the PM gain is now known, The validity of equation 5.3 for this data can be tested. For each frequency of table 5.3 the rms noise was calculated from equation 5.3. The results agreed rather well with the experimental values listed except, of course, for the two frequencies 50 Hz and 100 Hz. In conclusion, it is safe to affirm that the noise of the light source is given by the shot noise result from 5 Hz to 1 KHz.

5.2.5.3.- Source noise as a function of bandwidth.

More noise measurements were done on the full photon flux emerging from the light source. Tables 5.6 and 5.7 show these measurements done at 8.33 Hz and 1 KHz respectively. Applying equation 5.3 to this data confirms that the source

Q	total photo-current (μA)	RMS noise (pA)	ENBW (Hz)	$\frac{RMSnoise}{\sqrt{ENBW}}$ (pA/$\sqrt{Hz}$)
1	0.06	355	1571.0	9.0
2	0.06	260	785.4	9.3
5	0.06	168	314.2	9.5
10	0.06	118	157.1	9.4
20	0.06	84	78.5	9.5
50	0.06	53	31.4	9.5
100	0.06	35	15.7	8.8

Table 5.4: RMS noise as a function of bandwidth at a center frequency of 1 KHz.

Q	total photo-current (μA)	RMS noise (pA)	ENBW (Hz)	$\frac{RMSnoise}{\sqrt{ENBW}}$ (pA/$\sqrt{Hz}$)
1	0.061	60	13.10	16.6
2	0.061	34	6.50	13.3
5	0.061	17	2.60	10.5
10	0.061	11	1.31	9.6
20	0.061	8	0.65	9.9
50	0.061	5	0.26	9.8
100	0.061	4	0.1	11.1

Table 5.5: RMS noise as function of bandwidth at a center frequency of 8.33hz

Q	total photo-current (μA)	RMS noise (pA)	ENBW (Hz)	$\frac{RMSnoise}{\sqrt{ENBW}}$ (pA/$\sqrt{Hz}$)
1	4.93	350	13.10	96.7
2	4.92	260	6.54	101.7
5	4.92	150	2.62	92.7
10	4.92	110	1.31	96.1
20	4.91	70	0.65	86.8
50	4.91	40	0.26	78.4
100	4.91	25	0.13	69.1

Table 5.6: Source noise at 8.33 Hz as function of the ENBW

Q	total photo-current (μA)	RMS noise (pA)	ENBW (Hz)	$\frac{RMSnoise}{\sqrt{ENBW}}$ (pA/$\sqrt{Hz}$)
1	4.89	3200	1571.0	80.7
2	4.89	2300	785.4	82.1
5	4.88	1500	314.2	84.6
10	4.88	1100	157.1	87.8
20	4.87	760	78.5	85.8
50	4.87	470	31.4	83.9
100	4.86	300	15.7	75.7

Table 5.7: Source noise at 1 KHz as function of the ENBW

noise is shot noise even at these high intensities. Note that these are the usual intensities involved in the free precession experiments described later in the course of this work.

5.2.5.4.- Source noise as a function of total intensity.

The light source noise was also found to be proportional to the square root of the total light intensity indicating once again that equation 5.3 is applicable and that the source noise is shot noise. This can be readily checked by comparing table 5.4 to 5.7 or table 5.5 to 5.6. Moreover, noise was also checked to be proportional to $\sqrt{G}$.

5.2.6.- Photomultiplier noise

This noise has to do with the multiplication process on each dynode of the PM tube. We cannot assume that the pulse rate at each stage is uniform but we will assume that it obeys a Poisson distribution.

1°/ Case of one dynode:

Let r be the height of a pulse arriving per second, p_r the probability of having such a pulse height and N the number of pulses/sec.

$$\text{The count rate (of pulse height r)} = N\,p_r \qquad (5.4)$$

per second. Therefore, we have

$$\text{Noise amplitude} \propto \sqrt{N\,p_r}\;r \qquad (5.5)$$

which means that

$$\text{Noise power} \propto N\, p_r\, r^2 \tag{5.6}$$

Since we are in a situation where the incoming pulses are of different heights, the total noise power is then

$$\text{Total noise power} \propto \sum_{r=0}^{\infty} N\, p_r\, r^2 \tag{5.7}$$

$$\propto N\langle r^2 \rangle \tag{5.8}$$

If we assume that the distribution of heights is a Poisson distribution we have

$$\langle \mu \rangle = \sigma^2 = \langle (r - \mu)^2 \rangle \tag{5.9}$$

where σ is the standard deviation and μ the mean. From the last equation we can easily show that

$$\langle r^2 \rangle = \mu + \mu^2 \tag{5.10}$$

thus

$$\text{Total noise power} \propto N\,(\mu + \mu^2) \tag{5.11}$$

On the other hand, if the distribution of heights were uniform

$$\text{Total noise power (uniform)} \propto N\,\mu^2 \tag{5.12}$$

From 5.11 and 5.12 we can write a correction factor R as

$$R = \frac{\text{Total noise power(Poisson)}}{\text{Total noise power(uniform)}} = 1 + \frac{1}{\mu} \qquad (5.13)$$

Equation 5.13 suggests that the effect of one dynode is to multiply the noise power of the light source by $(1 + \frac{1}{\mu})$. The mean μ is effectively equal to the gain per stage. Thus

$$\mu = \sqrt[9]{G} \qquad (5.14)$$

but G=4550, therefore $\mu = 2.55$ and $R = 1.4$. This value is just a first estimate of μ since we used the value of G assuming a uniform pulse height distribution.

2°/ Case of the 9 dynodes altogether:

According to reference[Bre 55]

$$\frac{\langle r_t - \mu_t \rangle^2}{\mu_t^2} = \frac{1}{\mu - 1} \qquad (5.15)$$

where r_t is the total number of electrons detected after the 9 dynodes and μ_t is the mean number of electrons produced after all the stages. This equation reduces to

$$\frac{\langle r^2 \rangle}{\mu^2} - 1 = \frac{1}{2.55 - 1} = 0.65 \qquad (5.16)$$

or

$$\langle r^2 \rangle = 1.65\, \mu^2 \qquad (5.17)$$

Using equations 5.8 together with 5.17, the correction ratio for 9 stages reads

$$R_t = \frac{\text{Total noise power(Poisson)}}{\text{Total noise power(uniform)}} = \frac{N\,1.65\,\mu^2}{N\,\mu^2} \qquad (5.18)$$

thus

$$R_t = 1.65 \qquad (5.19)$$

Now, the value of the gain can be corrected, and we find

$$G = \frac{4550}{1.65} = 2758 \qquad (5.20)$$

From this value of G a new value of μ can be calculated using 5.14. We find $\mu = 2.41$; this implies that $R_t = 1.71$. This iterative process is applied once again until it converges to a fixed limit of μ, R_t and G. Finally, we find that

$$\mu = 2.40 \;;\; R_t = 1.71 \;;\; G = 2661 \qquad (5.21)$$

Note that the main contribution to this photomultiplier noise arises from the first dynode. This is made clear by the value of the so-called correction factor R which is equal to 1.42 in the case of one dynode and 1.71 in the case of 9 dynodes.
The actual value of the PM gain estimated from noise measurements is then 2661 instead of 4550.

5.2.7.-Estimation of the total photon flux:

The determination of the total number of photons arriving from the light source onto the detector per second and unit solid angle is now possible. Figure 5.11 shows the set-up

used in order to measure J. The PM tube was positioned 36cm away from the light source. Before getting to the PM, light is made to go through an orifice 6.4 mm in diameter. The interference filter was used to cut down the light intensity to prevent the PM from saturating. The PM is working at minimum gain (G=2661) and the I/V converter set to 1 V/μAmp. Under these conditions, the total current detected at the output of the PM tube was I = 6.68 μAmps. This quantity was obtained after subtracting the effect of the ambient light. The number of photons impinging on the photocathode per second is

$$J\,(\text{photons/sec}) = \frac{I}{e\,G} = 1.6\text{x}10^{10} \qquad (5.22)$$

Taking the effect of the interference filter (transmission T_f = 15.3%) and the quantum efficiency of the photocathode (QE = 17.6%) into account, we obtain the photon flux emerging from the source per unit time

$$J = \frac{I}{eG\,QE\,T_f} = 5.8\text{x}10^{11}\ \text{photons/sec} \qquad (5.23)$$

The solid angle used is determined by the area of the diaphragm and the distance from the source to the tube

$$d\Omega = \frac{A}{d^2} = 2.48\text{x}10^{-4}\ \text{Str.} \qquad (5.24)$$

Hence the total photon flux per unit time and unit solid angle is

$$J = 2.34\text{x}10^{15}\ \text{photons/sec.Str} \qquad (5.25)$$

5.2.8.-Direct absorption experiments

The direct absorption measurements are concerned with the absorption of unpolarised light by unpolarised target vapour, in contrast to free precession experiments where the target is already polarised. Light was passed through the vapour in the Washington cell (fig. 5.9) after cooling down the stem to liquid nitrogen temperature. The stem was inserted into a 3/4 inch diameter copper tubing filled with plasticine in order to insure maximum thermal contact. Shields prevented nitrogen vapours from reaching the PM tubes and these, in turn, were also thermally isolated with polystyrene sheets in order not to affect their outputs through temperature changes. PM2 was used to monitor the incoming light intensity, whereas PM1 was used to look at any changes at the scattered light.

The ratio R of the intensity seen by PM1 to that seen by PM2 was recorded by a computer as the stem cooled from room temperature down to nitrogen temperature. The experiment was performed three times and yielded the following changes in R

$$A_1 = 2.3\% \; ; \; A_2 = 0.9\% \; ; \; A_3 = 0.96\% \; ; \; A_{av} = 1.4\% \qquad (5.26)$$

We see that the results are not very reproducible; this is probably due the very small quantity of Hg contained in the cell.

5.2.9.- Free precession experiments

Figure 5.10 shows the general set-up used to observe

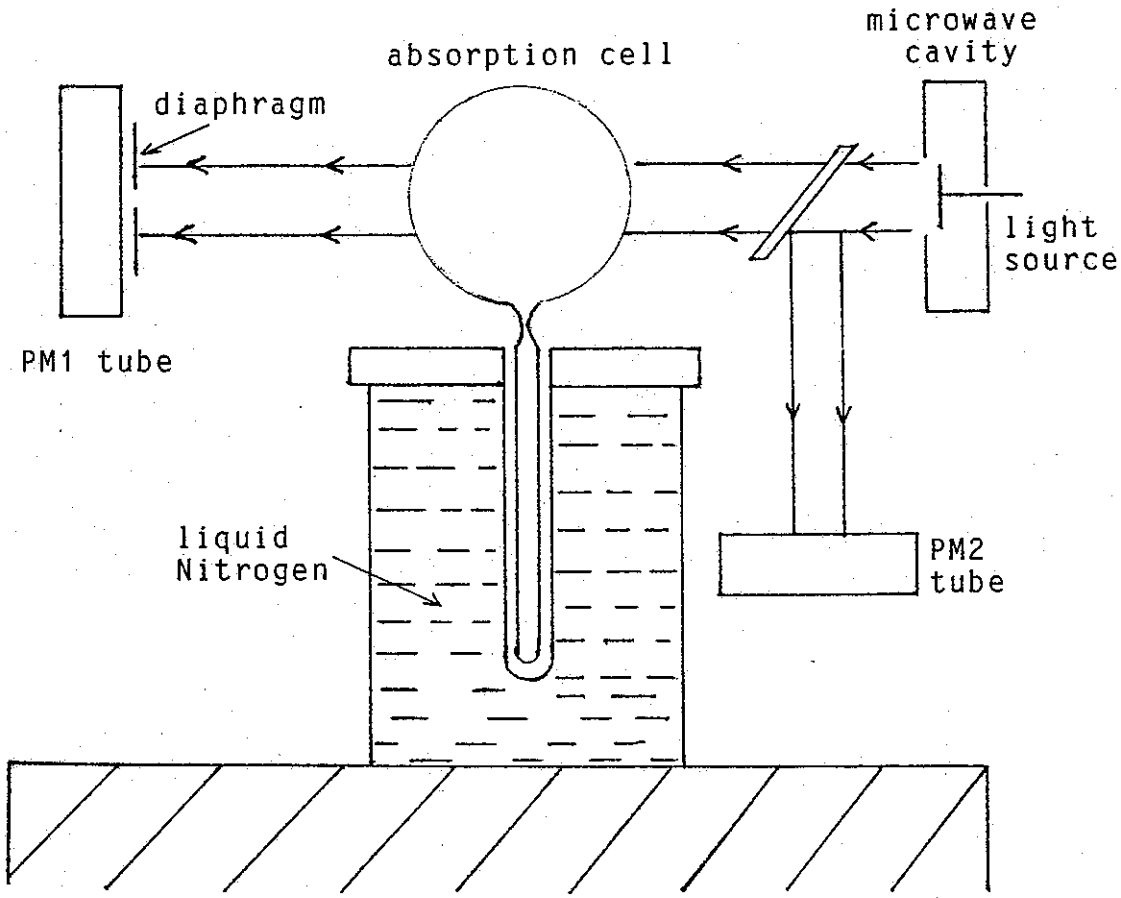

Figure 5.9: Experimental setup used to measure the light absorbed by Hg in the Washington cell. PM2 monitors the source light intensity whereas PM1 monitors the absorbed light by the cell. The transmitted light intensity is measured when the stem is at room temperature and when it is at liquid N_2 temperature.

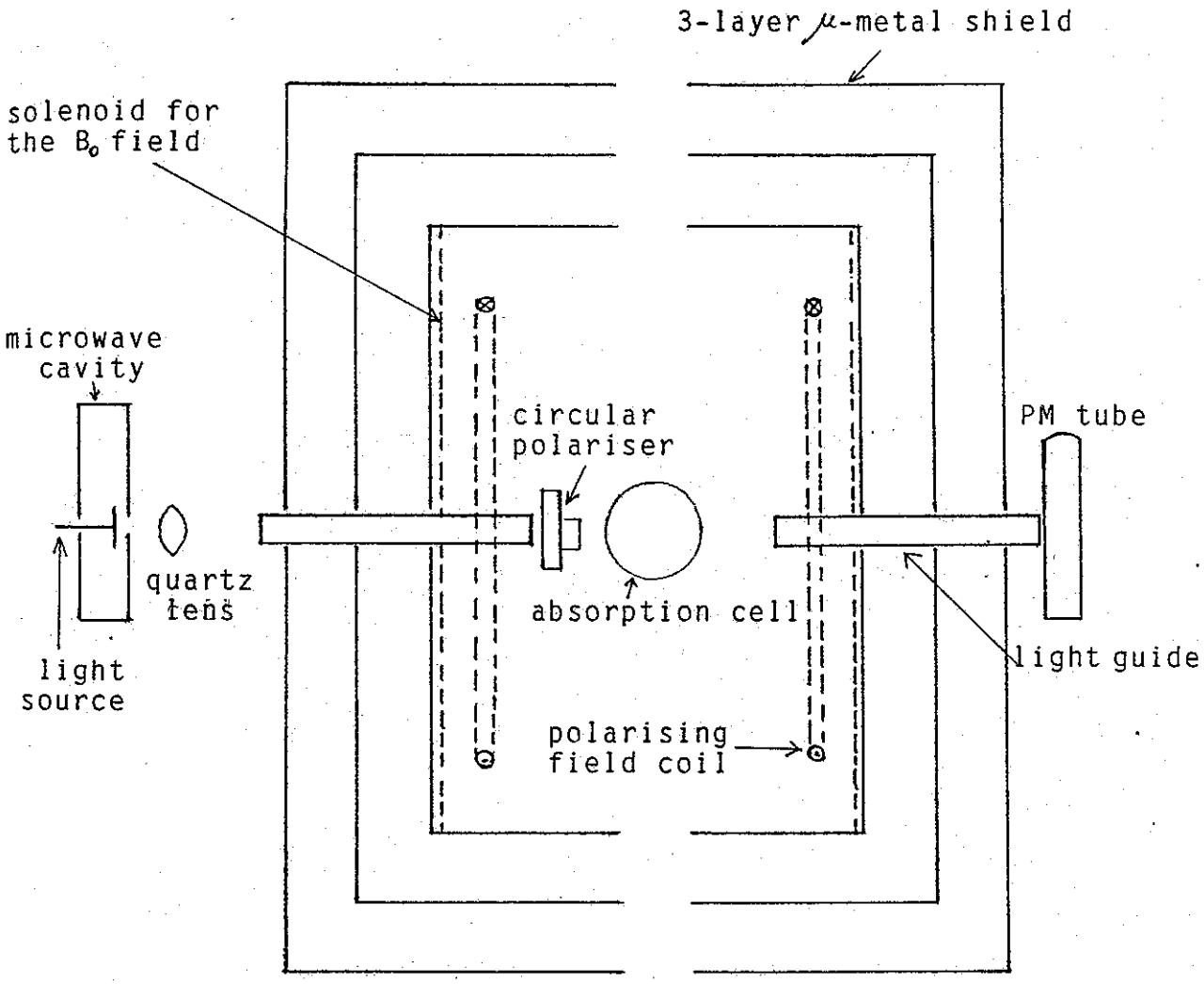

Figure 5.10: General setup of the Hg optical pumping experiment in the 3-layer μ-metal shield.

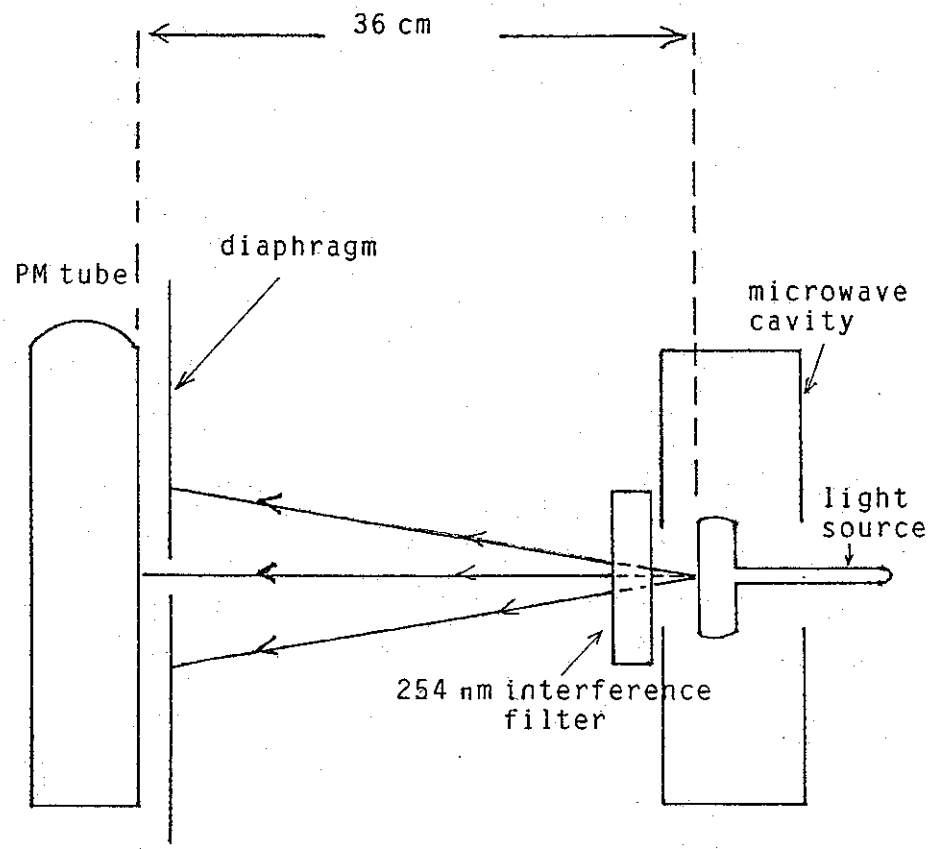

Figure 5.11: Experimental setup used to measure the total photon flux emerging from the light source.

precession of mercury atoms in the Washington cell. The cell is mounted in the same 3-layer μ-metal shield used in the Cs experiments (section 4.3.7.1). Two 22 mm holes were made on opposite sides in order to shine light through the cell perpendicular to the vertical 10 mGauss magnetic field B_0 generated by the coil mentioned in section 4.3.7.3 . A new 3-turn square Helmholtz coil 35 cm high with a separation of 31 cm is used to generate a rather stronger field $B_p >> B_0$, perpendicular to B_0, parallel to the light beam. The circular polariser (LP + λ/4 plate) was positioned just in front of the absorption cell and after the light guide. Had the polariser been placed before the light guide, the polarisation of the incoming light would have been partially destroyed by multiple reflections in the guide. We also used a quartz lens at the entrance of the guide, positioned in such a way that it collected most of the light emerging from the source and concentrated it into the guide. A second light guide was used on the detection side to transmit most of the light emerging from the absorption cell onto the photomultiplier.

The experimental procedure used was as follows:
A magnetic field B_p about four times B_0 is applied to the Hg vapour for a time comparable to the total relaxation time in this cell, about 10 secs, thereby polarising the atoms by the circularly polarised light beam along B_p. B_p is then switched off very quickly, leaving the atomic spins to precess around the remaining magnetic field B_0. The precession occurs around B_0 at the Larmor frequency corresponding to this field. However, because of the finite relaxation processes involved, such as the affect of the container walls, the magnetic field gradients and

the polarising light, this nutation around B_0 does not last for ever but decays with a time constant τ. This atomic behaviour is readily monitored by the transverse σ polarised light beam (as it is explained in chapter 2, section 2.5), giving a damped oscillating signal at the output of the PM tube.

The signal is amplified, filtered and then sampled by a 16 bit ADC under computer control. The computer program given in appendix A6 was written for that purpose. It controls the 16 bit ADC and stores data into memory. The rate at which the data was taken was monitored by an external clock (a frequency synthesizer), we used a rate of 300 reads per second.

The data was then plotted on the screen and finally analysed. One can use the program to calculate the signal amplitude, the rms noise in any portion of the data and subsequently, the signal to rms noise ratio. Furthermore, one can also fit an exponential to the signal in order to determine the decay time constant involved. Figure 5.12 shows such a free precession signal. The output of the PM tube was fed to the current to voltage converter described in Section 5.2.3. This was set to 1 V/μAmp conversion ratio and an upper corner frequency of 16 Hz. The output voltage was then fed to the PAR (section 5.2.5) set on the pass band mode with a 8.33 Hz centre frequency and Q = 5. The bandwidth at these settings is then 2.6 Hz (equation 5.2). The PAR also allowed an AC amplification of 50. The total DC signal emerging from the current to voltage converter was 9.5 V which is equivalent to a photomultiplier current of 9.5 μAmps.

5.3. - Discussion of the Results

By reference to figure 5.12 we can estimate the signal strength S. We will call S the " modulation depth " (MD) which is defined as the difference between the maximum and minimum amplitudes. We will also be calling " noise " the rms noise present with the signal and " S/N " the MD to rms noise ratio. Taking into account the gain introduced by the PAR as well as the effect of the low pass filter present in the I/V converter (which reduces the signal to 89% at 8 Hz) we find that S = 27mV. On the other hand, the total dc incoming light (DC) is 9.5v. This yields a ratio

$$\frac{S}{DC} = 0.28\,\% \qquad (5.27)$$

This value represents the amount of light being absorbed by the vapour in this type of free precession experiment and will be compared to absorption percentages as measured in direct absorption experiments.

Determination of T_p, T_R and the degree of polarisation achieved:

Before considering such a comparison, we will first calculate the atomic polarisation achieved in the sample. In other words, the proportion of Hg atoms whose spins could be orientated along the polarising field B_p under the action of the pumping light. The expression of such a polarisation P is developed in appendix 2. We showed that

$$P = \frac{T_R}{T_R + T_p} P_L \qquad (5.28.a)$$

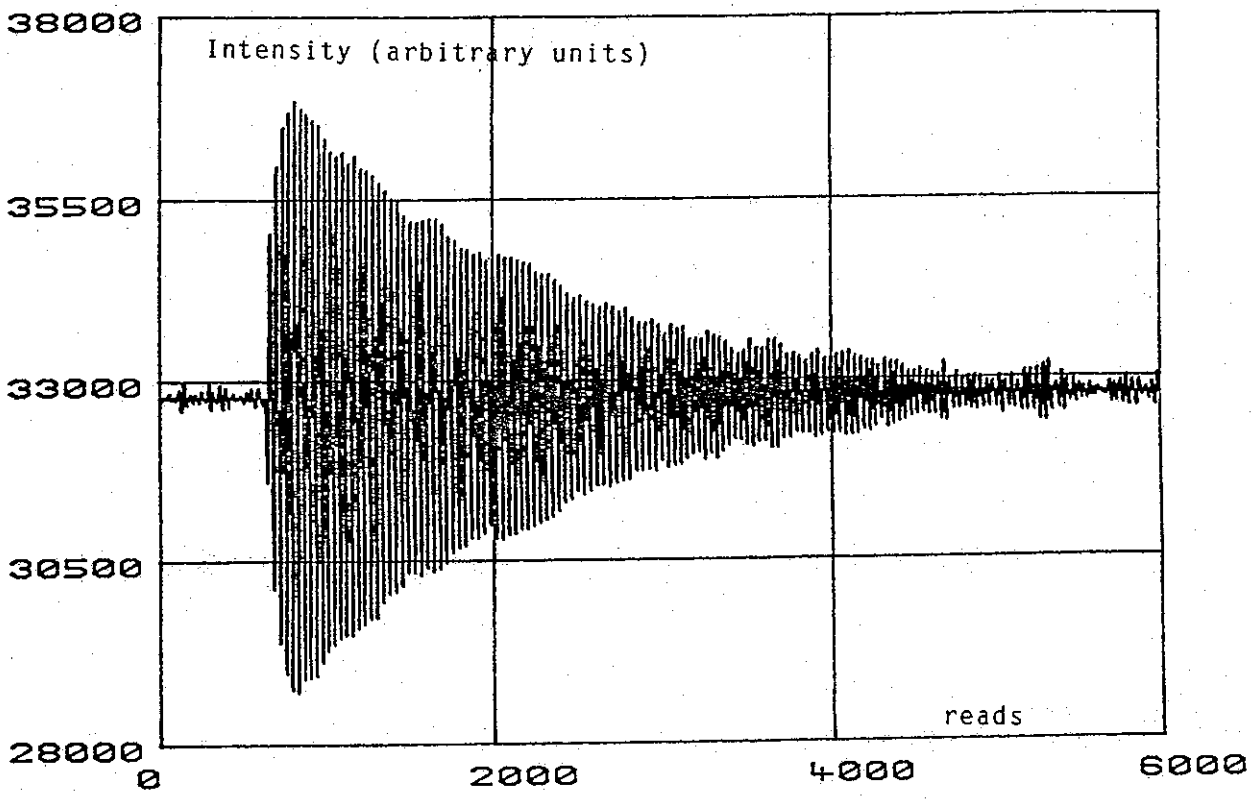

Figure 5.12: Hg free precession signal in a 10 mGauss magnetic field. 300 reads correspond to 1 second.

The light beam in this experiment is being used to polarise and detect so the light polarisation P_L comes in twice and the atomic polarisation becomes

$$P = \frac{T_R}{T_R + T_p} P_L^2 \qquad (5.28.b)$$

where T_R is the wall relaxation time and T_p the pumping time. P_L is a measure of how well the incident light is circularly polarised (section 5.2.4.), assumed to be 80% for the present set up. In order to determine T_R and T_p the data of figure 5.12 was analysed. An exponential curve was fitted to the decaying envelope which resulted in a total relaxation time $\tau = 4.5$ secs. This relaxation time is related to T_R and T_p by the relation (appendix 2)

$$\frac{1}{\tau} = \frac{1}{T_R} + \frac{1}{T_p} \qquad (5.29)$$

The same experiment was repeated with half the total incident light but the total relaxation time τ remained unchanged. This suggests that the pumping time T_p is rather long compared to T_R and an experimental measurement of T_p in this manner has rather poor precision. T_p could have been measured experimentally by combining the results of this experiment with those of some other technique (like the technique of relaxation in the dark developed by Franzen (1959) [Fra 59]), but we preferred to calculate T_p theoretically. This calculation is detailed in appendix 3 in which it is shown that

$$T_p = \frac{V}{1/3\sigma\ell J} \qquad (5.30)$$

where V is the volume of the cell (0.36 litres), ℓ = 7.5 cms is the light path in the cell, $\sigma = 2.533 \times 10^{-17}$ m^2 is the effective light absorption cross-section calculated in appendices A4 and A7 and finally, J is the total photon current entering the vapour. J is equal to the value of the total emitted photon flux from the source (equation 5.25) multiplied by the solid angle $d\Omega$ used in the experiment. The latter was rather complicated to evaluate theoretically and had to be measured experimentally. The measurement was done by setting up an experiment outside the μ-metal shield on the bench with the PM tube in place of the absorption cell. The light intensity was then measured with and without the lens and the guide tube, a ratio which is equal to the ratio of the corresponding solid angles. Knowing the two intensities as well as the solid angle when no lens and guide tube are used enables us to calculate the solid angle $d\Omega$ in presence of the lens and guide tube. We measured

$$d\Omega = 8.85 \times 10^{-2} \text{ Str.} \qquad (5.31)$$

Taking the transmission of the LP (17.5%), the λ/4 plate (83.4%) and the cell wall (74%) into account and the fact that only the ^{204}Hg line does the pumping (there is 58.2% ^{204}Hg in the source) we calculate J to be

$$J = 1.31 \times 10^{13} \text{ photons/sec} \qquad (5.32)$$

This is the actual number of photons per second interacting with the Hg vapour in the cell in the free precession experiment. Consequently, T_p can easily be calculated from

equation 5.30 from which we find

$$T_p = 44 \text{ secs} \tag{5.33}$$

Knowing T_p and τ, T_R is evaluated from equation 5.29

$$T_R = 5 \text{ secs} \tag{5.34}$$

P (equation 5.28.b) can now be calculated and reads

$$P = 6.5\ \% \tag{5.35}$$

Comparison between the direct and free precession experiments:

We can make use of the results elaborated in the direct absorption experiment (section 5.2.8). We recall that the absorption percentages obtained in that experiment are

$$A_1 = 2.3\%;\ A_2 = 0.9\%;\ A_3 = 0.96\%;\ A_{av} = 1.4\%$$

Note that the target was unpolarised. This is equivalent to saying that 50% of the atomic spins are parallel to the light beam and the other 50% anti-parallel to it. Therefore, if the target were fully polarised one would expect these percentages to be doubled. However, we showed in the free precession experiment that the atomic polarisation achieved was 6.5% (equation 5.35). This would result in

$$A_1' = 0.299\%;\ A_2' = 0.117\%;\ A_3' = 0.125\%;\ A_{av}' = 0.182\% \tag{5.36}$$

where the A_i' 's are now light absorption percentages by the vapour in a direct measurement.

These results can now be compared with the value obtained in the free precession experiment where we found (equation 5.27) that 0.28% of the light was absorbed. This result is not in total disagreement with the quantities in (5.36). On the other hand it agrees very well with A_1' and is of the same order as the rest of the A_i' 's.

As far as the relaxation time T_R is concerned (equation 5.34), it seems rather short. The cell is coated with a layer of teflon for which spin preservation properties are known to be good with Hg vapours. Previous experiments done at the University of Washington, two years ago, with the very same cell gave T_R = 120 secs. The magnetic fields involved do not seem to be the source of such a deterioration. The polarising field is reasonably homogeneous across the cell ($\delta B \approx 200\,\gamma$) for which the relaxation time would be bout 180secs. Moreover, the 10mGauss analysing field is very homogeneous across the cell ($\delta B < 1\,\gamma$). Consequently, we think that such a deterioration in T_R is probably caused by the high background pressure existing in the cell. T_R is then shortened through atomic collisions with foreign gas atoms. The high background pressure could have built up from leaks through the glue used to seal the cell ends (section 5.2.2) or due to the action of UV light on the walls. We think that UV light can make odd atoms come off the cell walls.

The signal to noise ratio was about 80 when the stem of the light source was maintained at 23°C, a temperature that

gave the maximum S/N.

The other parameter that is worth mentioning at this stage is the amplitude of the polarising magnetic field B_p. The S/N was found to be a maximum when $B_p \approx 4B_0$, a compromise which made $B_{eff} = B_p + B_0$ reasonably parallel to the light beam without introducing too much inhomogeneity into the B field present during the polarising period.

5.4. - Summary and Conclusion

We presented in the course of this chapter the work that was done to set up a mercury optical pumping experiment in a 3-layer μ-metal magnetic shield. For that purpose, a 2537 Å Hg light source was fabricated as well as a highly stabilised microwave generator that served to drive it. The noise from this source was measured rather carefully and was shown to be purely of shot noise when f>3Hz. We also showed that there is another source of noise and that is the photomultiplier noise due to the electron multiplication processes in the tube. From measurements of these two noises the PM gain was calculated which allowed us to determine the total photon flux emerging from the light source. The optical pumping experiment was then carried out in a 10mGauss magnetic field. The signal to noise ratio (S/N) was estimated to be about 80 with an integration time of 0.4 secs, the wall relaxation time T_R was found to be 4 secs and the pumping time T_p was 44 secs. Reasonable agreement between the observed peak to peak modulation and a direct light absorption experiment was achieved.

Although the results detailed in this chapter were

obtained with a sealed cell unlike the neutron storage volume in the main experiment, they represent a significant step towards the design and understanding of a suitable system.

The next chapter is concerned with measurements carried out in a 5 litre coated metal storage volume.

CHAPTER VI

A Prototype Mercury Magnetometer for the Neutron EDM Experiment

6.1.- Introduction

We shall be concerned, in the course of this chapter, with the design, the construction and the testing of a mercury magnetometer. More precisely, we are aiming to optically polarise Hg atoms in a 5-litre aluminium container coated with polystyrene to minimise sticking and spin flip. In the first stage of the experiment the vapour in the 5-litre container was polarised directly. In the second stage the atoms were polarised in a small aluminium chamber (0.16 litre in volume) and then transferred to the big bottle in order to look for free precession.

Since Hg tends to stick to surfaces, we shall have to calculate the different filling and emptying time constants involved and then measure them experimentally to see how well the theory agrees with the experiment. We shall also use the results obtained in the previous chapter in order to make an estimate of the way the system ought to behave.

Finally, the results of these experiments will allow us to design a Hg magnetometer for the EDM experiment and the performances likely to be attained.

6.2.-General outline of the system

We used a light source made up of 58% ^{204}Hg, and a target

of natural Hg in which ^{199}Hg represent about 17% of the total. There are two reasons for utilizing such concentrations. First, the very high cost of pure Hg isotopes, and secondly the non-availability of such elements when the experiment started. There are three consequences for using such mixtures:

1.Only 58% of the light source will be effective.

2.The fact that other components in the target like ^{204}Hg and the ^{201}Hg(F=5/2) component overlap with the 204 source component reduces the light that could be absorbed by ^{199}Hg.

3.Finally, even if the sample polarisation were 100%, the ratio of the modulation depth to the total DC light would be rather small because much of the light is not absorbed by the 199 component.

We shall start off this chapter by giving an overall view of the experimental set-up, then examine it in more detail, and finally present the experiments performed and the results obtained.

Figure 6.1 shows the overall set-up of the magnetometer. A 5.4 litre aluminium cylinder is positioned in the 3-layer μ-metal magnetic shield (section 4.3.7.1) in which a 10 mGauss vertical field generated by a cylindrical solenoid exists (section 4.3.7.3). On top of this vessel sits a smaller cylindrical chamber (0.16 litres in volume) communicating with it through a 2 mm hole. We shall call the big chamber A and the small one B. Outside, at the top of the shield there is a glass Hg container which is joined to the small chamber by some glass tubing. The small vessel can be filled with Hg vapour from the bead and then emptied into the big vessel through the 2 mm hole. A non

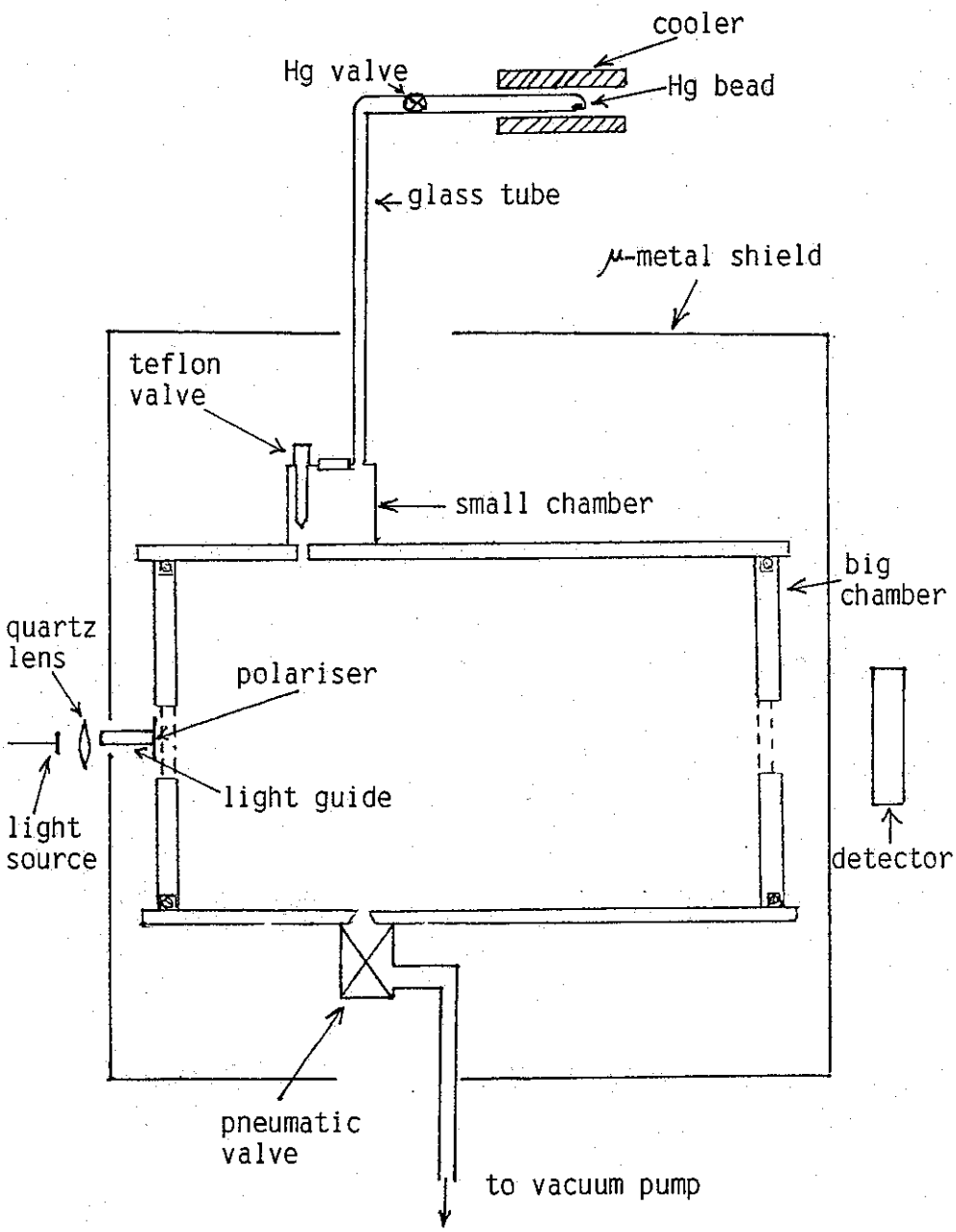

Figure 6.1: General setup of the Hg optical pumping experiment in the Aluminium chamber. the diagram is not to scale.

magnetic pneumatic valve connects A to a pumping system when it is necessary to remove mercury vapour from A.

A second magnetic field perpendicular to the axis of the shield is generated by a set of Helmholtz coils surrounding the big chamber.

Light shining from outside the shield crosses A through quartz windows to a photomultiplier placed on the other side of the shield. Light is first collected by a quartz lens which focuses it into a light guide. It is then circularly polarised before it crosses the big chamber. The DC component of the photomultiplier current, converted into a voltage, is read on a digital multimeter while the AC component is amplified by a PAR variable Q band-pass amplifier and displayed on a scope or read by a 16 bit ADC.

Without going into detail as yet, let us mention that three types of experiments were done with this piece of apparatus.

1. Study the flow of Hg between different parts of the system and compare the relevant time constants with theory.
2. Polarise the vapour in the large chamber and attempt to account for the properties of the free precession signals observed.
3. Polarise Hg vapour in the small chamber, transfer it to the larger volume and, again, attempt to account for the free precession signals observed.

The details of these experiments are laid out in the following section after giving a more complete description of different items of the whole system.

6.3.- Detailed description of the apparatus

6.3.1.- The analysing chamber

The term "analysing chamber" is given to the big vessel as opposed to the "polarising chamber" given to the small volume. This terminology will be more apparent in the following sections. The analysing chamber is a 5.4 litre aluminium cylinder made up of a 23 cm diameter ring, 13cm high, with two aluminium plates. The bottom plate contains a 1 cm hole through which the system can be evacuated. A hole, 2.5 cm from the center, communicates with the small chamber. Two 1 inch diameter holes sealed with quartz windows, 4 cm in diameter and 3 mm thick, exist in the aluminium ring on opposite sides. The two plates seal onto the cylindrical ring by means of two Viton O-rings. This chamber is very similar to the one used in the Caesium experiments (section 4.4.2) where a more comprehensive description is provided. The vacuum system and the pneumatic valve utilized are also described in the chapter dealing with Caesium and precisely in section 4.4.3.

6.3.2.- The polarising chamber

Figure 6.2 shows the small polarising aluminium vessel. It has a volume of 0.16 litre (i.e. 1/34 the volume of the big chamber), a diameter of 6.63 cm and is 4.5 cm high. A quartz window 3.5 cm in diameter is sealed in the top to allow polarising light to enter and a teflon pneumatically actuated needle valve controls access to the large volume through a 2 mm diameter hole. The 8 mm recess in the top of the small volume seals to the mercury source. Before the

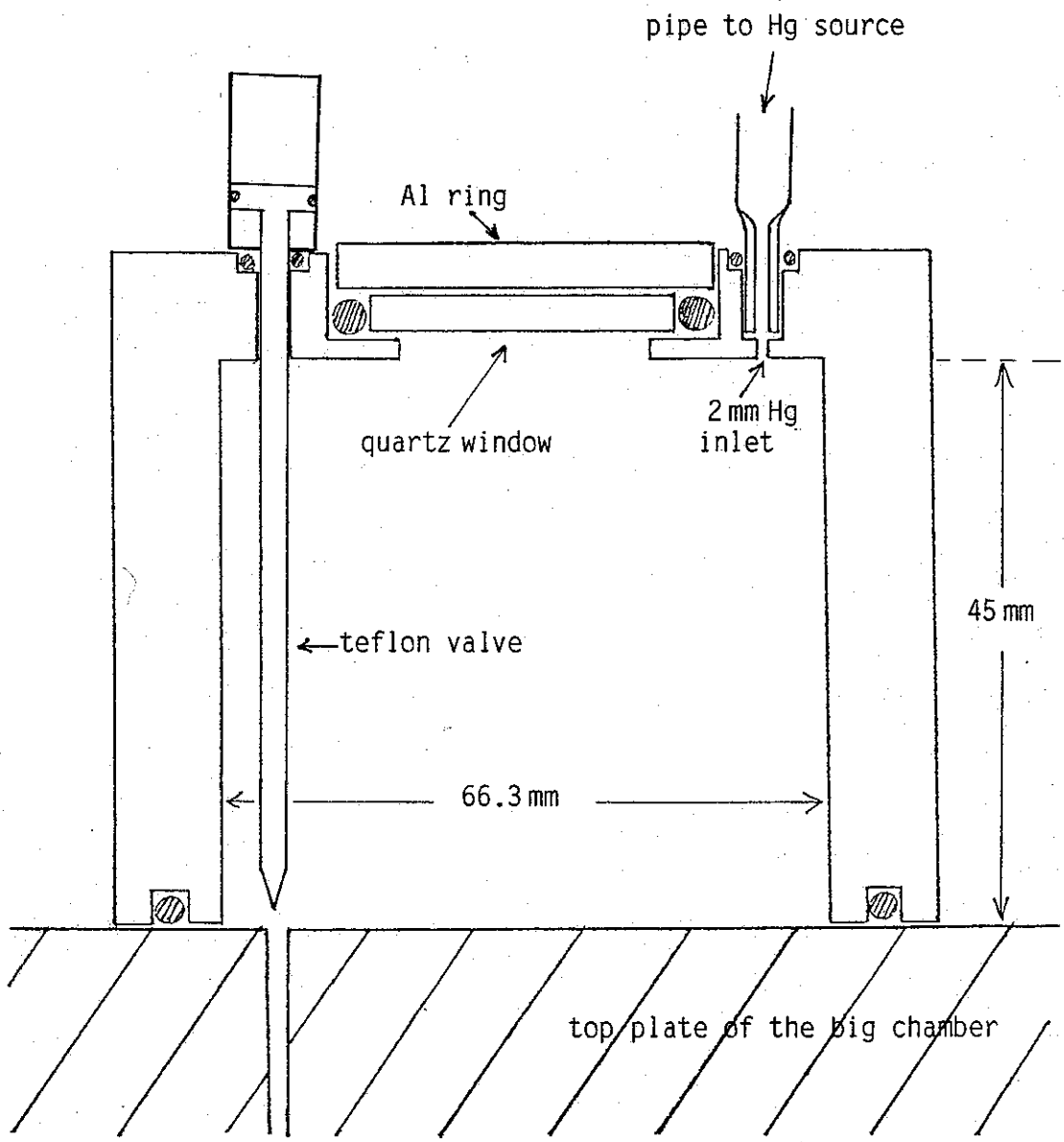

Figure 6.2: The small polarising Aluminium chamber.

system is pumped out the small chamber is tightly clamped down to the big volume.

6.3.3.- Coating the vessel

Very special care was taken coat every region of the apparatus. Each piece was thoroughly washed with a detergent called "Decon 90", rinsed with de-ionised water and finally dried in a hot stream of filtered air. We used a solution of polystyrene in toluene which was made in our laboratory. The polymerisation procedure and the way the fluid was applied on surfaces is explained in section 4.3.4.2. The O-rings and the teflon valve were coated with some Fomblin grease because polystyrene does not stick well on teflon. The choice of polystyrene is not unique and other kinds of coating ought to be tried. Polystyrene was chosen because it was used successfully in the past with polarised neutrons and Hg atoms in small quartz cells [Lam 88].

6.3.4. - The Hg Bead

A drop of natural Hg was placed in a Γ-shaped glass tube. The open bottom end of the tube fits into the recess in the small chamber leaving the Hg at the other end outside the shield. A manually operated tap near the bead prevents evaporation of Hg while the system is being pumped or out of use for an extended period of time. The Hg was cleaned by successive distillation in a separate vacuum system before being distilled into the tube which fits into a

block of aluminium cooled by a semi-conductor cooler similar to the one used in section 5.2.1.3. During the experiment it is kept below 0°C in order not to fill up the apparatus with Hg.

6.3.5. - The Magnetic Fields Involved

Two magnetic fields are generated inside the shield.

6.3.5.1. The transverse Polarising Field

It is made up of a one turn pair of Helmholtz coils 40cm in diameter with a separation of 20cm, positioned in such a way that the generated field is along the light beam (perpendicular to the B_0 field). Figure 6.3 shows the profile of this field when a current of 1.11 Amps generates a field at the centre of 50mGauss. The x-axis represents different positions along the horizontal axis passing through the two sets of holes in the shield. When the big chamber is in the shield, it extends over the interval 13cm - 35cm. In this region the field is rather homogeneous and maybe improved by reducing it even further if necessary. The vertical component of the field was not measured but precautions were taken to prevent the big vessel from touching the coil. In the following, we will be referring to this field by B_p.

6.3.5.2. - The Analysing Field

This is the field as described in section 4.3.7.3. It is generated by a solenoid along the axis of the shield, and

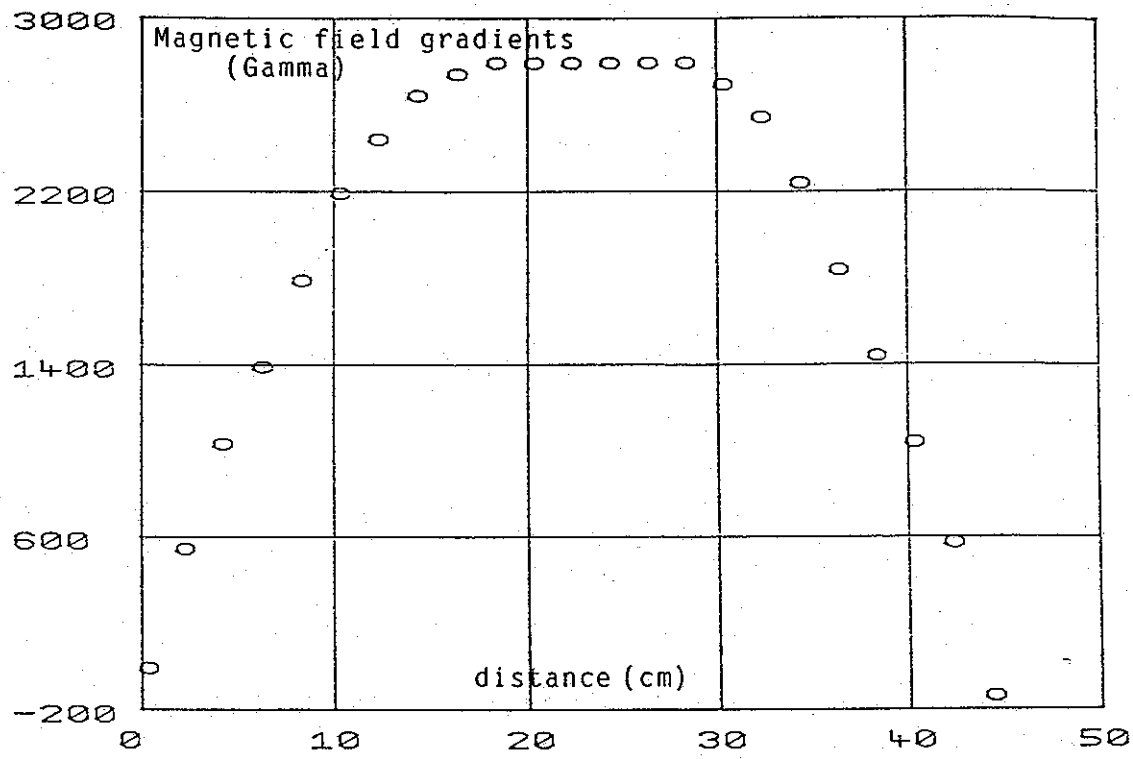

Figure 6.3: Profile of the polarising field as a function of position in the 3-layer μ-metal shield. The measurements are taken along the light beam axis.

is usually run to give 10mGauss. However, it can be easily altered by connecting a resistor in parallel with the coil as we have done on some occasions.

6.4. - Light Absorption Experiments

6.4.1. - Experimental Procedure

In the first stage of the experiment we used the absorption of light by mercury vapour to monitor the flow of the gas around the apparatus. Absorption signals allow us to determine the time it takes to fill up the polarising chamber from the Hg bead and measure the time it takes to fill up and pump out the big chamber. We started off with all the valves open except the Hg valve (the one used to isolate the bead) (see figure 6.1).

1. The system was pumped out to a background pressure of about 10^{-4} torr.
2. The teflon valve was then closed.
3. The Hg manual valve was opened to fill up the small volume.
4. The vacuum valve is then closed.
5. Hg is admitted to the analysing vessel after opening the teflon valve.

Since Hg atoms absorb some of the light beam (the amount of absorption depends on the quantity of Hg) the output of the photomultiplier tube decreases at a rate which depends on the conductance of the system.

In fact there are two stages to the process. There is a first short period while the small chamber shares the gas with the big one, and then the slower filling up process

when gas is transferred from the region of the of Hg bead. Each stage is characterised by a time constant which we will calculate and then measure experimentally. Another time constant calculated and measured is the one associated with evacuation of the system by the vacuum pump.

6.4.2. - Calculation of the Time Constants Involved

The detailed calculations of the filling up process of the big vessel are outlined in appendix 5. In the present section, we will only state the main assumptions made and give the final results.

6.4.2.1. - The Analysing Chamber Filling Time

The system considered is made up of three sub-systems :

1. The Hg container whose volume is taken to be negligible compared to the other two sub-systems.
2. The small chamber having a volume V_s.
3. The big chamber with a volume V_b.

The conductance of the connections (tubes, apertures ...etc...) are C_1 between B and the Hg container, and C_2 between B and A. We will be calling p_0 the Hg pressure in the Hg container, $p_s(t)$ the pressure in B, and $p_b(t)$ the one in A. We will assume that p_0 keeps constant throughout the transfer and thereafter.

The procedure consists of opening the Hg valve (see figure 6.1) until B is filled to pressure $p_s = p_0$. Then open the teflon valve (the vacuum valve is of course kept closed all the way through) to fill up A. There will

first be a sharing of the gas between B and A and then a filling up period of the two volumes B and A from the bead until the system reaches equilibrium.
The equations governing the flow of Hg in the system can be written as

$$V_s \frac{dp_s}{dt} = (p_0(t) - p_s(t))\, C_1 - (p_s(t) - p_b(t))\, C_2 \qquad (6.1)$$

$$V_b \frac{dp_b}{dt} = (p_s(t) - p_b(t))\, C_2 \qquad (6.2)$$

This system of differential equations is solved in appendix 5. Taking the instant the teflon valve is opened as the beginning of time, we find

$$p_s(t) = \frac{C_2}{V_2} \frac{p_0}{(m_2 - m_1)} [\exp(+m_1 t) - \exp(+m_2 t)] + p_0 \qquad (6.3)$$

$$p_b(t) = p_0\, [(d+e) \exp(+m_1 t) - (d+f) \exp(+m_2 t) + 1] \qquad (6.4)$$

where

$$m1 = \frac{1}{2}(-a - \sqrt{a^2 - 4b}) \;\; ; \;\; m_2 = \frac{1}{2}(-a + \sqrt{a^2 - 4b}) \qquad (6.5)$$

$$a = \frac{C_1 + C_2}{V_s} + \frac{C_2}{V_b} \;\; ; \;\; b = \frac{C_1 C_2}{V_s V_b} \qquad (6.6)$$

$$d = \frac{C_1 + C_2}{(m_2 - m_1) V_2} \;\; ; \;\; e = \frac{m_1}{m_2 - m1} \;\; ; \;\; f = \frac{m_2}{m_2 - m_1} \qquad (6.7)$$

From equation 6.3. we verify that at $t = 0$, $p_s(0) = p_0$ and at $t \rightarrow \infty$, $p_s(\infty) = p_0$. Similarly, from equation 6.4. we see that at $t = 0$, $p_b(0) = 0$ whereas at $t \rightarrow \infty$, $p_b(\infty) = p_0$. Therefore, the solutions show well that the ultimate pressure reached by the system, at equilibrium, is the pressure of the bead p_0 at a given temperature. Knowing that $V_s = 0.16$ litre, $V_b = 5.4$ litre, $C_1 = 0.0113$ l/sec and $C_2 = 0.081$ l/sec (C_1 and C_2 are calculated in appendix 5) we find

$$\tau_{sb} = 1.94 \text{ sec.} \tag{6.8}$$

$$\tau_b = 9.3 \text{ mins.} \tag{6.9}$$

where τ_{sb} is the time constant of the sharing process of the gas between the two chambers, and τ_b the total filling time constant for the chamber.

6.4.2.2. - The Analysing Chamber Emptying Time

It is determined by the conductance of the vacuum valve and the pipe work associated with it. We calculated the total conductance (by adding up the different contributions of the different parts of this system) C_3 to be 1.5 l/sec for air. This is multiplied by the ratio of the velocity of Hg to the velocity of air ($v_{Hg}/v_{air} = 0.39$), thus the conductance C_3 becomes 0.58 l/sec for Hg. The time constant defined by

$$\tau_e = \frac{V_b}{C_3} \tag{6.10}$$

is then equal to 9.2 secs.

6.4.3. - Measurement of the Time Constants

The three time constants calculated theoretically in the previous section are now to be measured experimentally. We made sure that we were working with thin vapours so that light absorption is always linear with increasing pressure. For that reason, the Hg bead was usually run at -16°C ; this resulted in absorption percentages of a few percents.

6.4.3.1. - Measurement of the Filling Time

The procedure, as explained in 6.4.1., involves filling up the small chamber first and then opening the teflon valve to fill the big chamber keeping the vacuum valve shut. First there is a sharing of the vapour between the two chambers in a relatively short time τ_{sb} and then the whole system fills from the source with a time constant τ_b.

1. Measurement of τ_b:

The first attempts of measuring τ_b from a bead maintained at -24.5°C were rather disappointing. Instead of finding τ_b, equal to that calculated from equation 6.9 we obtained values of the order of a few hours.

We initially thought that Hg might stick to the walls of the big container and then come off very slowly. However, this possibility was tested and proved to be wrong. Some Hg was admitted into A and then pumped out. After closing both the teflon and the vacuum valves, we monitored the

light intensity for a few hours and then opened the vacuum valve. If Hg had been coming off the walls there would have been a steady decrease in light intensity over the few hours and when the valve was opened the initial light level would have been recovered. Nothing of the sort was observed. The light intensity remained constant during the experiment. The same check was done on the small chamber and the glass tubing connecting it to the bead. Hg did not seem to be sticking there either.

Eventually, we considered the possibility that the Hg bead might be rather dirty. This would decrease the emitting surface area of the bead considerably, and slow down the evaporation process. The Hg container was then tapped a few times to move the bead and uncover a new surface. This resulted in an immediate improvement in τ_b as shown in figure 6.4 where the rapid drop of intensity when the teflon valve was opened can be seen. This was followed by a rather long rate of drop of the intensity until the bead was disturbed again.

We made a computer fit to this long process and found it to happen with a time constant of the order of 2.5 hours. However, a fit to the last part of the graph (following the second disturbance) resulted in a time constant τ_b = 10 mins which is in very reasonable agreement with the calculated value of 9.3 minutes (equation 6.9). At the end of this run, the vacuum valve was opened and the light intensity returned to its initial value.

2. Measurement of τ_{sb}:

The measurement of τ_{sb} was less troublesome. The small chamber was filled up and the teflon valve opened. Light

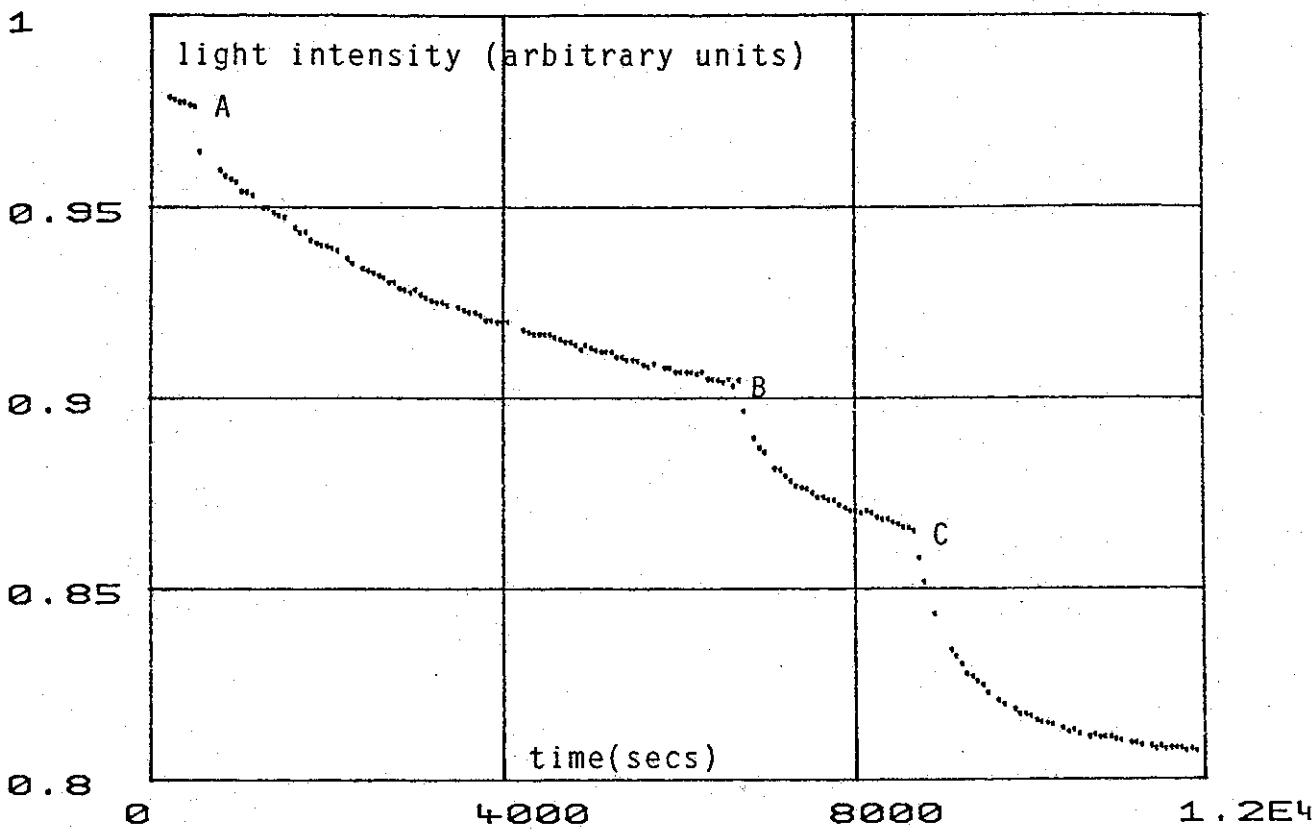

Figure 6.4: The big chamber filling up process. In A the teflon valve was opened. B and C indicate the points at which the bead was disturbed (tapped).

intensity drops rather quickly compared to the decrease seen when filling up the big chamber. Figure 6.5 shows such an experimental curve. In this run, the chamber was pumped out once the sharing process seemed to be complete. A computer fit to this data resulted in a time constant τ_{sb} = 3 secs which has to be compared with the theoretical value of 1.94 secs calculated above.

6.4.3.2.-Measurement of the emptying time

Figure 6.6 shows a run to measure the time it takes to pump out the chamber. After some Hg is admitted to the vessel, the teflon valve is closed and the vacuum valve is opened. The light intensity then recovers with a time constant τ_e determined by the conductance of the pumping system. Once again, the agreement between the measured value of τ_e and the calculated one is rather good. Fitting the curve in figure 6.6, we find that τ_e = 9 secs (the calculated value is 9.2 secs).

To conclude this section, we give in table 6.1 a summary of the results obtained so far.

	τ_{sb}	τ_b	τ_e
Theory	1.94 sec	9.3 mn	9.2 sec
Experiment	3.0 sec	10.0 mn	9.0 sec

Table 6.1

where τ_{sb} is the time constant for the gas sharing process between the two chambers, τ_b is the big chamber total filling time constant, and τ_e is the big chamber emptying

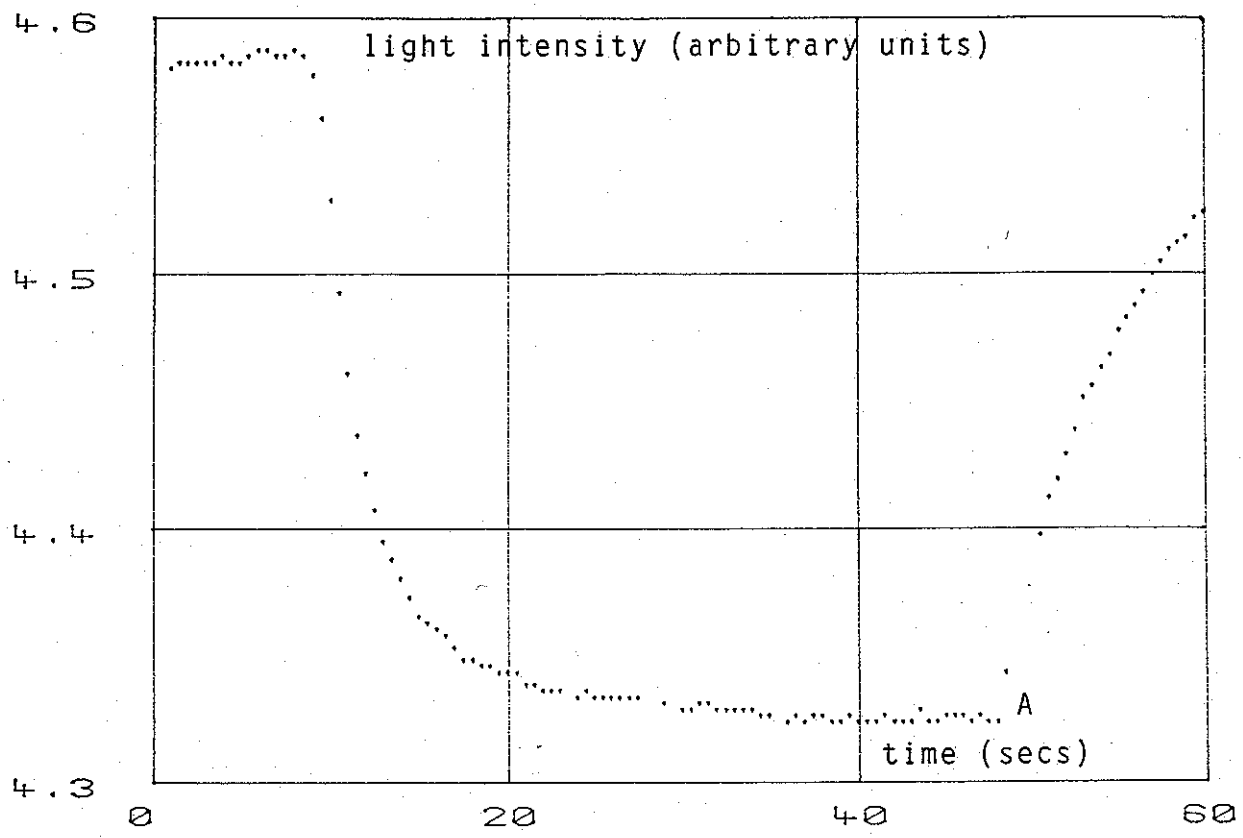

Figure 6.5: The gas sharing process between the two chambers. This quick decay (τ_{sh}=3 secs) appears as soon as the teflon valve is opened.
The chamber was pumped out at A.

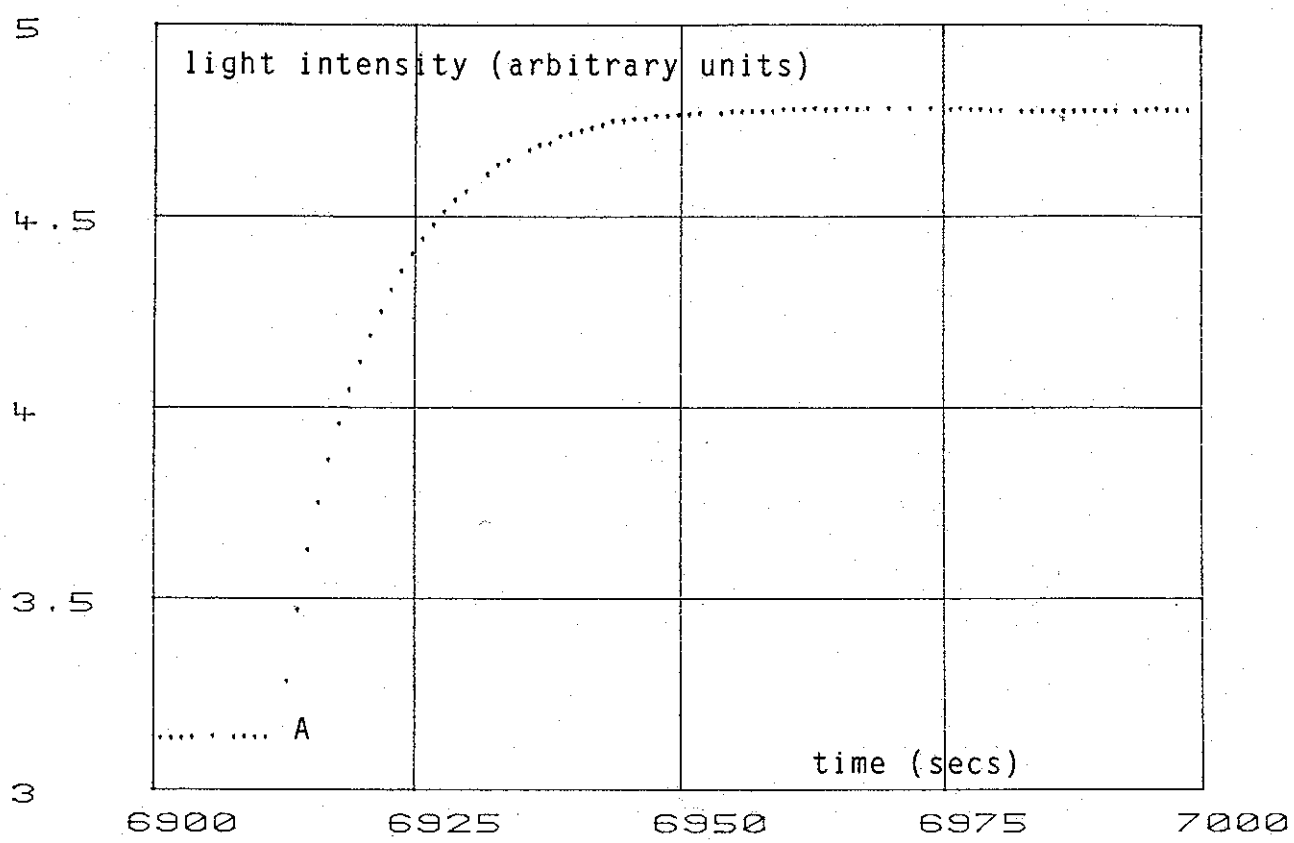

Figure 6.6: The big chamber pumping out process. We measure a time constant τ_e=9 secs. Hg is pumped out at A.

time constant.

Knowing these different time constants should help us to understand the transfer processes of Hg in the system and explain the results obtained when free precession is observed.

6.5.- Free precession experiments

6.5.1.- Introduction

Having succeeded in monitoring the Hg flow in the apparatus from one chamber to another, we are now ready to try to do some free precession experiments with the vapour. As a first step, we shall describe an experiment that is rather similar to the one done on the quartz sealed off cell (see section 5.2.9). But, this time, it will be done in the 5.4 litre aluminium container whose walls have been treated with polystyrene. The second stage of the experiment will involve polarisation of vapour in the small chamber using a second light source and observation of free precession in the large chamber after transferring the polarised atoms, a procedure which we hope to copy in the EDM experiment by mixing polarised mercury atoms with the neutrons.

We shall give the calculations done to determine under what conditions the experiment is feasible, describe the experimental procedure used for each experiment, and finally discuss the results obtained.

6.5.2.- Preliminary calculations

In what follows are some calculations that were done either to make sure that the experiment is likely to be successful or to evaluate some parameter needed in the analysis.

6.5.2.1.- Pumping time in the big chamber

This can be calculated from the value measured in the experiments done with the quartz cell (equation 5.33) and equation 5.30. Using this equation both for the quartz cell and the aluminium chamber results in

$$T_p = \frac{V_b}{V_q}\frac{\ell_q}{\ell_b} T_{pq} \qquad (6.11)$$

where $V_q = 0.36$ litre and $\ell_q = 7.5$ cm are the volume and the diameter of the quartz cell respectively. T_p is the pumping time in the big vessel and $T_{pq} = 44$ secs the one in the quartz cell. Since $V_b = 5.4$ litres and $\ell_b = 23$ cm we obtain

$$T_p = 215 \text{ secs} \qquad (6.12)$$

Equation 6.11 is correct only if the same light source is used in both cases which is true in this experiment.

6.5.2.2.- Effects of shining the light in a small region of the chamber

In this experiment the light beam is effectively

"squeezed" by the optical elements used (lens and light guide). It then crosses the chamber through a rather small region, about 1/50 of the total volume. However, when the experiment was done using the quartz cell the beam was assumed to be covering the whole volume. Therefore, the question is - does this squeezing effect affect the pumping rate?

It turns out that it does not. Provided the light path length is the same before and after squeezing the beam, and provided the density of atoms is the same outside and inside the region crossed by the beam, the pumping rate remains the same. When one atom is outside the beam another atom inside would have twice the probability of being pumped. However, one important condition for this to be true is that the probability of absorption in the beam is not too large as is the case with a laser. The intensity of our light source is rather weak compared to a laser. If the light beam is very intense the number of excited atoms could be rather big and the density of atoms capable of absorbing light becomes smaller.

6.5.2.3.- **Magnetic field gradients**

We are mainly concerned with the effects of the polarising field gradients on the relaxation time, i.e. evaluate the relaxation time T_B under the effect of field inhomogeneities arising with B_p. This is expressed as

$$T_B = \frac{\pi^2}{\gamma^2 \delta B^2 t} \qquad (6.13)$$

where γ is the gyromagnetic ratio of Hg, δB the field gradients across the chamber and t the mean transit time.

According to figure 6.3, δB is of the order of 200 Gamma. The mean free path in the big chamber is equal to 12.2 cm which results in a transit time $t = 6.9 \times 10^{-4}$ secs. Putting all this together yields

$$T_B = 90\text{secs} \qquad (6.14)$$

This was obtained in a field of 50 mGauss and should be improved by working at a lower intensity.

As far as the analysing field B_0 is concerned, it is substantially more homogenous than B_p and should not cause any problem. However, this statement could be checked when the free precession signal is obtained. One would lower B_0 and record the change in both the signal amplitude and relaxation time. Indeed, this was done and the results are presented below.

6.5.2.4.- Calculation of the light absorption cross-section

The purpose behind the following calculation is to determine the contribution of the actual pumping spectral line to the total absorbed light. As we know, from chapter 5, the pumping is done through the ^{204}Hg line component acting on the ^{199}Hg(F=1/2) absorption line. However, both the source and the target are not pure ^{204}Hg and ^{199}Hg respectively, but involve all the other isotopic components. The light source contains 58.2% of ^{204}Hg whereas the target consists of natural mercury which contains 16.84% of ^{199}Hg. The abundance of the other components can be found in table 5.1 for the case of the target and in table A4.2 for the source.

Although the other components do not contribute to the pumping process, they, on the other hand, are absorbed by some absorption lines of the target. In order to calculate the contribution of the pumping component it is necessary (among other parameters) to calculate the effective absorption cross-section. The detailed calculations are given in appendix 4, so we will only present the main results for the moment. The numerical computation of these results is given in the computer program listed in appendix 7.

Since the source is an ensemble of different isotopic lines, the incoming intensity on the chamber can be written as

$$I_{in} = I_0^{204} + I_0^{202} + I_0^{201(F=5/2)} + \ldots\ldots \qquad (6.15)$$

where $I_0^j = A^j\ (2F+1)/[(2J+1)(2I+1)]$ is the share of a given component j to the total incident beam. On the other hand, the light scattered by the vapour is

$$I_{out} = I_0^{204}\ \exp{-k(\Sigma_{204}^{204} + \Sigma_{202}^{204} + \ldots.)}$$

$$+ I_0^{202}\ \exp{-k(\Sigma_{204}^{202} + \Sigma_{202}^{202} + \ldots.)} + \ldots. \qquad (6.16)$$

where

$$k = n\,x \qquad (6.17)$$

n is the density of the target vapour (atoms/m^3), and x is the light path length in the vapour i.e. the diameter of the chamber.

Σ_i^j is the light absorption cross-section of the source component j with the target component i. It is defined as

$$\Sigma_i^j = A_i \frac{1}{N_{g\,i}} \sigma_i^j \qquad (6.18)$$

where A_i is the abundance of component i in the target and $N_{g\,i}$ is the ground state degeneracy of the isotope i. σ_i^j is the effective cross section per atom. It depends firstly on the overlap O_i^j of source line j with target line i, secondly on the total probability $(\Sigma b_r)_i$ of optical transition with σ^+ light to the excited level, and finally on the peak cross section $\sigma(\omega_0)$ involving two components of exactly the same centre wavelength and a 100% overlap. It is defined as (appendix 4)

$$\sigma(\omega_0) = \frac{3\lambda^2}{2\pi} \frac{\gamma}{\Delta_i'} (\pi \log 2)^{1/2} \qquad (6.19)$$

where λ is the wavelength of the incoming light, Δ_i' is the Doppler width of the line i in the target and γ is the inverse of the excited state lifetime. Substituting the numerical values of λ, Δ_i' and γ (given in appendix 4) in 6.19 we find

$$\sigma(\omega_0) = 6 \times 10^{-17}\ m^2 \qquad (6.20)$$

The overlap function O_i^j is worked out in appendix 4 and reads

$$O_i^j = \frac{1}{\sqrt{(a_i^j)^2 + 1}} \exp -\left(4(\beta_i^j)^2 \left[\frac{1}{(a_i^j)^2} + \frac{1}{((a_i^j)^2 + 1)} \right] \right) \qquad (6.21)$$

where α_i^j is the ratio of the Doppler width of the source to the Doppler width of the target, and $\beta_i^j = (\omega_{0j} - \omega_{0i})/\Delta_i$. $\omega_{0j}/2\pi$ is the centre frequency of the source component j, $\omega_{0i}/2\pi$ is the centre frequency of the target component i and $\Delta_i = \Delta_i'/\sqrt{\log 2}$. The actual expression of σ_i^j is

$$\sigma_i^j = \sigma(\omega_0)\, O_i^j\, (\Sigma b_r)_i \qquad (6.22)$$

When the computer program of appendix 7 is run, we find that for the pumping component 204 with 199(F=1/2)

$$\sigma_{199(F=1/2)}^{204} = 2.553 \times 10^{-17}\ m^2 \qquad (6.23)$$

which is the figure used in calculating the pumping time T_p in equation 5.30. Using the same computer program we could also evaluate the contribution of the pumping component to the total absorbed light. We find that out of the total absorbed source light by the target only 18% is due to the 204 line absorbed by the 199(F=1/2) component.

6.5.3.- Free precession experiments in the big chamber

6.5.3.1.- Experimental procedure

The apparatus has already been shown in figure 6.1. Before the experiment was realised, the whole system was baked to 80°C. This was done by passing a current through a thick constantan wire (which is non magnetic) wound around the two chambers. The baking lasted for about 4 hours during which the system was continuously evacuated. The final background pressure attained was 10^{-4} torr.

The measurements were started by closing the teflon valve with the Hg bead at a temperature of -20°C and opening the glass tap to fill the small chamber. The vacuum valve was then closed and the teflon valve opened to let Hg vapour into the big chamber. The light intensity I_0 as recorded by the photomultiplier tube then started falling steadily until the teflon valve was closed when the intensity reached a lower level I. The value of I is given by

$$I(n) = I_0 \exp-(n\sigma\ell_b) \qquad (6.24)$$

where n is the Hg density, ℓ_b is the diameter of the big chamber and σ is the atomic light absorption cross-section.

The quantity $(I_0 - I)/I_0$ is then related to the Hg density in the vessel. Equation 6.24 is just a simplified version of the actual equation that relates to the existing conditions in our experiment where many lines emitted by the source induce several transitions in the target atoms.

The next step in the procedure consists of applying the magnetic field B_p for a time comparable to the total relaxation time τ of the vapour magnetisation in the chamber. If τ is unknown to start with, one has to repeat the experiment with different values of τ until the free precession signal is optimised. The atoms are subjected to two perpendicular magnetic fields B_p and B_0, with B_p usually chosen to be a few times bigger than B_0 so that the angular momentum transmitted from the pumping light to the vapour points mainly in the direction of B_p.

After the target is believed to be fully polarised the B_p field is turned off leaving the atoms to precess around B_0 alone. This will result in the precession of the sample

magnetisation around B_0 in a plane perpendicular to it (we will take this plane as the xy-plane and the z-direction along B_0). This behaviour is translated into a modulation of the light beam at the Larmor frequency associated with B_0 (see chapter 2 for more details). A sinusoidal decaying signal is then observed, and processed in the same way outlined in section 5.2.9 (i.e. amplified, filtered ...etc...). Once the decaying signal is over, the vacuum valve is opened and the system is pumped out and ready to be used again. The light intensity recovers its initial value I_0.

6.5.3.2. - **Results**

A first experiment was done to test whether a light guide would be of any help on the detection side. It turned out that it did not. The longer the guide one puts in, the smaller the signal. In fact, this should not be surprising because the nearer to the chamber the detection device is the more " odd " the light rays it collects. The meaning of the word "odd " is any light that was reflected on the chambers walls or scattered by the atoms i.e. any light that did not cross the chamber in a straight line but was somehow scattered due to the relatively wide incident beam. Consequently, we decide to use just the PM tube, far enough from the chamber but not too much to make the S/N small.

In this section, we will only give the results obtained and defer the explanations to the discussion section below.

Figure 6.7 shows the result of an experiment done in an analysing field $B_0 \approx 10$ mGauss. The signal to noise ratio is

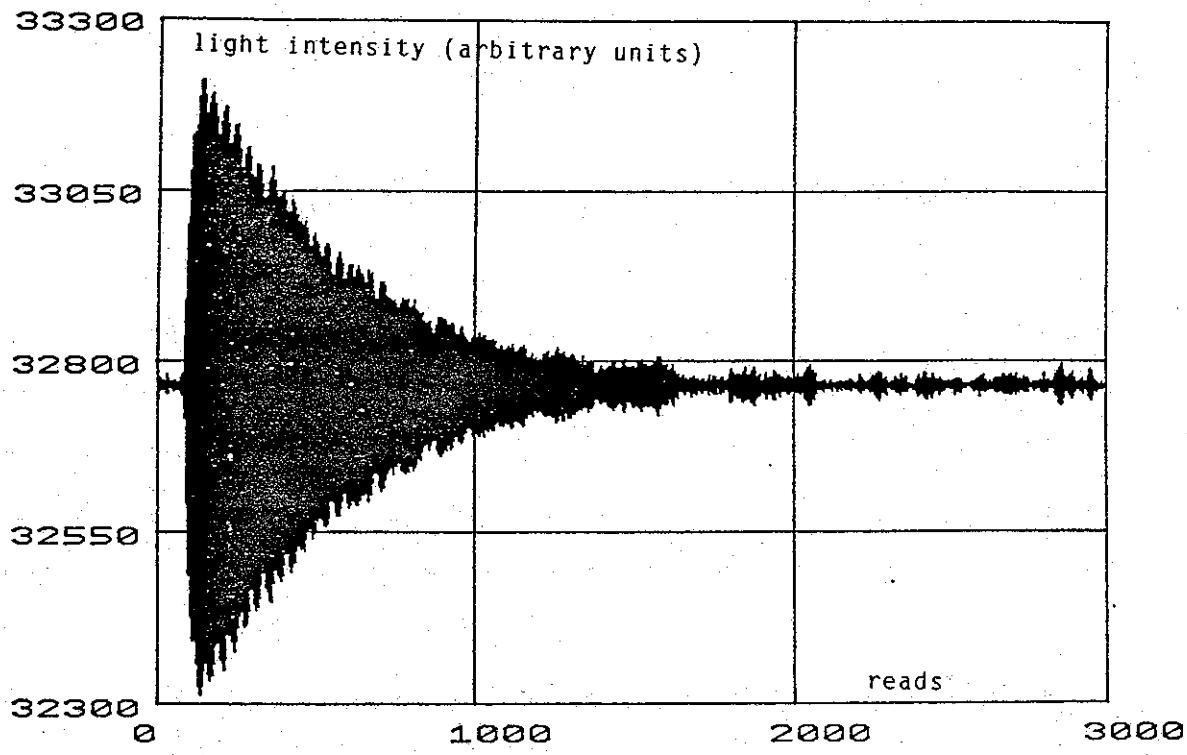

Figure 6.7: Mercury free precession in a 10 mGauss magnetic field. 50 reads correspond to 1 second.

about 150 whereas the total relaxation time $\tau \approx 10$ secs. The frequency of the oscillations is $f_0 = 8.06$ Hz from which the exact value of B_0 can be calculated.

$$B_0 = \frac{2\pi f_0}{\gamma} \qquad (6.25)$$

where $\gamma = 4768.97 \times 10^4$ $sec^{-1}.T^{-1}$ for ^{199}Hg. We find that $B_0 = 10.62$ mGauss. The integration time used is about 0.8sec (the bandwidth used on the PAR is 1.26Hz). The photomultiplier tube was working at the usual gain of 2661 and the ADC set to take 50 reads/sec. The low-pass filter used in the current to voltage converter reduces the output to 89%. The total incident light intensity was 10 volts and the intensity transmitted by the vapour was 5.5 volts. This amounts to 45% absorption.
As far as the polarising field is concerned, we worked at $B_p = 1.5\, B_0$. This was determined experimentally, B_p was changed until we obtained the best possible signal.

6.5.3.3.-Free precession in a low B_0 field

Another area of investigation is the behaviour of the signal with the amplitude of the analysing field B_0. If field gradients are affecting the total relaxation time τ, then reducing the field B_0 ought to make τ longer. In order to change the intensity of B_0 a resistor was connected in parallel with the B_0 coil. The resonance frequency was adjusted to the new value on the PAR as well

as the bandwidth. The integration time was still 0.8 sec.

We first reduced B_0 to half its value ie. $B_0 = 5$ mGauss. Figure 6.8 shows the signal obtained. The new resonance frequency is 4.1 Hz. The polarising field giving the best signal seems to be $B_p = 3\,B_0$. The signal to noise ratio is about 184 which is a 20% increase from the last run. However, the relaxation time τ does not seem to have changed. The total incoming light intensity is similar to the one used with $B_0 = 10$ mGauss, it is 10.3 volts. The amount of absorption was also similar i.e. 45%.

The B_0 field was further reduced to 1 mGauss. The resonance frequency at this field is now 1Hz. The detected signal is shown in figure 6.9. It exhibits a factor of two improvement in the signal amplitude from the one obtained at 10mGauss, and a S/N of 126. However, the relaxation time still seems to be unchanged. We notice that the rms noise level has increased. This is probably the 1/f noise from the light source showing at such a low frequency of 1Hz. The same incident light intensity and absorption ratio were used. The polarising field is about six times the B_0 field.

6.5.3.4.-Free precession amplitude as a function of Hg density

One measurement that seemed interesting to do is the variation of free precession amplitude with the density of Hg admitted to the chamber. Figure 6.10 shows such a variation when the density is monitored by observing the percentage of light absorbed. The optimum in this system occurs for 60% absorption.

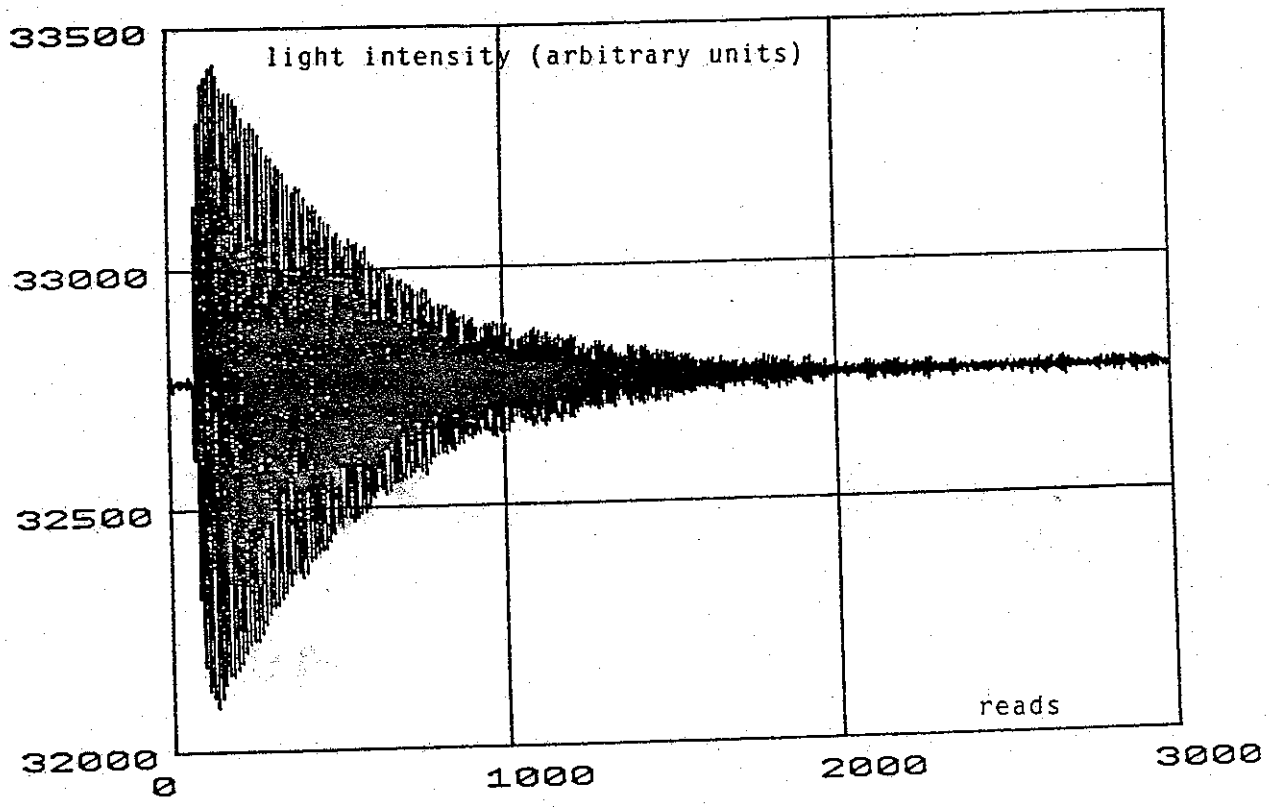

Figure 6.8: Mercury free precession in a 5 mGauss magnetic field. 50 reads correspond to 1 second.

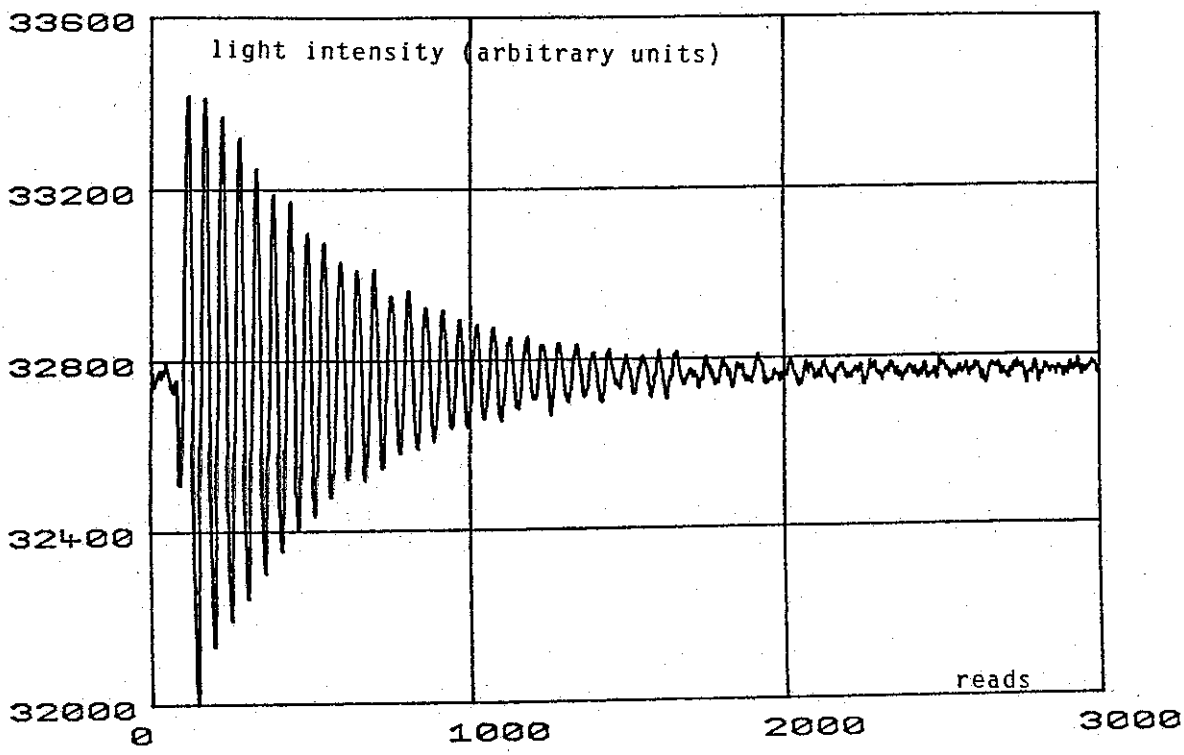

Figure 6.9: Mercury free precession in a 1 mGauss magnetic field. 50 reads correspond to 1 second.

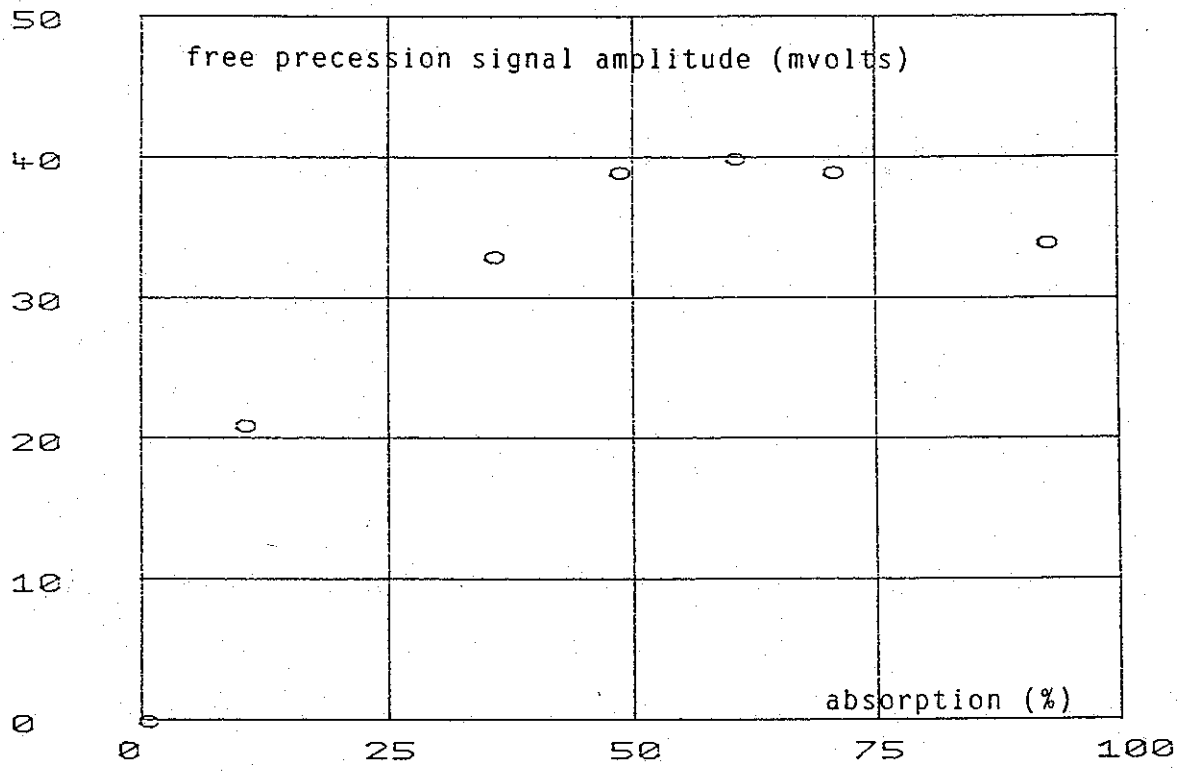

Figure 6.10: Variation of free precession signal amplitude with the amount of mercury admitted.

6.5.3.5.-Performances of a new source

By the time these experiments were done a new light source was made. In order to test it we decided to make use of it in the experiment. The light intensity was rather large compared to the old source, and thus in order not to exceed the allowed photomultiplier current the PM tube was covered with a polythene sheet which absorbs 54% of the incoming light. Taking this into account, the equivalent intensity used was 18.5 volts. The amount of Hg admitted to the chamber was such that the transmitted light through the vapour is 45% of the total beam. The experiment was done in a 10mGauss analysing field and a 15mGauss polarising field B_p. The Q of the tuned amplifier was set to 10 and the resonance frequency to 8.06 Hz. The signal obtained is shown in figure 6.11. Although the relaxation time is still 10 secs, the S/N of 254 seems to be a good improvement.

6.5.3.6.-Free precession at 50°C

Another experiment performed with this new light source consisted of heating up the chamber to some temperature and looking for a free precession signal at that temperature. The vessel was heated to 95°C and then allowed to cool down. In figure 6.12 we can see the signal obtained in the normal way when the temperature on cooling was 50°C. The S/N was then about 270, and more importantly the relaxation time has doubled to 20 secs. The chamber was then allowed to cool down to room temperature and a new signal was

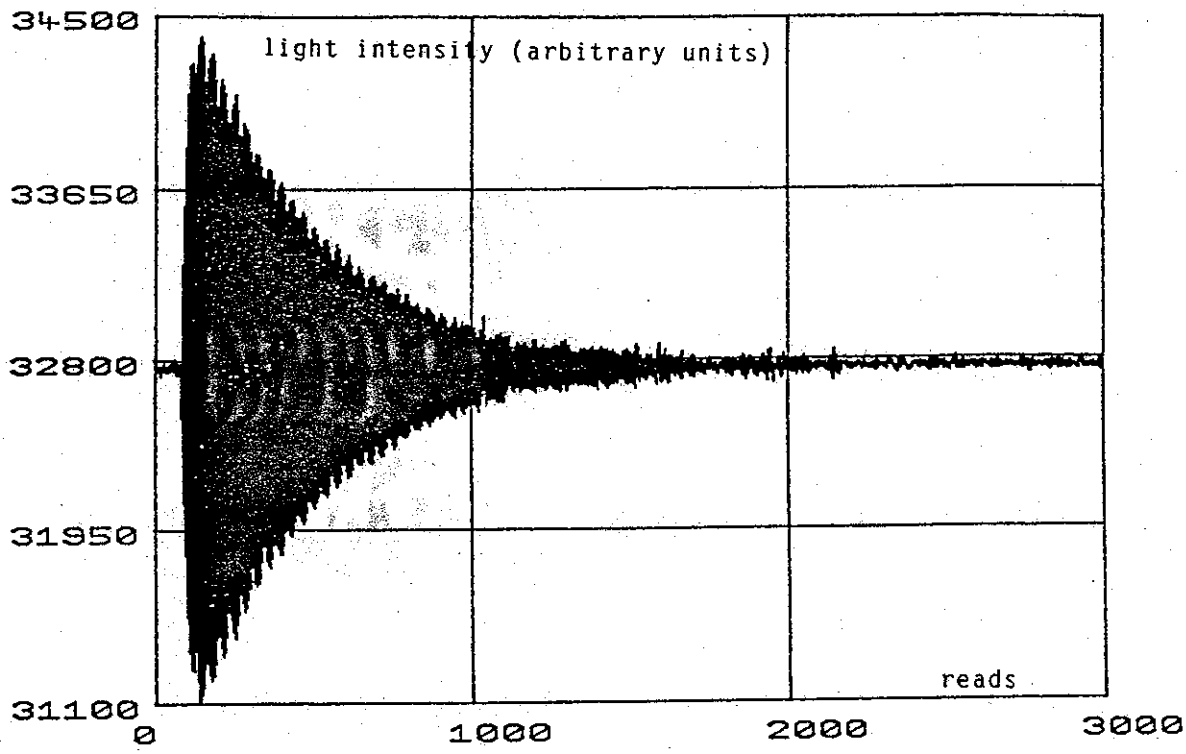

Figure 6.11: Mercury free precession in a 10 mGauss magnetic field using the new light source. 50 reads correspond to 1 second.

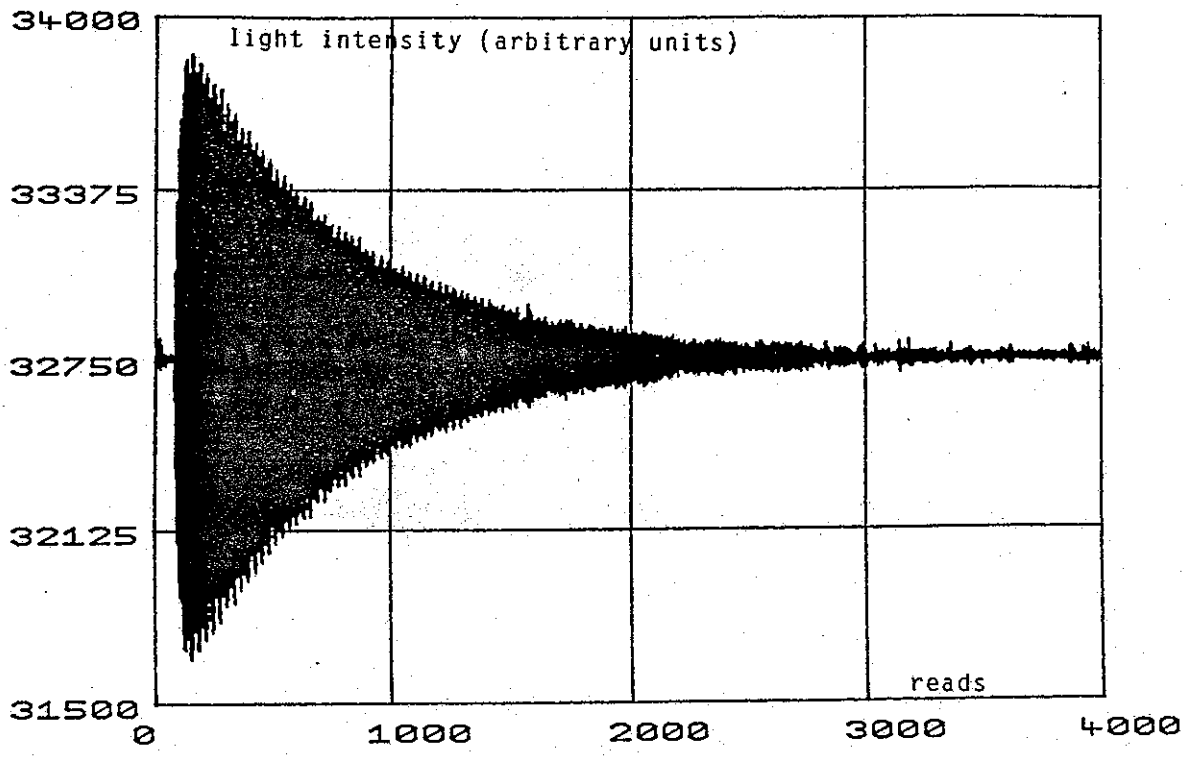

Figure 6.12: Mercury free precession in a 10 mGauss magnetic field using the new light source. The chamber is at a temperature of 50 °C. 50 reads correspond to 1 second.

taken, giving S/N = 225 and a relaxation time of 10 secs.

The improvement in relaxation time on heating and the associated improvement in S/N may be due to a reduced sticking time on the walls. Unfortunately the improvement does not persist when the system is cooled down again.

6.5.4.- Discussion

The signals obtained in these experiments seem to be of a satisfactory S/N level. Nevertheless, the relaxation times involved are rather short. We showed that the cause of relaxation is not originated by the magnetic field gradients. Reducing the analysing field B_0 to 1/10 of its value did not affect the total relaxation time although the signal amplitude did improve by a factor of 2. The reason is that at such a low field (1 mGauss), the polarising field was 6 times bigger than B_0 (i.e. 6 mGauss), while $B_p = 1.5\, B_0$ when $B_0 = 10$ mGauss. The bigger the ratio B_p/B_0 the more the effectively ($B_0 + B_p$) is aligned with the pumping light beam and the polarisation is improved.

Using the new light source allowed us to double the total incoming photon flux and thus half the pumping time but this did not have any effect on the total relaxation time τ.

The prime cause for relaxation must be the walls. We calculate that a depolarising surface area of 12 mm^2 can shorten the relaxation time to 10 secs (the total area is 177×10^3 mm^2). An area as small as that could well have been missed out in the coating process, especially around the windows or the O-ring grooves. Another depolarising factor could be the presence in the coating of the inhibitor used

to keep styrene as a monomer. We also estimate that if the inhibitor constitutes 1% of the polystyrene coating and if we assume that there is complete spin destruction upon hitting an inhibitor molecule, it would only take 1% of the inhibitor to cause a 10 sec relaxation time.

The experiment performed at 50°C shows an improvement by a factor of 2 in the relaxation time τ. It confirmed that the S is proportional to τ since both of them improved by the same factor. The reason for such an improvement at high temperature is due to the reduction in the atoms' dwelling time on the chamber walls which shortens the interaction time between an atomic spin and the depolarising site.

Quantitative analysis:

First, we shall calculate what the signal amplitude to the total light (S/DC) is from the free precession signal obtained at 10 mGauss and 45% light absorption, and then extrapolate S/DC in the case where 10% of the light is absorbed.

Secondly, we shall assume a 10% absorption and calculate S/DC for the same degree of polarisation as that achieved in the experiment.

1. From figure 6.7 we can calculate the ratio of the signal amplitude to the total DC light level

$$\frac{S}{DC} = \frac{15.4 \times 10^{-3}}{10.08} = 0.153\ \% \qquad (6.26)$$

In this experiment the absorption was 45%. Using figure 6.10 we can calculate what the ratio S/DC would be for a 10% total absorption. We find that S/DC = 0.089%.

2. Taking τ_R = 9 secs and τ_p = 215 secs and substituting in (5.28.b) we obtain the polarisation of ^{199}Hg as

$$P = 1.3\ \% \qquad (6.27)$$

Let us take the case where the Hg admitted reduces the intensity by 10%. This means that 1.8% is due to the actual pumping component, namely 204 with 199(F=1/2) component. We recall from section 6.5.2.4 that this component constitutes 18% of the total absorption and thus a 1.8% contribution to the total 10%. This amount refers to an unpolarised target. A system which gives 1.8% absorption when it is unpolarised would give a modulation of 3.6% of the incident light if the system were 100% polarised when the spin vector precesses about the magnetic field at the Larmor frequency.

We established in equation 6.27 that only 1.3% of the target is polarised. Consequently, the resulting modulation in the absorption is 3.6%x1.3% = 0.047% at the precession frequency. This value is about half 0.089%.

An explanation for that is the tendency of the pumping light to be reflected by the aluminium chamber walls and thus contribute to the pumping process more than once. It appears that the average effect resulted in doubling the light beam doing the pumping.

Noise estimation:

Let us estimate the rms noise present in the signal. Taking I = 5μAmps as a typical photomultiplier current

recorded after the vapour has been admitted to the big chamber and assuming the noise at the input of the photomultiplier tube to be purely shot noise, i.e

$$i_{RMS} = (2\,q\,I\,\Delta f)^{\frac{1}{2}} \qquad (6.28)$$

we find that, at the output of the photomultiplier tube

$$\frac{\text{RMS noise}}{\text{DC}} = 0.0019\% \qquad (6.29)$$

or

$$\frac{\text{DC}}{\text{RMS noise}} = 5\text{x}10^{4} \qquad (6.30)$$

where we took the Q of the tuned amplifier to be 10 and a center frequency of 8 Hz.

This figure is to be compared with the values observed in the experiment. These usually vary between 0.0018% and 0.0040%. In figure 6.7 this ratio is equal to 0.0018% which is in very good agreement with the calculated value.

6.5.5.- Transfer of a polarised gas from one chamber to another

This section is concerned with an attempt to polarise Hg atoms in the small chamber and then transfer them to the big one where their precession around B_0 is observed.

6.5.5.1.- Experimental procedure

The new light source was set up at the top of the shield in order to shine light onto the small chamber (see figure 6.1) at a distance of 28 cm. A quartz lens (5 cm of focal

length and 4 cm in diameter) was positioned 6 cm away from the source, whereas both linear polarisers and the $\lambda/4$ plate were placed near the source because the $\lambda/4$ plate was slightly magnetic. The beam subtends a solid angle $d\Omega = 0.35$ Str at the chamber.

The operating sequence adopted is as follows:
1. Once Hg is thought to be completely pumped in the small chamber, the teflon valve is then opened for a time T_f to fill the big chamber with polarised Hg atoms.
2. A $\pi/2$ pulse generated by the same coil used to generate the B_p field is applied for a time T_m to flip the spins from the z-direction (along the axis of the shield) to the xy-plane. Being in the presence of the B_0 field, the atomic spins start precessing around it at the Larmor frequency f_0.
3. This precession is then monitored in the same usual way by shining light across the big chamber.

A similar free precession signal to the ones obtained previously is then expected. As far as the detection is concerned, we will be using exactly the same items that we have used so far.

6.5.5.2.- Preliminary calculations

Figure 6.13 shows the circuit generating the $\pi/2$ pulse. The manual switch can either be set to connect the coil to a DC current supply (generating the field B_p when necessary) or to an AC/open circuit position. Once on position B, a square pulse T_m seconds long from a timer is used to activate the Hg relay and an AC current at the

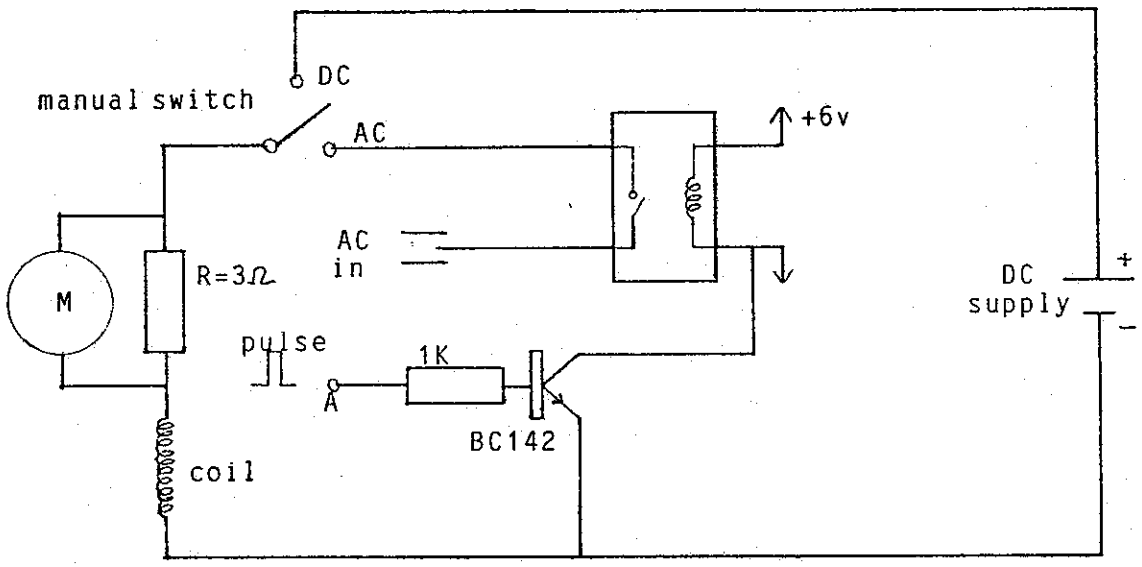

Figure 6.13: A DC field is obtained when the switch is in the DC position. An AC field is produced for the duration of the pulse applied at A when the switch is in the AC position.

resonance frequency is fed to the coil.

In order to test this technique, we polarised Hg atoms in the big chamber along B_p. Once this is switched off the atoms precess around B_0. Before the precession has died out we applied a $\pi/2$ pulse at the Larmor frequency and with the appropriate strength. This makes the signal disappear by flipping the spins along B_0 provided they are "picked up" with the right phase which is a matter of pure luck. We succeeded in reducing the signal to 20% of its amplitude. Fortunately, this problem of phase between the $\pi/2$ pulse and the precessing spins is irrelevant in the transfer experiment since we will be flipping spins which are all along the B_0 field and not in a precession motion.

Strength of the $\pi/2$ pulse:

This can be calculated from the following formula

$$\gamma B T_m = \phi \qquad (6.31)$$

where ϕ is the angle through which the spins are rotated under the action of B in a period of time T_m. In this experiment $\phi = \pi/2$. If the flipping is done in 2 secs we find that $B = B_0/32$ i.e. 0.31 mGauss which requires 7 mAmps peak in the 40 cm diameter Helmholtz coil generating the pulse. However, when the experiment was done, we found that a 2 sec pulse at 0.51 mGauss intensity gave the optimum signal. The disagreement between the calculated value and the experimental one is of no surprise since the 8 Hz field is expected to be attenuated by the aluminium walls to a certain extent.

Estimation of the possible pumping time:

This can be calculated from the value obtained when the pumping was done in the big vessel (T_p = 44 secs). Using equation 6.11 we find that T_p = 32 secs. Since we are using the new light source to pump the small chamber T_p = 16 secs because this source is twice as bright as the old one. Moreover, the solid angle used in this case is about 4 times bigger, therefore T_p = 4 secs. This estimation of T_p assumes the case of a thin target as it was the case when the pumping was done in the big chamber.

6.5.5.3.- Results

We showed in figure 6.10 that a maximum signal was obtained when 55% of the incoming light is absorbed. Consequently, it is worth setting the vapour pressure in the small chamber such that the same amount of light is absorbed. This can be done by looking at the amount of absorption in the big chamber after the gas has been transferred. This amount would then be equal to $0.55 \frac{V_s}{V_b} \frac{\ell_b}{\ell_s} = 8.3\%$. V_s and V_b are the volume of the small and the big chamber respectively, ℓ_b is the diameter of the big chamber and ℓ_s the height of the small chamber. We first measured the time it takes to absorb 8.3% in the big chamber for a given bead temperature and then calculate the time it takes to absorb 55% of the vapour in the small chamber. We find that opening the Hg manual valve for 28 secs would achieve such an absorption. However, using the bead temperature to monitor the amount of absorption is

rather unreliable. One has to make sure that the vapour is in equilibrium at any given temperature which implies waiting for a long enough time for that to take place. Nevertheless, a better way to run the experiment would be to fill the small chamber, admit some polarised Hg into the big chamber, and look at the signal amplitude at different bead pressures. The teflon valve is opened for a fixed time T_f but the Hg bead temperature is varied. We found that for T_f = 2.4 secs the best signal amplitude was obtained at a bead temperature of -3.2°C giving an absorption of 10.2% in the big chamber.

This signal is shown in figure 6.14. We can now calculate the absorption in the small chamber using the following relation

$$\text{Abs(small)} = \text{Abs(big)} \frac{V_b}{V_s} \frac{\ell_s}{\ell_b} \frac{1}{(1 - \exp(-2.4/3))} \qquad (6.32)$$

The last term takes into account the fact that the teflon valve is opened for 2.4 secs only and the time constant for sharing the gas between the two chambers is 3 secs. Equation 6.32 yields 37.4% absorption. This actually represents the ratio $(I_0 - I)/I_0 = (1-\exp-(n\sigma\ell_s))$ from which we find that the amount of absorption used in the small chamber $n\sigma\ell_s$ = 47%. This figure is in good agreement with the absorption of 55% which gave maximum signal in the big chamber (see figure 6.10). Moreover, the geometry of the two vessels is not the same, so the amount of reflected light contributing to the absorption is also different.

The total analysing light intensity used was 8.6 volts. The $\pi/2$ pulse was applied for 2 secs just after the teflon valve was closed. In fact, we arranged for the timer

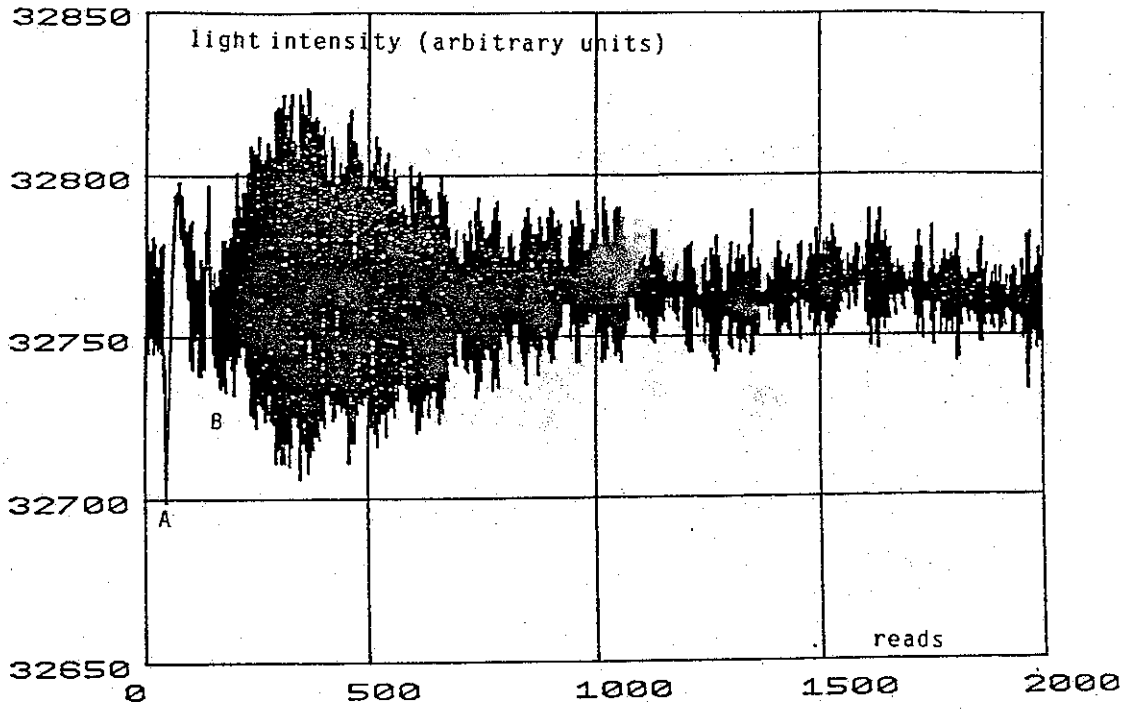

Figure 6.14: The mercury vapour was polarised in the small chamber and the free precession signal observed in the big chamber. 50 reads correspond to 1 second. The transfer was done at A (for 2.4 secs) and the $\pi/2$ pulse applied (for 2 secs) at B.

activating the teflon valve to initiate a second timer once the valve is closed. This second timer was then used to send a pulse to the $\pi/2$ pulse generating circuit. The signal to noise ratio achieved is 15.5 with a Q of 10 in the tuned amplifier.

However, there is still a correction factor on this figure due to the time required to fill the big chamber (2.4 secs) and apply the $\pi/2$ pulse (2 secs). Assuming that the average loss for the filling up process is 1.2 sec we end up with a 3.2 secs loss out of the 10 secs relaxation time measured in the big vessel. In other words, this reduces the signal to 68% of its actual size. Consequently the actual signal to noise ratio should be 23.

6.5.5.4.- Discussion

Although the signal to noise ratio obtained is rather poor, we showed that polarised mercury vapour can be transferred from one vessel to another and detect the spin precession around an applied magnetic field in the second chamber. One likely explanation for the poor S/N is a short relaxation time in the small chamber. This could be checked by polarising and analysing in the small chamber just like it was done in the big vessel. An estimation of the wall relaxation time in the small chamber from the relaxation time measured in the big vessel gives $T_R = 3$ secs, assuming the walls of both chambers to be similar. Combining this with the pumping time $T_p = 4$ secs gives a total relaxation time of 1.7 sec, which is rather short. However, this is only a rough estimate of the relaxation time and the state of the small chamber walls

should be examined more carefully.

As suggested earlier, the effect of the inhibitor mixed with polystyrene should be investigated and we may attempt to remove the inhibitor. The two chambers will also be recoated and the relaxation time remeasured.

We also intend to use a smaller quartz cylinder in the big chamber to get rid of reflection problems since quartz transmits the majority of the UV light. Furthermore, there should not be big stresses on the cylinder walls to affect the polarisation of the pumping light. This problem can occur with aluminium cylinders fitted with flat quartz windows. If these are fixed rather tightly the window can easily develop stresses.

Finally, using a smaller analysing chamber reduces the proportions between the analysing and the polarising chamber, which allows us to use a smaller vapour pressure in the polarising volume to obtain the same absorption in the analysing volume.

Radiation trapping:

Radiation trapping effects can cause some trouble. If the pressure is too high in the polarising cell, trapped radiation can cause a reduction in the amount of polarisation achieved. Let us assume a σ^+ polarised light beam incident on an atomic system whose ground state and excited state are F = 1/2 states. This beam can only excite the $\mu_F = -1/2$ ground sub-level to the $m_F = +1/2$ excited state. However, the spontaneous decay back to the ground state can take place by

a/ emitting a σ^- polarised photon and the atom goes to the

$\mu_F = -1/2$ sub-level. In this case the net angular momentum gain is zero.

b/ or emitting a π polarised photon and the atom goes to the $\mu_F = +1/2$ sub-level. This photon is generally emitted in a direction perpendicular to the direction of the incoming photon. Before leaving the cell, the π photon can then meet another atom, if the target pressure is high enough, and excite it from the $\mu_F = +1/2$ state to the $m_F = +1/2$ state, thus causing a depletion of the $\mu_F = +1/2$ state and a reduction in the sample polarisation.
As far as our experiment is concerned it is then more effective to use a long thin polarising volume to get rid of any radiation scattered at right angle to the main pumping beam. However, the polarising chamber cannot be made as long as one wishes because of existing magnetic field gradients.

Another improvement to the experiment would be to use purer isotopes both in the light source and the target. The fact that the source contains only 58% ^{204}Hg reduces these values by a factor of 0.58. Furthermore, the amounts of ^{204}Hg and ^{201}Hg in natural mercury add up to about 20% and ^{199}Hg constitutes 17% of the total. Both ^{204}Hg and ^{201}Hg(F=5/2) lines overlap with the 204 line from the source, therefore they absorb a total of $20/(17+20) = 54\%$ of the incoming 204 line. This makes only 46% of the 204 source line available for ^{199}Hg in the target. Consequently, there should be an improvement in S/N of 4. It is then certainly worthwhile utilizing purer mercury isotopes at the ILL for the source as well as the target.

CHAPTER VII

Design of the ILL Mercury Magnetometer

We finish this thesis by presenting the Mercury magnetometer we think should be used in the EDM experiment at ILL. We first give the experimental layout to be adopted and then estimate its performance.

7.1 -Experimental set-up

First of all, independently of the new magnetometer system, the EDM bottle is rotated through 90° about the horizontal axis (Figure 7.1). This reduces the displacement of the mean position of the neutrons by gravity. Furthermore, the volume of the storage bottle will be increased to 20 litres in order to increase the neutron storage time.

As far as the new magnetometer is concerned, mercury atoms are polarised inside a small chamber fixed to the bottom of the main neutron vessel. A first intense UV light source positioned at the lower part of the 4-layer μ-metal magnetic shield is used to do the polarisation. Once the vapour is transferred from the polarising chamber to the neutron storage vessel, the Hg precession signal around the 10mGauss field is monitored with a second light beam which we will call the analysing beam. This beam does not have to be intense, but just strong enough to monitor the Hg precession. It should be weak enough not to speed up the relaxation process or cause a release of electrons in the chamber that would break down the applied **E** field

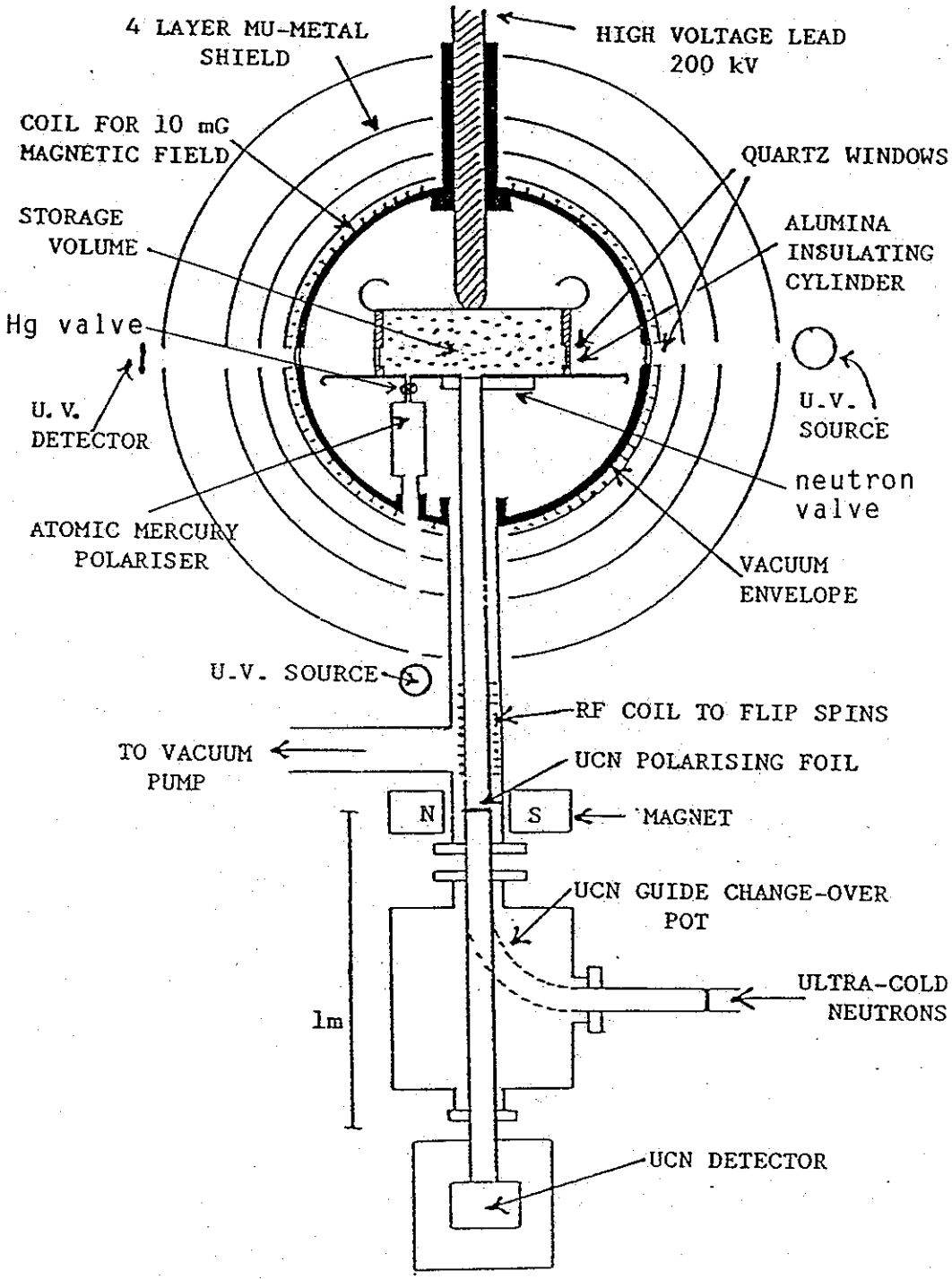

Figure 7.1 : The new arrangement of the neutron EDM apparatus at ILL.

which is the reason for not polarising Hg inside the storage vessel but have a separate polarising volume. Each time the neutrons are admitted to the big chamber, Hg atoms are also transferred from the small volume to the big one. By registering the decaying Hg sinewave in the neutron storage vessel a computer program is used to fit the data and calculate the Hg resonance frequency in the applied magnetic field.

For a given direction of the electric field E and a given value of the neutron $\pi/2$ pulse strength, a typical operating sequence would be

1. Close the Hg valve and polarise the atoms.
2. Open the neutron valve and fill the storage vessel.
3. Close the neutron valve, open the Hg valve and admit the polarised vapour.
4. Close the Hg valve.
5. Apply a $\pi/2$ pulse for both Hg and neutrons (8Hz for Hg and 30Hz for the neutrons).
6. Monitor the Hg precession using the analysing beam.
7. Apply the second $\pi/2$ neutron pulse coherent with the first one.
8. Open the neutron valve. Since Hg is moving much faster than the neutrons it will be pumped out of the system while the neutrons are directed onto the UCN detector to count them.

Since Hg atoms are about 100 times faster than the ultra cold neutrons used, the Hg vapour is admitted to the storage vessel after this is filled with neutrons and the neutron valve closed.

7.2 -Expected Performance:

From the results obtained at Sussex which are given in Chapter 6, we can estimate the S/N achievable at ILL. A computer program working with simulated data having the same S/N calculates the Hg precession frequency and the precision in that frequency.

Before such an estimation is done we have to make sure that the experiment at ILL works in the same sort of conditions existing at Sussex. For instance, the analysing photon flux has to be similar in order to use the same noise figure measured at Sussex. Let us start by estimating the analysing photon counting rate R as seen by the photomultiplier tube at ILL. Figure 7.2 shows the optical path of the analysing beam. The solid angle $d\Omega_s$ subtended at the source by the lens is $d\Omega_s = 1.96 \times 10^{-3}$ Str. The product P_s of the source surface area by $d\Omega_s$ is equal to 2.22×10^{-3} Str.cm^2. Similarly, the solid angle $d\Omega_v$ subtended by the window that is on the detector side is $d\Omega_v = 4.91 \times 10^{-4}$ Str.cm^2. The window surface area times $d\Omega_v$ is $P_v = 2.41 \times 10^{-3}$ Str.cm^2 which is very similar to P_s. Taking into account the transmission of light through the different optical components as measured in chapter 5, we can estimate the counting rate detected by the PM tube. A typical photon flux emerging from the light source is $J = 2.34 \times 10^{15}$ photons/sec. str. The circular polariser transmits 14.6%, the 4 windows and the lenses transmit 61% altogether, the two polystyrene layers on the storage vessel windows transmit 80% and the quantum efficient of the PM tube is 17.6%. Multiply all these factors together and the solid angle $d\Omega_{source}$ yields a counting rate

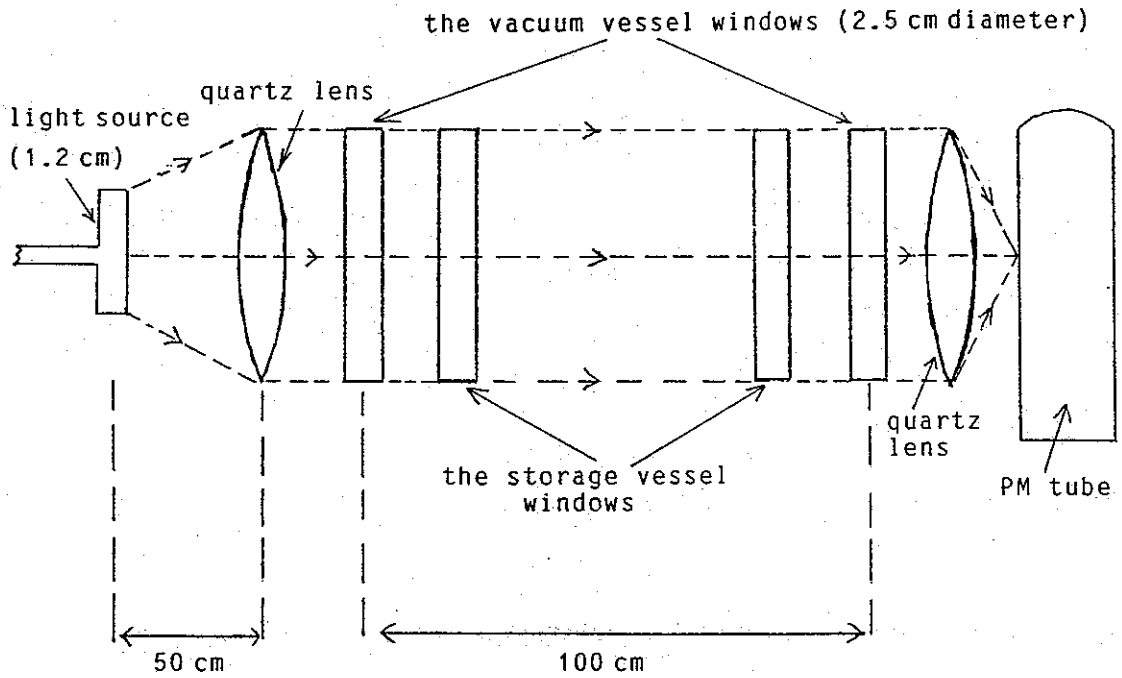

Figure 7.2 : Optical path of the analysing beam in the ILL setup.
The diagram is not to scale.

$$R = 5.75 \times 10^{10} \text{ photoelectrons/sec} \qquad (7.1)$$

The usual photomultiplier current used at Sussex (see Chapter 6) is about 10μAmp. This corresponds to a counting rate of 2.35×10^{10} photoelectrons/sec which is in the same range as R. Consequently, a direct comparison between the two set-ups can be drawn, namely we expect the detected noise to be the same as the one measured at Sussex (see chapter 6) ie. 0.0018% of the total incident light when the data is collected every 0.4 secs.

Degree of polarisation that will be achieved :

We consider the polariser volume to be a cylinder 35cm long and 7.5cm in diameter totalling a 1.55 litre volume. It can be a quartz cylinder coated with either polystyrene or teflon which should give a total relaxation time of at least 50secs. The magnetic field inside the 4-layer μ-metal shield was checked to be perfectly homogeneous over a 35cm distance. We intend to use the set-up shown in figure 7.3. The solid angle subtended at the source by the lens is $d\Omega = 0.22$ Str. The polariser transmits 14.6%, whereas the lens, the quartz window, the vacuum vessel and the coating transmit 72% altogether. If the photon flux emitted by the lamp is taken to be equal to the one measured at Sussex by the intense source, ie. $J = 4.68 \times 10^{15}$ photons/sec.Str, using equation 5.30 results in a pumping time

$$T_p = 4.8 \text{ secs.} \qquad (7.2)$$

Assuming a wall relaxation time of 50 secs, one can then

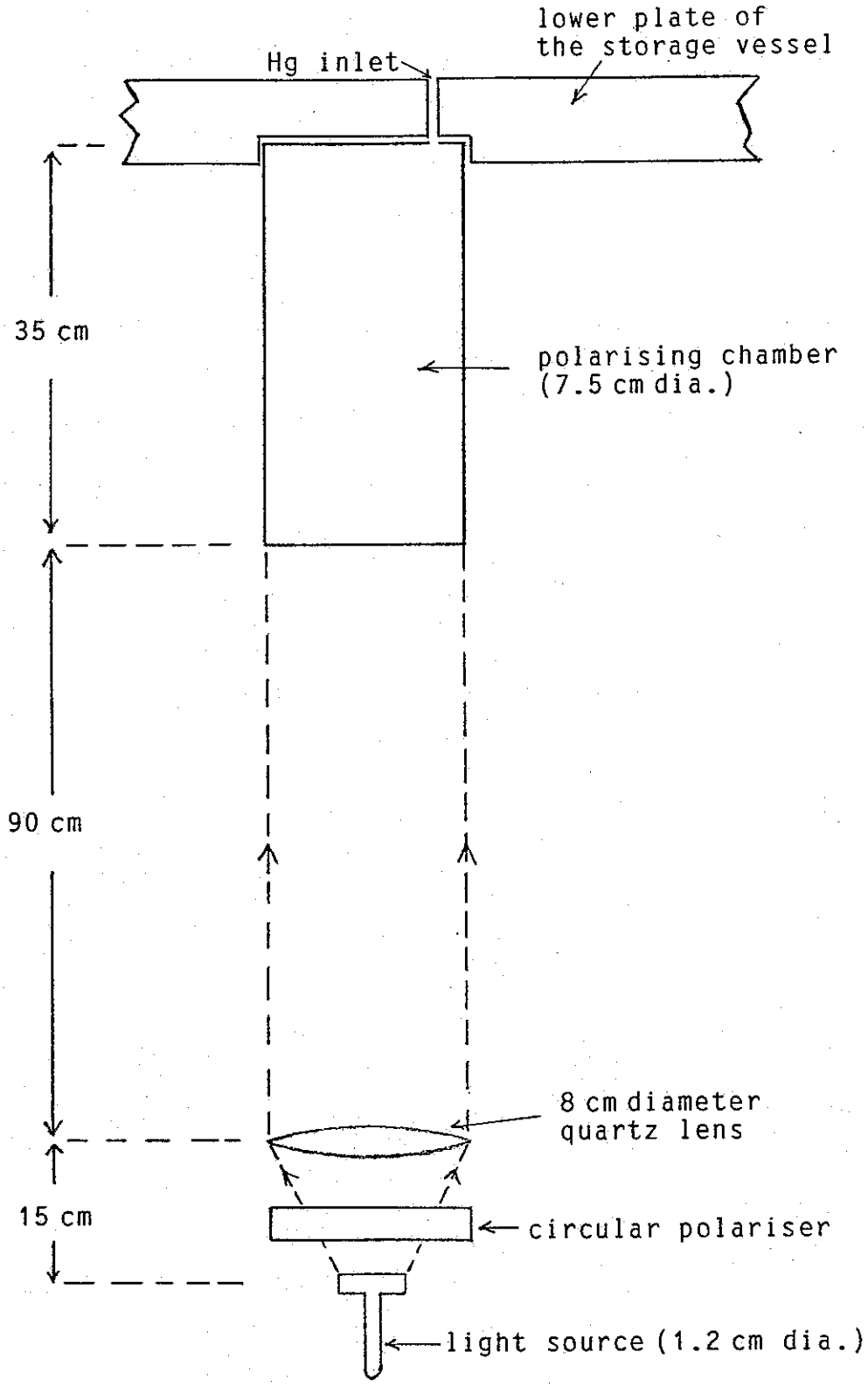

Figure 7.3 : Setup for polarising Hg that will possibly be used at ILL.

achieve a polarisation (using equation 5.28a)

$$P = 73\% \tag{7.3}$$

Where the incoming light is assumed to be 80% polarised.

Signal to Noise Ratio in the Main Vessel :

Assume a mean free path λ_{pol} of 1 meter for the light in the polariser volume. In the storage vessel this would be

$$\lambda = \lambda_{pol} \frac{V_b}{V_s} \tag{7.4}$$

where V_b = 20 litres and V_s = 1.55 litres. Therefore, λ = 12.9 m. If an unpolarised vapour is admitted to the storage vessel, the amount of absorption it experiences is equal to

$$A_{unp} = \frac{d}{\lambda} \tag{7.5}$$

where d = 40 cm is the diameter of the vessel. Thus A_{unp} = 3.1%. For a 100% polarised target, the modulation depth would then be 6.2% of the incident light when the spin vector precesses about the magnetic field at the Larmor frequency. But the actual target will be 73% polarised and the light beam 80% polarised. Therefore, the amount of modulation that we will achieve is S=3.62%. Since one can assume that the noise at 8Hz (which was checked to be shot noise from the source) will be of the same order as in the Sussex experiment ie. 0.0018% of the total light, with an integration time of 0.4 secs, we have

$$\left(S/N\right)_{.4sec} = \frac{3.62\%}{0.0018\%} = 2012 \qquad (7.6)$$

We will probably be taking, in the actual experiment, data with an integration time of 20 msecs (ie. 50 reads/sec), thus this figure has to be multiplied by $\sqrt{0.02/0.4}$. Therefore

$$S/N = 450 \qquad (7.7)$$

which is the signal to noise ratio calculated at the beginning of the decay signal.

Precision in the frequency measurement:

Assuming a relaxation time of 100 secs in the storage vessel, the S/N after 100 secs drops by a factor 1/e from the initial value and becomes equal to 166. Entering this figure of S/N in the computer program which does the data fit yields

$$\frac{\sigma_f}{f} = 2.54\text{x}10^{-7} \qquad (7.8.a)$$

for unfiltered noise, and

$$\frac{\sigma_f}{f} = 2.49\text{x}10^{-7} \qquad (7.8.b)$$

for a noise filtered with a band pass filter with a 0.01sec integration time.

This is better than the figure of $5.53\text{x}10^{-7}$ achieved by the UCN magnetometer.

7.3 -Conclusion

The work in this thesis is primarily concerned with the development of a new magnetometer system for the neutron EDM experiment at ILL (Grenoble).

We established that the best atomic system to use is probably spin polarised mercury atoms. They are easy to polarise and can be stored for long periods of time (few tens of seconds) provided the container walls are adequately coated. The Hg resonance frequency in a 10 mGauss field (this is the value of the field used in the EDM experiment) is 8 Hz and the neutron frequency is 30 Hz. Computer simulation shows that the Hg pulse applied at the same time as the neutron $\pi/2$ pulse alter the neutron count at the end of the cycle by a significant proportion of the order of the neutron counting statistics. The effect is calculable, however, and can be allowed for during data processing.

Magnetic field monitoring with Hg atoms is directly achieved by measuring the Larmor precession frequency rather than calculating it through some other parameter, like degree of polarisation, as it is the case in a Helium magnetometer.

We showed that Hg atoms can be polarised and stored in an Aluminium container 5.4 litres in volume coated with polystyrene. We obtained a good signal to noise ratio of 250. However, the wall relaxation time was rather short and amounted to only 10 seconds. Nevertheless, there is still quite a few changes that could be implemented in the experiment in order to improve both S/N and the relaxation time. We established that using pure isotopes in both the

light source and the target should improve the signal to noise ratio by a factor of 4. While this thesis was being written, a S/N of 1500 was obtained using 90% separated isotopes in both target and source.
In order to obtain more useful pumping light, we should use a larger quarter wave plate than the one we have been using so far (it is only 1.5 cm in diameter).

As far as improving the wall relaxation time, separation of the inhibitor from Styrene before polymerisation is certainly worth trying. It is believed that the presence of the inhibitor in the polystyrene wall coating may be the main cause of relaxation. Nevertheless, a mere recoating of the vessel could result in a better lifetime. We showed that an uncoated surface area as small as 1/10000 of the total area of the 5.4 litre volume could result in a 10 second relaxation time.

We also succeeded in polarising Hg atoms in a separate small Aluminium side chamber and in transferring them to the main chamber . The signal to noise ratio was only 23, but the main achievement, as far as this thesis is concerned is the fact that such a transfer could be done. One can now work on improving it in order to use such a technique in the ILL experiment. An immediate improvement that comes to mind is the use of a longer polarising chamber, probably made of quartz, in order to eliminate any trapped radiation problems.

Concerning the implementation of this technique in the neutron EDM experiment, we estimated that by using pure isotopes and provided we achieve a Hg wall lifetime of 100 seconds, the precision to which the magnetic field is measured is $\sigma_f / f = 2.5 \times 10^{-7}$. This is better than what the

neutrons provide ($\sigma_f/f = 5.53\times10^{-7}$) but a further improvement is certainly helpful. A limiting theoretical figure was calculated to be ~ 2.3×10^{-9}.

Compared to other magnetometer systems, Hg seems to be the best. Helium atoms can only achieve a precision of $\sigma_f/f = 9.5\times10^{-7}$. In addition, ^{3}He polarisation is rather difficult to measure. Another magnetometer system that was considered in this thesis is a Caesium system.
The tendency for Caesium to form a metallic layer on the walls causing a **E** field breakdown makes it a less likely system to use.

REFERENCES

[Alt 86] I.S.Altarev et-al, JETP Lett. **44**, 460 (1986).

[Bar 61] J.P.Barrat and C.Cohen-Tannoudji, J.Phys. Paris **22**, 329,443 (1961).

[Ben 56] P.Bender, Thesis Princeton University (1956).

[Bla 56] A.Blandin and J.P.Barrat, Compt. Rend. de l'Academie des Sciences **243**, 2041 (1956).

[Blo 40] F.Bloch and A.Siegert, Phys. Rev. **57**, 522 (1940).

[Blo 46] F.Bloch, Phys. Rev. **70**, 460 (1946).

[Bre 55] E.Breitenberger, Progress in Nuclear Physics **4**, 65 (1955).

[Bro 52] J.Brossel and F.Bitter, Phys. Rev. **86**, 308 (1952).

[Cag 58a] B.Cagnac, J. Phys. Radium **19**, 863 (1958).

[Cag 58b] B.Cagnac, J.Brossel and A.Kastler, Compt. Rend. **246**, 1827 (1958).

[Cag 58c] B.Cagnac and J.Brossel, Compt. Rend. **249**, 77 (1958).

[Cag 71] B.Cagnac, Ann. Phys. (Paris) **6**, 467 (1961).

[Chr 64] J.H.Christenson, J.W.Cronin, V.L.Fitch and R.Turlay, Phys. Rev. Lett. **13**, 138 (1964).

[Coh 62] C.Cohen-Tannoudji, Ann. Phys. (Paris) **7**, 423, 469 (1962).

[Col 63] F.D.Colegrove, L.D.Schearer and G.K.Walters, Phys. Rev. **132**, 2561 (1963).

[Cor 77] A.Corney, Atomic and Laser Spectroscopy, Clarendon Press Oxford (1977).

[Deh 57] H.G.Dehmelt, Phys. Rev. **105**, 1924 (1957).

[Fra 59] W.Franzen, Phys. Rev. **115**, 850 (1959).

[Fra 86] P.W.Franks, Thesis University of Sussex, (1986).

[Fri 57] J.I.Friedman and V.L.Telegdi, Phys. Rev. **105**, 1681 (1957).

[Gar 57] R.L.Garwin et al, Phys. Rev. **105**, 1415 (1957).

[Gui 57] M.A.Guiochon et al, Comp. Rend. **243**, 1859 (1956).

[Hap 72] W.Happer, Rev, Mod. Phys. **44**, 169 (1972).

[Kas 50] A.Kastler, J. Phys. (Paris) **11**, 255 (1950).

[Kas 66] A.Kastler, Comp. Rend. Acad. Sciences (Paris) Vol.262, serie B, 624 (1966).

[Lam 87] S.K.Lamoreaux, Thesis University of Washington (1987).

[Lam 88] S.K.Lamoreaux, Institut Laue-Langevin Internal Report 88LA01T (1988).

[Lud 57] G.Luders and B.Zumino, Phys. Rev. **106**, 385 (1957).

[Mes 65] A.Messiah, Quantum Mechanics Vol 2, North Holland Publishing Company - Amsterdam (1965).

[Mit 71] A.C.G.Mitchell and M.W.Zemansky, Resonance Radiation and Excited Atoms, Cambridge University Press (1971).

[Mug 81] S.F.Mughabghab et al, Neutron Cross Sections Vol.1, Part A, Acad Press (1981).

[Pau 55] W.Pauli, Niels Bohr and the Development of Physics, London Pergamon (1955).

[Pav 77] M.Pavlovic and F.Laloe, J. de Phys. **31**, 173 (1970).

[Pen 90] J.M.Pendlebury, Private communication (1990).

[Pur 50] E.M.Purcell and N.F.Ramsey, Phys. Rev. **78**, 807 (1950).

[Ram 49] N.F.Ramsey, Phys. Rev. **76**, 996 (1949).

[Ram 56] N.F.Ramsey, Molecular Beams, Oxford University

Press (1956).

[Ram 79] N.F.Ramsey, Proposal to Use a ^{3}He Optically Pumped Magnetic Field Monitor in Neutron EDM Experiments, Harvard University Report (1979).

[Ram 84] N.F.Ramsey, Acta Physica Hungarica **55** (1-4), 117 (1984).

[Rob 58] H.G.Robinson et al,Bull. Am. Phys. Soc. **3**, 9 (1958).

[Sch 63] L.Schiff, Phys. Rev. **132**, 2194 (1963).

[Skr 61] G.V.Skrotskii and T.G.Izyumova, Soviet Phys. Usp. **4**, 177 (1961).

[Smi 90] K.F.Smith, Private Communication (1990).

[Smi 90] K.F.Smith, Physics Letters B Vol. 234, number 1,2 , 191 (1990).

[Wu 57] C.S.Wu et al Phys. Rev. **105**, 1413 (1957).

APPENDIX 1

Modulation of a light beam by precessing absorbing atoms

Let us assume a completely polarised atomic system with a ground state total angular momentum F = 1/2 and J = 0, and an excited state with F = 1/2 and J = 0. This is the case of an ensemble of ^{199}Hg atoms subjected to a σ^+ polarised 2537 Å resonance radiation. The ground state is a $^1S_0$ and the excited state a $^3P_1$.

We also assume a quantisation axis in the direction θ,ϕ and a magnetisation **M** in this same direction. The state $|\psi\rangle$ describing such a system in the ground state is

$$|\psi\rangle = \mathrm{Sin}\frac{\theta}{2}\, e^{i\phi/2}\, |-1/2\rangle + \mathrm{Cos}\frac{\theta}{2}\, e^{-i\phi/2}\, |+1/2\rangle \qquad (A1.1)$$

We then apply a magnetic field **B** in the z-direction and shine a σ^+ polarised light beam in the x-direction.

Let us calculate the probability of finding the system in the excited $^3P_1$ state under the action of such a light beam.

The electric vector **E** of the incoming light beam (σ^+ polarised) can be written as

$$\mathbf{E} = \frac{E}{\sqrt{2}}(\mathbf{j} + i\mathbf{k}) \qquad (A1.2)$$

if it was σ^- polarised it would be $\mathbf{E} = \frac{E}{\sqrt{2}}(\mathbf{j} - i\mathbf{k})$.

The position of the electron making the transition is

$$\mathbf{r} = x\mathbf{i} + y\mathbf{j} + z\mathbf{k} \qquad \text{(A1.3)}$$

therefore

$$\mathbf{E}.\mathbf{r} = \frac{E}{\sqrt{2}}(y + iz) \qquad \text{(A1.4)}$$

The spherical tensor components of $\mathbf{r}$ are defined by

$$r_0 = z$$

$$r_- = \frac{1}{\sqrt{2}}(x - iy) \qquad \text{(A1.5)}$$

$$r_+ = \frac{-1}{\sqrt{2}}(x + iy)$$

therefore

$$y = \frac{i}{\sqrt{2}}(r_+ + r_-) \qquad \text{(A1.6)}$$

The probability of making an electric dipole transition to the $^3P_1$ state is

$$P = |\langle \tfrac{1}{2}\tfrac{1}{2}|\mathbf{E}.\mathbf{r}|\psi\rangle|^2 + |\langle \tfrac{1}{2}-\tfrac{1}{2}|\mathbf{E}.\mathbf{r}|\psi\rangle|^2 \qquad \text{(A1.7)}$$

which is the sum of the transition probabilities from the superposition state $|\psi\rangle$ to either of the $|F\,M_F\rangle$ excited states.

In the $|J\ M_J\rangle|I\ M_I\rangle$ representation the ground state levels are $|00\rangle|\tfrac{1}{2}+\tfrac{1}{2}\rangle$ and $|00\rangle|\tfrac{1}{2}-\tfrac{1}{2}\rangle$ whereas the excited states $|FM_F\rangle$, they are written as

$$|\tfrac{1}{2}\tfrac{1}{2}\rangle = \frac{-1}{\sqrt{3}}|10\rangle|\tfrac{1}{2}\tfrac{1}{2}\rangle + \sqrt{\frac{2}{3}}|11\rangle|\tfrac{1}{2}-\tfrac{1}{2}\rangle \qquad \text{(A1.8)}$$

and

$$|\tfrac{1}{2}-\tfrac{1}{2}\rangle = -\sqrt{\frac{2}{3}}|1-1\rangle|\tfrac{1}{2}\tfrac{1}{2}\rangle + \frac{1}{\sqrt{3}}|10\rangle|\tfrac{1}{2}-\tfrac{1}{2}\rangle \qquad \text{(A1.9)}$$

note that we do have $\langle\tfrac{1}{2}\tfrac{1}{2}|\tfrac{1}{2}-\tfrac{1}{2}\rangle = 0$ therefore

$$|\langle\tfrac{1}{2}\tfrac{1}{2}|\mathbf{E}.\mathbf{r}|\psi\rangle|^2 = |\left(\frac{-1}{\sqrt{3}}\langle\tfrac{1}{2}\tfrac{1}{2}|\langle 10| + \sqrt{\frac{2}{3}}\langle\tfrac{1}{2}-\tfrac{1}{2}|\langle 11|\right)\mathbf{E}.\mathbf{r}\left(|00\rangle\right.$$

$$\left.\mathrm{Sin}\frac{\theta}{2}e^{i\phi/2}|\tfrac{1}{2}-\tfrac{1}{2}\rangle + |00\rangle\mathrm{Cos}\frac{\theta}{2}e^{-i\phi/2}|\tfrac{1}{2}\tfrac{1}{2}\rangle\right)|^2 \qquad \text{(A1.10)}$$

Note that when including the electronic spin states, $|\psi\rangle$ is written as

$$|\psi\rangle = \mathrm{Sin}\frac{\theta}{2}e^{i\phi/2}|00\rangle|\tfrac{1}{2}-\tfrac{1}{2}\rangle + \mathrm{Cos}\frac{\theta}{2}e^{-i\phi/2}|00\rangle|\tfrac{1}{2}\tfrac{1}{2}\rangle \qquad \text{(A1.11)}$$

Also note that the $|IM_I\rangle$ states do not act on $\mathbf{E}.\mathbf{r}$, thus

$$|\langle\tfrac{1}{2}\tfrac{1}{2}|\mathbf{E}.\mathbf{r}|\psi\rangle|^2 = |\frac{-1}{\sqrt{3}}\langle 10|\mathrm{Cos}\frac{\theta}{2}e^{-i\phi/2}\mathbf{E}.\mathbf{r}|00\rangle +$$

$$\sqrt{\frac{2}{3}}\langle 11|\mathrm{Sin}\frac{\phi}{2}e^{i\phi/2}\mathbf{E}.\mathbf{r}|00\rangle|^2$$

$$= |\frac{-1}{\sqrt{3}}\mathrm{Cos}\frac{\theta}{2}e^{-i\phi/2}\frac{E}{\sqrt{2}}\langle 10|y+iz|00\rangle +$$

$$\sqrt{\frac{2}{3}}\mathrm{Sin}\frac{\theta}{2}e^{i\phi/2}\frac{E}{\sqrt{2}}\langle 11|y+iz|00\rangle|^2 \qquad \text{(A1.12)}$$

But (see Woodgate page 162),

$$\langle 10|y+iz|00\rangle = i\langle 10|z|00\rangle = i\sqrt{B} \qquad \text{(A1.13)}$$

$$\langle 11|y+iz|00\rangle = \langle 11|y|00\rangle = \frac{i}{\sqrt{2}}\sqrt{B} \qquad \text{(A1.14)}$$

where $\sqrt{B}$ is a reduced matrix element dependent on the other commun quantum numbers (like n) and a radial integral. Therefore

$$|\langle \tfrac{1}{2}\tfrac{1}{2}|\mathbf{E}.\mathbf{r}|\psi\rangle|^2 = E^2 B|\frac{-1}{\sqrt{3}}\mathrm{Cos}\frac{\theta}{2}e^{-i\phi/2}\frac{i}{\sqrt{2}} + \sqrt{\frac{2}{3}}\mathrm{Sin}\frac{\theta}{2}e^{i\phi/2}\frac{1}{\sqrt{2}}\frac{i}{\sqrt{2}}|^2$$

$$= \frac{E^2 B}{6}|-\mathrm{Cos}\frac{\theta}{2}e^{-i\phi/2} + \mathrm{Sin}\frac{\theta}{2}e^{i\phi/2}|^2 \qquad (A1.15)$$

Now we use the fact that

$$|ae^{i\phi/2} + be^{-i\phi/2}|^2 = a^2 + b^2 + 2ab\mathrm{Cos}\phi \qquad (A1.16)$$

where a and b are real, therefore

$$|\langle \tfrac{1}{2}\tfrac{1}{2}|\mathbf{E}.\mathbf{r}|\psi\rangle|^2 = \frac{E^2 B}{6}(1 - 2\mathrm{Sin}\frac{\theta}{2}\mathrm{Cos}\frac{\theta}{2}\mathrm{Cos}\phi)$$

$$= \frac{E^2 B}{6}(1 - \mathrm{Sin}\theta\mathrm{Cos}\phi) \qquad (A1.17)$$

Similarly we obtain

$$|\langle \tfrac{1}{2}-\tfrac{1}{2}|\mathbf{E}.\mathbf{r}|\psi\rangle|^2 = \frac{E^2 B}{6}(1 - \mathrm{Sin}\theta\mathrm{Cos}\phi) \qquad (A1.18)$$

The total probability of equation (A1.7) is then

$$P = \frac{E^2 B}{3}(1 - \mathrm{Sin}\theta\mathrm{Cos}\theta) \qquad (A1.19)$$

In our experiment, the magnetisation **M** is in the xy-plane, for which $\theta=\pi/2$ and $\mathrm{Sin}\theta=1$, therefore

$$P = \frac{E^2 B}{3}(1 - \cos\phi) \qquad (A1.20)$$

$\phi = \omega t$ where ω is the precession frequency of the sample magnetisation around the applied B field. Hence

$$P = \frac{E^2 B}{3}(1 - \cos\omega t) \qquad (A1.21)$$

indicating a modulation in light absorption at the frequency ω.

APPENDIX 2

Solution to the Rate equations for the ^{199}Hg System

Let us consider a simplified model of the energy levels of ^{199}Hg, in which the ground state is made up of two Zeeman states 1 and 2 having spin projection quantum numbers $\mu_F = -1/2$ and $\mu_F = +1/2$ respectively. Let the excited state be made up of level 3 with $m_F = -1/2$ and level 4 with $m_F = +1/2$. Let this system of atoms be subjected to the action of a light beam made up of γ% left circularly polarised light (σ^+) and $(1-\gamma)$% right circularly polarised light (σ^-). We define the overall polarisation of this beam as

$$P_L = \frac{\gamma - (1-\gamma)}{\gamma + (1-\gamma)} = 2\gamma - 1 \qquad \text{(A2.1)}$$

We also define the following probabilities as follows:
$-P_{1,2} = P_{2,1} = \frac{1}{2T_R}$ the probabilities per atom and per unit time of having a transition from 1 to 2 (or 2 to 1) under the action of the relaxation processes influencing the system.
$-P_{1,4} = \gamma\frac{1}{T'_p}$ and $P_{2,3} = (1-\gamma)\frac{1}{T'_p}$. $P_{1,4}$ is the probability per unit time of having a transition from 1 to 4 per atom due the σ^+ light component and $P_{2,3}$ the probability per unit time of having a transition from 2 to 3 per atom due to the σ^- component.

$-P_{3,1} = \alpha\frac{1}{\tau}$, $P_{3,2} = (1-\alpha)\frac{1}{\tau}$, $P_{4,1} = \alpha'\frac{1}{\tau}$ and $P_{4,2} = (1-\alpha')\frac{1}{\tau}$.
$P_{3,1}$ is the probability per unit time of having a

spontaneous emission from 3 to 1. $P_{3,2}$, $P_{4,1}$ and $P_{4,2}$ are similarly defined. α is the relative transition strength from 3 to 1 and α' is the relative transition strength from 4 to 1. τ is the lifetime of levels 3 and 4 assumed to be the same.

One can now write the rate equations for the evolution of the populations of all the four levels.

$$\frac{dn_1}{dt} = -n_1 P_{1,2} + n_2 P_{2,1} - n_1 P_{1,4} + n_4 P_{4,1} + n_3 P_{3,1}$$

$$= (n_2 - n_1)\frac{1}{2T_R} - n_1 \frac{\gamma}{T'_p}(1-\alpha') + n_2 \frac{(1-\gamma)}{T'_p}\alpha \qquad (A2.2)$$

$$\frac{dn_2}{dt} = -n_2 P_{2,1} + n_1 P_{1,2} - n_2 P_{2,3} + n_3 P_{3,2} + n_4 P_{4,2}$$

$$= -(n_2 - n_1)\frac{1}{2T_R} - n_2 \frac{(1-\gamma)}{T'_p}\alpha + n_1 \frac{\gamma}{T'_p}(1-\alpha') \qquad (A2.3)$$

$$\frac{dn_3}{dt} = -n_3 P_{3,1} - n_3 P_{3,2} + n_2 P_{2,3}$$

$$= \frac{-n_3}{\tau} + n_2 \frac{(1-\gamma)}{T'_p} \qquad (A2.4)$$

$$\frac{dn_4}{dt} = -n_4 P_{4,1} - n_4 P_{4,2} + n_1 P_{1,4}$$

$$= \frac{-n_4}{\tau} + n_1 \frac{\gamma}{T'_p} \qquad (A2.5)$$

At equilibrium, we have $dn_3/dt = dn_4/dt = 0$, thus

$$n_3 = n_2 \frac{(1-\gamma)}{T'_p}\tau \qquad (A2.6)$$

$$n_4 = n_1 \frac{\gamma}{T'_p}\tau \qquad (A2.7)$$

Subtracting (A2.2) from (A2.3) and putting $n_2 - n_1 = n$ and $n_1 + n_2 = N$ we obtain

$$\frac{d(n_2-n_1)}{dt} = -\frac{n}{T_R} - 2n_2\frac{(1-\gamma)}{T'_p}\alpha + 2n_1\frac{\gamma}{T'_p}(1-\alpha') \qquad (A2.8)$$

Since $n_2 = \frac{N+n}{2}$ and $n_1 = \frac{N-n}{2}$ we have

$$\frac{dn}{dt} = -n\left[\frac{1}{T_R} + \frac{1}{T'_p}(\alpha + \gamma(1-\alpha'-\alpha))\right] - \frac{N}{T'_p}\left[\alpha + \gamma(\alpha'-1-\alpha)\right] \qquad (A2.9)$$

We define the degree of polarisation as

$$P = \frac{n}{N} \qquad (A2.10)$$

Therefore equation (A2.9) can be written in the form

$$\frac{dP}{dt} = -\Gamma_R P - \Gamma'_p P(\alpha + \gamma(1-\alpha'-\alpha)) + \Gamma'_p(\gamma(1-\alpha') - (\alpha(1-\gamma)) \qquad (A2.11)$$

where $\Gamma_R = \frac{1}{T_R}$ and $\Gamma'_p = \frac{1}{T'_p}$. We have $\alpha = 1/3$ and $\alpha' = 2/3$, thus

$$\frac{dP}{dt} = -\Gamma_R P + \frac{1}{3}\Gamma'_p[(2\gamma-1) - P] \qquad (A2.12)$$

but $2\gamma-1$ is the polarisation of the light beam as expressed in equation (A2.1), hence

$$\frac{dP}{dt} = -\Gamma_R P + \frac{1}{3}\Gamma'_p(P_L - P) \qquad (A2.13)$$

If we call pumping time the quantity T_p defined as

$$\frac{1}{T_p} = \frac{1}{3}\Gamma'_p = \Gamma_p \qquad (A2.14)$$

equation (A2.13) can then be written under the form

$$\frac{dP}{dt} + (\Gamma_R + \Gamma_p)\, P = \Gamma_p\, P_L \qquad \text{(A2.15)}$$

The solution to this equation is

$$P(t) = \frac{\Gamma_p\, P_L}{\Gamma_R + \Gamma_p}\left(1 - \exp-(\Gamma_R + \Gamma_p)t\right) \qquad \text{(A2.16)}$$

We can easily see that at equilibrium (i.e $t \longrightarrow \infty$) the optimum atomic polarisation attained is

$$P_\infty = \frac{\Gamma_p P_L}{\Gamma_R + \Gamma_p} \qquad \text{(A2.17)}$$

If the light beam is 100% σ^+ polarised (i.e $\gamma=1$, $P_L=1$) then

$$P_\infty = \frac{\Gamma_p}{\Gamma_R + \Gamma_p} \qquad \text{(A2.18)}$$

If the light beam is 100% σ^- polarised (i.e $\gamma=0$, $P_L=-1$) then

$$P_\infty = -\frac{\Gamma_p}{\Gamma_R + \Gamma_p} \qquad \text{(A2.19)}$$

If the light beam is 50% σ^+ and 50% σ^- polarised (i.e $\gamma=1/2$ and $P_L=0$), then $P_\infty = 0$.

APPENDIX 3

Derivation of the Expression of the Pumping Time T_p

We are concerned in this appendix with the derivation of equation (5.30). Let us consider the ^{199}Hg atomic system $^1S_0$ ground state and $^3P_1$ excited state. Both states have two Zeeman components. The M_F changing decay rate is twice as probable as the M_F conserving one. This can be shown by writing the expression of the four states in the $|JM_J>|IM_I>$ representation and then compute the radiative transition operator between two states involved in the transition.
Let N_+ = total population in the ground state with $M_F = +1/2$ and N_- = total population in the ground state with $M_F = -1/2$. If $N = N_+ + N_-$, $n = N_+ - N_-$, $n_+ = N_+/V$ and $n_- = N_-/V$, we can see that $N_- = -\frac{1}{2}(n - N)$ and $N_+ = \frac{1}{2}(n + N)$.
Suppose this atomic system is subjected to the action of a σ^+ polarised light beam. In a time t, the N_- population decreases by a factor of 1/3 and N_+ increases by a factor of 1/3. We can then write the equation of evolution of the difference between N_+ and N_- as

$$\frac{d(N_+ - N_-)}{dt} = R\, I_0 \exp-(n_- \sigma x) \qquad (A3.1)$$

where $R = 2/3$ is the relative transition probability for the upwards transition involving a change in M_F (i.e from $M_F = -1/2$ to $M_F = +1/2$). We also introduced n_- in the exponential term because only the atoms in the $M_F = -1/2$ of the ground state are excited. I_0 is the total incoming photon flux which we will call J, x is the distance

travelled by the beam in the vapour and σ is the light absorption cross-section per atom. If we assume the case of a thin target we can write that

$$\exp-(n_- \sigma x) \approx n_- \sigma x \qquad \text{(A3.2)}$$

therefore equation (A3.1) takes the form

$$\frac{d(N_+ - N_-)}{dt} = \frac{2}{3} J n_- \sigma x \qquad \text{(A3.3)}$$

Substituting for $(N_+ - N_-)$ and n_- we obtain

$$\frac{dn}{dt} = \frac{1}{3} \frac{J\sigma x}{V} (N - n) \qquad \text{(A3.4)}$$

Introducing the degree of atomic polarisation $P = n/N$, this equation becomes

$$\frac{dP}{dt} = \frac{1}{3} \frac{J\sigma x}{V} (1 - P) \qquad \text{(A3.5)}$$

At $t = 0$, $P(0) = 0$ and the solution of (A3.5) is

$$P(t) = 1 - \exp-(t/T_p) \qquad \text{(A3.6)}$$

where

$$T_p = \frac{V}{1/3\sigma x J} \qquad \text{(A3.7)}$$

The quantity we defined as the total pumping time of the vapour.

APPENDIX 4

Calculations of the Effective Light Absorption Cross-section in a Hg Vapour

We are concerned here, of course, with the 2537 Å Hg intercombination line incident on a Hg vapour. We assume that both the source and the target are not pure but contain a mixture of Hg isotopes. We defined, in equation 6.19,as the light absorption cross-section of the source component j with the target component i the quantity

$$\Sigma_i^j = A_i \frac{1}{N_{g\,i}} \sigma_i^j \qquad \text{(A4.1)}$$

where A_i is the abundance of component i in the target and $N_{g\,i}$ is the ground state degeneracy of the isotope i. For example, for the even isotopes $N_{g\,even} = 1$, but $N_{g\,199} = 2$ and $N_{g\,201} = 4$. σ_i^j is the effective light absorption cross-section per atom defined by

$$\sigma_i^j = \sigma(\omega_0)\, O_i^j\, (\Sigma b_r)_i \qquad \text{(A4.2)}$$

where $(\Sigma b_r)_i$ is the total probability of optical transition with σ^+ light to the excited level for each target component i. In table A4.1 we give $(\Sigma b_r)_i$ for each component [Cag 61]. O_i^j is a factor describing the extent to which source component j overlaps with target component i. $\sigma(\omega_0)$ is the peak cross-section involving two components of exactly the same centre wavelength and complete overlap.

Overlapping Lines	$\sum b_r$ for σ^+ light
204 – 204	1
204 – 199-1/2	2/3
204 – 201-5/2	2
202 – 202	1
200 – 200	1
198 – 198	1
198 – 201-3/2	4/3
199-1/2 – 199-1/2	2/3
199-1/2 – 204	1
199-1/2 – 201-5/2	2
199-3/2 – 199-3/2	4/3
199-3/2 – 201-1/2	2/3
201-1/2 – 201-1/2	2/3
201-1/2 – 199-3/2	4/3
201-3/2 – 201-3/2	4/3
201-3/2 – 198	1
201-5/2 – 201-5/2	2
201-5/2 – 204	1
201-5/2 – 199-1/2	2/3

Table A4.1

In what follows is a detailed calculation of both $\sigma(\omega_0)$ and O_i^j.

Let $\sigma(\omega)$ be the frequency dependent absorption cross-section given by [Cor 77]

$$\sigma(\omega) = \frac{3\lambda^2}{2\pi}\left[\frac{\gamma^2/4}{(\omega-\omega_0')^2+\gamma^2/4}\right] \qquad (A4.3)$$

which exhibits a Lorentzian shape of height 1 and width γ. ω is the frequency of the incoming light being considered, ω_0' is the centre frequency for the absorbing atom and may be a value influenced by Doppler shift due to the motion of the atom. Let ω_0 be the unshifted value for an atom at rest.

We then assign to the atom to have a probability distribution over the thermal speeds. Thus

$$\sigma(\omega) = \int_0^\infty \frac{3\lambda^2}{2\pi}\left[\frac{\gamma^2/4}{(\omega-\omega_0')^2+\gamma^2/4}\right] p(\omega_0')\,d\omega_0' \qquad (A4.4)$$

where $p(\omega_0')d\omega_0'$ is the probability for an atom to have an angular frequency between ω_0' and $\omega_0' + d\omega_0'$. We have

$$\int_0^\infty p(\omega_0')\,d\omega_0' = 1 \qquad (A4.5)$$

Since the Lorentzian shape is much more smaller than $p(\omega_0')$ (it is about 1MHz wide as opposed to the width of $p(\omega_0')$ which extends over more than 1000 MHz) , it behaves like a δ function and the integral in (A4.4) becomes

$$\sigma(\omega) = p(\omega)\int_0^\infty \frac{3\lambda^2}{2\pi}\left[\frac{\gamma^2/4}{(\omega-\omega_0')^2+\gamma^2/4}\right] d\omega_0' \qquad (A4.6)$$

Doing the integration results in

$$\sigma(\omega) = p(\omega)\,\frac{3\lambda^2}{4}\,\gamma \qquad \text{(A4.7)}$$

The quantity $p(\omega)$ is given by

$$p(\omega) = \frac{2}{\sqrt{\pi\Delta}}\,\exp-[4(\omega-\omega_0)^2/\Delta^2] \qquad \text{(A4.8)}$$

where Δ is a quantity proportional to the true Doppler half-width Δ'

$$\Delta = \frac{\Delta'}{\sqrt{\text{Log}2}} \qquad \text{(A4.9)}$$

and

$$\Delta' = 2\,\frac{\omega_0}{c}\left[\frac{2kT}{M}\,\text{Log}2\right]^{\frac{1}{2}} \qquad \text{(A4.10)}$$

c is the velocity of light in free space, T is the temperature of the target, k is the Boltzman constant and M is the mass of the radiating atom. Δ' can also be written under the form

$$\Delta' = 7.16\text{x}10^{-7}\,\nu_0\left(\frac{T}{A}\right)^{\frac{1}{2}} \qquad \text{(A4.11)}$$

where A is the atomic weight of the radiating particle and $\nu_0 = \frac{c}{\lambda}$.

Substituting for $p(\omega)$ in (A4.7), we have

$$\sigma(\omega) = \frac{3\lambda^2}{2\pi}\,\frac{\gamma}{\Delta'}\,(\pi\text{Log}2)^{\frac{1}{2}}\,\exp-[4(\omega-\omega_0)^2/\Delta^2] \qquad \text{(A4.12)}$$

The peak value $\sigma(\omega_0)$ of $\sigma(\omega)$ is obtained at $\omega = \omega_0$.

Therefore

$$\sigma(\omega_0) = \frac{3\lambda^2}{2\pi}\frac{\gamma}{\Delta'}(\pi \mathrm{Log}2)^{\frac{1}{2}} \qquad (A4.13)$$

which is the expression used in section 6.5.2.2.4 equation 6.20 . Since $\lambda = 2537$ Å , $\gamma = 1/\tau$ (where $\tau = 1.18\times10^{-7}$ sec. is the lifetime of the $^3P_1$ level), $T = 294^\circ K$ (we assume the target to be at room temperature) and $A = 199$, we have

$$\frac{\Delta'}{2\pi} = 1030 \text{ MHz} \qquad (A4.14)$$

and

$$\sigma(\omega_0) = 6\times10^{-17} \text{ m}^2 \qquad (A4.15)$$

Let us now find an expression for the overlap O_i^j. It is defined for a thin source as the weighted cross-section over the incoming spectrum and expressed as

$$O_i^j = \left\langle \frac{\sigma(\omega)}{\sigma(\omega_0)} \right\rangle = \frac{\int_0^\infty I^j(\omega)\,[\sigma_i(\omega)/\sigma(\omega_0)]\,d\omega}{\int_0^\infty I^j(\omega)\,d\omega} \qquad (A4.16)$$

where we introduced the index i for the target and j for the source. The light spectral profile $I^j(\omega)$ emitted by the source is assumed to have a Gaussian shape, i.e

$$I^j(\omega) = B \exp-[4(\omega-\omega_{0j})^2/\Delta_j^2] \qquad (A4.17)$$

where Δ_j is defined through equation (A4.9) , $\omega_{0j}/2\pi$ is the centre frequency for the source and B is a constant. Substituting for $\sigma_i(\omega)$, $\sigma(\omega_0)$ and $I^j(\omega)$ in equation (A4.16) we find

$$O_i^j = \frac{\int_0^\infty \exp-[4(\omega-\omega_{0\,j})^2/\Delta_j^2]\,\exp-[4(\omega-\omega_{0\,i})^2/\Delta_i^2]\,d\omega}{\int_0^\infty \exp-[4(\omega-\omega_{0\,j})^2/\Delta_j^2]\,d\omega} \qquad (A4.18)$$

After integration we obtain

$$O_i^j = \frac{1}{\sqrt{(\alpha_i^j)^2+1}} \exp-\left(4(\beta_i^j)^2\left[\frac{1}{(\alpha_i^j)^2}+\frac{1}{((\alpha_i^j)^2+1)}\right]\right) \qquad (A4.19)$$

where we put

$$\alpha_i^j = \frac{\Delta_j}{\Delta_i}$$

$$\beta_i^j = \frac{\omega_{0\,j}-\omega_{0\,i}}{\Delta_i} \qquad (A4.20)$$

Because of the small differences in the atomic weights of the different isotopes, we assumed $\Delta'_j/2\pi = 1200$ MHz to be the same for all, and $\Delta'_i/2\pi = 1030$ MHz. The source temperature was taken to be equal to 400°K and the target temperature to 294°K.

Finally, a detailed picture of the different light components existing in both the source and the target is presented in figure A4.1. The components at the bottom represent the absorption lines of ^{199}Hg corresponding to σ^+ transitions in an unpolarised target.These are drawn for natural Hg used in the resonance experiments of chapter 6. However, the spectral lines at the top of the picture represent the emission lines from the source used in those same experiments for which the isotopic abundances are given in table A4.2. The x-axis corresponds to the different positions of the lines in the frequency domain.

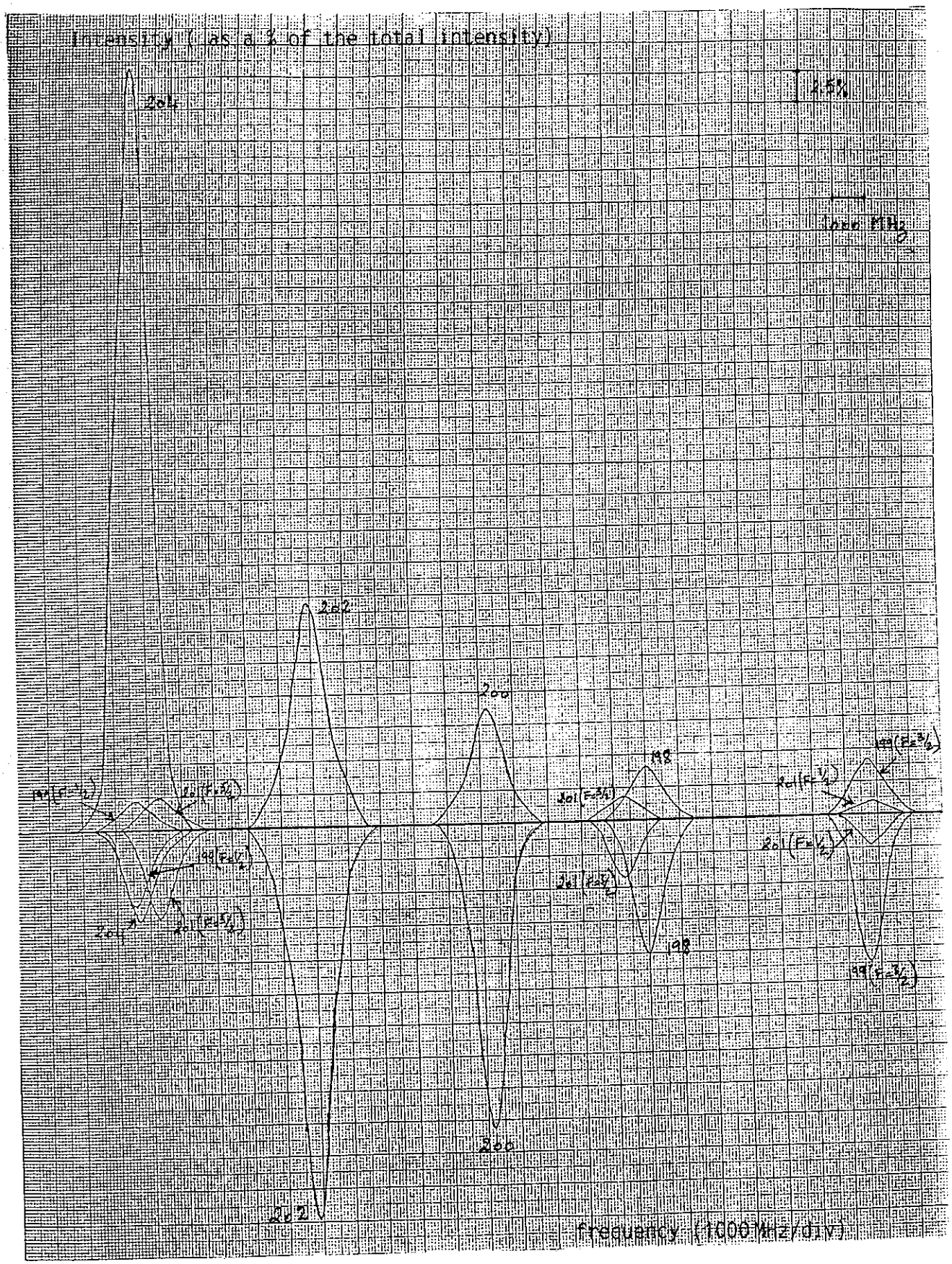

Figure A4.1: Diagram showing the target absorption lines (on the lower side of the axis) and the source emission lines(on the upper side).The target is natural Hg, whereas the source is made up of a mixture given in table A4.2. On the vertical axis, each division corresponds to 2.5% of the total intensity.

Isotope	204	202	201	200	199	198
Abundance (%)	58.20	17.05	5.26	8.78	6.50	4.10

Table A4.2: Hg isotopic abundance from Harwell used in the light source.

The scale on this axis is 1000 MHz per division. The width of each line is determined by its Doppler-width calculated using equation (A4.11). The y-axis corresponds to the strength of each line. We just took the quantity $A_i\ (\Sigma b_r)_i\ /N_{gi}$ to represent the strength of each target line. A_i, $(\Sigma b_r)_i$ and N_{gi} were all defined in the begining of this appendix. As far as the source is concerned, we took the quantity

$$I_0^j = F^j\ A^j \qquad \text{(A4.21)}$$

to represent the strength of the line. A^j is the abunbance of source line j, and F^j is defined by

$$F^j = \frac{(2F+1)}{(2J+1)(2I+1)} \qquad \text{(A4.22)}$$

for each source component j. The different F^j values are summarised in table A4.3.

Isotope	$2J+1$	$2I+1$	$2F+1$	$\frac{2F+1}{(2J+1)(2I+1)}$
204	3	1	3	1
202	3	1	3	1
201-5/2	3	4	6	1/2
201-3/2	3	4	4	1/3
201-1/2	3	4	2	1/6
200	3	1	3	1
199-3/2	3	2	4	2/3
199-1/2	3	2	2	1/3
198	3	1	3	1

Table A4.3: Summary of the F' factors used to determine the intensity of each source component.

APPENDIX 5

Calculations of the Equilibrium Pressure in the Experiment of Chapter VI

The system considered is made up of three sub-systems :

1. The Hg container whose volume is taken to be negligible compared to the other two sub-systems.
2. The small chamber having a volume V_s.
3. The big chamber with a volume V_b.

The conductance of the connections (tubes, appertures ...etc...) are C_1 between V_s and the Hg container, and C_2 between V_s and V_b. We will be calling p_0 the Hg pressure in the Hg container, $p_s(t)$ the pressure in V_s, and $p_b(t)$ the one in V_b. We will assume that p_0 keeps constant throughout the transfer and thereafter.

The procedure consists of opening the Hg valve (see figure 6.1) until V_s is filled to pressure $p_s = p_0$. Then open the teflon valve (the vacuum valve is of course kept closed all the way through) to fill up V_b. There will first be a sharing of the gas between V_s and V_b and then a filling up period of the two volumes V_s and V_b, from the bead, until the system reaches equilibrium.

The equations governing the flow of Hg in the system can be written as

$$V_s \frac{dp_s}{dt} = (p_0(t) - p_s(t))\, C_1 - (p_s(t) - p_b(t))\, C_2 \qquad (A5.1)$$

$$V_b \frac{dp_b}{dt} = (p_s(t) - p_b(t))\, C_2 \qquad (A5.2)$$

Differentiating the two sides of equation (A5.1) with respect to time we obtain

$$V_s \frac{d^2 p_s}{dt^2} = -C_1 \frac{dp_s}{dt} - C_2 \frac{dp_s}{dt} + C_2 \frac{dp_b}{dt} \qquad (A5.3)$$

Using equation (A5.2), we have

$$V_s \frac{d^2 p_s}{dt^2} = -(C_1 + C_2) p'_s + \frac{C_2^2}{V_b}(p_s - p_b) \qquad (A5.4)$$

Using equation (A5.1), we end up with the differential equation describing the evolution of the pressure in V_s,

$$p''_s + \left(\frac{C_1 + C_2}{V_s} + \frac{C_2}{V_b}\right) p'_s + \frac{C_1 C_2}{V_s V_b} p_s = \frac{C_2 C_1}{V_s V_b} p_0 \qquad (A5.5)$$

Let us put

$$a = \left(\frac{C_1 + C_2}{V_s} + \frac{C_2}{V_b}\right) ; \; b = \frac{C_1 C_2}{V_s V_b} ; \; c = b p_0 \qquad (A5.6)$$

The general form of the solution of equation (A5.5) is given by

$$p_s(t) = A \exp(+m_1 t) + B \exp(+m_2 t) + \frac{c}{m_1 m_2} \qquad (A5.7)$$

where m_1 and m_2 are the solutions of the following equation

$$m^2 + am + b = 0 \qquad (A5.8)$$

i.e

$$m1 = \frac{1}{2}\left(-a - \sqrt{a^2 - 4b}\right) \;;\; m_2 = \frac{1}{2}\left(-a + \sqrt{a^2 - 4b}\right) \qquad (A5.9)$$

note that $m_1 m_2 = b$ and $c = bp_0$.

At $t = 0$ (i.e when we open V_b), $p_s = p_0$ and thus $A = -B$.

Moreover, we have according to equation (A5.1) $p_2' = -\frac{C_2}{V_b} p_0$ at $t = 0$.

Differentiating equation (A5.7) and setting $t = 0$ we obtain

$$-\frac{C_1}{V_s} p_s = m_1 A + m_2 B = (m_1 - m_2) A \qquad (A5.10)$$

or

$$A = \frac{C_2}{V_s} \frac{1}{(m_2 - m_1)} p_0 \qquad (A5.11)$$

The final form of the solution is then

$$p_s(t) = \frac{C_2}{V_2} \frac{p_0}{(m_2 - m_1)} [\exp(+m_1 t) - \exp(+m_2 t)] + p_0 \qquad (A5.12)$$

We verify that at $t = 0$ $p_s = p_0$, and when $t \longrightarrow \infty$ $p_s = p_0$

Writing equation (A5.1) under the form

$$p_b = \frac{V_b}{C_2} p_s' + \frac{(C_1 + C_2)}{C_2} p_s - \frac{C_1}{C_2} p_0 \qquad (A5.13)$$

and substituting for p_s' (calculated from equation A5.12), we end up with an expression of the pressure in the big vessel in the form

$$p_b(t) = p_0 [(d+e) \exp(+m_1 t) - (d+f) \exp(+m_2 t) + 1] \qquad (A5.14)$$

where

$$d = \frac{C_1 + C_2}{(m_2 - m_1)V_s} \quad ; \quad e = \frac{m_1}{m_2 - m1} \quad ; \quad f = \frac{m_2}{m_2 - m_1} \qquad (A5.15)$$

we see that at $t = 0$, $p_b(0) = 0$ whereas at $t \longrightarrow \infty$, $p_b(\infty) = p_0$. Therefore, the solution shows well that the ultimate pressure reached by the system, at equilibrium, is the pressure of the bead p_0 at a given temperature.
The conductance C_1 of the pipework connecting the Hg bead to the small chamber is calculated to be equal to 0.0113 l/sec. for Hg. Whereas, the conductance of the 2 mm long and 2 mm diameter hole connecting the two chambers is $C_2 = 0.081$ l/sec. for Hg atoms. Note that the ratio of the velocity of air molecules to that of Hg atoms is equal to 0.39.

```
 10REM SAVE"ADPLOT3"
 20*KEY10"OLD|MMODE131|MLISTO7|MVDU14|ML.|M"
 30*KEY0"32767+273*EXP(-(X-6156)/400)"
 40REM N% HB in bank%, LB in bank%+1
 50D%=0:REM No points already stored
 60?&0405=0:?&FE6E=16:MODE128
 70DIM MC% 100
 80M%=20000
 90Y1=32200:Y2=33200
100C%=80
110DIM bank% M%
120T%=bank%+M%
130?&F8=(bank%+28) MOD 256              :REM START OF DATA LO BYTE
140?&F9=(bank%+28) DIV 256              :REM START OF DATA HI BYTE
150:
160a$="Take new data ?":PROCans:IF A$="Y" PROCdata
170a$="Graph data ?":PROCans:IF A$="Y" PROCplot
180a$="SAVE data ?":PROCans:IF A$="Y" PROCsave
190a$="LOAD data from disk ?":PROCans:IF A$="Y" PROCload
200GOTO 160
210:
220DEF PROCdata
230?&206=MC% MOD 256                    :REM REPLACE IRQ2 VECTORS
240?&207=MC% DIV 256                    :REM REPLACE IRQ2 VECTORS
250                                     :REM PROGRAM 16BIT
260                                     :REM 2 8 BIT READS OF THE USER PORT
270                                     :REM IRQ2V INTERUPT VIA CB1 ON 6522
280                                     :REM LINE 350 = JMP &DE89 FOR BBC/B
290                                     :REM LINE 350 = JMP &E60C FOR MASTER
300                                     :REM INTERUPT ON CB1 PROG
310?&FE62=0                             :REM PORT B SET TO I/P MODE
320?&FE6C=238                           :REM CB2 HIGH
330PRINT"Memory available for ";INT((M%-2-1-25-C%-D%*2)/2);" reads"
340INPUT "Number of reads ?"N%:D%=D%+N%
350?(bank%+2)=C%/80
360C%=C%+80
370?bank%=D% MOD 256
380?(bank%+1)=D% DIV 256
390$(bank%+3)=TIME$
400FORPASS=0TO1                         :REM SET FOR 2 ASSEMBLER PASSES
410P%=MC%
420
430[OPT PASS*2
440       PHA:TXA:PHA:TYA:PHA             \SAVE STATUS
450       LDA£16:STA&FE6E                 \DISABLE FURTHER INTERUPTS ON CB1
460       LDA&FE6D:ORA £16:STA &FE6D      \CLEAR CB1 INTERUPT FLAG
470       LDA£1:STA&0405                  \SET INTERUPT FLAG
480       LDY£2                           \SET LOOP COUNTER
490.loop  LDA£206:STA&FE6C                \CB2 LOW
500       LDA&FE60:STA(&F8)               \READ ADC
510       INC &F8                         \INCREMENT STORE POINTER LO BYTE
520       BNE high                        \BRANCH IF < 255
530       INC &F9                         \INCREMENT STORE POINTER HI BYTE
540.high  LDA£238:STA&FE6C                \CB2 HI
550       DEY:BNE loop                    \BRANCH TO LOOP FOR HI BYTE
560       LDA£144:STA&FE6E                \ENABLE INTERUPTS ON CB1
570       PLA:TAY:PLA:TAX:PLA             \RESTORE STATUS
580       JMP &E60C                       \RETURN TO BASIC
```

```
590]NEXT PASS
600
610FOR I%=1 TO N%
620?&FE6E=144
630IF?&0405=0THEN630
640?&405=0
650NEXT
660?&FE6E=16
670PRINT:a$="Save data to disk ?":PROCans:IF A$="Y" PROCsave
680ENDPROC
690:
700DEF PROCplot
710PROCaxes
720PROCpoints
730INPUTTAB(0,3)"Name Y axis = "a$:VDU26:PRINTTAB(8,1)a$:VDU28,0,31,79,28
740INPUTTAB(0,3)"Name X axis = "a$:VDU26:PRINTTAB(40,24)a$:VDU28,0,31,79,28
750PRINTTAB(0,3);:a$="Graph to printer?":PROCans:IF A$="Y" PROCgraph
760a$="Change axes?":PROCans:IF A$="Y" GOTO 710
770a$="Calculate Ymax,Ymin?":PROCans:IF A$="Y" PROCmax:PROCfindx
780a$="Fit a curve?":PROCans:IF A$="Y" PROCadd
790a$="Graph to printer?":PROCans:IF A$="Y" PROCgraph
800a$="Calculate noise?":PROCans:IF A$="Y" PROCnoise
810a$="Calculate Signal/noise?":PROCans:IF A$="Y" GOTO 830
820ENDPROC
830PROCmax:INPUT"Noise in which interval? ":PROCnoise:PROCston
840ENDPROC
850DEF PROCans
860PRINTa$;" (Y/N) ";:A$=GET$:PRINTA$:IFA$<>"Y"ANDA$<>"N"GOTO860
870ENDPROC
880
890DEFPROCaxes:LOCAL W,N,NX,NY
900PRINT"No data points available = ";D%
910INPUT"Xmin,Xmax="X1,X2
920PRINT"Y range is ";Y1;" to ";Y2;" change it (Y/N) ";:A$=GET$
930IF A$="Y" OR A$="y" INPUT'"Ymin,Ymax="Y1,Y2:GOTO 940
940CLS:CLG:VDU28,0,31,79,28:W=Y2-Y1:N=0:PROCintervals
950NY=N:W=X2-X1:N=0:PROCintervals
960NX=N:VDU5:@%=&0500
970FOR N=0 TO NY:W=200+N*800/NY
980MOVE 0,W+10:PRINT(Y1+(Y2-Y1)*N/NY)
990MOVE 100,W:PLOT 21,1200,W:NEXT
1000FOR N=0 TO NX:W=100+N*1100/NX
1010MOVE W-30,180:PRINT(X1+(X2-X1)*N/NX)
1020MOVE W,200:PLOT 21,W,1000:NEXT:VDU4
1030ENDPROC
1040DEF PROCintervals:LOCAL I
1050IF W<1 THEN W=W*10:GOTO 1050
1060IF W>1E6 THEN W=W/10:GOTO 1060
1070I=3
1080IFABS(W/I-INT(W/I+.001))<.001THEN1110
1090I=I+1:IF I<6GOTO1080
1100W=W*10:GOTO 1070
1110N=I:ENDPROC
1120
1130DEF PROCpoints
1140VDU5
1150BA%=bank%+28+2*X1
1160x=X1+1
1170y=256*?BA%+?(BA%+1):BA%=BA%+2
1180MOVE FNX,FNY
1190FOR x=X1+2 TO X2
```

```
1200y=256*?BA%+?(BA%+1):BA%=BA%+2
1210DRAW FNX,FNY
1220NEXT
1230VDU4
1240ENDPROC
1250
1260DEF PROCgraph
1270a$="Large print?":PROCans
1280IFA$="Y"GOTO1290ELSEGOTO1330
1290*FX108,1
1300*RUN BDUMP2
1310*FX108,0
1320GOTO1360
1330*FX108,1
1340*RUN BDUMP1
1350*FX108,0
1360VDU2,1,27,1,64,1,27,1,33,1,1,1,27,1,108,1,12,3
1370VDU2:PRINT
1380PRINTD$:PRINT
1390PRINT"Comments":FORI%=T%-80 TO T%-C% STEP -80:PRINT$I%:NEXT
1400VDU3
1410a$="Reprint graph?":PROCans:IF A$="Y" GOTO 1270
1420ENDPROC
1430
1440DEF PROCsave
1450INPUT"Filename (7 char max)="Q$
1460PRINT"Comment, one line max"
1470INPUTLINE""A$:$(T%-C%+80)=A$
1480OSCLI"SAVE "+Q$+" "+STR$~bank%+"+"+STR$~M%
1490ENDPROC
1500:
1510DEF PROCload
1520INPUT'"Filename (7 char max)="Q$
1530OSCLI"LOAD "+Q$+" "+STR$~bank%
1540REM BA%=bank%+28
1550REM FORI%=0 TO 10
1560REM y=256*?BA%+?(BA%+1):BA%=BA%+2
1570REM PRINTy
1580REM NEXT
1590C%=80*?(bank%+2)
1600D%=?bank%+256*?(bank%+1)
1610D$=$(bank%+3):PRINT"Data was saved on ";D$
1620PRINT"Comments":FORI%=T%-80 TO T%-C% STEP -80:PRINT$I%:NEXT
1630ENDPROC
1640:
1650DEF FNX=100+(x-X1)*1100/(X2-X1)
1660DEF FNY=200+(y-Y1)*800/(Y2-Y1)
1670:
1680DEF PROCadd
1690INPUTLINE"Y(X) = "E$
1700X=X1:x=X1:y=EVAL(E$)
1710MOVE FNX,FNY
1720FOR x=X1 TO X2 STEP (X2-X1)/100
1730X=x:y=EVAL(E$)
1740PLOT 5,FNX,FNY
1750NEXT
1760a$="Another curve?":PROCans:IF A$="Y" GOTO 1690
1770ENDPROC
1780:
1790DEF PROCnoise
1800S1=0:S2=0:MS=0:RMS=0
```

```
1810INPUT"Xmin,Xmax= "Xmin,Xmax
1820BA%=bank%+28+2*Xmin-2
1830FOR x=Xmin TO Xmax-2
1840y=256*?BA%+?(BA%+1):BA%=BA%+2
1850S1=S1+y:S2=S2+y^2
1860REM PLOT 69,FNX,FNY
1870NEXT
1880N=Xmax-Xmin-1
1890MS=(S2/N)-(S1/N)^2
1900RMS=SQR(MS)
1910PRINT"RMS noise (bits) = ";RMS
1920PRINT"RMS noise (mv) = ";RMS*0.1526
1930ENDPROC
1940:
1950DEF FNy(I%)
1960BA%=bank%+28+2*I%
1970=256*?BA%+?(BA%+1)
1980:
1990DEF PROCmax
2000INPUT"Enter Xmin,Xmax where the max and min are likely to be: " XX1,XX2
2010Ymax=FNy(XX1):Ymin=Ymax
2020FOR I%=XX1 TO XX2
2030IF Ymax<FNy(I%) Ymax=FNy(I%)
2040IF Ymin>FNy(I%) Ymin=FNy(I%)
2050NEXT
2060PRINT"Ymax = "Ymax," ";:PRINT"     Ymin = "Ymin," ";
2070PRINT"      Ymax-Ymin = "Ymax-Ymin
2080ENDPROC
2090:
2100DEF PROCston
2110PRINT"S/N = "(Ymax-Ymin)/RMS
2120ENDPROC
2130:
2140DEF PROCfindx
2150FOR I%=XX1 TO XX2
2160IF Ymax=FNy(I%) PRINT"X(Ymax)= "I%+1
2170IF Ymin=FNy(I%) PRINT"X(Ymin)= "I%+1
2180NEXT
2190ENDPROC
2200:
```

```
 10 REM SAVE"OLAP"
 20 VDU14
 30 DIM omega$(18):DIM A(9,9):DIM beta(9,9):DIM beta1(9,9):DIM Sig(9,9)
 40 DIM abdt(9):DIM br(9):DIM weight(9):DIM B(9,9):DIM Seff(9,9):DIM F(9)
 50 DIM abds(9):DIM Cross(9,9):DIM Iin(9):DIM E(9):DIM Ng(9):DIM Satom(9,9)
 60 DIM atom(9):DIM D(9,9)
 70 dels=1200*2*PI*1E6/SQR(LN(2)):del=1030*2*PI*1E6/SQR(LN(2))
 80 DATA -1.5333E10,-1.0116E10,-1.4679E10,-6.78E8,6.881999999E9,-4.812E9,
    6.738000001E9,-1.5429E10,0
 90 DATA  204,202,201-5,201-3,201-1,200,199-3,199-1,198
100 :
110 FOR I%=1 TO 18
120 READ omega$(I%)
130 NEXT
140 :
150 FORJ%=1 TO 9
160   FORI%=1 TO 9
170   REM IF J%<=I% A(J%,I%)=EVAL(omega$(J%))-EVAL(omega$(I%))
180   A(J%,I%)=EVAL(omega$(J%))-EVAL(omega$(I%))
190   NEXT
200 NEXT
210 :
220CLS
230 :
240 FORJ%=1 TO 9
250   FORI%=1 TO 9
260   REM PRINT TAB(7*J%+5,I%+5) A(J%,I%)
270   NEXT
280 NEXT
290 :
300 PRINT TAB(25,1) "Line profile weighting factors (Overlaps)"
310 PROClabel
320 FORJ%=1 TO 9
330   FORI%=1 TO 9
340   beta(J%,I%)=2*PI*A(J%,I%)/del:beta1(J%,I%)=beta(J%,I%)^2
350   alfa=dels/del
360   alfa1=alfa^2:alfa2=alfa1+1:alfa3=SQR(alfa2):alfa4=1/alfa1:alfa5=1/alfa2
370   alfa6=1/alfa3
380   Sig(J%,I%)=alfa6*EXP(-4*beta1(J%,I%)*(alfa4+alfa5))
390   REM PRINT"Sig="Sig(J%,I%)
400   NEXTI%
410 NEXTJ%
420 :
430 @%=&20408
440 FORJ%=1 TO 9
450  FORI%=1 TO 9
460  IF Sig(J%,I%)>1E-5 THEN PRINT TAB(7*J%+5,I%+5) Sig(J%,I%)
470  REM PRINT TAB(7*J%+5,I%+5) Sig(J%,I%)
480  NEXT
490 NEXT
500 :
510 PRINT:PRINT
520 PRINT"  Overlap=(1/sqr(1+a^2))exp-4b^2(1/a^2+1/(1+a^1)) with a=alpha,b=beta"
530 PRINT
540 PRINT"  alpha=delta(source)/delta(target) ; beta=(Wos-Wot)/delta(target)"
550 PRINT
560 PRINT"  delta is the Doppler width ; Wo is the centre frequency(rad)"
570 PRINT
580 PRINT TAB(12) "Do you want to display next page ? (Y/N)"
```

```
590 IF GET$="Y" THEN GOTO 620
600 END
610 :
620 REM These are the abundances (in the target)
630 REM of 204,202,201-5,201-3,201-1,200,199-3,199-1,198 respectively
640 abdt(1)=.0685:abdt(2)=.2980:abdt(3)=.1322:abdt(4)=.1322:abdt(5)=.1322
650 abdt(6)=.2313:abdt(7)=.1684:abdt(8)=.1684:abdt(9)=.1002
660 :
670 REM br(I%) are the (sum of br's)/Ng for each component
680 REM Ng=2 for 199,Ng=4 for 201,Ng=1 for even isotopes
690 Ng(1)=1:Ng(2)=1:Ng(3)=4:Ng(4)=4:Ng(5)=4:Ng(6)=1:Ng(7)=2:Ng(8)=2:Ng(9)=1
700 REM The sum of br's is the strenght of each component for sigma+ light
710 REM they are given in Cagnac's thesis
720 br(1)=1:br(2)=1:br(3)=1/2:br(4)=1/3:br(5)=1/6:br(6)=1:br(7)=2/3:br(8)=1/3
730 br(9)=1
740 :
750 FOR I%=1 TO 9
760 weight(I%)=br(I%)*abdt(I%)
770 NEXT
780 :
790 FOR I%=1 TO 9
800 atom(I%)=weight(I%)*Ng(I%)/abdt(I%)
810 NEXT I%
820 :
830 FOR J%=1 TO 9
840   FOR I%=1 TO 9
850   B(J%,I%)=weight(J%):D(J%,I%)=atom(J%)
860   REM PRINT B(J%,I%)
870   NEXT I%
880 NEXT J%
890 :
900 FOR J%=1 TO 9
910   FOR I%=1 TO 9
920   Seff(J%,I%)=B(J%,I%)*Sig(J%,I%)*6*1E-17
930   Satom(J%,I%)=D(J%,I%)*Sig(J%,I%)*6*1E-17
940   NEXT I%
950 NEXT J%
960 :
970 CLS
980 PRINT TAB(35,1) "n.Sigma for target absorber"
990 PROClabel
1000 @%=&10408
1010 FOR J%=1 TO 9
1020   FOR I%=1 TO 9
1030   IF Seff(J%,I%)>1E-22 THEN PRINT TAB(7*J%+5,I%+5) Seff(J%,I%)
1040   NEXT I%
1050 NEXT J%
1060 :
1070 PRINT:PRINT:PRINT:
1080 PRINT TAB(12) "Do you want to display next page ? (Y/N)"
1090 IF GET$="Y" THEN GOTO 1120
1100 END
1110 :
1120 CLS:PRINT TAB(30,1) "Effective cross-section per atom":PROClabel
1130 @%=&10408
1140 FOR J%=1 TO 9
1150   FOR I%=1 TO 9
1160   IF Satom(J%,I%)>1E-22 THEN PRINT TAB(7*J%+5,I%+5) Satom(J%,I%)
1170   NEXT I%
1180 NEXT J%
1190 :
```

```
1200 REM These are the (2F+1)/(2J+1)(2I+1) values
1210 REM for 204,202,201-5,201-3,201-1,200,199-3,199-1,198 respectively
1220 F(1)=1:F(2)=1:F(6)=1:F(9)=1:F(3)=1/2:F(4)=1/3:F(8)=1/3:F(5)=1/6:F(7)=2/3
1230 REM These are the source abundances in the same order
1240 abds(1)=.582:abds(2)=.1705:abds(3)=.0526:abds(4)=.0526:abds(5)=.0526
1250 abds(6)=.0878:abds(7)=.065:abds(8)=.065:abds(9)=.041
1260 :
1270 PRINT:PRINT:PRINT:
1280 PRINT TAB(12) "Do you want to display next page ? (Y/N)"
1290 IF GET$="Y" THEN GOTO 1310
1300 END
1310 CLS:PROClabel
1320 Sum=0
1330 FOR J%=1 TO 9
1340   FOR I%=1 TO 9
1350   Cross(J%,I%)=Seff(J%,I%)*abds(I%)*F(I%)
1360   Sum=Sum+Cross(J%,I%)
1370   NEXTI%
1380 NEXT J%
1390 :
1400 FORJ%=1 TO 9
1410  FORI%=1 TO 9
1420  IF Cross(J%,I%)>1E-25 THEN PRINT TAB(7*J%+5,I%+5) Cross(J%,I%)
1430  REM PRINT TAB(7*J%+5,I%+5) Cross(J%,I%)
1440  NEXT
1450 NEXT
1460 :
1470 @%=&20309:PRINT:PRINT:PRINT
1480 PRINT "   The 204--199-1/2 component represents ";Cross(8,1)/Sum;
     "  of the total light"
1490 :
1500 PRINT:PRINT:PRINT
1510 PRINT TAB(12) "Do you want to display next page ? (Y/N)"
1520 IF GET$="Y" THEN GOTO 1540
1530 END
1540 CLS
1550 @%=&00305
1560 Itot=0
1570 FORI%=1 TO 9
1580 Iin(I%)=abds(I%)*F(I%)
1590 PRINT"Iin(";omega$(I%+9);")= ";Iin(I%)
1600 Itot=Itot+Iin(I%)
1610 NEXT
1620 :
1630 PRINT
1640 PRINT"Total incoming light intensity I(tot) = ";Itot
1650 PRINT
1660 :
1670 PRINT
1680 PRINT:a$="List results as a function of k ?":PROCans:IF A$="Y"GOTO1710
1690 PROCresult
1700 END
1710 FOR K=1E16 TO 1E17 STEP 1E16
1720 PRINT"k=n.x=";K;:PROCpressure
1730 PROCresults
1740 NEXT
1750 END
1760 :
1770 DEF PROCresult
1780 INPUT"What is the value of k=n.x ;  "K;:PROCpressure
1790 C=0:D=0:Seff(8,1)=B(8,1)*Sig(8,1)*6*1E-17
```

```
1800 PRINT
1810 PRINT"c is the x-section of an isotope from the source with the ensemble"
1820 PRINT"of all the isotopes present in the target"
1830 PRINT
1840 FOR I%=1 TO 9
1850 C=0
1860   FOR J%=1 TO 9
1870   C=C+Seff(J%,I%)
1880   NEXT J%
1890 PRINT"c= ";C;
1900 E(I%)=Iin(I%)*EXP(-C*K)
1910 PRINT TAB(25)"Iin(";omega$(I%+9);") exp-kc = ";E(I%);
1920 PRINT TAB(55) "exp-c.k =";E(I%)/Iin(I%)
1930 D=D+E(I%)
1940 NEXT I%
1950 :
1960 PRINT
1970 PRINT"Total output light from the target (Iout) = ";D:PRINT
1980 PRINT"Ratio of total output light to incoming light (Iout/Itot)= ";D/Itot
1990 PRINT
2000 PRINT "1-exp-(k.c[204--199-1/2]) = ";(1-EXP-(K*Seff(8,1))):PRINT
2010 :
2020 D1=0
2030 FOR I%=1 TO 9
2040 C=0:Seff(8,1)=0
2050   FOR J%=1 TO 9
2060   C=C+Seff(J%,I%)
2070   NEXT J%
2080 E(I%)=Iin(I%)*EXP(-C*K)
2090 D1=D1+E(I%)
2100 NEXT I%
2110 :
2120 PRINT"Total output light without [204--199-1/2] component (Ia)= ";D1
2130 PRINT
2140 PRINT"(Ia-Ib)/Itot =";(D1-D)*100/Itot;" %"
2150 GOTO 1670
2160 ENDPROC
2170 :
2180 REM END
2190 :
2200 DEF PROClabel
2210 PRINT TAB(42,2) "Target"
2220 PRINT TAB(1,5) "Source"
2230 FOR I%=10 TO 18
2240 PRINT TAB(7*(I%-9)+7,4) omega$(I%)
2250 PRINT TAB(2,(I%-9)+5) omega$(I%)
2260 NEXT
2270 ENDPROC
2280:
2290 DEF PROCresults
2300 C=0:D=0:Seff(8,1)=B(8,1)*Sig(8,1)*6*1E-17
2310 FOR I%=1 TO 9
2320 C=0
2330   FOR J%=1 TO 9
2340   C=C+Seff(J%,I%)
2350   NEXT J%
2360 E(I%)=Iin(I%)*EXP(-C*K)
2370 D=D+E(I%)
2380 NEXT I%
2390 PRINT "1-exp-(k.c[204--199-1/2]) = ";(1-EXP-(K*Seff(8,1)));
2400 D1=0
```

```
2410 FOR I%=1 TO 9
2420 C=0:Seff(8,1)=0
2430   FOR J%=1 TO 9
2440   C=C+Seff(J%,I%)
2450   NEXT J%
2460 E(I%)=Iin(I%)*EXP(-C*K)
2470 D1=D1+E(I%)
2480 NEXT I%
2490 PRINT TAB(40) "(Ia-Ib)/Itot =";(D1-D)*100/Itot;" %"
2500 ENDPROC
2510 :
2520DEF PROCans
2530PRINTa$;" (Y/N) ";:A$=GET$:PRINTA$:IFA$<>"Y"ANDA$<>"N"GOTO2530
2540ENDPROC
2550 :
2560 DEF PROCpressure
2570 P=0
2580 kb=1.38E-23:T=294:x=.23
2590 P=7.5E-3*(K*kb*T)/x:PRINT"  Pressure (Torr)=";P;
2600 Tb=3214/(8.164-LOG(P)):PRINT"  Tbead (C)=";(Tb-273.15)
2610 REM pressure(T)=10^(8.164-3214/T)
2620 REM gives p(torr) given T(K) for Hg
2630 ENDPROC
2640 :
```